NPL Report CMAM 26

February 1999

A systematic assessment of the 'magnomic' method of high frequency hydrophone calibration

B Zeqiri, P N Gélat and M Hodnett
Centre for Mechanical and Acoustical Metrology
National Physical Laboratory
Teddington
Middlesex
United Kingdom
TW11 0LW

ABSTRACT

This document represents the technical report for Milestone (d) of Project 2.3(i) of the DTI NMS Acoustics Programme for 1995-1998 entitled "Establish service for hydrophone calibration in the frequency range 20 to 60 MHz". The actual title of Milestone (d) is "Validate interferometer calibration method by use of the magnomic calibration method."

The aim of this Milestone was to attempt to corroborate hydrophone calibrations based on the NPL primary standard laser interferometer, by using an independent technique termed the 'magnomic' method. This method utilises the theoretical modelling of propagating acoustic waves of finite amplitude within the plane-wave region of a 10 MHz transducer. This document describes in detail a number of aspects of the theoretical and experimental work carried out. The plane-wave algorithm used to predict the acoustic waveform at various measurement positions is presented. An important facet of the work has been an investigation of the pressure distribution generated by the transducer at various distances from the transducer face through beam-plotting, work which has demonstrated significant departures from the required plane-wave behaviour. Also presented are the results of experimental studies of other aspects of the 'magnomic' calibration method.

Finally, calibration results are presented for four Marconi membrane hydrophones covering the frequency range 10 to 60 MHz. Derived sensitivity values are compared with those obtained from a range of other methods, including the NPL primary standard laser interferometer. The main conclusion drawn from the studies is that the 'magnomic' calibration method is not currently appropriate for use as a standard high frequency calibration technique.

© Crown Copyright 1999
Reproduced by permission of the Controller of HMSO

ISSN 1369-6785

National Physical Laboratory
Teddington, Middlesex, UK, TW11 0LW

Extracts from this report may be reproduced provided the source is acknowledged and the extract is not taken out of context.

Approved on behalf of the Managing Director, NPL,
by Graham Torr, Head, Centre for Mechanical and Acoustical Metrology

CONTENTS

1 INTRODUCTION 5
1.1 MOTIVATION 5
1.2 MILESTONE SUMMARY 5
2 REPORT LAYOUT 7
3 PRINCIPLES OF THE 'MAGNOMIC' METHOD 9
4 THEORY - THE FINITE AMPLITUDE PROPAGATION OF PLANE-WAVES 11
4.1 OVERVIEW 11
4.2 THEORY 11
4.2.1 Solution in terms of normalised quantities 11
4.2.2 Solution in terms of acoustic pressure 13
4.3 PROGRAMMING 15
4.4 VALIDATION 16
4.4.1 Comparison with results produced by Fubini and Fay 16
4.4.2 Comparison with results given by the routine used in Mitome (1989) 19
4.4.3 Validation of solution in terms of acoustic pressure 22
4.5 NONLINEAR PROPAGATION OF A MEASURED PULSE 23
4.6 SENSITIVITY OF THE MAGNITUDE OF THE FIRST 6 HARMONICS TO THE UNCERTAINTY IN THE MAXIMUM PRESSURE AT THE SOURCE 24
4.7 SUMMARY 25
5 MEASUREMENT SYSTEMS AND DEVICES 26
5.1 SCANNING TANK 26
5.2 THE 'MAGNOMIC' TRANSDUCER 26
5.3 TRANSDUCER DRIVE SYSTEM 26
5.4 WIDE BANDWIDTH AMPLIFIER 27
5.5 REFERENCE HYDROPHONES USED DURING MILESTONE 27
5.6 MEASUREMENT PROCEDURES 28
5.6.1 Alignment 28
5.6.2 Waveform acquisition 29
6 RESULTS - ANCILLARY STUDIES 30
6.1 PLANE-WAVE BEHAVIOUR OF THE TRANSDUCER - BEAM-PLOTTING OF THE TRANSDUCER FIELD 30
6.1.1 Measurement protocol 30
6.1.2 Results 31
6.2 EFFECT OF WINDOWING AND TRUNCATION OF THE ACOUSTIC WAVEFORM 35
6.2.2 Effects of truncation on the variation of the magnitude of the fundamental with distance 40

6.2.3 Effects of truncation on a calibration using the 'magnomic' method 44
6.3 MEASUREMENTS MADE USING THE LARGE APERTURE HYDROPHONE. 49
6.3.1 Waveforms acquired using the 75 mm hydrophone 50
6.3.2 Measurements of nonlinear loss 53
6.3.3 Axial dependence of nonlinear loss 58
6.3.4 Axial variation of generated second harmonic component 59
6.4 EXPERIMENTAL INVESTIGATIONS OF THE 'TRANSDUCER CORRECTION' 60
6.4.1 Low drive level measurements 60
6.4.2 Drive setting behaviour for the axial dependence of the fundamental signal level 65
6.5 THE EFFECT OF DECONVOLUTION 66
7 RESULTS - 'MAGNOMIC' CALIBRATIONS 69
7.1 INVESTIGATION OF WAVEFORM ACQUISITION REPEATABILITY 69
7.2 'Magnomic' hydrophone calibration 75
7.2.1 Overall description 75
7.2.2 Hydrophone IP016 76
7.2.3 Hydrophone IP010 79
7.2.4 Hydrophone IP901 82
7.2.5 Hydrophone IP904 85
7.3 CORRECTING FOR TRANSDUCER IMPERFECTIONS 88
8 DISCUSSION 91
9 SUMMARY 94
10 ACKNOWLEDGEMENTS 96
11 REFERENCES 97
APPENDIX A HIGH FREQUENCY 'MAGNOMIC' HYDROPHONE CALIBRATION 98
APPENDIX B MEMBRANE HYDROPHONE REFERENCE SENSITIVITIES 111
APPENDIX C GAIN VALUES FOR AMPLIFIER 55391001 124
APPENDIX D TRANSFER FUNCTION OF A HYDROPHONE 125

1 INTRODUCTION

This document constitutes the final report of Milestone (d) of the NMSPU deliverable 2.3 (i) whose title is "Establish service for hydrophone calibration in the frequency range 20 to 60 MHz". The actual title of the Milestone is "Validate interferometer calibration method by use of the magnomic calibration method". This report covers work carried out over the period January to November 1998.

1.1 MOTIVATION

In recent times, the need to provide high resolution images of small body structures has led to an increasing number of medical ultrasound applications being developed that use acoustic frequencies in excess of 20 MHz. Specifically, these are diagnostic devices used to perform short-range imaging in tissue. Skin scanners that interrogate layers of the epidermis have been developed, operating at 20 MHz, and intravascular devices formed by transducer elements mounted on catheters are utilised in blood vessel imaging, at frequencies of typically 30 MHz. The acoustic pressure amplitudes and frequencies employed in these applications cause the ultrasound propagating in the tissue to undergo finite amplitude distortion, whereby energy is transferred to higher harmonic multiples of the fundamental frequency component. Thus, there will be a significant amount of acoustic energy present at frequencies up to and in excess of 60 MHz from a drive frequency of 15 MHz or above. In order to assess patient safety in terms of exposure to ultrasound, the acoustic fields produced by these devices must be measured.

The established method of measuring acoustic fields is to use a calibrated hydrophone, and alongside the wide commercial availability of devices, standards are in place which describe hydrophone calibration in the range 0.5 MHz to 15 MHz (IEC 60866, IEC 61101), and the methods appropriate in evaluating diagnostic ultrasound fields in this range (IEC 61102). However, the characterisation of high frequency fields places greater demands on hydrophone performance, and it is only in recent times that hydrophones with the required bandwidth (in excess of 60 MHz) and spatial resolution (0.1 mm or better) have become available. Thus, there is a need to develop techniques to calibrate hydrophones accurately over an extended frequency range. The work described here has concentrated on the investigation of the suitability of the so-called 'magnomic' method to provide a means of calibrating such hydrophones at frequencies up to 60 MHz.

1.2 MILESTONE SUMMARY

Previously during this NMSPU deliverable, a number of Marconi membrane hydrophones were calibrated over the frequency range 5 to 60 MHz using the NPL primary standard laser interferometer. This work, undertaken under Milestone (b): "Establish interferometer calibration method", has been summarised in the NPL report CMAM(INT)001 (Esward et al. 1997). Although the poor signal-to-noise ratio for measurements of displacement at these elevated frequencies compromised measurement accuracy, reference calibrations were carried out on four membrane hydrophones and these are listed in Section 5.5 along with their sensitivity values at 10 MHz.

The aim of Milestone (d) reported here was to investigate systematically a second method for deriving absolute calibration of hydrophones up to 60 MHz, which will henceforth be referred

to as the 'magnomic' method. Obtaining independent corroboration of the interferometer values was considered crucial in validating the interferometer calibrations.

The basis of this second method, whose concept is described in detail in Section 3, utilises the theoretical modelling of finite amplitude propagation of ultrasound in water. Previous work undertaken on this topic has been summarised in an NPL Internal document, which has now been included for reference purposes in Appendix A of this document. As well as describing the principles behind the 'magnomic' method, the report tabulates end-of-cable open-circuit sensitivities of two reference hydrophones, IP027 and IP767, both of which malfunctioned during the course of the project and are no longer usable. It is therefore not possible to compare the results of the current study directly with those calibrations. However, fortunately, during the early stages of this deliverable, 'magnomic' calibrations of IP767 and IP027 were transferred to a number of other hydrophones, including IP016 and IP901 which are used in the current study.

2 REPORT LAYOUT

A pivotal part of the analysis procedure employed lies in the plane-wave propagation algorithm used and this is described in detail in Section 4. It allows the time-domain acoustic waveform acquired close to the face of the transducer to be propagated to any distance, thereby permitting the degree of distortion and the harmonic content of the waveform at any measurement site of interest to be predicted.

Section 4 describes the propagation algorithm used and presents a MATLAB implementation of the routine which has been validated using well known limiting forms which appear in the literature.

Section 5 provides a breakdown of the experimental measurement systems and the protocols used, with the experimental studies being undertaken using the NPL beam-plotting facility.

Some key studies undertaken to understand the 'magnomic' method and provide a validation for the technique are given in Section 6. These ancillary studies include the following:

- a fundamental assumption of the 'magnomic' method relates to the existence of plane-wave propagation in the transducer field. This is tested in Section 6.1, where data is presented derived from scanning of the field using small hydrophones at various distances from the transducer;

- the effect of windowing and truncation on the acoustic signals acquired with attention being paid to the effect on the fundamental component which is crucial in estimating the nonlinear loss: this is examined in Section 6.2;

- a 75 mm diameter membrane hydrophone is used to determine the plane-wave nonlinear loss, this aspect represents a new feature in the current study and results obtained using this hydrophone are presented in Section 6.3;

- an investigation of the variation in acoustic pressure along the acoustic axis of the transducer, Section 6.4. If propagation were truly plane-wave, then for low amplitude propagation of pulses, the signal should only alter due to small signal absorption of the water path. Variations in this anticipated behaviour were ascribed in the original 'magnomic' calibration to transducer imperfections. The method of correcting for these is crucial to the calibration method;

- the effect of deconvolution of the acquired waveforms using the theoretical hydrophone response is covered in Section 6.5, particular emphasis being placed on measurements made using the 75 mm large-aperture hydrophone described in Section 6.3.

Section 7 describes the calibrations which have been attempted on the four wide-bandwidth Marconi membrane reference hydrophones.

- in Section 7.2, these calibrations have been carried out in various ways, without directly correcting for transducer imperfections;

- the potential effect of transducer imperfections, or deviations from plane-wave behaviour, is described briefly in Section 7.3.

Finally, Sections 8 and 9 discuss and summarise the results obtained and assess the appropriateness of the 'magnomic' method.

3 PRINCIPLES OF THE 'MAGNOMIC' METHOD

The 'magnomic' method of hydrophone calibration is described in detail in Appendix A. For this reason, only an overview of the basic methodology will be given in this Section, essentially highlighting only the most important characteristics of the technique.

Ultrasound propagation in water has long been established as a nonlinear process (Carstensen et al, 1980). Depending on the properties of the medium, the acoustic frequency and initial pressure amplitude of the acoustic wave, a plane-wave will suffer progressive and cumulative distortion in the time-domain as it propagates. When the frequency content of the propagating waveform is considered, there are two main consequences of the nonlinear propagation:-

- the magnitude of the starting frequency component (referred to as the fundamental) undergoes an enhanced loss over and above that expected through (small signal) absorption in water;

- higher frequency harmonics of the fundamental frequency (integer multiples of the fundamental frequency) are generated during the propagation.

The frequency content of the distorted waveform and the resultant loss in the fundamental are linked, a feature which is utilised in the 'magnomic' hydrophone calibration method in the following way. Providing an accurate propagation model exists describing the propagation of the plane-wave, then by measuring the fundamental loss directly and comparing this with theory, it is possible to predict the frequency content of the acoustic wave at any particular measurement position. By comparing this with the electrical output of the hydrophone at the same measurement point, a broadband calibration of its sensitivity can be derived at integer frequencies of the fundamental.

In principle, therefore, the 'magnomic' method provides an attractive means of calibrating a hydrophone up to and beyond frequencies of 100 MHz (Bacon 1982). There are, however, certain explicit requirements for the method, perhaps the most difficult to achieve being the need for plane-wave propagation, which if not met will render the theoretical model applied invalid.

For the calibrations described in Appendix A, it can be seen that the method has been implemented using the so-called plane-wave region of a large diameter (19 mm) transducer operating at 10 MHz. Here, providing the excitation of the transducer is pulsed, it is possible to resolve in time the plane-wave component (emanating from the flat face of the transducer) from the edge-wave component (travelling from the periphery or rim of the transducer). Some calculations of the 'usable' distance, i.e. the region where the plane and edge-waves are sufficiently separable, are given in Appendix A. For this transducer, using a pulse length of 270 ns, propagation distances of up to 110 mm can be readily be used.

Although in concept such an approach may be used to isolate a plane-wave, one major practical difficulty encountered is the fact that commercially-available transducers are far from ideal, and even close to the transducer face, well within the time interval identified by Equation A.1 of Appendix A, a plane-wave is not produced. Due to these deviations from idealised behaviour, even using low transducer drive conditions where no nonlinear distortion occurs, the pulse amplitude does not attenuate as it should assuming only absorption in water,

but can actually increase with distance. Within Appendix A, this effect has been ascribed to non-uniformities in the transducer backing, and in the calibration method described, an attempt has been made to overcome this by using the following measurement procedure:

- two measurement positions are identified, one as close to the source as possible (during this study, 5 mm was used) and a second at the site used for the calibration, where the plane and edge-waves are sufficiently distinct (in the study a separation of 70 mm was used);

- two drive voltage levels are identified, the highest of which generates the harmonic-rich waveform at the calibration site. The second, the low drive waveform, is of sufficiently low acoustic pressure such that propagation between the two sites indicated above is linear;

- the calibration process involves acquiring two acoustic waveforms (high and low drive) at both these near and far distances.

From the two high drive waveforms, the nonlinear loss between the two measurement positions is calculated and this is used to obtain an estimate of the source pressure. Through this, using an algorithm which describes reliably the finite amplitude propagation of a plane-wave, the harmonic content of the acoustic waveform at the farthest measurement distance is predicted. This is then compared with the frequency content of a hydrophone waveform measured when the device is positioned at the greater distance.

The two low drive waveforms are used to establish an estimate of the 'transducer imperfection correction'. It is not clear from Appendix A exactly how this correction is applied to adjust the source waveform measured close to the face in the high drive case. An investigation of how this could potentially be applied provided one of the identified work topics of the current report.

Other aspects of the 'magnomic' method reported in Appendix A worthy of mention are the need to window the acoustic waveform to ensure the plane-wave and edge-wave are indeed separated. Additionally, as an acoustic pulse is used, a single frequency is not generated at the source but a range of frequencies are propagated in the initial acoustic disturbance.

4 THEORY - THE FINITE AMPLITUDE PROPAGATION OF PLANE-WAVES

4.1 OVERVIEW

As part of this project, it is clearly important to develop a means of modelling the propagation of a one-dimensional wave in a dissipative fluid. This Section describes the approach that has been used. Results have been compared with those in Mitome (1989) and Bacon (1986). A slightly modified version of the solution in terms of the acoustic pressure has also been obtained.

The 'magnomic' method of hydrophone calibration relies on the ability to predict the way in which an initial one-dimensional pulse is distorted when propagating nonlinearly within water. As described in Appendix A, the sensitivity of the hydrophone may be estimated by comparing with a measured waveform at that position.

The aim of the work presented within this report was to investigate a range of methods for calibrating the hydrophones using the basic 'magnomic' methodology, although ideally it would be preferable to calibrate the hydrophone without any *a priori* knowledge of the hydrophone response. One of the alternative techniques is to use the known low frequency (10 MHz) sensitivity of the hydrophone. Using this route the influence of calibration accuracy becomes important and this is investigated in Section 5.6 for the first five harmonics.

4.2 THEORY

4.2.1 Solution in terms of normalised quantities

From Mitome (1989), an exact solution for finite-amplitude plane sound waves in a non-compressible viscous, dissipative fluid is given by:

$$P(T,X) = D_0 \frac{\partial}{\partial T} \ln \left[\int_{-\infty}^{T} e^{-\frac{1}{D_0}\left(\frac{(T-T')^2}{2X} - \Psi_1(T')\right)} dT' \right] \qquad (1)$$

where

$$T = \omega\left(t - \frac{x}{c_0}\right), \quad X = \frac{x}{x_c}, \quad D_0 = \frac{2}{\Gamma}, \quad P = \frac{p}{p_0} \text{ and } \Psi_1(T') = \int_{-\infty}^{T'} P(T'',0)\,dT''$$

- x is the positive direction of propagation
- t is time
- p is the acoustic pressure amplitude
- p_0 is the pressure magnitude at source
- c_0 is the local velocity and the index 0 refers to quantities relevant to infinitesimal sound waves
- x_c is the shock formation distance in a lossless fluid
- Γ is the Gol'dberg number.

In order to compare the results obtained using this formulation with those given by the code in Bacon (1986), equivalencies between the variables used in each reference are provided in the remainder of this section.

From Bacon (1986),

$$\frac{\partial U}{\partial \sigma} = U\frac{\partial U}{\partial \tau} + \frac{1}{\Gamma}\frac{\partial^2 U}{\partial \tau^2} \tag{2}$$

where U is the normalised particle velocity. This equation is known as Burgers' equation. σ and τ represent the same quantities as X and T respectively.

The following substitution is made:

$$U = \frac{2}{\Gamma\varphi}\frac{\partial \varphi}{\partial \tau} = \frac{\partial \psi}{\partial \tau} \tag{3}$$

where φ and ψ are functions of σ and τ.

Substituting Equation (3) into Equation (2) and integrating w.r.t. τ yields:

$$\frac{\partial \psi}{\partial \sigma} = \frac{1}{2}\left(\frac{\partial \psi}{\partial \tau}\right)^2 + \frac{1}{\Gamma}\frac{\partial^2 \psi}{\partial \tau^2} \tag{4}$$

But from Equation (2),

$$\psi = \frac{2}{\Gamma}\ln|\varphi|, \frac{\partial \psi}{\partial \tau} = \frac{2}{\Gamma\varphi}\frac{\partial \varphi}{\partial \tau} \text{ and } \frac{\partial \psi}{\partial \sigma} = \frac{2}{\Gamma\varphi}\frac{\partial \varphi}{\partial \sigma}$$

Substituting into Equation (4) gives:

$$\frac{\partial \varphi}{\partial \sigma} = \frac{1}{\Gamma}\frac{\partial^2 \varphi}{\partial \tau^2} \tag{5}$$

If the variables are re-labelled, this equation is analogous to the linear diffusion equation. The solutions to this type of equation are known. Consider Equation (3) at $\sigma = 0$:

$$\left(\frac{1}{\varphi}\frac{\partial \varphi}{\partial \tau}\right)_{\sigma=0} = \frac{\Gamma}{2}U(\tau,0)$$

$$\Rightarrow \left|\varphi(\tau_1,0)\right| = \exp\left[\frac{\Gamma}{2}\int^{\tau_1} U(\tau,0)d\tau\right] \tag{6}$$

This will be re-written as:

$$\Phi(\tau_1) = \exp\left[\frac{\Gamma}{2}\int^{\tau_1} U(\tau,0)d\tau\right]$$

Equation (7) forms the initial condition of Equation (5). The solution of Equation (5) for φ, subject to (7), is given by [4]:

$$\varphi(\tau,\sigma) = \frac{1}{\sqrt{\frac{4\pi\sigma}{\Gamma}}}\int_{-\infty}^{+\infty}\Phi(\tau_1)e^{-\frac{(\tau-\tau_1)^2\Gamma}{4\sigma}}d\tau_1$$

Let

$$\varphi_1(\tau_1) = \int^{\tau_1} U(\tau,0)d\tau$$

From Equation (3),

$$U = \frac{2}{\Gamma\varphi}\frac{\partial\varphi}{\partial\tau} = \frac{2}{\Gamma}\frac{\partial}{\partial\tau}\ln|\varphi|$$

and hence,

$$U(\tau,\sigma) = \frac{2}{\Gamma}\frac{\partial}{\partial\tau}\ln\left[\right.$$

By comparing Equations (1) and (11), and noting that $D_0 = 2/\Gamma$, it can be seen that the normalised pressure and the normalised velocity defined respectively in Mitome (1989) and Bacon (1986) are in fact equivalent quantities.

4.2.2 Solution in terms of acoustic pressure

In practice, it is perhaps more convenient to deal with non-normalised quantities. It may be shown (Hamilton and Blackstock (1997)) that the Burgers equation may be presented as:

$$\frac{\partial p}{\partial x} - \frac{\delta_0}{2c_0^3}\frac{\partial^2 p}{\partial\tau^2} = \frac{\beta p}{\rho_0 c_0^3}\frac{\partial p}{\partial\tau}$$

where

$$\delta_0 = \frac{1}{\rho_0}\left[\frac{4}{3}\mu + \mu_B + \kappa\left(\frac{1}{c_v} - \frac{1}{c_p}\right)\right] \qquad (13)$$

and

- μ is the shear viscosity
- μ_B is the bulk viscosity
- κ is the thermal conductivity

- c_p and c_v are the specific heat coefficients at constant pressure and volume respectively
- ρ_0 is the density of the medium
- c_0 is the velocity of sound in the unperturbed medium.

Here, p is the acoustic pressure, x is the distance of propagation and $\tau = t - x/c_0$ is retarded time. δ_0 is known as the diffusivity of sound and is related to the Gol'dberg number as follows:

$$\delta_0 = \frac{2\beta p_0}{\Gamma \rho_0 \omega} \tag{14}$$

where

- β=1+B/(2A) (equal to 3.5 for water)
- p_0 is the maximum value of the pressure at t=0.

To a first order approximation, it may be shown (Hamilton and Blackstock (1997)) that δ_0 is related to the attenuation α as follows:

$$\delta_0 \approx \frac{2\alpha c_0^3}{\omega^2} \tag{15}$$

where α<<k, and k=ω/c_0 is the wave number. For water and at the frequencies which are considered here (of the order of MHz), this holds true. Note that it is more convenient to express the diffusivity of sound in terms of the attenuation of the medium. The terms in Equation (13) are often not known to a great accuracy.

In order to solve Equation (12), a solution of the following form is assumed:

$$p(x,t) = \frac{\rho_0 \delta_0}{\beta} \frac{\partial}{\partial \tau} \ln \psi(x,\tau) \tag{16}$$

where

$$\psi(x,\tau) = e^{\frac{\beta}{\rho_0 \delta_0} \int_{\tau} p(x,\tau')\, d\tau'} \tag{17}$$

Substituting Equation (17) into Equation (12) yields:

$$\frac{\partial \psi}{\partial x} = \frac{\delta_0}{2c_0^3} \frac{\partial^2 \psi}{\partial \tau^2} \tag{18}$$

Note that the procedure is analogous to that used in Section 4.2.1

The solutions to this equation are known from the linear diffusion equation (Hamilton and Blackstock (1997)):

$$\psi(x,\tau) = \left(\frac{c_0^3}{2\pi x \delta_0} \right)^{\frac{1}{2}} \int_{-\infty}^{+\infty} \psi(0,\tau) e^{\frac{c_0^3 (\tau - \tau')^2}{2x\delta_0}} d\tau' \tag{19}$$

Substituting into Equation (16) gives the expression for the acoustic pressure:

$$p(x,\tau)=\frac{\rho_0\delta_0}{\beta}\frac{\partial}{\partial\tau}\ln\left[\left(\frac{c_0^3}{2\pi x\delta_0}\right)^{\frac{1}{2}}\int_{-\infty}^{+\infty}e^{-\frac{c_0^3(\tau-\tau')^2}{2x\delta_0}+\frac{\beta}{\rho_0\delta_0}\int^{\tau'}p(0,\tau'')d\tau''}d\tau'\right] \qquad (20)$$

Hence, the initial time history of a pressure pulse may then be propagated throughout the medium. This equation is in fact analogous to Equation (1).

4.3 PROGRAMMING

This Section deals with the implementation of Equation (1), i.e. the solution for normalised pressure. Equation (20) is coded up in much the same way. Hence, a detailed explanation on how Equation (20) has been implemented is not considered here.

In order to implement Equation (1), a similar approach as in Mitome (1989) has been used. The main difficulty lies in the evaluation of the integral with the infinite integration range. However, it can be noted that outside specific boundaries, the exponential term will have a negligible contribution to the overall value of the integral. In Mitome (1989) it is suggested that the lower and upper integration limits be respectively set to T - (-2 $X D_0 \ln C$)$^{1/2}$ and T + (-2 $X D_0 \ln C$)$^{1/2}$. For accurate results, taking $C = 10^{90}$ is usually sufficient. In fact if D_0 is large (i.e. Γ is small), taking $C = 10^{30}$ is adequate. Note that the larger the value of C, the larger the integration range. Hence, more accurate results may be obtained at the expense of longer computation times.

In order to evaluate this integral, a Romberg quadrature routine has been used (Press 1992). Another problem is that of the evaluation of the indefinite integral in Equation (9) in the case of a sampled initial waveform. In order to obtain accurate results whilst using a quadrature routine, it is necessary to be able to evaluate the integrand at any point within the integration range. In order to do so, a cubic interpolation routine has been included so that this may be possible. Note that, as the integral is indefinite, it is assumed that, if the sampled waveform starts at $T = 0$, $\int^{T'} P(T'',0)dT'' = \int_0^{T'} P(T'',0)dT''$.

The derivative with respect to T is evaluated by calculating the gradient of the time history obtained for a specific value of X and D_0.

Hence, given an initial time history, it is possible to propagate this time history throughout the medium. Also, the Fourier transforms of the time histories obtained at different values of X may be evaluated so that the variation of the harmonic content of the initial waveform may be plotted as a function of normalised propagation distance. In the case where the initial waveform is a sine wave, these plots may be compared with the Fubini and Fay solutions for low values and high values of X respectively (Mitome 1989).

4.4 VALIDATION

4.4.1 Comparison with results produced by Fubini and Fay

In Mitome (1989), results have been produced for $P(T,0) = \sin(T)$ with $D_0 = 0.01$, 0.1 and 0.3 (i.e. $\Gamma = 200$, 20 and 20/3). Plots of the changes in waveform during propagation for $X \in [0,5]$ (i.e. $\sigma \in [0,5]$) as well as comparison with the Fubini and Fay solutions in the frequency domain for the first 5 harmonics have been obtained. These results have been reproduced and good agreement has been obtained. The changes in waveform during propagation are found below, in Figures 4.1, 4.2 and 4.3.

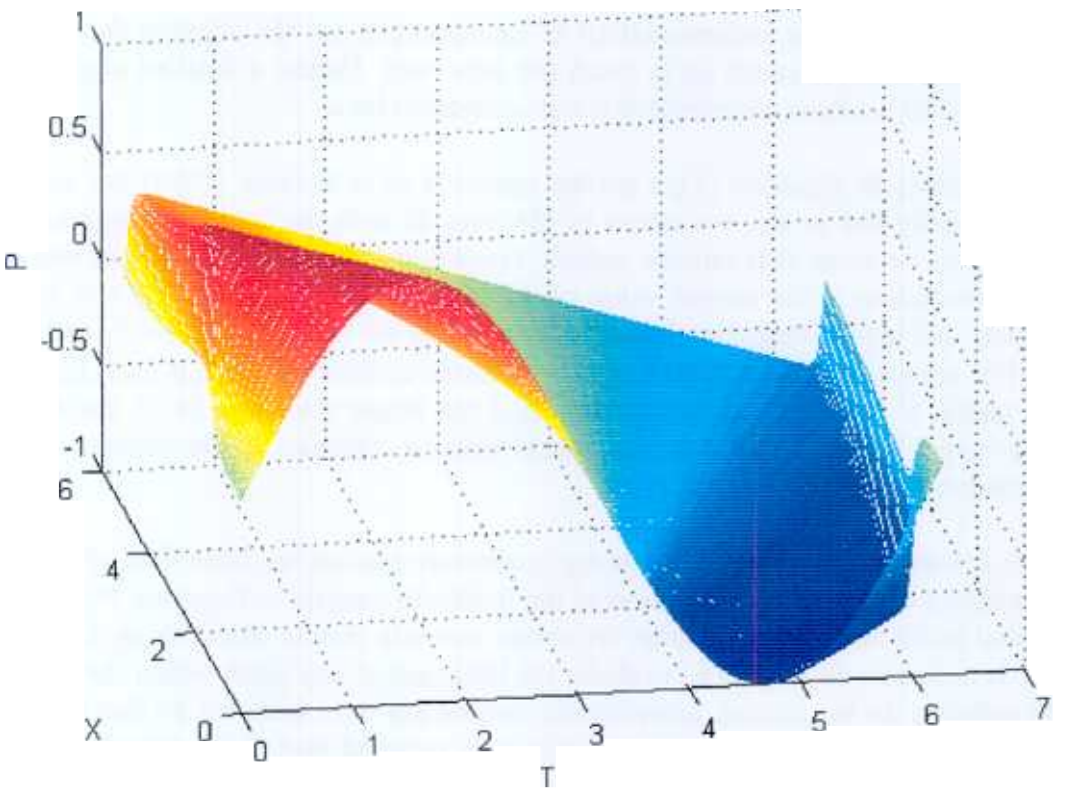


Figure 4.1: $D_0 = 0.01$

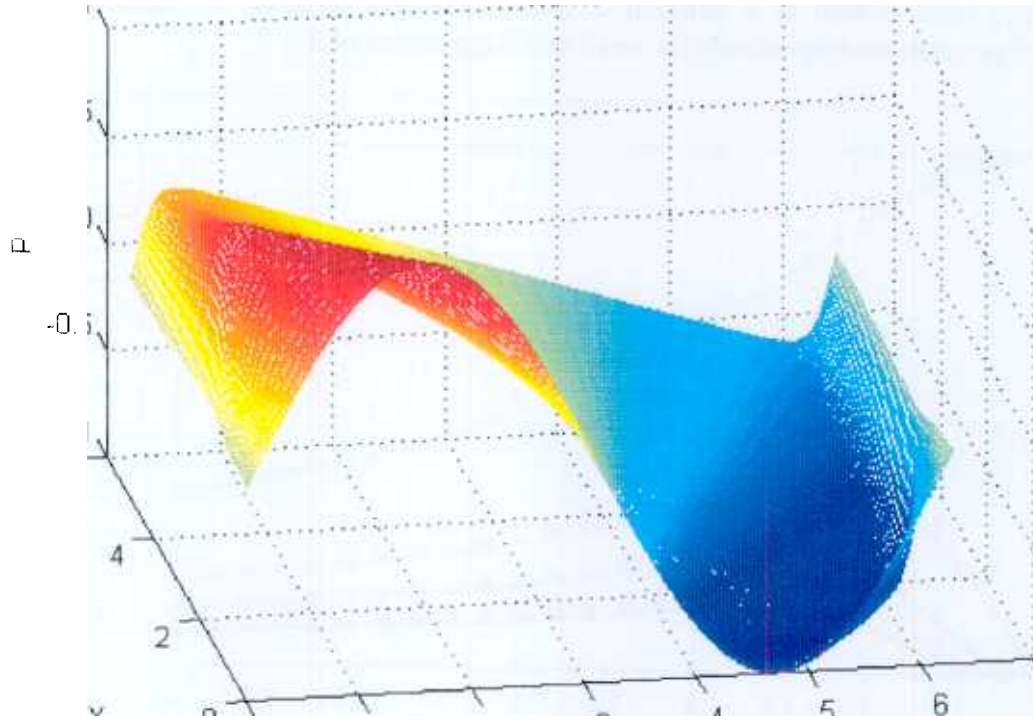


Figure 4.2 D_0 0.03

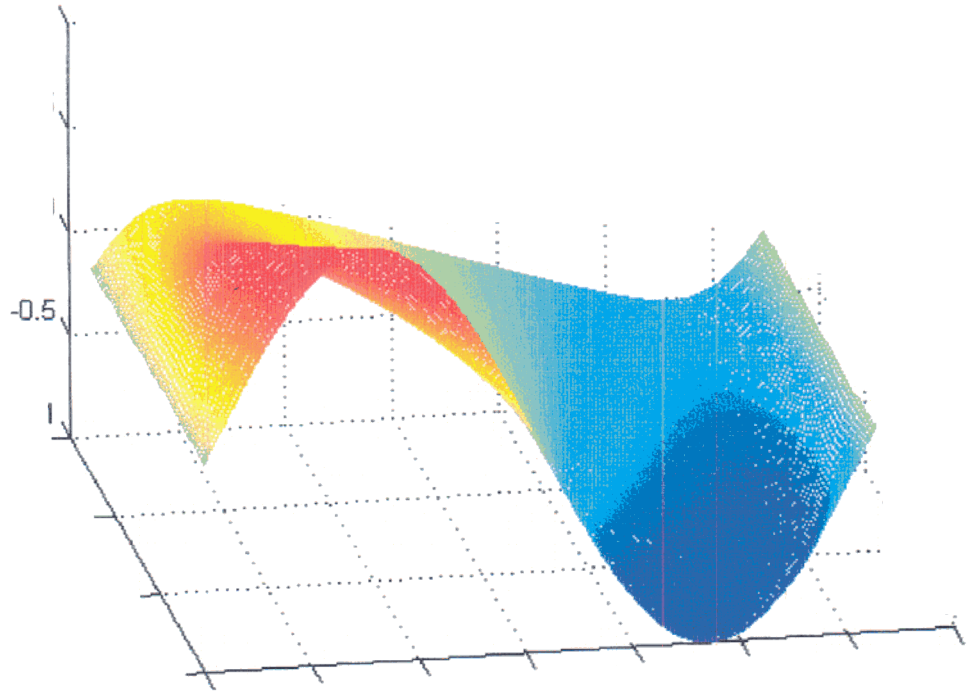


Figure 4.3 D_0

Below, in Figures 4.4, 4.5 and 4.6, the magnitude of the first 5 harmonics (fundamental and next four harmonics, denoted f1-f5) of the propagated waveforms depicted in Figures 4.1, 4.2 and 4.3, have been plotted as a function of non-dimensional distance X, together with the Fubini and Fay solutions respectively for small and large values of X.

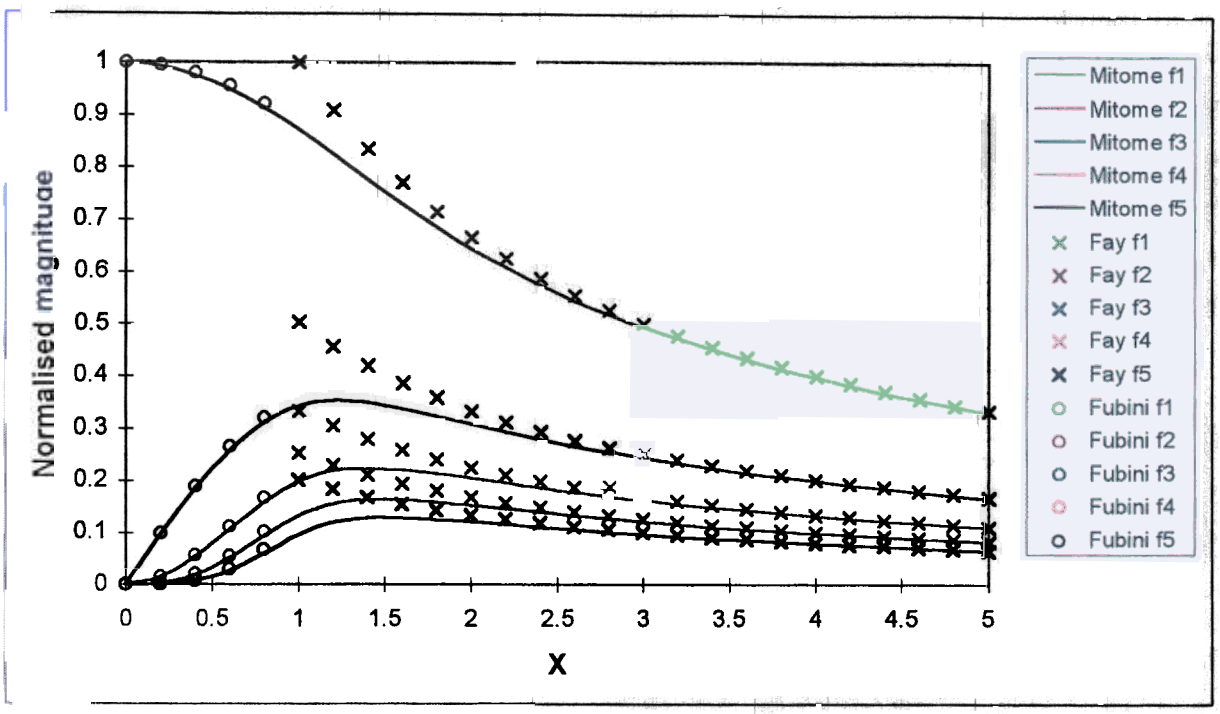


Figure 4.4: D_0=0.03

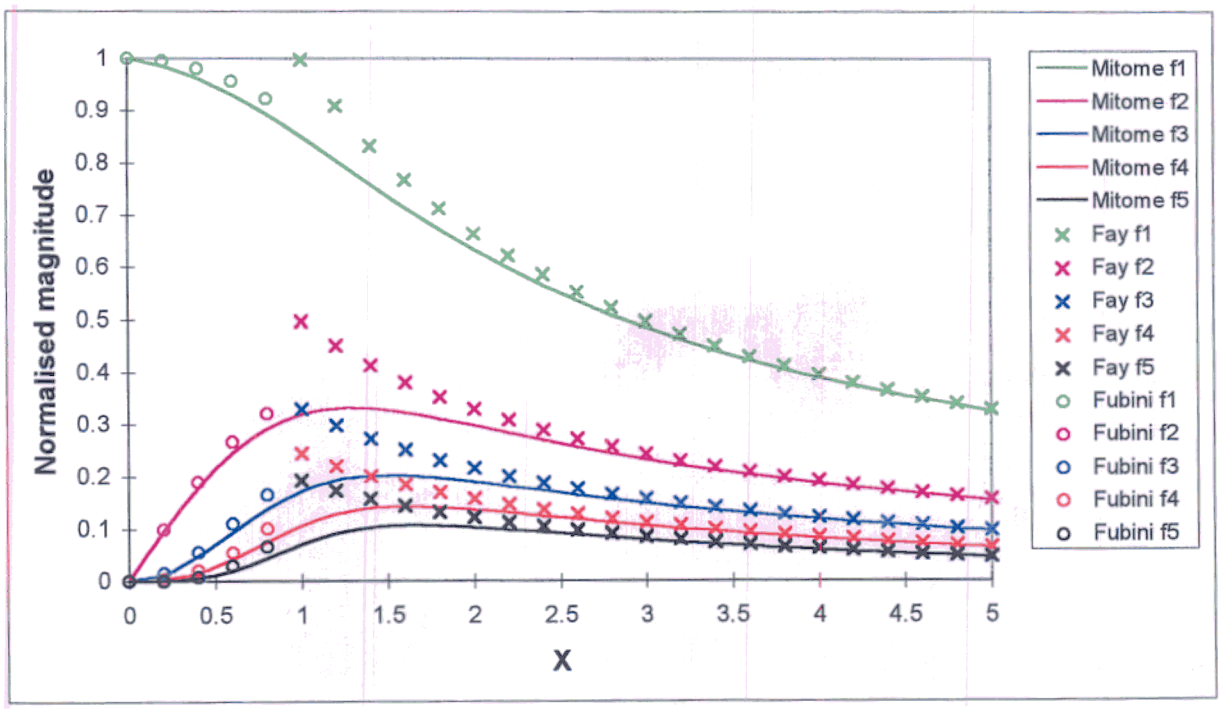


Figure 4.5: $D_0 = 0.1$

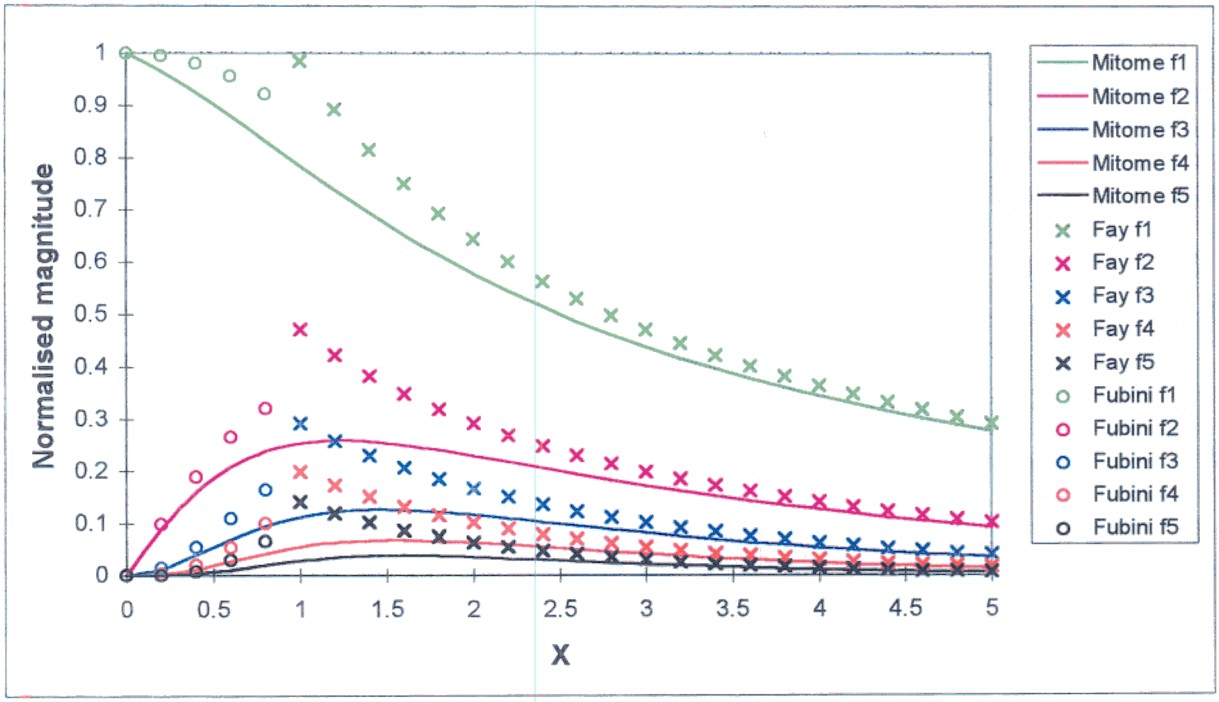


Figure 4.6: $D_0 = 0.3$

4.4.2 Comparison with results given by the routine used in Mitome (1989)

The routine providing the propagated normalised pressure waveform in Bacon (1986) has been translated from Pascal to MATLAB and results have been compared in order to further validate the codes.

In Section 4.4.1, the code was validated for waveforms defined for all values of T. Here, the case where the initial waveform is a sampled pulse is considered. Plots of the changes in waveform during propagation have been obtained for the following cases: $P(T,0)$ is a pulsed negative sine wave between 0 and 2π and $P(T,0)$ is a Hanning-windowed pulsed sine wave between 0 and 2π. D_0 has been taken as 0.3 (i.e. Γ=20/3) and $X \in [0,5]$ (i.e. $\sigma \in [0,5]$). See Figure 4.7 and 4.8.

Note that there are some slight discrepancies between the results produced by the two codes. This is possibly due to the fact that, in the code used in Bacon (1986), no quadrature routine as such has been implemented. The infinite integral in Equations (1) and (11) had been approximated by means of a summation.

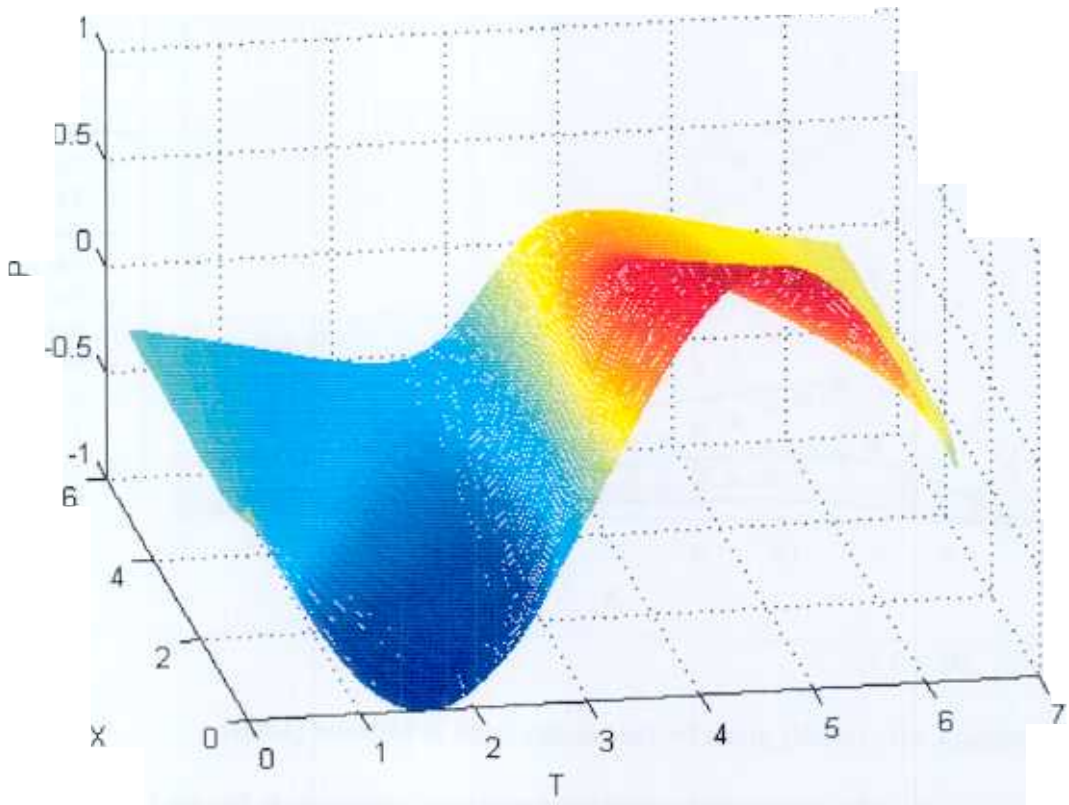


Figure 4.7a: Negative pulsed sine wave propagated using original MATLAB code

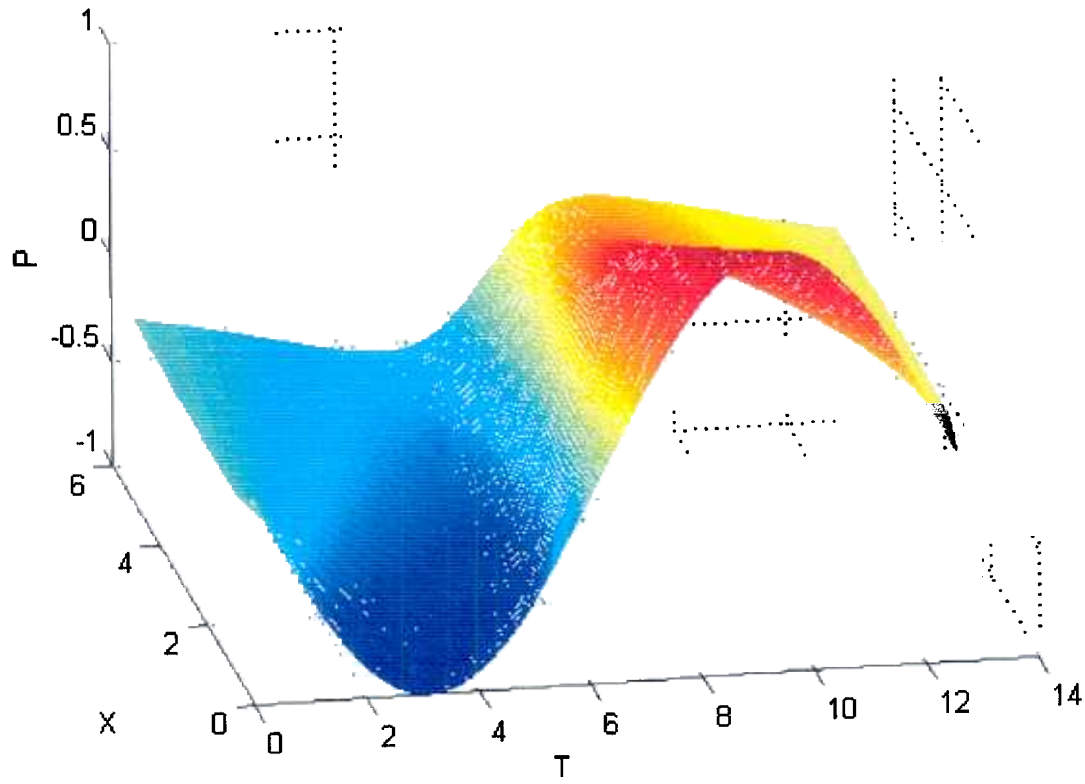


Figure 4.7b: Negative pulsed sine wave propagated using PASCAL code from Bacon (1986) translated into MATLAB

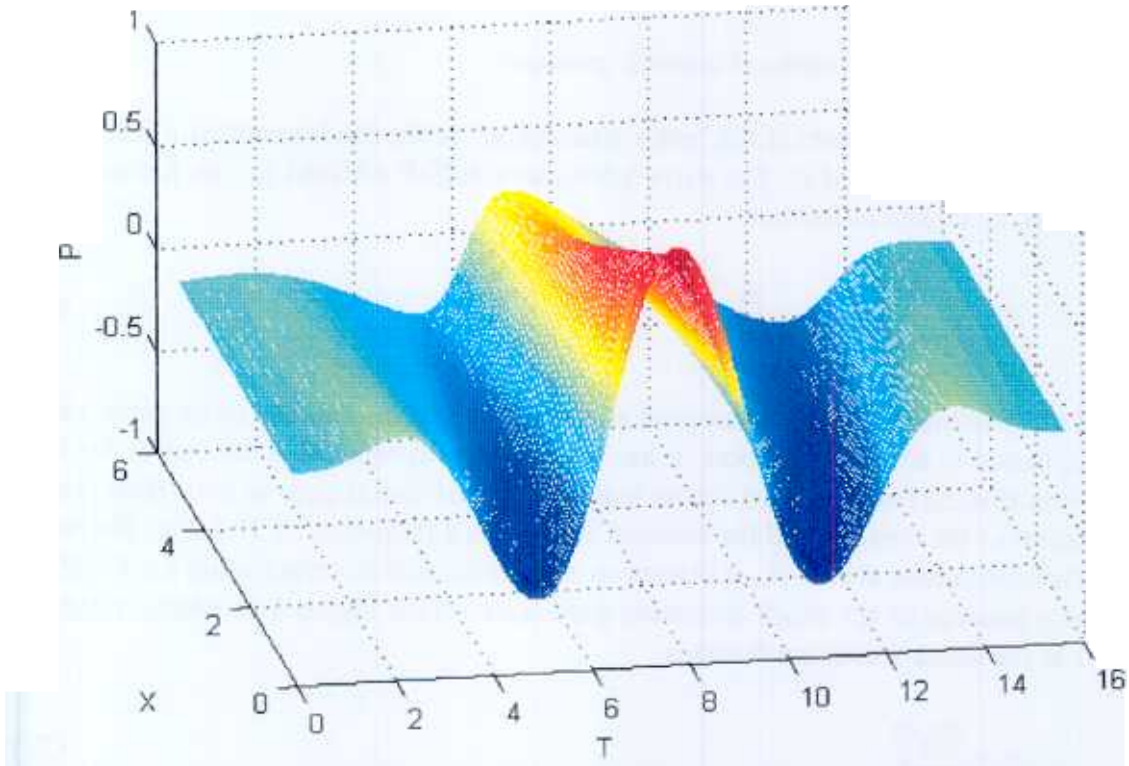


Figure 4.8a: Hanning-windowed sine wave propagated using original MATLAB code

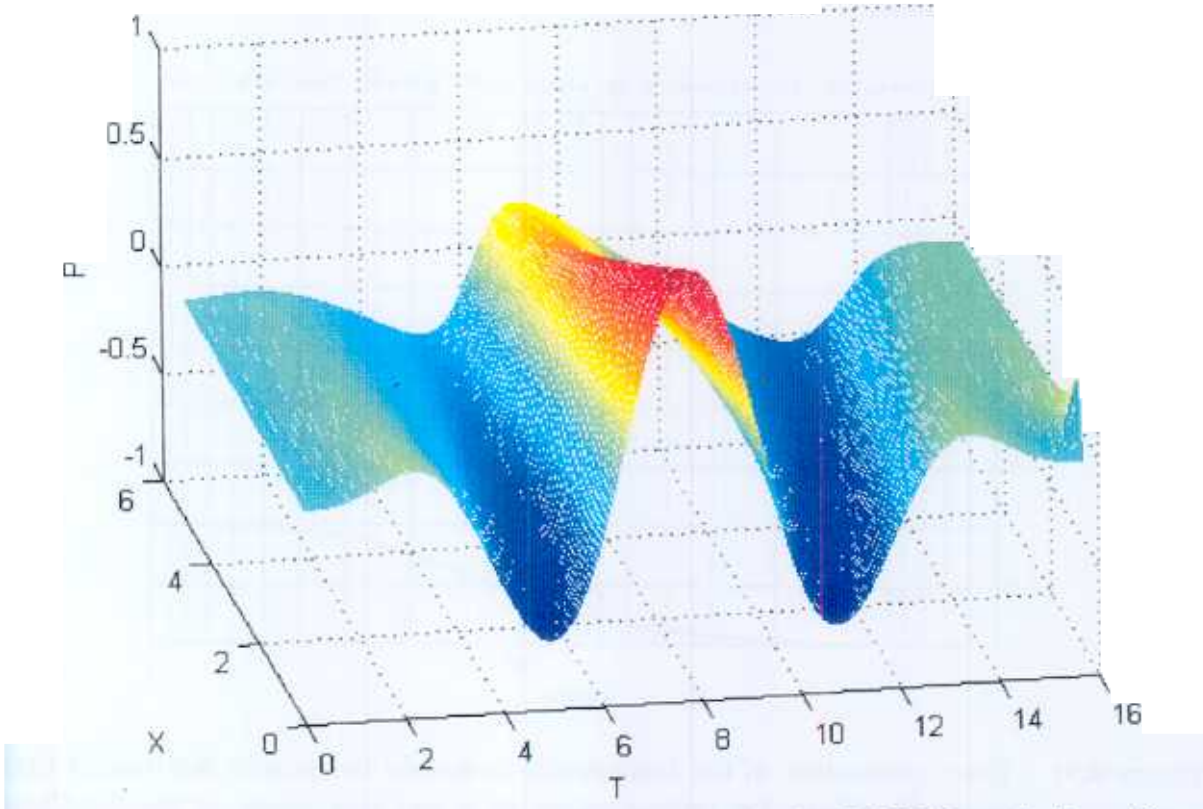


Figure 4.8b: Hanning-windowed sine wave propagated using PASCAL code from Bacon 1986) translated into MATLAB

Results have also been obtained for other values of X and D_0. Similarly, good agreement has been seen.

4.4.3 Validation of solution in terms of acoustic pressure

Blackstock (1964) provides plots of the "extra attenuation" of the fundamental as a function of distance for different values of Γ. The extra attenuation *EXDB* suffered by the fundamental, expressed in dB, is defined as follows:

$$EXDB = -20\log_{10}\left(\frac{B_1}{e^{-\alpha x}}\right)$$

where B_1 is the magnitude of the fundamental at a distance of x, normalised to its initial value. *EXDB* is expressed in dB. In this report, it has been chosen to reproduce the curves for Γ=2 and Γ=5. Note that *EXDB* is defined for an initial sinusoidal disturbance at x=0. Here, water has been chosen as the medium and the sinusoid at x=0 has a frequency of 10 MHz. The value of the pressure magnitude at x=0, p_o, is chosen so as to produce the correct value for Γ. *EXDB* is plotted as a function of the shock formation parameter σ (see Figure 4.9) which is defined so that σ=1 at the shock formation distance.

$$\sigma = \frac{\beta p_0 kx}{\rho_0 c_0^2} \tag{22}$$

Note that if $x = x_c = \frac{\rho_0 c_0^3}{\beta\omega p_0}$, the shock formation distance, $\sigma = 1$

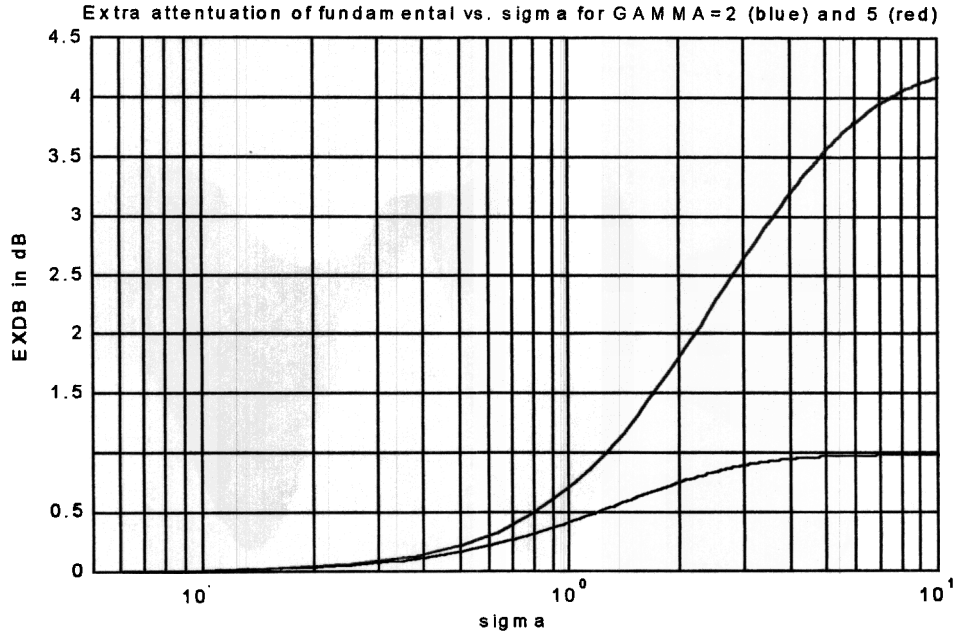


Figure 4.9: Extra attenuation of the fundamental frequency component that results from nonlinear effects, for various values of σ and two values of the Gold'berg parameter, Γ (2: blue curve and 5:red curve).

The sensitivity of the fundamental loss to values of σ and Γ can be seen in Figure 4.9. It is clearly of interest to evaluate typical values of these parameters for the experimental configuration used for 'magnomic' measurements presented within this report. An upper estimate for the peak-pressure generated at the face of the 10 MHz transducer is 0.64 MPa, which, for the propagation distance of 70 mm, corresponds to a σ value of 3 at the measurement site. For these parameters, Γ has a value of 17.

4.5 NONLINEAR PROPAGATION OF A MEASURED PULSE

The 'magnomic' method has been concerned with measurements of attenuated acoustic pressure waveforms at a propagation distance of 110 mm from the face of the transducer (see Appendix A). Beyond this distance, there is interference between the plane-wave and edge-wave from the transducer, and the method is no longer valid (for pulse lengths of about 270 ns and a transducer of diameter 19 mm). If the fundamental component has a frequency of 10 MHz and it is required that 110 mm be at least twice the shock formation distance (corresponding to $\sigma \geq 2$), the maximum initial value of the pressure must be at least 0.27 MPa (Appendix A).

To get an idea of what kind of waveforms can be expected, a measured pulse has been propagated using equation (20) and results for initial maximum pressures ranging between 0.27 and 0.36 MPa (obtained by scaling the pulse appropriately) have been obtained for x=0.11 m in water. The different degrees of distortion are shown in Figure 4.10. Note that some low-pass filtering has been used on the measured waveform so as to reduce noise levels.

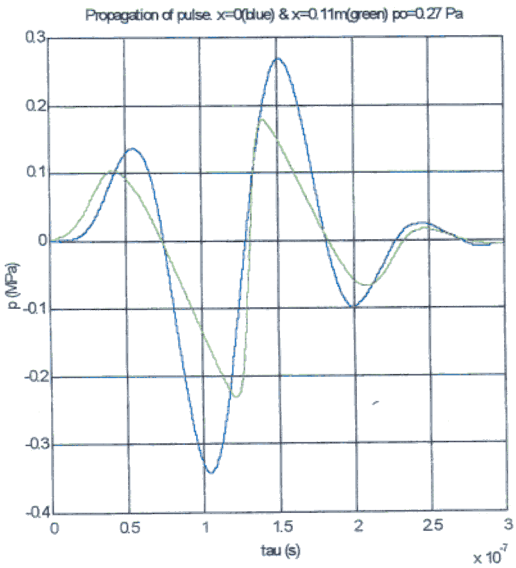


Figure 4.10a

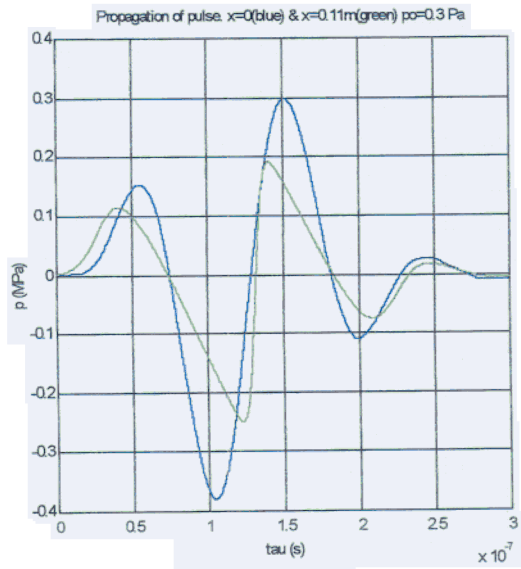


Figure 4.10b

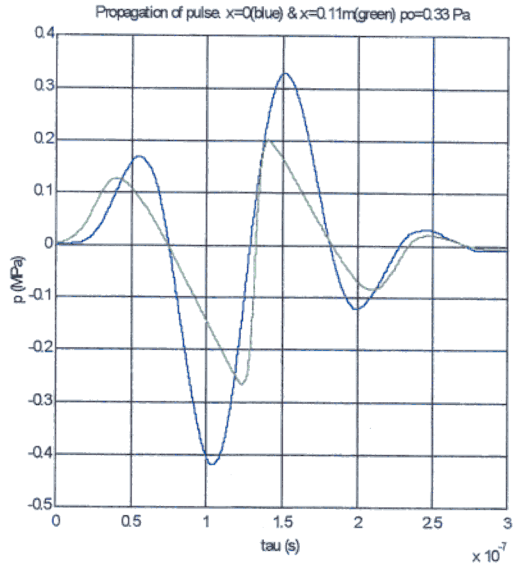


Figure 4.10c

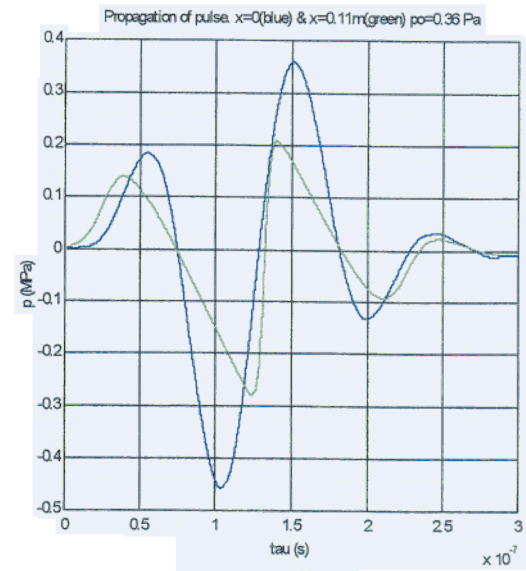


Figure 4.10d

Figures 4.10: Initial and distorted pulse at propagation distance of 0.11 m of fundamental frequency 10 MHz for various values of the maximum initial pressure: 0.27 MPa [a]; 0.30 MPa [b]; 0.33 MPa [c] and 0.36 MPa [d].

4.6 SENSITIVITY OF THE MAGNITUDE OF THE FIRST 6 HARMONICS TO THE UNCERTAINTY IN THE MAXIMUM PRESSURE AT THE SOURCE

Using the known sensitivity of the hydrophone at 10 MHz, it may be possible to propagate the waveform measured at the face (5 mm) forward to the measurement position (70 mm) in order to predict the harmonic components. In practice, there will always be an uncertainty in determining the value of the pressure at the face of the hydrophone due to the uncertainty in hydrophone calibration. This will lead to an uncertainty in the initial magnitude of the harmonics and hence an uncertainty as to how these will vary with distance (since the propagation in the medium is nonlinear, the initial magnitude of the pulse will affect the way in which the harmonics vary with distance).

The following analysis provides some insight into how the values of the magnitudes of the first 6 harmonics are affected when there is a ±3% uncertainty in the initial maximum value of the pressure: this is a typical uncertainty value for a hydrophone calibrated at 10 MHz on the NPL primary standard laser interferometer. All harmonic magnitudes are normalised to the initial magnitude of the fundamental and have been evaluated at a distance of x=110 mm. The initial pulse is the same as that used in Section 4.5.

	Fundamental	2nd harmonic	3rd harmonic	4th harmonic	5th harmonic	6th harmonic
p_0=0.27MPa-3%	0.5958	0.1311	0.0627	0.0311	0.0165	0.0094
p_0=0.27MPa	0.5888	0.1300	0.0635	0.0319	0.0171	0.0099
p_0=0.27MPa 3%	0.5818	0.1289	0.0641	0.0325	0.0176	0.0103
p_0=0.30MPa-3%	0.5708	0.1268	0.0649	0.0333	0.0183	0.0109
p_0=0.30MPa	0.5633	0.1253	0.0652	0.0337	0.0188	0.0112
p_0=0.30MPa+3%	0.5558	0.1237	0.0655	0.0340	0.0191	0.0115
p_0=0.33MPa-3%	0.5468	0.1217	0.0657	0.0343	0.0195	0.0119
p_0=0.33MPa	0.5388	0.1199	0.0657	0.0345	0.0198	0.0121
p_0=0.33MPa+3%	0.5310	0.1182	0.0657	0.0345	0.0200	0.0124
p_0=0.36MPa-3%	0.5237	0.1165	0.0656	0.0345	0.0202	0.0125
p_0=0.36MPa	0.5155	0.1147	0.0653	0.0344	0.0203	0.0127
p_0=0.36MPa+3%	0.5074	0.1129	0.0650	0.0343	0.0205	0.0128
p_0=0.39MPa-3%	0.5018	0.1117	0.0648	0.0341	0.0205	0.0129
p_0=0.39MPa	0.4933	0.1100	0.0643	0.0339	0.0206	0.0129
p_0=0.39MPa+3%	0.4850	0.1085	0.0637	0.0336	0.0206	0.0130

Table 4.1: Uncertainty in predictions of the relative magnitudes of the first 6 harmonics arising from hydrophone calibration uncertainty

From Table 4.1, it is of interest to note that the higher frequency components are relatively insensitive to uncertainties in the calibration of the hydrophone, particularly at the high drive levels. For the highest drive case, the variation in the levels of the higher harmonics is generally less than ±1%. The variation in the level of the fundamental is typically greater, being ±1.2% for the lowest drive case (a) and increasing to ±1.7% for the highest drive.

4.7 SUMMARY

A solution to Burgers' equation describing the propagation of a one-dimensional wave in a non-compressible viscous, dissipative fluid has been implemented and validated. Results have been checked by means of comparison with the work produced in Mitome (1989) as well as through a PASCAL routine obtained from Bacon (1986) which has been translated into MATLAB. The code has also been modified so that it is also possible to work directly with acoustic pressure, rather than normalised pressure. Results using this code have been compared with those given in Blackstock (1964). In all cases, good agreement has been obtained.

5 MEASUREMENT SYSTEMS AND DEVICES

This Section describes the experimental facilities, devices, and procedures used to characterise the transducer and provide the source waveforms for use with the Mitome code described in Section 4.

5.1 SCANNING TANK

The transducer measurements and waveform acquisitions were performed using the NPL Beam Plotting Facility. This consists of a 0.7 x 0.4 x 0.5 m water tank, over which is positioned a scanning rig. The rig has two independent carriages and mounts, each with longitudinal, vertical, transverse, angular and tilt adjusters, making ten degrees of freedom in total. One mount houses the transducer, and the other the hydrophone. The linear resolution of the system is 2.5 μm, with the angular resolution 0.0036°. The scanning system is controlled by a HP 9000 Series 200 computer.

The hydrophones and preamplifier used are described in detail in Sections 5.4 and 5.5. The preamplifier signal was connected to a Tektronix 2430A digital oscilloscope, where appropriate averages were taken of the acquired signals. The data was then passed to the HP computer for storage and analysis. A software routine was employed to convert the acquired waveform data to ASCII text, for analysis in MATLAB. Additionally, for some of the measurements of the loss in the fundamental frequency component, the hydrophone/amplifier output was connected to a LeCroy 9450A oscilloscope, and the FFT magnitudes monitored directly from the display.

5.2 THE 'MAGNOMIC' TRANSDUCER

The transducer used to generate the plane-wave nonlinear acoustic field was identical to the one used in the original 'magnomic' calibration study reported in Appendix A. Made by Panametrics, the 10 MHz transducer was of diameter 19.1 mm (0.75"). The transducer type number was V315, its serial number 88868. The drive system used to drive the transducer is described in Section 5.3.

5.3 TRANSDUCER DRIVE SYSTEM

The drive and acquisition system used is illustrated schematically in Figure 5.1. The HP 8165A synthesiser generator was triggered by the Lyons box to produce a single cycle sine-wave pulse at 10 MHz. The output of the HP generator was fed to an ENI A300-L power amplifier, which provided a nominal gain of 55 dB over a frequency range of 0.3 to 35 MHz. The output from the amplifier was passed through an in-line fuse before connection to the transducer. To ensure low power dissipation in the transducer and hence minimise crystal heating, the drive system was restricted to a pulse repetition rate of 50 Hz. The output from the Lyons box was also used to trigger the oscilloscope, with the separation distance between the transducer and hydrophone then derived from the product of the time-delay between the electrical drive signal and the received acoustic pulse, and the sound propagation velocity of the water in the test tank.

It should be noted that results presented within this report were generated using two different ENI A300L power amplifiers. The first of these generated an acoustic waveform which

exhibited two major cycles within the pulse which were of similar magnitude. Unfortunately, this amplifier eventually showed signs of instability at high drive levels and could not be used for any 'magnomic' calibrations. However, it provided useful information on certain aspects of the technique. A second power amplifier was used for the 'magnomic' calibrations, and this was characterised by a shorter acoustic pulse, which had a single major cycle.

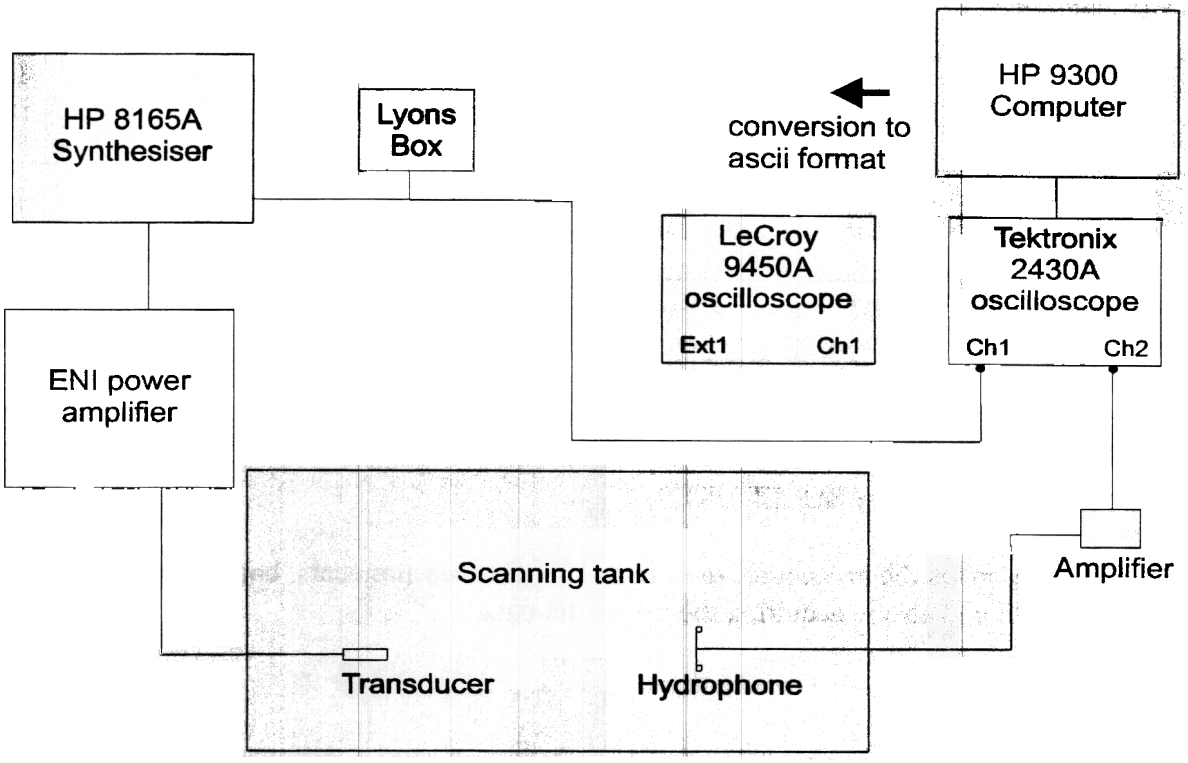


Figure 5.1: Schematic diagram of the transducer drive and waveform acquisition system used in this study

5.4 WIDE BANDWIDTH AMPLIFIER

The studies were completed using Input B of the wide-bandwidth amplifier 55391001. The gain of the amplifier over the frequency range of interest is tabulated in Appendix C. It should be noted that calibration figures presented for the hydrophones in Section 7 are all end-of-cable loaded, in keeping with the configuration used for the original interferometer measurements.

5.5 REFERENCE HYDROPHONES USED DURING MILESTONE

A range of devices were used during the characterisation measurements, and to generate the waveforms for analysis. These are shown in Table 5.1. The first four hydrophones were used to provide actual waveform data for use with the Mitome code (Section 4), with the 75 mm device used predominantly to make measurements of the decrease in the fundamental frequency amplitude as a function of position and drive setting.

Device type	Serial number	Film thickness (μm)	Active element diameter (mm)	E-of-C loaded sensitivity at 10 MHz (nV Pa^{-1})
GEC-Marconi 3598 bilaminar	IP016	2 x 25	0.5	59.1
GEC-Marconi 6526 unshielded bilaminar	IP010	2 x 9	0.2	21.7
GEC-Marconi 7603 shielded coplanar	IP901	9	0.5	27.6
GEC-Marconi 7603 shielded coplanar	IP904	9	0.5	34.4
GEC-Marconi 7609 bilaminar	IP002	2 x 25	75	Unknown

Table 5.1: Hydrophones used during field characterisation and signal acquisition

5.6 MEASUREMENT PROCEDURES

This Section describes the procedures used in making the measurements, both in characterising the acoustic field and also in acquiring the waveform data.

5.6.1 Alignment

A well-defined protocol was established for the purposes of system alignment, which is crucial in the context of high frequency waveform acquisition, and also in cross-axial beam plotting. The procedures were designed to ensure that the mechanical axis of translation of the beam-plotting tank scanning rig was coincident with the acoustic axis of the transducer.

First, the HP 8165A was set up with an output amplitude of 350 mV, which for all hydrophones provided a good signal-to-noise ratio. Alignment of the acquisition system when using the four main 'magnomic' hydrophones required carrying out an iterative procedure involving two measurement planes. The first of these planes was at a near-field position where the edge-wave and plane-wave components in the acoustic signal were clearly separable in time: delay times of typically 42 - 47 μs were used (corresponding to positions of 62 - 70 mm). The delayed time-base on the Tektronix oscilloscope was set up as required, according to the sound velocity and separation (X direction). In this first measurement plane, the observed edge-wave on the oscilloscope display was maximised by using the cross-axial adjusters on the hydrophone mount, in both Y and Z directions. Due to its coherent arrival for on-axis positions of the hydrophone, the edge-wave component was extremely sensitive to alignment - moves of ± 0.1 mm changed the peak signal level by as much as 30%.

The separation distance was then adjusted to that corresponding to a delay of around 220 μs (approximately 325 mm), and in this second measurement plane, the positive voltage on the oscilloscope was again maximised, this time by using the angular and tilt adjusters on the transducer mount. The transducer or hydrophone was then returned to its original separation (first measurement plane) where the signal maximisation procedure as described above was

repeated. Through repeated maximising processes at these two measurement planes, the system was deemed to be aligned when the peak-positive voltage in each of the planes read from the oscilloscope display was within 3% of the maximum in that plane. Finally, at the near plane, the tilt and rotation adjustment on the hydrophone was used to maximise the displayed signal. Data acquisition then commenced. This alignment procedure was carried out each time the hydrophone was changed, and at frequent points during the measurement runs.

For the 75 mm hydrophone (IP002), the large active element rendered the 'near and far' alignment procedure redundant. The sharp directional response of the device meant that adjustment of the tilt and rotation of the hydrophone only was performed in a single plane (42 to 47 μs) to maximise the displayed signal.

5.6.2 Waveform acquisition

After the system had been aligned as described in Section 5.6.1, the drive amplitude of the HP 8165A was decreased to 50 mV, and the temperature of the water measured. From this, the speed of sound in water was used to calculate the delay time corresponding to a hydrophone-transducer separation of 70 mm. Whilst observing the Tektronix 2430A display, the hydrophone was then moved to this position, with the acoustic pulse positioned such that the trigger 'T' was just before the first negative cycle. The timebase was set to 50 ns div^{-1}. Using the control software, the acoustic pulse was digitised, using typically 32 averages, and the waveform stored on the HP computer.

The delay time to 5 mm was then calculated, and the hydrophone moved as required, with the pulse and trigger position set up as described above. Again, the averaged waveform was digitised and stored.

Next, the HP 8165A amplitude was increased to 700 mV (the chosen 'high-drive setting'), and the hydrophone returned to its previous location, 70 mm. The cross-axial alignment was checked using the Y and Z adjusters, and the trigger positioned as required. The waveform was digitised and stored, and finally, the hydrophone was moved to 5 mm, positioned as required, and the acoustic waveform acquired, to complete the set of four waveforms required for one 'run'.

In later acquisition measurements, the magnitude of the fundamental frequency component was also measured, using the LeCroy 9450A oscilloscope at each position, for the two drive levels. The LeCroy was also used to produce the fundamental magnitudes as a function of position for the 75 mm hydrophone.

In all cases, the waveforms digitised by the Tektronix 2430A and stored on the HP computer were converted to an ASCII format by a suitable subroutine, and then analysed in MATLAB - this process is described in Section 7 to yield calibration values.

6 RESULTS - ANCILLARY STUDIES

In addition to the main calibration measurements performed during the project, a number of supporting studies investigating specific aspects of the 'magnomic' calibration method were carried out. These will now be described in detail.

6.1 PLANE-WAVE BEHAVIOUR OF THE TRANSDUCER - BEAM-PLOTTING OF THE TRANSDUCER FIELD

This Section describes a series of field characterisation measurements carried out on the 10 MHz transducer, to investigate the spatial distribution of ultrasound in the acoustic field and to assess how closely it approached the plane-wave required for the propagation algorithm.

The NPL Beam Plotting Facility was used to make the measurements, data being acquired using two hydrophone-amplifier combinations, one each of the membrane and needle types:

a) 0.2 mm unshielded bilaminar membrane hydrophone IP010, 2 x 9 μm film, into amplifier 55391001, input B (as used for the waveform acquisitions);

b) 0.075 mm needle probe hydrophone, 9 μm thick PVDF element, connected via a submersible preamplifier and a DC coupler to a power amplifier - this constituted the finest resolution device available.

Both the membrane and the needle hydrophone were used to investigate the spatial distribution over the centre of the beam using a fine resolution beam-plot, typically of step-size 50-100 μm. The membrane hydrophone was also used to make measurements of coarser resolution (0.25 mm steps) over the full width of the beam. For all measurements, the HP 8165A drive unit was set to 50 mV, ensuring that acoustic propagation would be in the linear regime. Additionally, to improve the signal-to-noise ratio, the bandwidth limit of the 2430A oscilloscope was limited to 20 MHz.

6.1.1 Measurement protocol

After the system had been aligned as described in Section 5.6.1, the hydrophone was located at the required position along the acoustic axis by measuring the water temperature and calculating the relevant delay-time according to the desired position. The diametrical beam scans were then performed. In all cases, scans were started on the acoustic axis, and were completed as 'half-scans', where the hydrophone was moved across the acoustic axis to a pre-determined limit (normally 10% of the maximum peak-positive acoustic pressure measured in the scan), back to the axis to check on the starting value, and then scanned across the beam on the other side of the axis. Specifically, the scans were carried out close to the transducer, in the region where the edge-wave component could adequately be gated out in time. The scans presented at each distance are only those derived in the 'horizontal' direction as good cylindrical symmetry was seen in the pressure distribution.

6.1.2 Results

The mechanical layout of the measurement system restricted the range of distances over which measurements could be performed using the membrane hydrophone to 5 mm and outwards, and so the needle-probe was used to investigate the field structure at 2 mm.

Figure 6.1 shows the scan performed at 2 mm from the output face of the transducer, which demonstrates that the local variation in acoustic pressure is significant, with a pressure minimum on axis whose value is only 50% of the peak in the plane. The maximum peak-positive pressure values measured in this case was of the order of 60 kPa.

Examination of Figure 6.1 and comparison with Figure 6.2 shows that by moving the measurement position out along the axis to 5 mm, the structure changes considerably for the needle hydrophone-measured case, with a larger flat region about the acoustic axis. Comparing this with the membrane hydrophone measurement (Figure 6.3) shows some differences: the local peaks around ±1.2 mm are similar for both cases, but the central region is flatter and better defined in the needle case. This may be due to the greater spatial-averaging of the 0.2 mm hydrophone but is more likely attributable to alignment or the directional response of the needle to non plane-wave components in the field.

Moving out further, to 10 mm (Figure 6.4), to 15 mm (Figure 6.5) and finally to 20 mm (Figure 6.6) shows that the beam begins to flatten out, with the central region less structured, and the normalised pressure values showing a smaller level variation. The actual measured maximum peak-positive pressure was of the order of 60 kPa, as noted previously.

Using the information contained in these plots, it is possible to build up a picture of the way the acoustic field is behaving close to the transducer. It is clear from the significant structure seen that the transducer is not producing a plane-wave. The fine structure observed may produce differences in the waveforms measured at 5 mm using the four 'magnomic' hydrophones, particularly when the respective spatial resolutions available are considered. It is probable that imperfections in the transducer crystal may be responsible for the major components of the structure seen, together with artefacts caused by the attachment of the electrodes, and possible transducer heating.

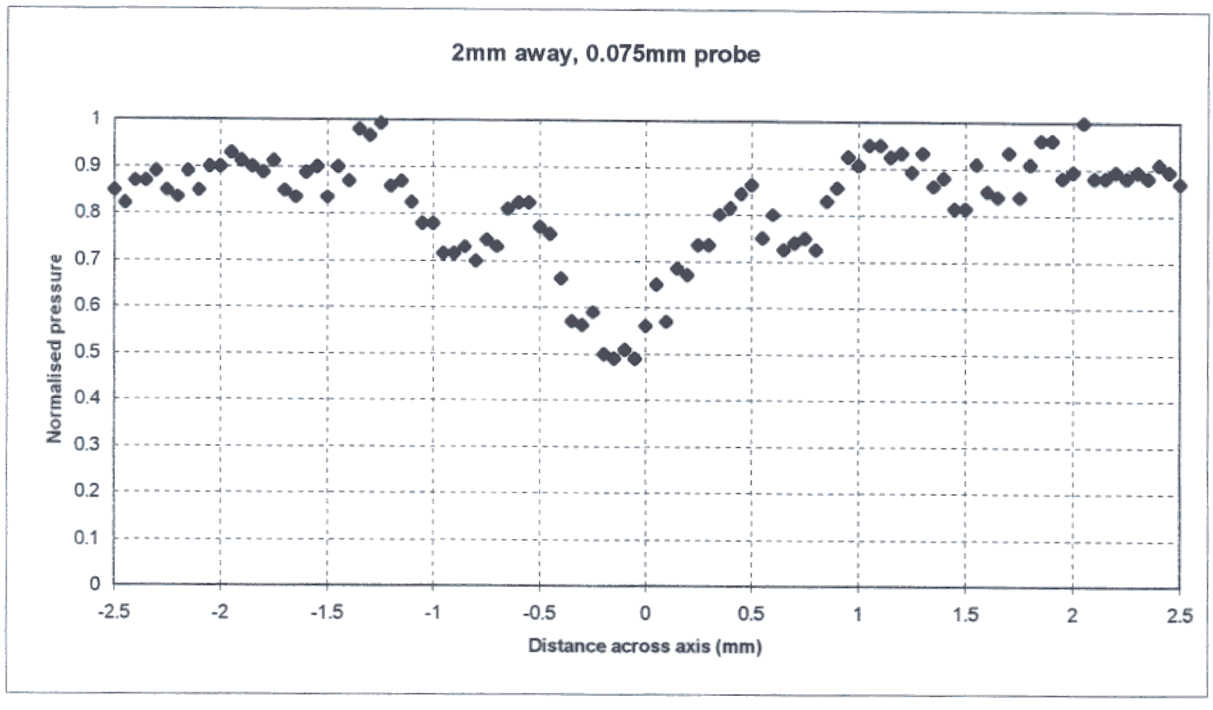


Figure 6.1: 50 μm resolution scan over centre of beam, 2 mm away from the transducer, using the 0.075 mm needle hydrophone

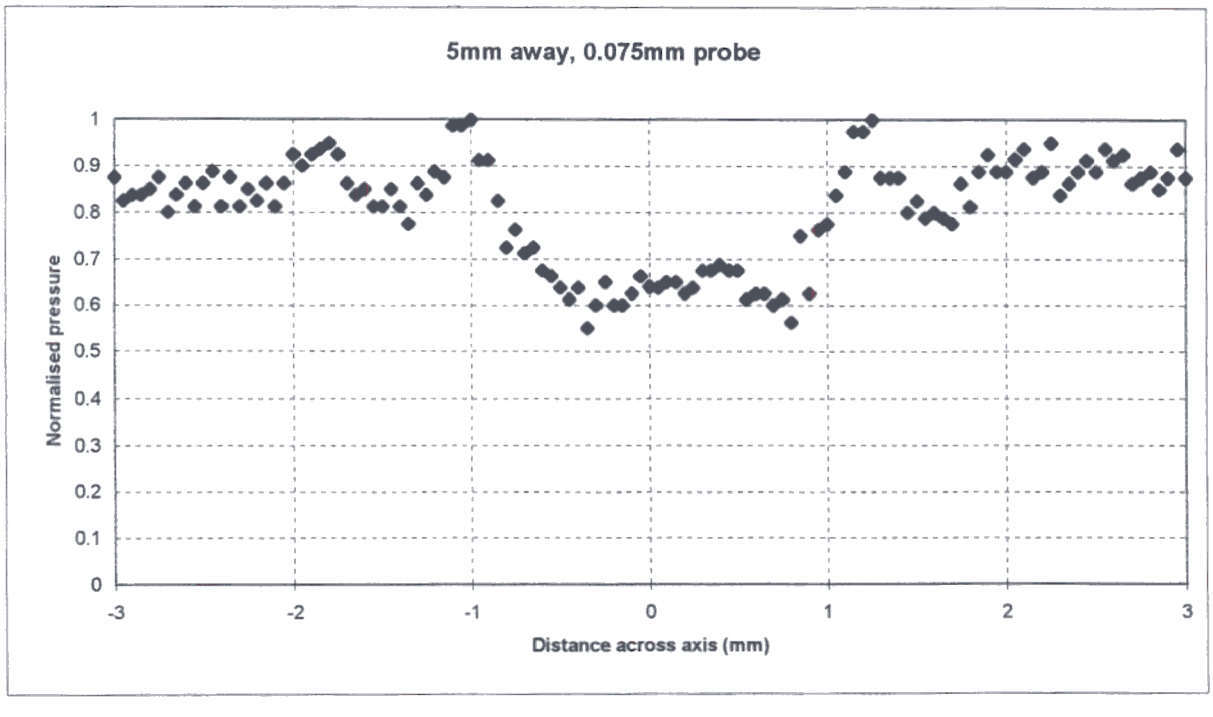


Figure 6.2: 50 μm resolution scan over centre of beam, 5 mm away from the transducer, using the 0.075 mm needle hydrophone

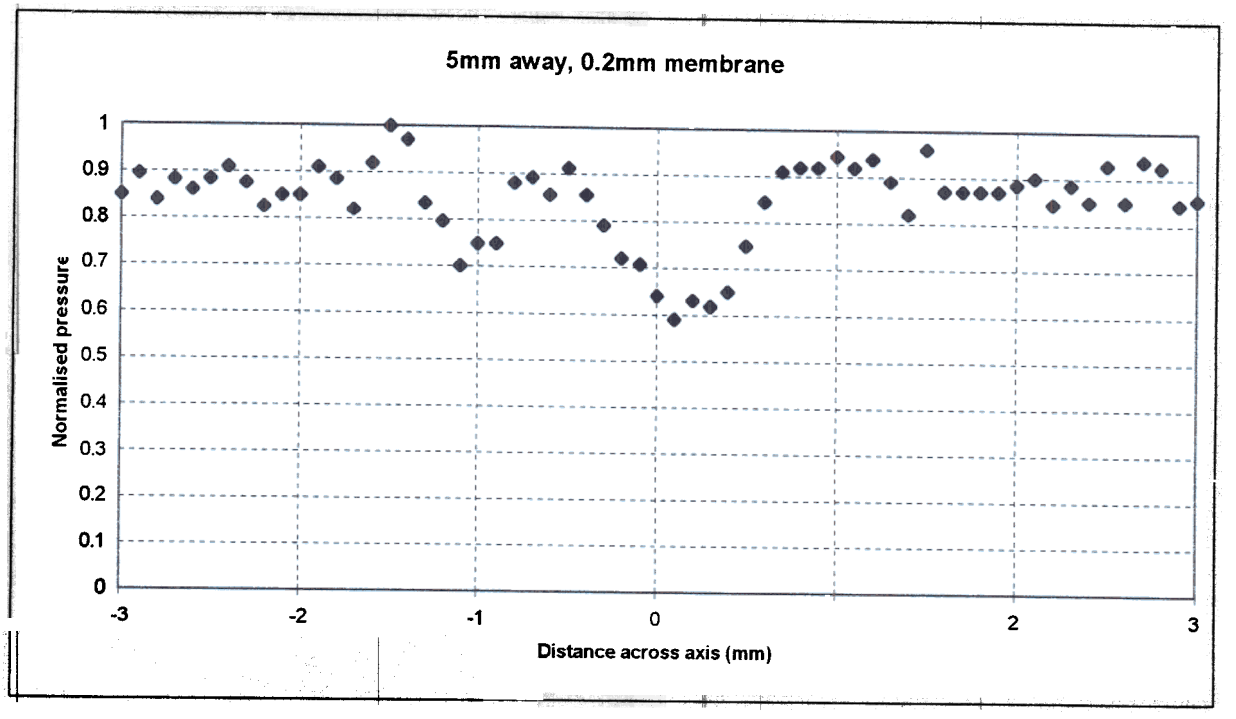


Figure 6.3: 100 μm resolution scan over centre of beam, 5 mm away from the transducer, using the 0.2 mm membrane hydrophone

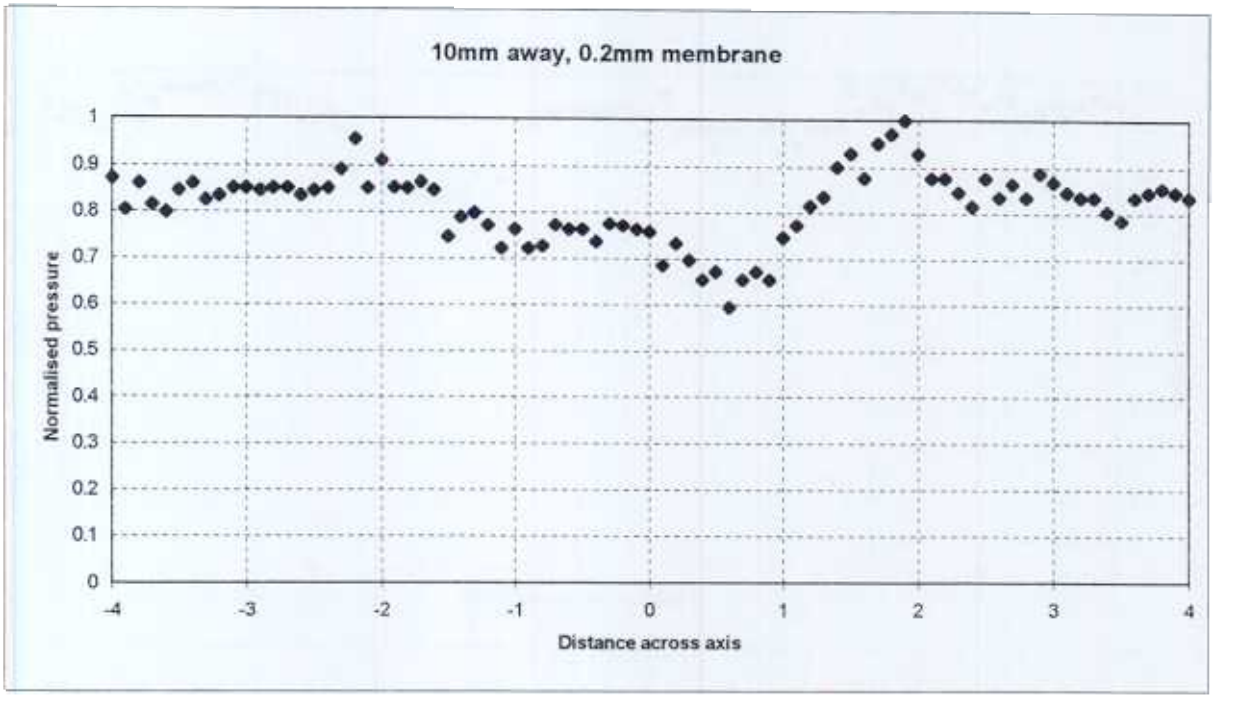


Figure 6.4: 100 μm resolution scan over centre of beam, 10 mm away from the transducer, using the 0.2 mm membrane hydrophone

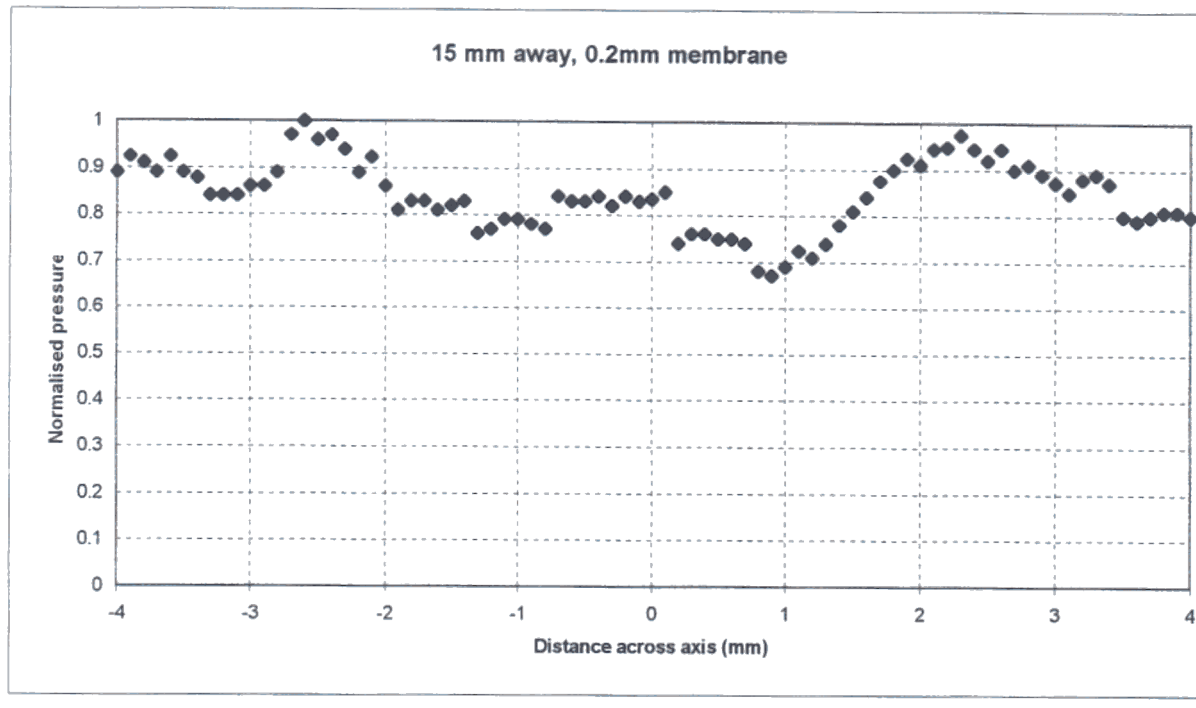


Figure 6.5: 100 μm resolution scan over centre of beam, 15 mm away from the transducer, using the 0.2 mm membrane hydrophone

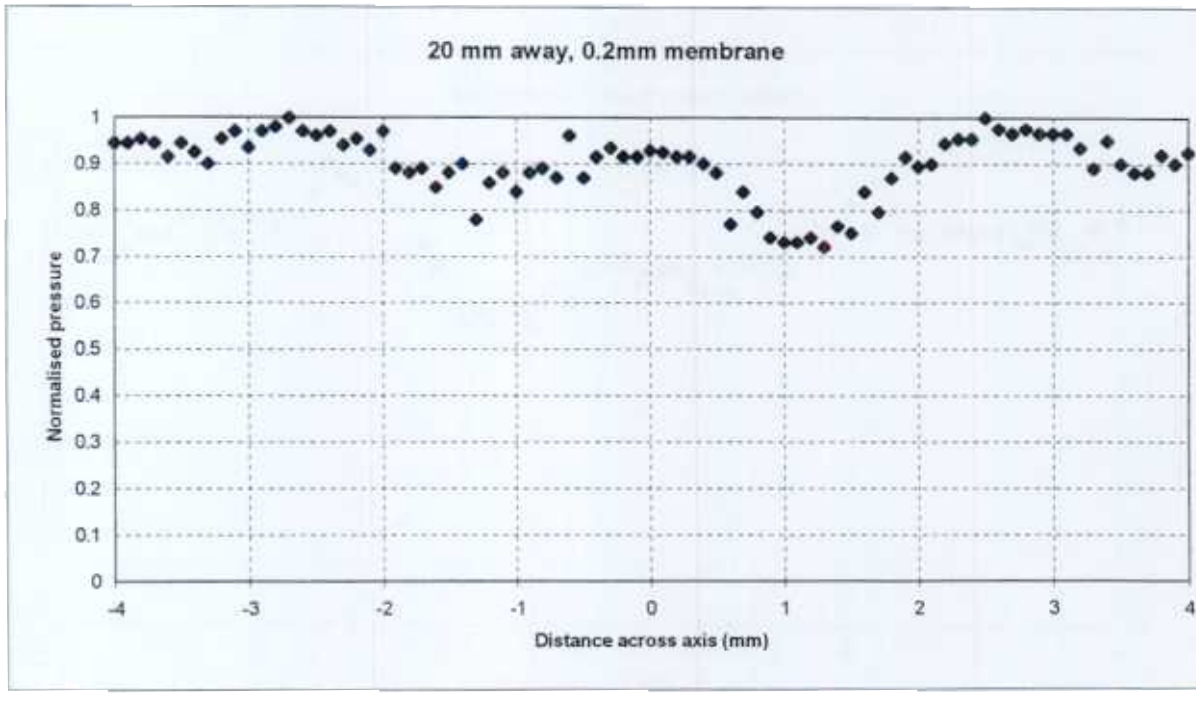


Figure 6.6: 100 μm resolution scan over centre of beam, 20 mm away form the transducer, using the 0.2 mm bilaminar membrane hydrophone

Figures 6.7 and 6.8 show scans performed over the entire transducer width at separations of 10 and 20 mm respectively, showing the edge-wave at the extremes of the scan before the signal levels tail off as the hydrophone passes over the edge of the transducer crystal.

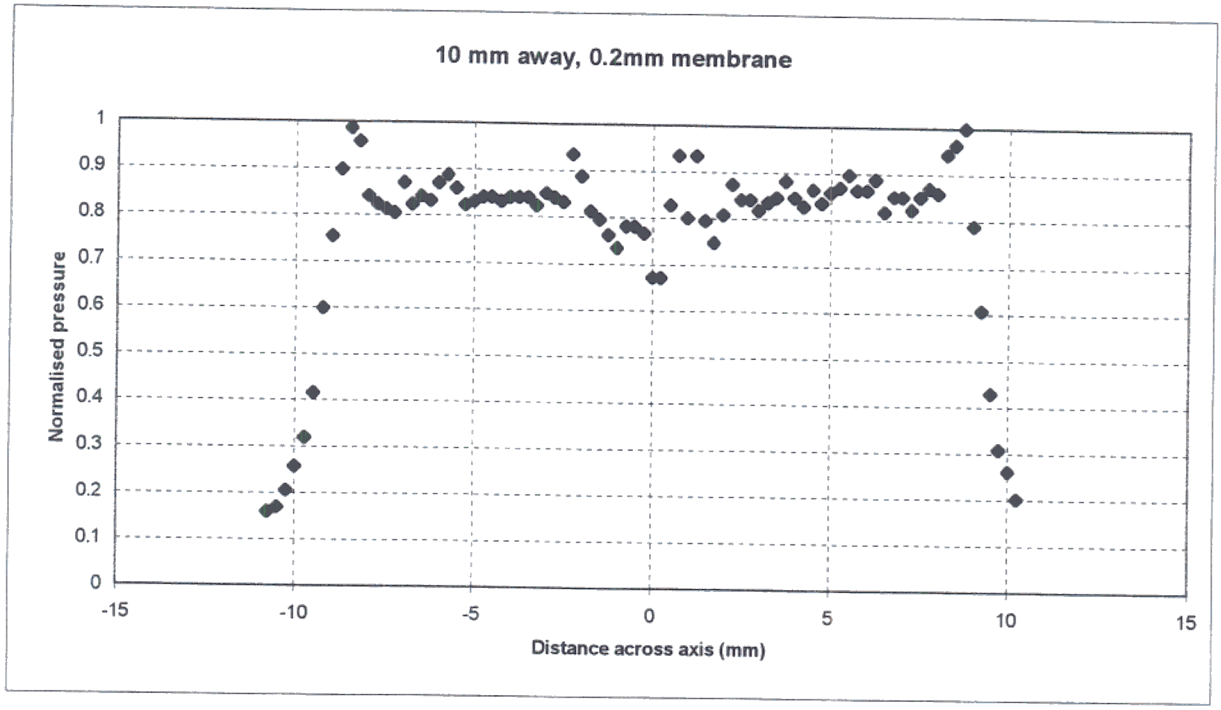


Figure 6.7: 250 μm resolution scan over centre of beam, 10 mm away from the transducer, using the 0.2 mm membrane hydrophone

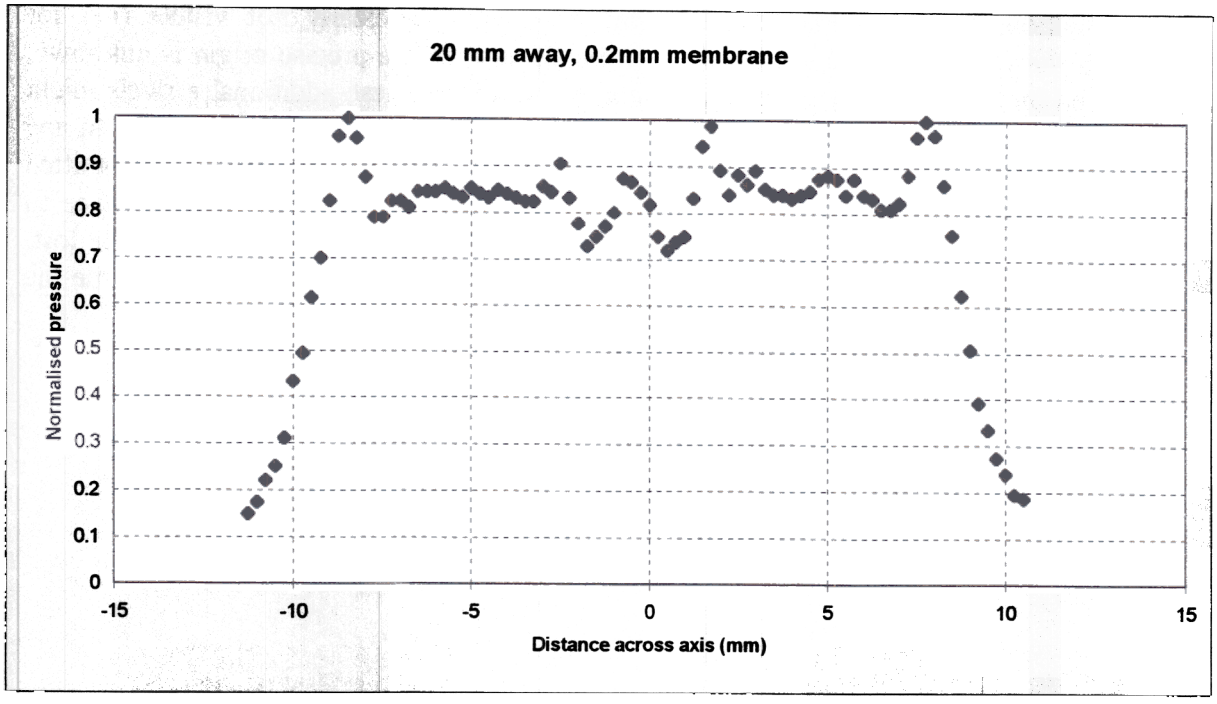


Figure 6.8: 250 μm resolution scan over centre of beam, 20 mm away from the transducer, using the 0.2 mm membrane hydrophone.

6.2 EFFECT OF WINDOWING AND TRUNCATION OF THE ACOUSTIC WAVEFORM

This Section describes the effects of windowing and truncation of the acoustic waveform.

6.2.1 Acquisition of time domain waveforms along the transducer axis

As identified earlier in this report, when a waveform is acquired at a given distance from the transducer along its axis, there will in general be a measurement position at which the edge-wave component will start to appear within the time window. Presented below are a set of graphs which show axial measurements of the acoustic waveform at different distances from the face of the transducer and the corresponding spectra (given in Figures 6.9 a, b and c). The bilaminar membrane hydrophone IP010 was used, along with the 10 MHz transducer driven at one of the intermediate drive levels used, 350 mV. In each of these Figures, x represents the distance between the hydrophone and the transducer.

From these figures, it is clear that beyond 40 mm, the edge-wave component starts to become significant. As the hydrophone is moved further away, the difference in arrival time between the edge and plane-wave components becomes smaller and the two start to overlap. Due to the effect this has on the spectrum, it is necessary to truncate the time-domain waveform to evaluate the magnitude of the fundamental. This is required to determine the high-drive nonlinear loss and therefore plays a pivotal role in the 'magnomic' technique. It can be seen that for distances close to the measurement site (located at 70 mm from the face of the transducer for the current study), this means that some of the acoustic information will be lost. As it is the magnitude of the fundamental that is of principal interest, the truncation position should ideally be selected so that there is minimal effect on the former quantity.

Even at positions where interference with the edge-wave is clearly not visible (i.e. for $x < 40$ mm), there appear to be subsidiary acoustic signals, whose precise origin is unknown, superimposed on the plane-wave after approximately 5 cycles. These additional arrivals might be produced from other parts of the crystal perhaps not vibrating in a piston fashion. In any case they probably are not part of the plane-wave excitation and should therefore be omitted during the truncation process. However, the plane-wave component has not had a chance to fall below the dynamic range of the A/D converter and some signal information will be lost. Hence, the frequency domain representation of the signal will be modified, as will also be the case for the signal acquired at the measurement site.

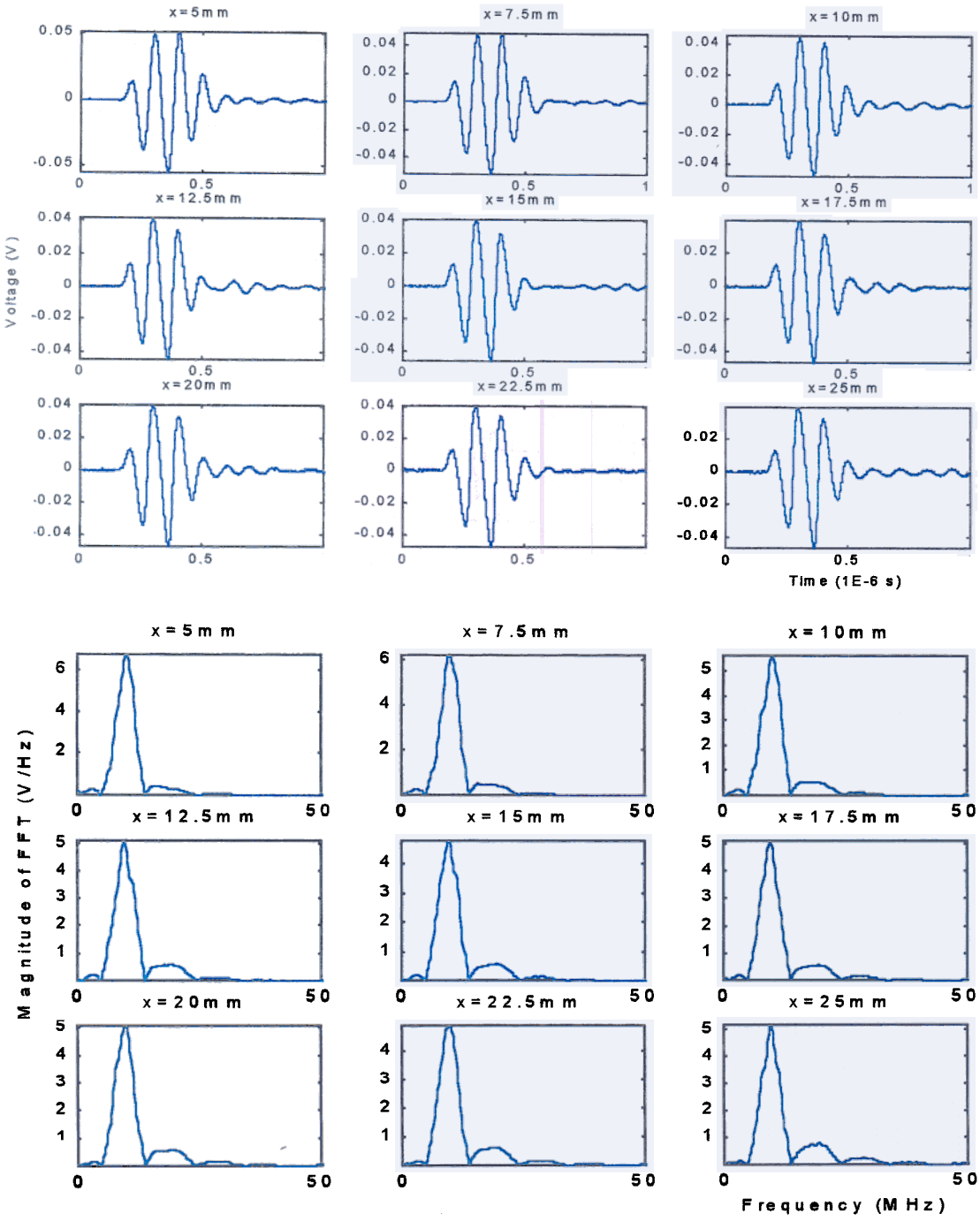


Figure 6.9a: Axial waveform acquisitions at a sampling frequency of 1 GHz and the corresponding spectra derived using a 1024 point FFT (x varies between 5 mm and 25 mm)

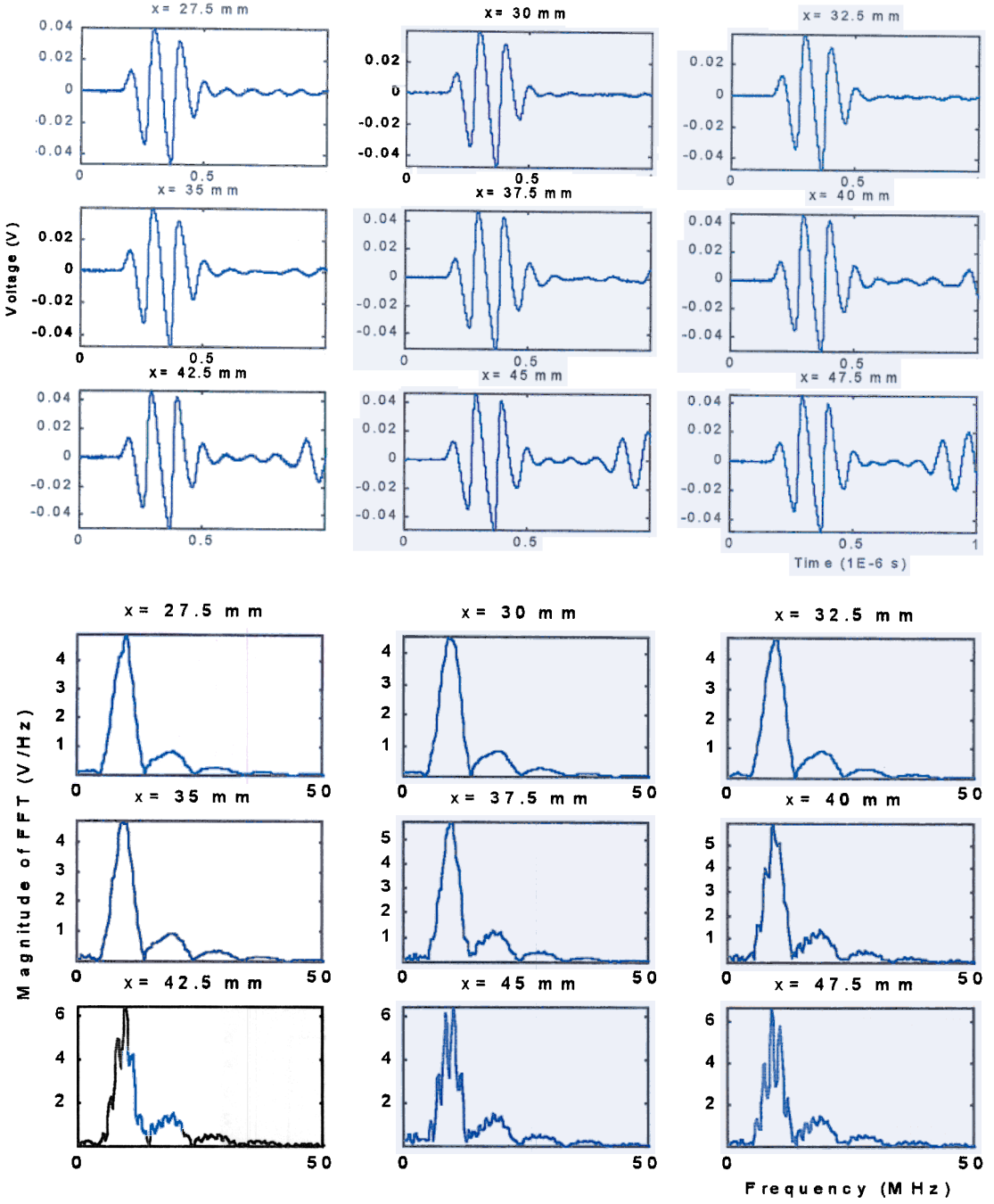


Figure 6.9b: Axial waveform acquisitions at a sampling frequency of 1 GHz and the corresponding spectra derived using a 1024 point FFT (x varies between 27.5 mm and 47.5 mm)

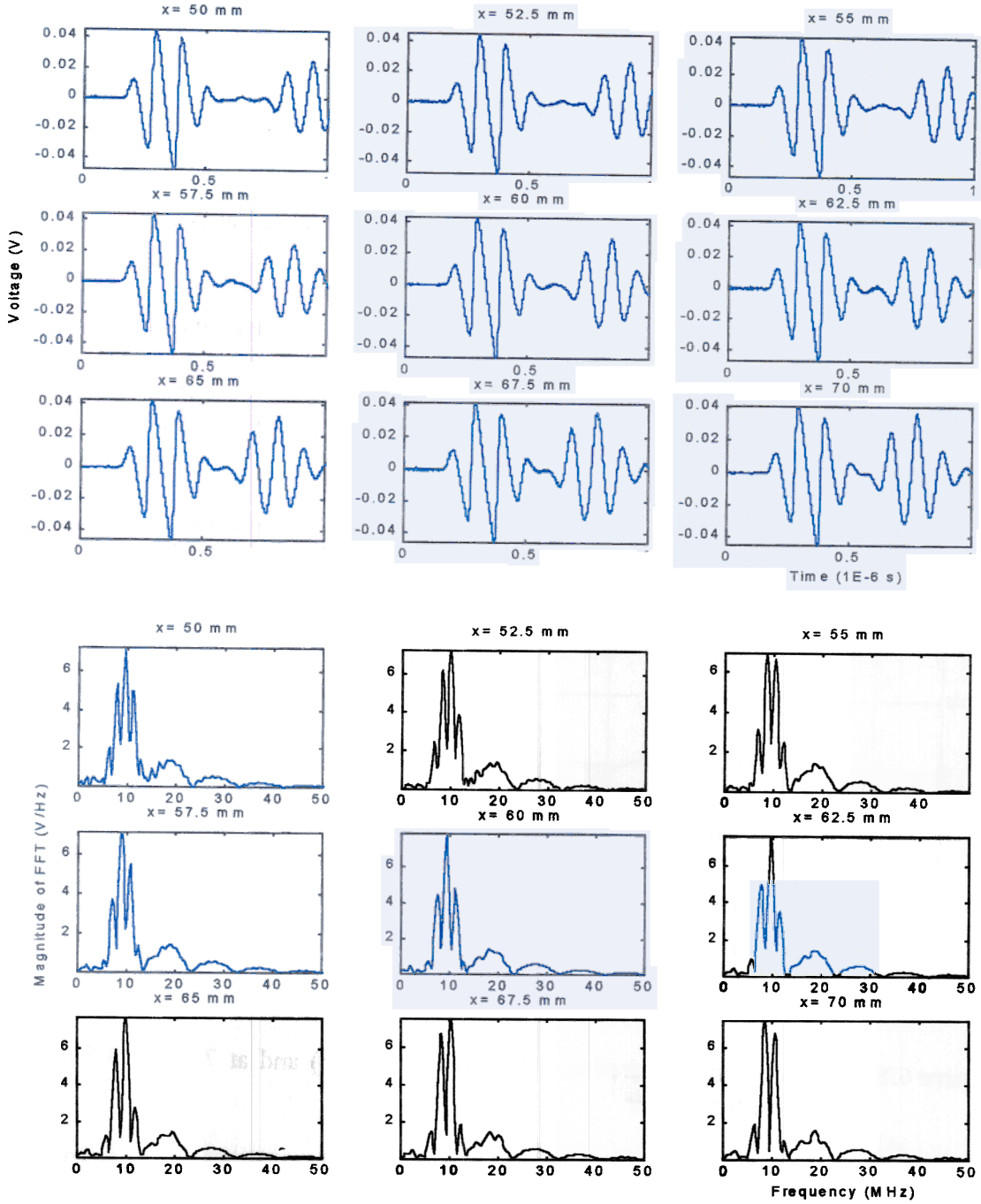


Figure 6.9c: Axial waveform acquisitions at a sampling frequency of 1 GHz and the corresponding spectra derived using a 1024 point FFT (x varies between 50 mm and 70 mm)

Due to the nature of the signals, it is thought adequate to use a rectangular window. When taking the FFT of the truncated waveform, Gibbs phenomenon effects are not really visible on the fundamental component, hence using another type of window is unlikely to improve results.

In order to get a broad idea of how the truncation of the signals acquired at the face of the transducer and at the measurement site can affect the value of the magnitude of the fundamental (hence introducing errors in the hydrophone calibration), two exercises will be

carried out. First, the time domain waveforms in Figures 6.9a to 6.9c will be truncated at various positions, and the value of the magnitude of the fundamental as a function of the distance between the face of the transducer and the hydrophone will be compared. Second, the calibration of a bilaminar hydrophone (ref. IP016) will be attempted by comparing the theoretically propagated waveform measured at the face of the transducer with that acquired at the measurement site.

6.2.2 Effects of truncation on the variation of the magnitude of the fundamental with distance

In order to investigate the influence of truncation, three different scenarios will be investigated.

Case A. The waveforms acquired at distances less than 40 mm from the face of the transducer are not truncated. Waveforms acquired at 40 mm and beyond are truncated so that the edge-wave is omitted (see Figure 6.10).

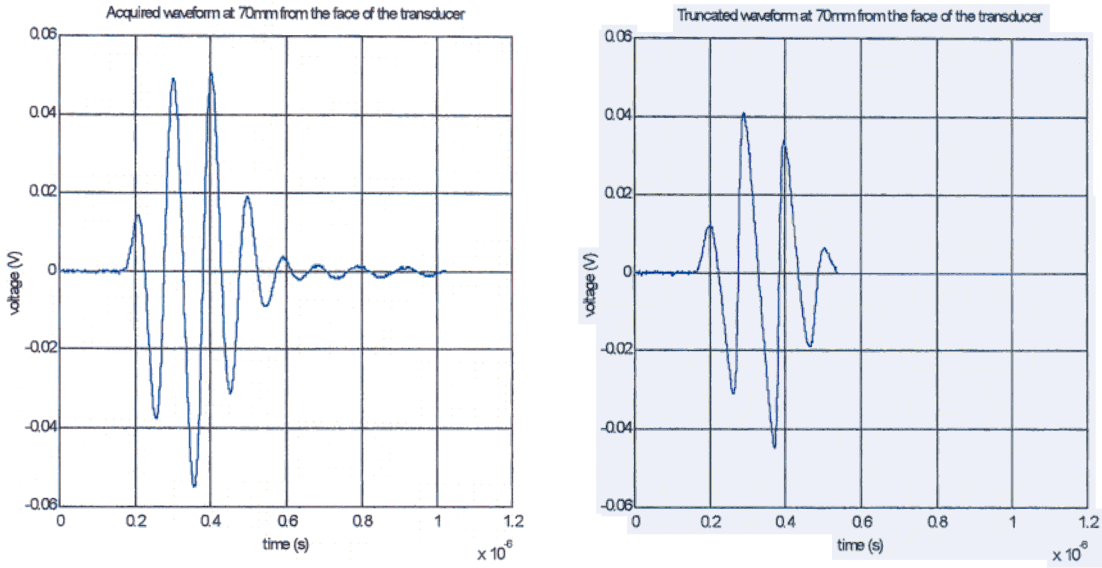


Figure 6.10: Waveforms acquired at 5 mm (no truncation) and at 70 mm (3.5 cycles) from face of transducer

Case B. The waveforms are now truncated so that 4.5 cycles are retained after truncation for measurement positions ranging between 5 and 10 mm and 3.5 cycles for positions beyond 10 mm. The truncated waveforms acquired at 5 and 70 mm from the face of the hydrophone are shown below in Figure 6.11.

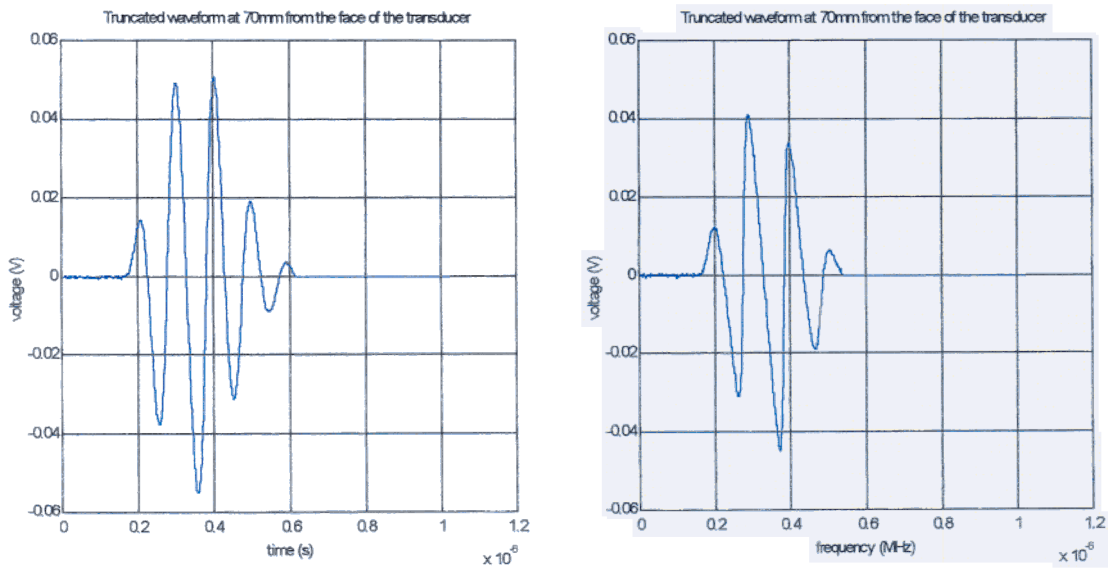


Figure 6.11: Waveforms acquired at 5 mm (4.5 cycles) and at 70 mm (3.5 cycles) from face of transducer

Case C. The waveforms have been truncated so that only 3 cycles are retained. Whatever precedes the first cycle has also been truncated since this is generally noise. The truncated waveforms for measurement positions at 5 mm and 70 mm from the face of the transducer are shown below in Figure 6.12.

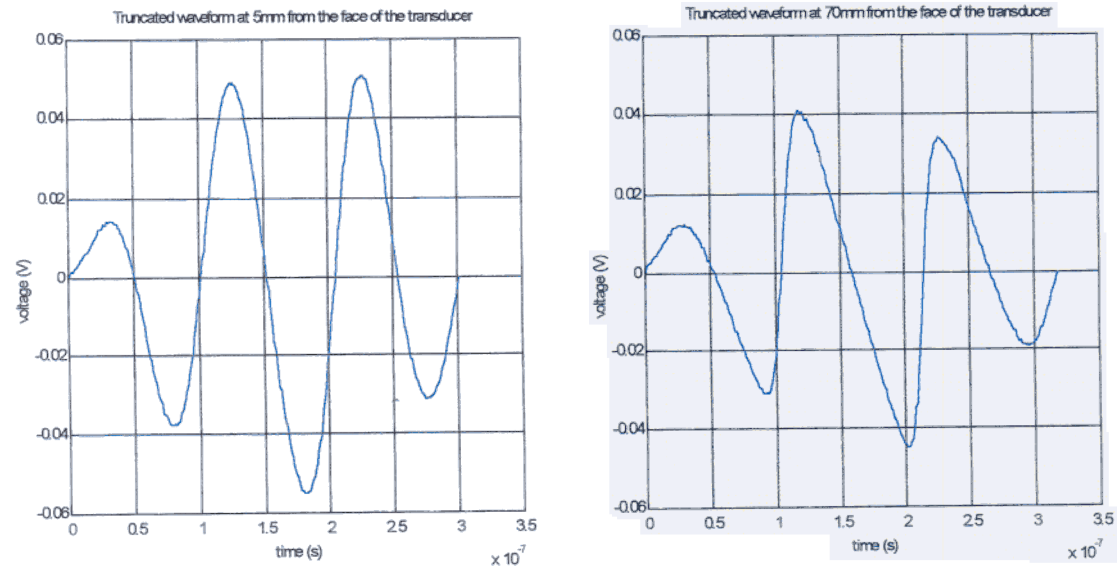


Figure 6.12: Waveforms acquired at 5 mm (3 cycles) and at 70 mm (3 cycles) from face of transducer

In order to visualise the effects of truncation on the frequency content of the waveforms, the FFT's of the time histories in Cases A, B and C have been superimposed.

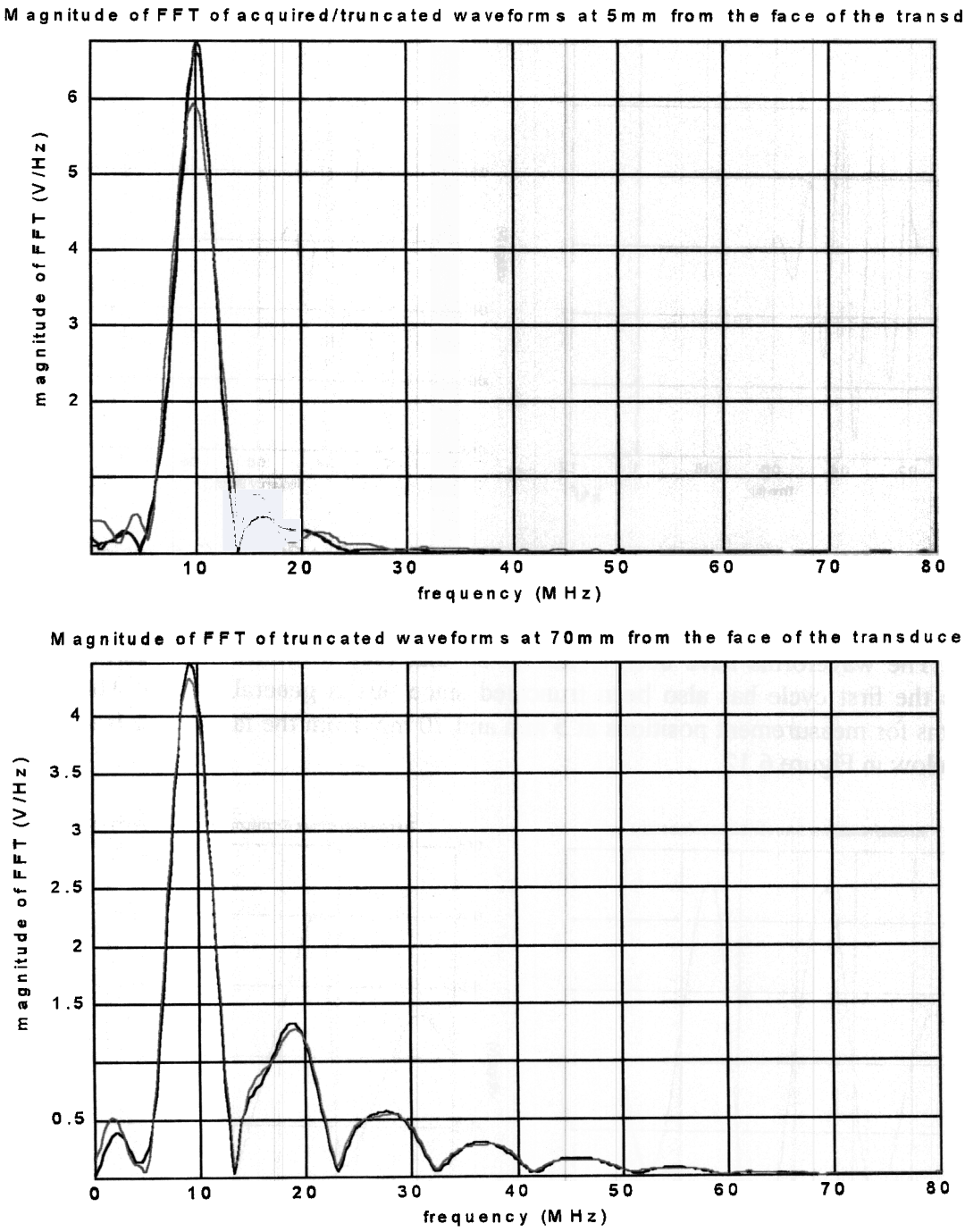


Figure 6.13: Magnitude of FFT's of waveforms in Cases A (—), B (—) and C (—) at 5 mm (the upper plot) and 70 mm (lower plot) from the face of the transducer.

Note that for the 70 mm position, only two frequency domain plots that are shown. This is because the time domain waveforms in Cases A and B have been truncated in the same place.

	Case A	Case B	Case C
Magnitude of fundamental at 5mm (V/Hz)	6.7503	6.6149	5.9368
Magnitude of fundamental at 70mm (V/Hz)	4.4513	4.4513	4.3229

Table 6.1: Maximum value of fundamental for truncation positions corresponding to Cases A, B and C.

Table 6.1 shows that, for the truncation positions considered, the magnitude of the fundamental varies by as much as 12% at the 5 mm position and 3% at 70 mm. Clearly, the results suggest that truncating after just 3 cycles is likely to lead to erroneous results in terms of estimating the magnitude of the fundamental at both the face of the transducer and the measurement site. This is to a certain extent predictable since a non-negligible section of the time domain waveform is omitted. Cases A and B show similar results for the magnitude of the fundamental at the face of the transducer. It is therefore likely that truncating the waveform after 4.5 cycles is in this case sufficient to yield a good estimate of the magnitude of the fundamental. However, it should be noted that the difference in fundamental level between Cases A and B is still 2% and this can have a significant influence on the reliable establishment of the nonlinear loss which forms such a pivotal part of the 'magnomic' technique (Section 7).

The variation of the magnitude of the fundamental frequency as a function of x is shown below in Figure 6.14. Note the large increase in the fundamental level exhibited close to the face of the transducer, as seen later in Figure 6.34.

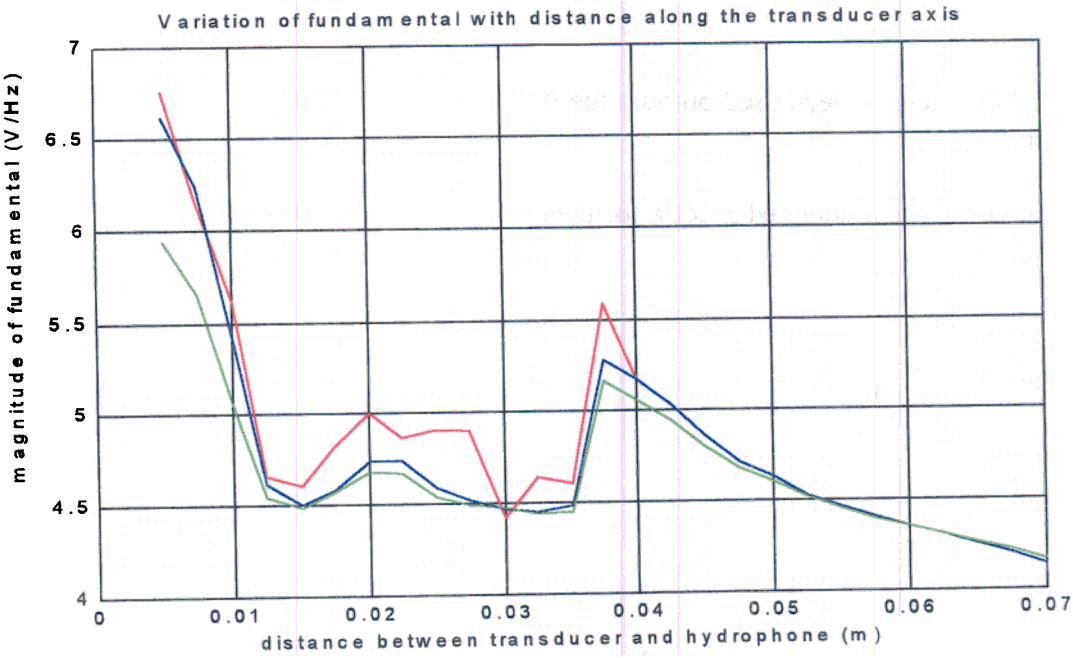


Figure 6.14: Variation of fundamental magnitude with distance between the transducer and hydrophone (IP010) for Cases A (—), B (—) and C (—). Drive level: 350mV.

It can be seen that selecting the appropriate truncation position plays an important role in establishing an estimate of the magnitude of the fundamental of the signals. Note that as the waveforms generally all have unwanted components superimposed on them after at least the fourth cycle, the above results only provide an insight into the effects of truncation. Also, the accuracy at which the magnitude of the fundamental may be determined is also dependent on the amount of points used on the FFT. Here, although signals have been acquired using a 1024 point FFT, the waveforms have been padded with zeros so as to increase frequency resolution: 4096 points in total having been used. The axial variation of the fundamental level is described in more detail in Section 6.4.

6.2.3 Effects of truncation on a calibration using the 'magnomic' method

The effects of truncation of the acquired time-domain waveforms on the derived hydrophone sensitivity values will be examined briefly. Waveforms have been acquired under the high drive conditions used for calibrations (700 mV) in order to ensure sufficient higher harmonic content. The bilaminar hydrophone IP016 has been used with the waveform acquired close to the face of the transducer being truncated at various points and then propagated theoretically using the algorithm described in Section 4. In order to convert the voltage waveform to a pressure waveform, the known 10 MHz sensitivity of the hydrophone has been used (see Appendix B for sensitivity data on hydrophone IP016). This approach assumes that the frequency response of the hydrophone is flat for the band of frequencies contained in the waveform acquired at the face of the transducer. Again, three specific cases have been identified.

Case A. The waveform at the 5 mm position is not truncated. At the 70 mm position, 4 cycles have been included, hence omitting the edge-wave.

Case B. 3 cycles have been used on both the waveform at the 5 mm position and that acquired at 70 mm.

Case C. 4 cycles have been used on both the waveform at the 5 mm position and that acquired at 70 mm.

The waveforms and associated spectra for these three cases are shown in Figures 6.15 to 6.17.

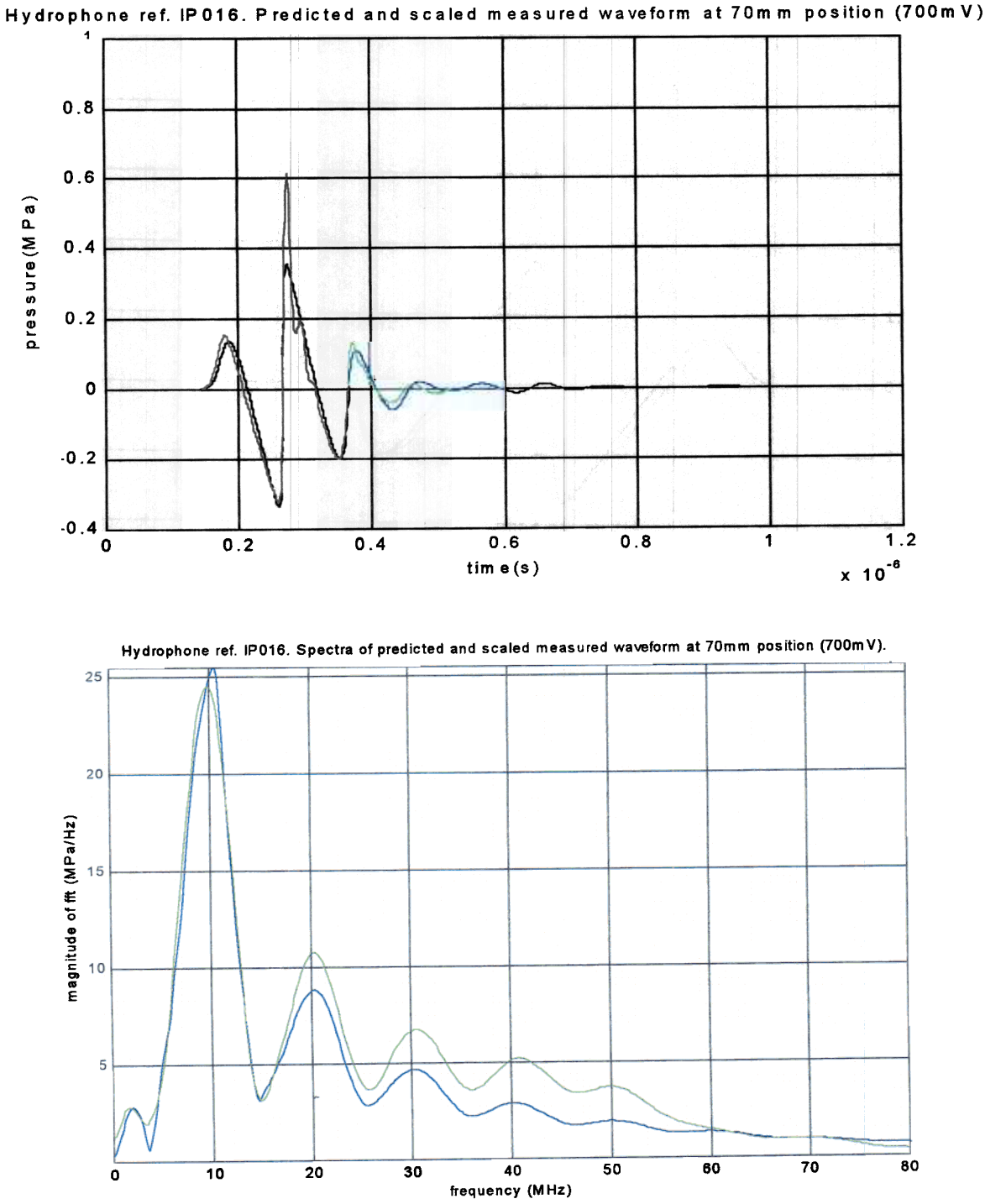


Figure 6.15: Predicted (–) and measured (–) waveforms at 70 mm from face of transducer presented both the in time and frequency domains, no truncation being carried out at the 5 mm position and four cycles being retained at 70 mm (Case A)

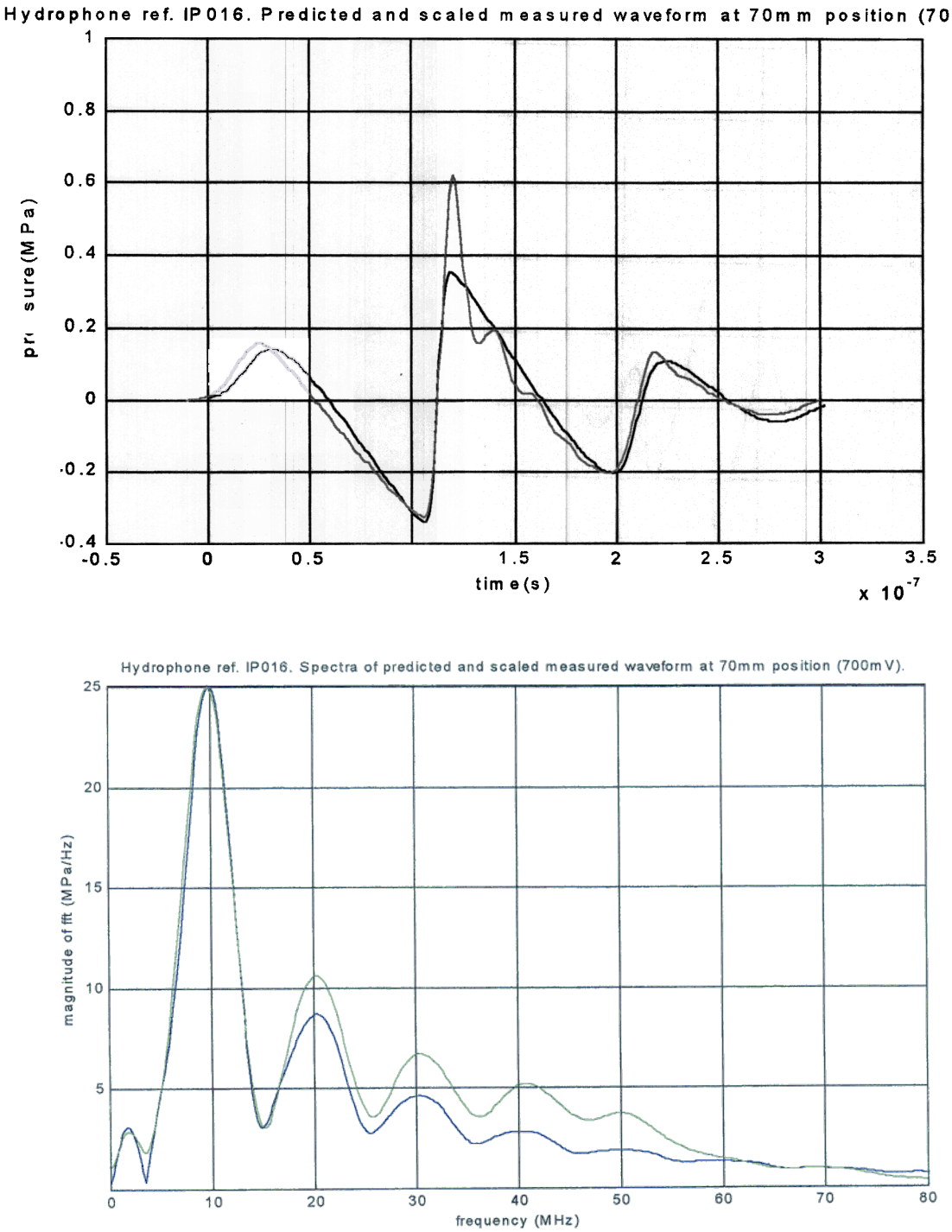


Figure 6.16: Predicted (–) and measured (–) waveforms at 70 mm from face of transducer presented both in time and frequency domains, three cycles being retained at both 5 mm and 70 mm (Case B)

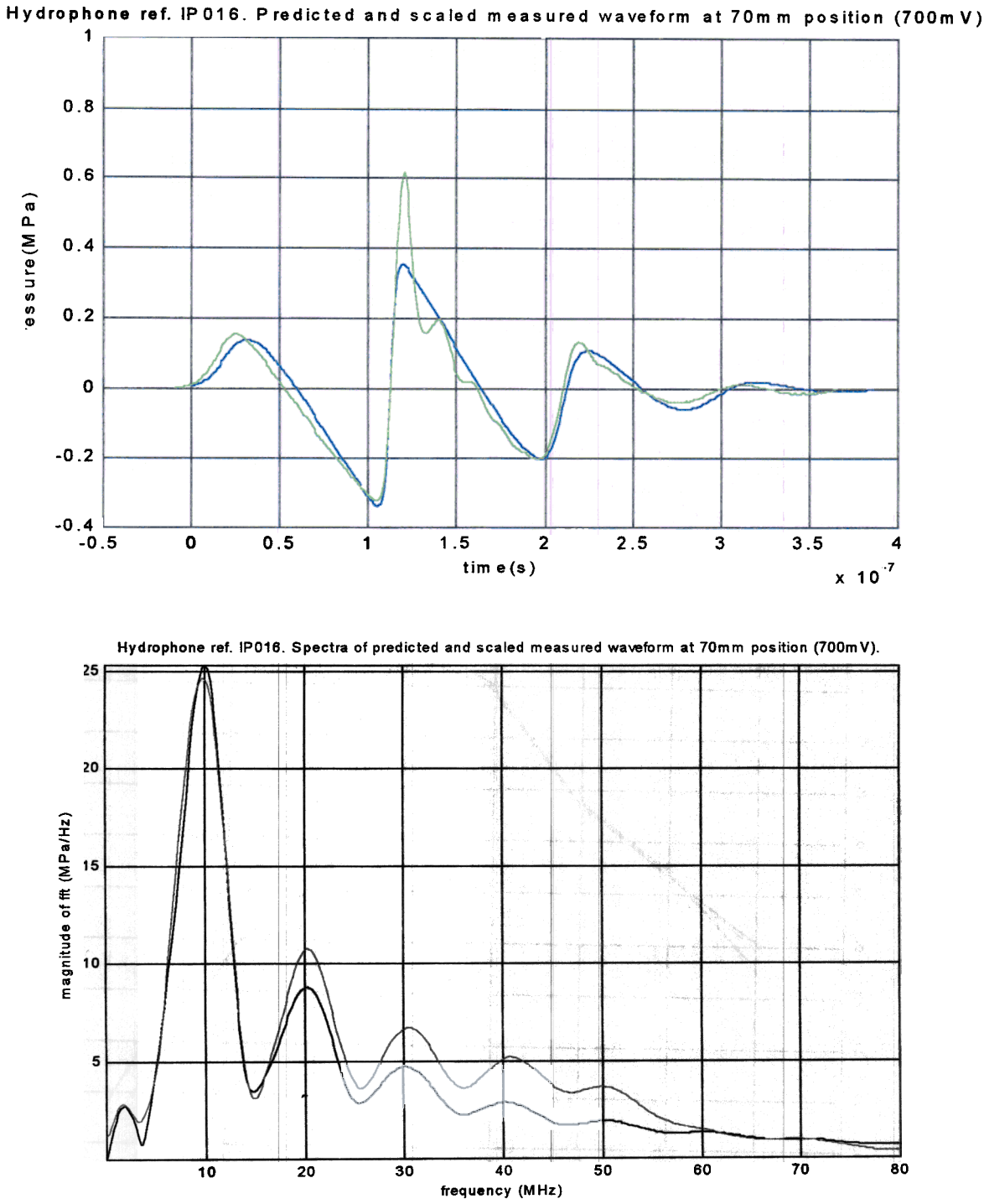


Figure 6.17: Predicted (–) and measured (–) waveforms at 70mm from face of transducer presented both in the time and frequency domains, four cycles being retained at both 5 mm and 70 mm (Case C).

	Case A	Case B	Case C
Magnitude of fundamental at the 5 mm position (V/Hz)	15.588	14.989	15.204
Magnitude of fundamental at the 70 mm position (V/Hz)	9.985	10.084	9.985
Predicted magnitude of fundamental of pressure at the 70 mm position (MPa/Hz)	25.48	25.06	25.26

Table 6.2: Maximum value of the fundamental for truncation positions corresponding to Cases A, B and C.

Table 6.2 shows that, for the truncation positions considered, the magnitude of the fundamental varies by as much as 3.8% at the 5 mm position and 1% at the 70 mm position. The predicted fundamental pressures derived by propagating the waveforms truncated in various ways, show a variation of up to 1.7%. These uncertainties are significant in relation to the required accuracy of the loss measurement.

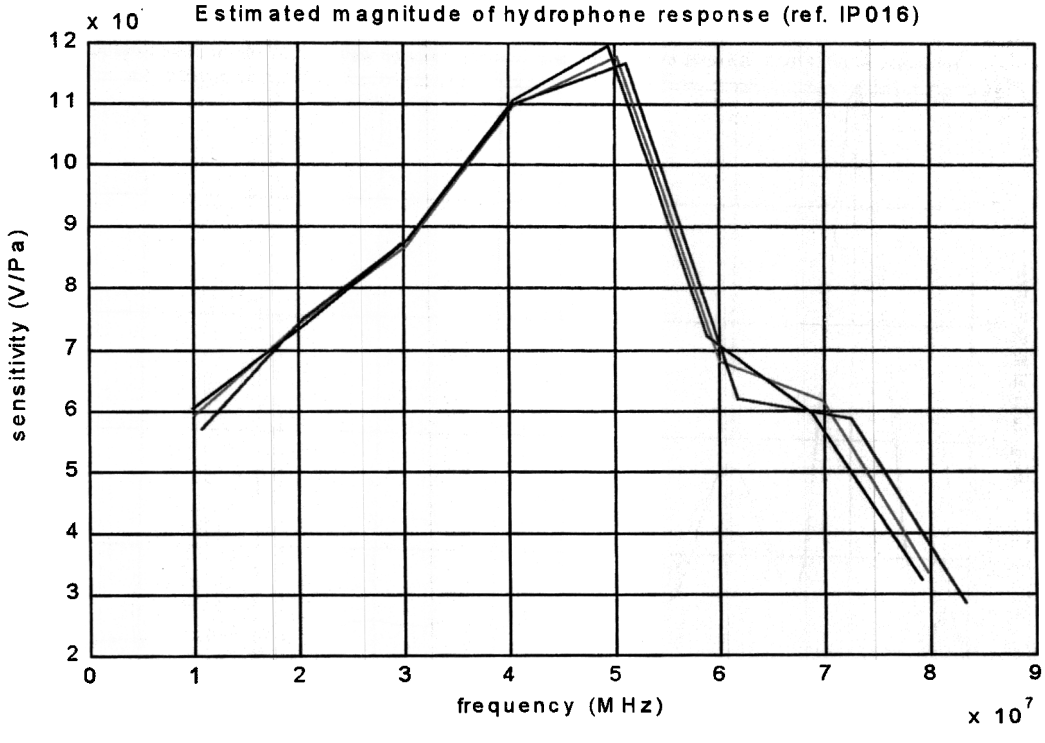


Figure 6.18: Magnitude of hydrophone response (end-of-cable, loaded, hydrophone IP016) estimated using the "magnomic" method for Cases A (—), B (—) and C (—)

Figure 6.18 shows the estimated hydrophone responses for Cases A, B and C using the 'magnomic' method. It can be seen that the position at which the time-domain waveform is truncated does not seem to significantly affect the estimate of the hydrophone response in this particular case, particularly for the harmonic frequencies. The results for the fundamental, fourth and fifth harmonics are summarised in Table 6.3.

	Case A	Case B	Case C
Estimated sensitivity at the fundamental (nV/Pa)	56.8	60.5	59.3
Estimated sensitivity at the fourth harmonic (nV/Pa)	110.0	110.5	109.6
Estimated sensitivity at the fifth harmonic (nV/Pa)	116.8	119.8	117.8

Table 6.3: End-of-cable loaded sensitivity of hydrophone (IP016) derived at the fundamental frequency along with the fourth and fifth harmonics (40 and 50 MHz).

Note the insensitivity of the higher frequency components to the truncation position, although it is equally clear that the derived sensitivity at the fundamental is sensitive to the truncation position. This tends to suggest that there is enough information in the truncated waveforms to carry out a calibration. Any significant discrepancies between the results obtained via the 'magnomic' method and other methods (e.g. interferometer calibration) are not likely to be due to windowing problems.

6.3 MEASUREMENTS MADE USING THE LARGE APERTURE HYDROPHONE

As highlighted in Section 3, the validity of the magnomic technique is based on a reliable determination of the nonlinear loss incurred during the propagation of a plane-wave between the two measurement sites of interest. This value for the nonlinear loss (L), defines the value of the nonlinear propagation parameter (σ) and consequently the harmonic content at the further position where the acoustic waveform is strongly distorted.

Section 6.1 demonstrated that the pressure distribution within the acoustic field of the 10 MHz transducer shows significant deviations from a true plane-wave, and the original work described by Bacon presented in Appendix A involved applying a correction to allow for these transducer imperfections. The objective of applying such a correction was in order to derive a value for the 'true' nonlinear loss.

An independent measurement of the plane-wave nonlinear loss would clearly be desirable as it may in itself provide a check of the 'transducer imperfection' corrections applied. This could be achieved through measurements made using a large aperture hydrophone, or a hydrophone of sufficient size such that it completely intercepts the transmitted acoustic beam. If this condition is met, the hydrophone essentially acts as a spatial-filter, resolving the plane-wave component of the acoustic wave perpendicular to its surface. This type of hydrophone has been applied by a number of workers to derive diffraction-insensitive measurements of the acoustic properties of materials (Costa et al. 1986; Zeqiri 1989; Costa et al. 1986a; Costa et al. 1990). The hydrophone used in this present study (details of which are given in Table 5.1), has an active element of diameter 75 mm and is therefore substantially larger than the transducer diameter (19.1 mm). The various aspects of the studies carried out using this hydrophone will now be discussed in detail.

6.3.1 Waveforms acquired using the 75 mm hydrophone

Figures 6.19 and 6.20 give the waveform acquired using IP002 at the low drive setting (50 mV) with the hydrophone positioned at respective distances of 5 mm and 70 mm. The orientation of the hydrophone was carefully adjusted to maximise the output voltage in both cases. The two spectra are shown in Figure 6.23.

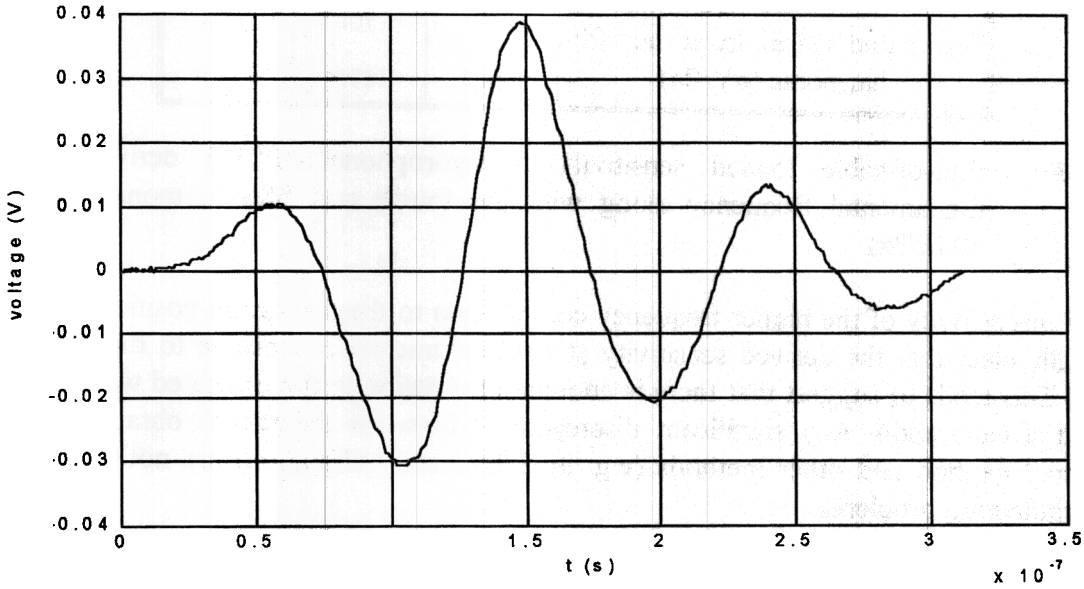


Figure 6.19: Waveform acquired using the 75 mm active element diameter hydrophone, IP002, determined at a distance 5 mm for the HP low-drive setting of 50 mV

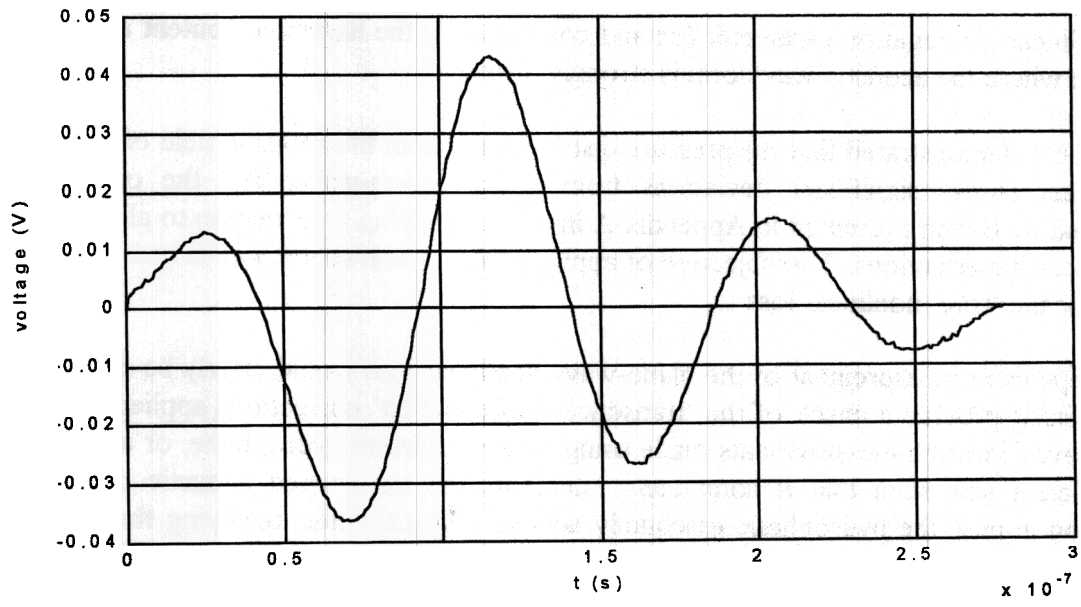


Figure 6.20: Waveform acquired using the 75 mm active element diameter hydrophone, IP002, determined at a distance of 70 mm for the HP low-drive setting of 50 mV.

Figures 6.21 and 6.22 give the waveform acquired using IP002 at the high drive setting with the hydrophone positioned at distances of 5 mm and 70 mm. Note the clear nonlinear distortion of the waveform observed at a separation of 70 mm, although, due to the limited bandwidth of the hydrophone, only the first two harmonics are detected as depicted in the two spectra shown in Figure 6.24.

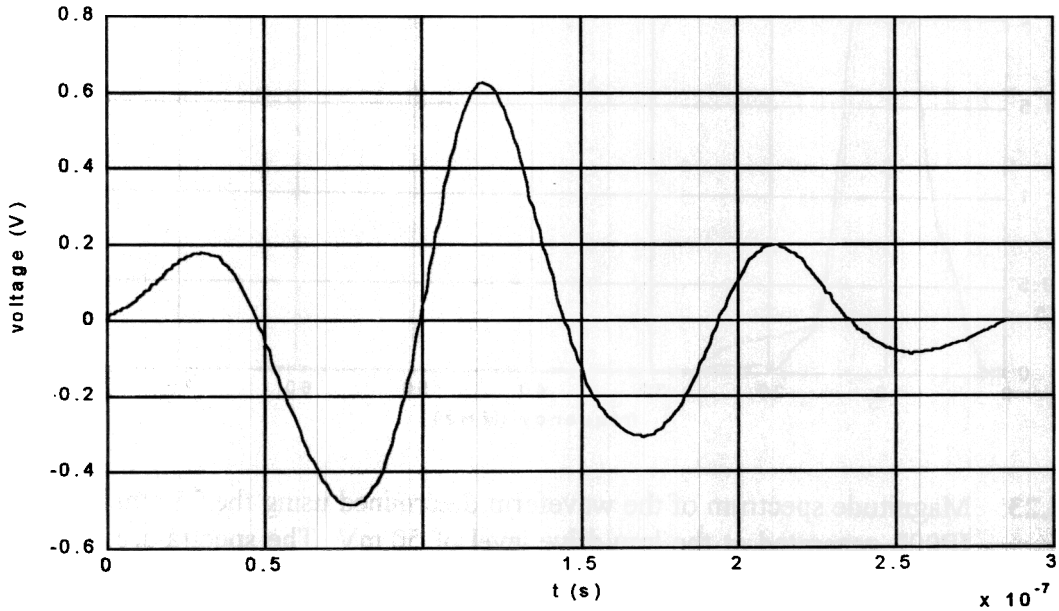


Figure 6.21: Waveform acquired using the 75 mm active element diameter hydrophone, IP002, determined at a distance of 5 mm for the HP high-drive setting of 700 mV

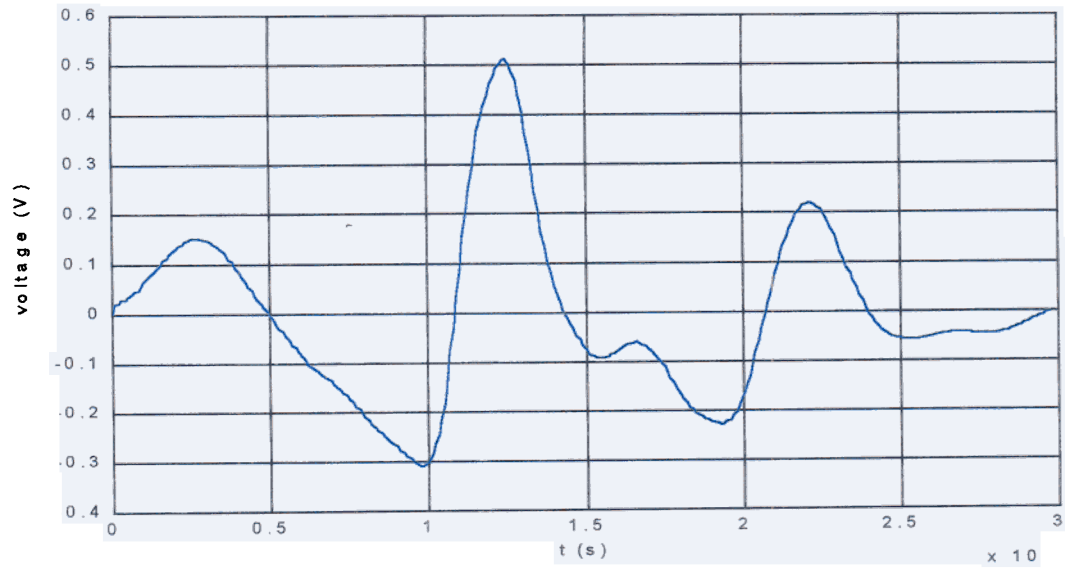


Figure 6.22: Waveform acquired using the 75 mm active element diameter hydrophone, IP002, determined at a distance of 70 mm for the HP high-drive setting of 700 mV

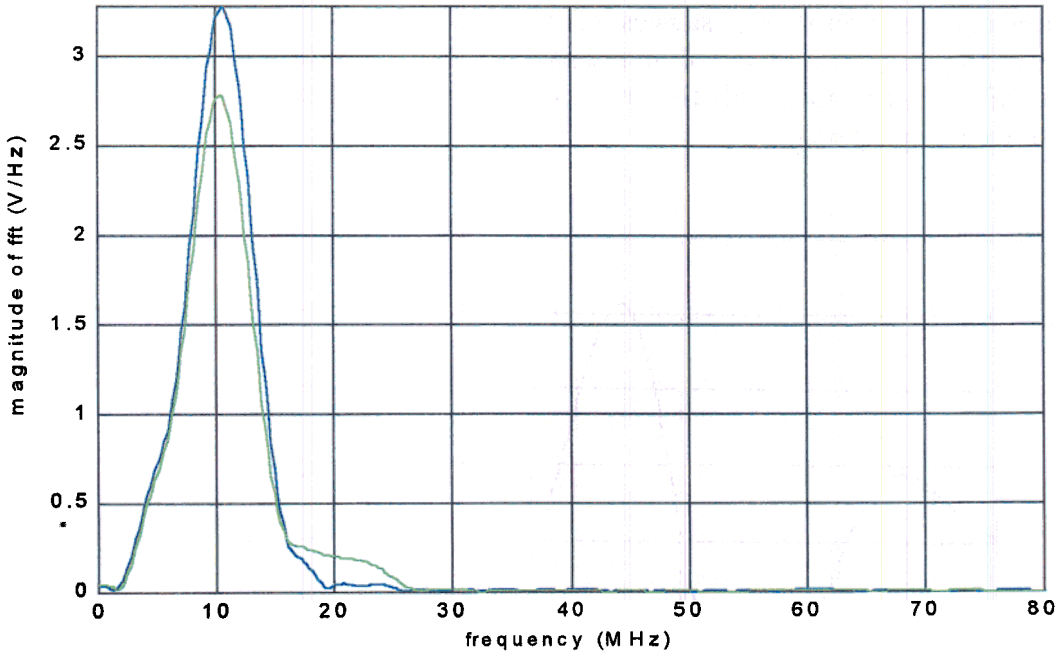


Figure 6.23: Magnitude spectrum of the waveform determined using the 75 mm hydrophone IP002 generated at the low-drive level of 50 mV. The spectra are shown with the hydrophone positioned at 5 mm (–) and 70 mm (–)

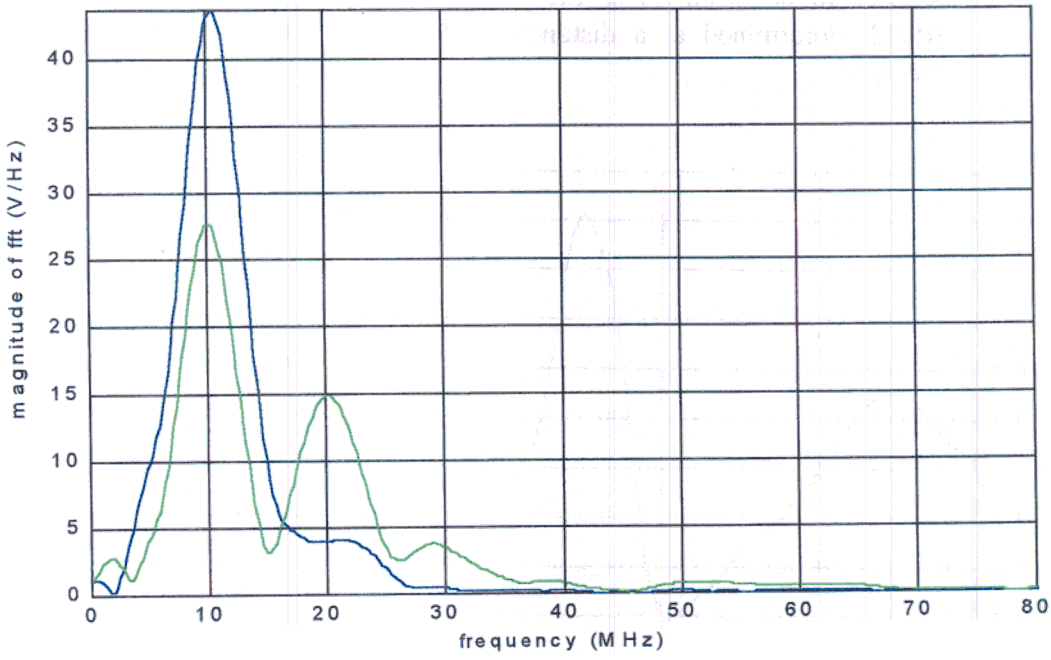


Figure 6.24: Magnitude spectrum of the waveform determined using the 75 mm hydrophone IP002 generated at the high-drive level of 700 mV. The spectra are shown with the hydrophone positioned at 5 mm (–) and 70 mm (–)

6.3.2 Measurements of nonlinear loss

Figure 6.25 shows the variation in the fundamental level with the HP function generator drive setting derived at the two principal measurement sites of interest, 5 mm and 70 mm. Here, the fundamental level has been taken as the peak in the response shown in Figure 6.24, the voltage values being determined using the LeCroy 9450A oscilloscope. The figure shows the clear falling off in the response at 70 mm with increasing drive resulting from nonlinear loss. It should be noted that the 5 mm position was chosen as the closest achievable separation.

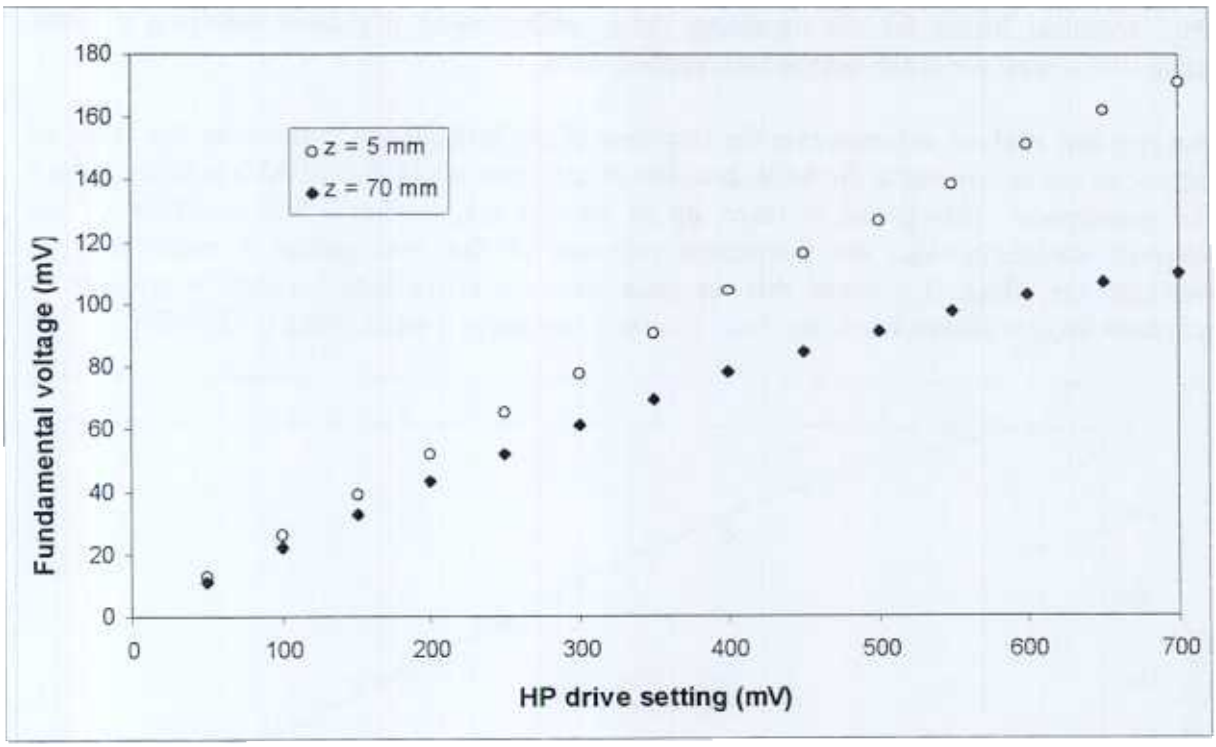


Figure 6.25: Variation of the fundamental level with the Hewlett Packard (HP) function generator drive setting measured using the 75 mm diameter membrane hydrophone (IP002). Measurements have been made at the two positions used for the 'magnomic' calibration, 5 mm and 70 mm

Even at 5 mm, some nonlinearity in the response is produced although this probably arises due to nonlinearities in the applied drive voltage itself. It corresponds to a reduction in the drive relative to the linear case of 3% at the 500 mV drive setting and 6% at the 700 mV drive setting. As the 'magnomic' method involves determining the pressure at the face, nonlinearities in the drive itself are of no relevance.

The dependence of the derived nonlinear loss, L, on the HP drive setting is shown in Figure 6.26, up to the maximum drive level of 700 mV. The figures have been corrected for small signal absorption in water using the 10 MHz absorption coefficient in water at 21.1°C. The relatively smooth dependence of L on the drive setting and the fact that at low drives, L tends to 1 (linear regime with no nonlinear loss) is very encouraging.

Throughout the 'magnomic' calibrations described in Section 7, the large aperture hydrophone IP002 was used to check the value of L obtained at the highest drive setting. Values obtained

over a number of days were extremely reproducible, being 0.754, 0.755, 0.752 and 0.758, giving a mean value of the nonlinear loss of 0.755 ± 0.6% where the Type A uncertainty is given using a coverage factor, k=2.

Also included in Figure 6.26 is the theoretical dependence of the nonlinear loss whose dependence was derived in the following way. First, the waveform determined at 5 mm (shown in Figure 6.21) was progressively scaled in absolute pressure terms and propagated through the Mitome routine until the computed nonlinear loss at 70 mm was equal to that observed at the high drive level i.e. 0.755. This required a pressure at the face of the transducer of 0.603 MPa. Nonlinear losses for the remaining drive settings were evaluated assuming a linear scaling of the pressure at the source with applied drive.

Note that this analysis assumes that the response of the hydrophone is flat over the range of frequencies which constitute the initial acoustic disturbance, which for IP002 is unlikely to be a valid assumption. This theme is taken up in Section 6.5, where a deconvolution of the measured waveform with the theoretical response of the hydrophone is undertaken to investigate the effect. It is found that the peak-pressures at the face required to produce an equivalent loss are higher when the 'true' acoustic waveform is used, being 0.636 MPa.

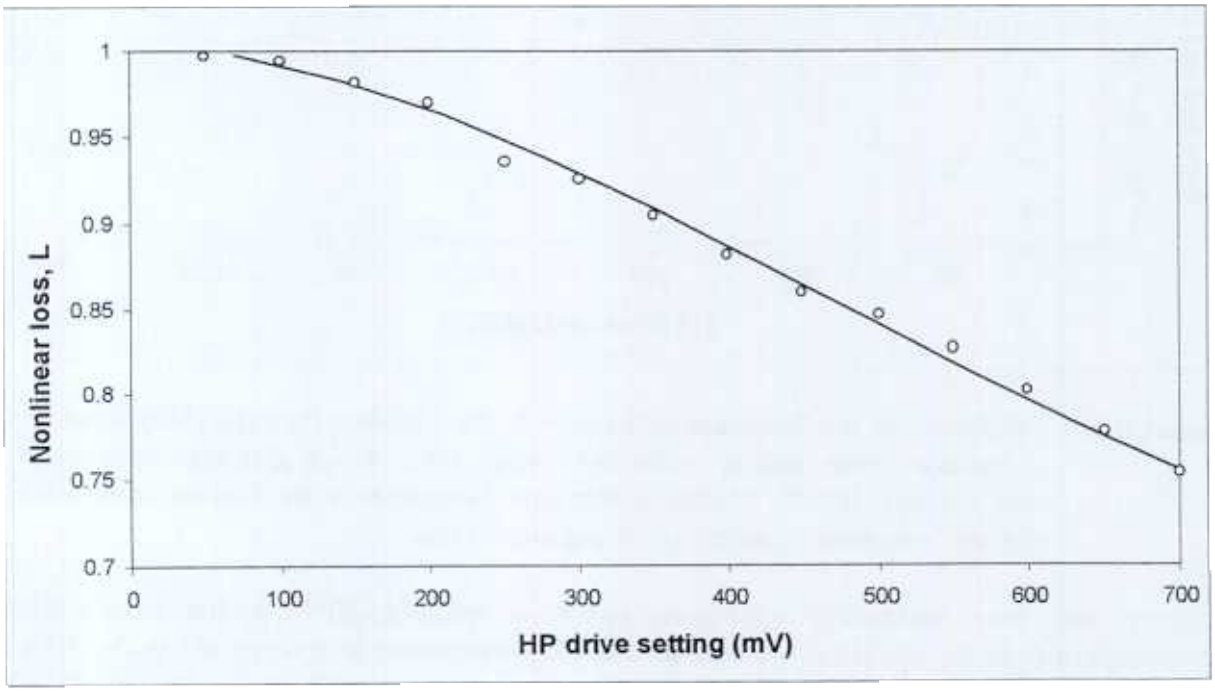


Figure 6.26: Comparison of measured (o) and predicted (–) nonlinear loss derived up to a Hewlett Packard function generator setting of 700 mV. Measurements have been made using the 75 mm large aperture hydrophone between measurements positions 5 mm and 70 mm. Predictions have been derived by propagating the waveform measured close to the face using the Mitome model.

Although there is some scatter in the experimental data points, the shape of the curve is reliably reproduced by the predictions. From Equation 22 given in Section 4, using the computed input pressure derived from the 75 mm hydrophone measurements, the value of σ is computed as 2.9.

The Mitome routine has been used to propagate the waveforms determined using the 75 mm hydrophone at the face of the transducer. Figure 6.27 gives the low-drive setting and represents a comparison of the waveforms predicted through propagating the 5 mm waveform forward to 70 mm with the waveform determined directly at the site. The agreement between the two waveforms is reasonable, the shape and amplitudes of the half-cycles being reliably reproduced.

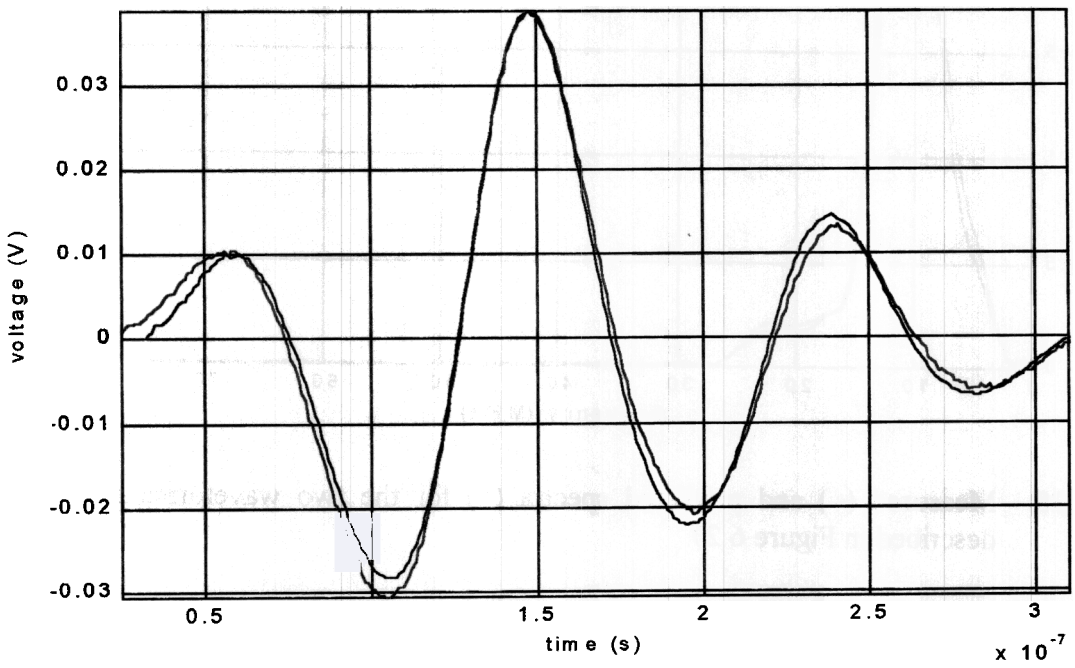


Figure 6.27: Comparison of the waveform measured using the 75mm bilaminar hydrophone, IP002, (–) and the predicted waveform (–). The latter was obtained by taking the measured waveform at the face of the hydrophone, propagating it forward using the Mitome routine and convolving the resultant acoustic waveform with the theoretical impulse response of the hydrophone.

The two predicted spectra are shown in Figure 6.28, again good agreement is exhibited.

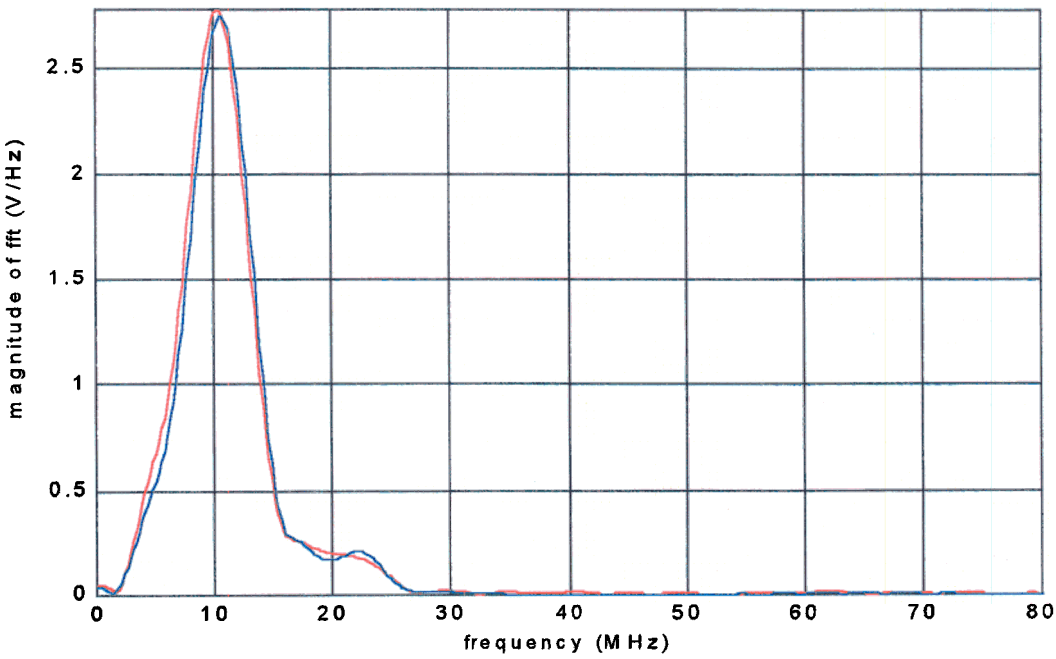


Figure 6.28: Measured (–) and predicted spectra (–) for the two waveforms shown and described in Figure 6.27

For the comparison of the observed high-drive waveforms, a model has been used to predict the response of the hydrophone and its basis may be found in Appendix D. There are some uncertainties regarding the appropriate electrical part of the model to use for such a large diameter active element hydrophone. In the calculated responses presented in the next few graphs, a capacitance value of 50 pF has been assumed.

Figure 6.29 portrays both the voltage waveform measured using the 75 mm hydrophone and that predicted from a waveform acquisition carried out at a distance of 5 mm. Measurements were made at the HP high drive setting of 700 mV. The 5 mm waveform has been propagated forward to the 70 mm measurement site using an input pressure of 0.60 MPa, and the true acoustic waveform has then been convolved with the theoretical hydrophone response to generate the predicted voltage waveform from the hydrophone. Again, the agreement between prediction and direct measurement is encouraging, the general features of the two waveforms being common.

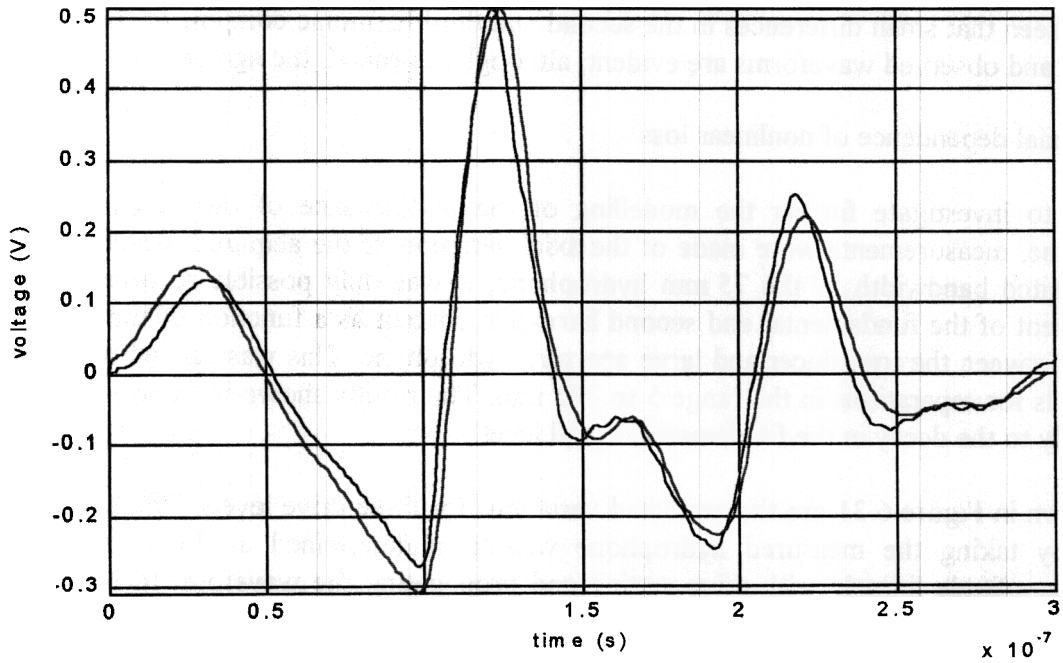


Figure 6.29: Comparison of the waveform measured using the 75mm bilaminar hydrophone, IP002, (–) and the predicted waveform (–), obtained by taking the measured waveform at the face of the hydrophone, propagating it forward using the Mitome routine and convolving the resultant acoustic waveform with the theoretical impulse response of the hydrophone.

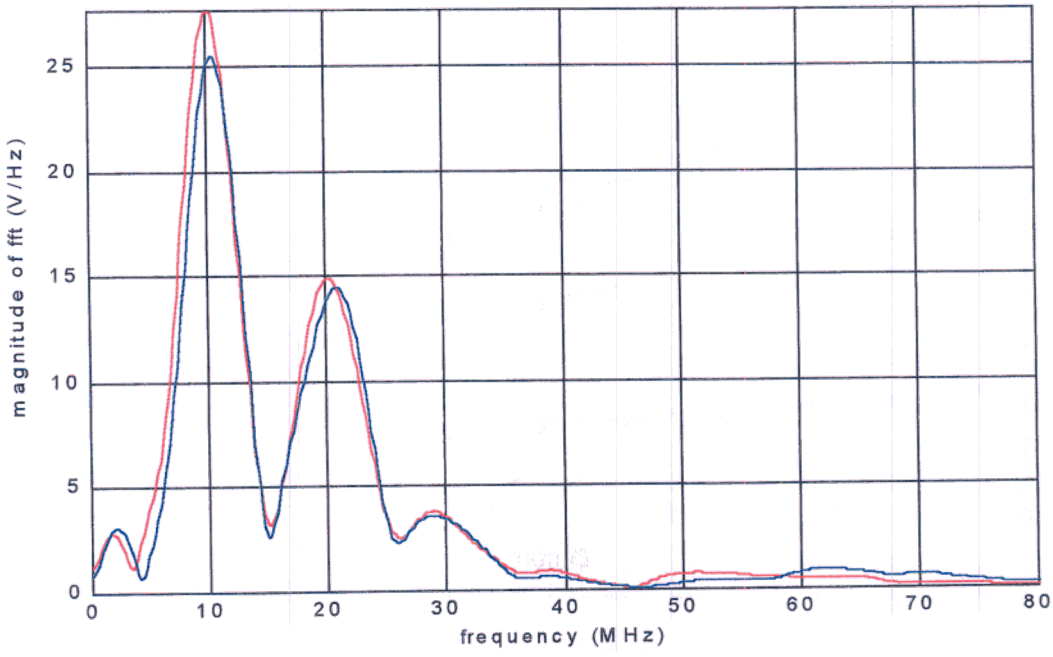


Figure 6.30: Measured (–) and predicted spectra (–) for the two waveforms shown and described in Figure 6.29

Figure 6.30 gives a frequency domain comparison of the two waveforms shown in Figure 6.29. It can be seen that small differences in the second and third harmonic components between the predicted and observed waveforms are evident, although in general, the agreement is good.

6.3.3 Axial dependence of nonlinear loss

In order to investigate further the modelling of the performance of the 75 mm diameter hydrophone, measurements were made of the axial variation of the acquired waveforms. Due to the limited bandwidth of the 75 mm hydrophone, it was only possible to investigate the development of the fundamental and second harmonic content as a function of the separation distance between the transducer and large aperture hydrophone. This was carried out at three drive levels for separations in the range 5 to 105 mm. The results shown in Figure 6.31 relate specifically to the decay in the fundamental signal level.

Also shown in Figure 6.31 are the predicted variations for three drive levels. These have been derived by taking the measured hydrophone waveform determined at 5 mm, scaling the acoustic amplitude linearly with drive setting and propagating the waveform forward to the measurement site of interest using the Mitome routine. Here, the true acoustic waveform has been convolved with the hydrophone response (see Appendix D) and the relative fundamental and second harmonic levels derived from an FFT of the predicted waveform. The fundamental is defined as the peak in the frequency spectrum. As the sensitivity of the 75 mm hydrophone is unknown, the predicted variation has been normalised to the experimental data points using the 15 mm measurement.

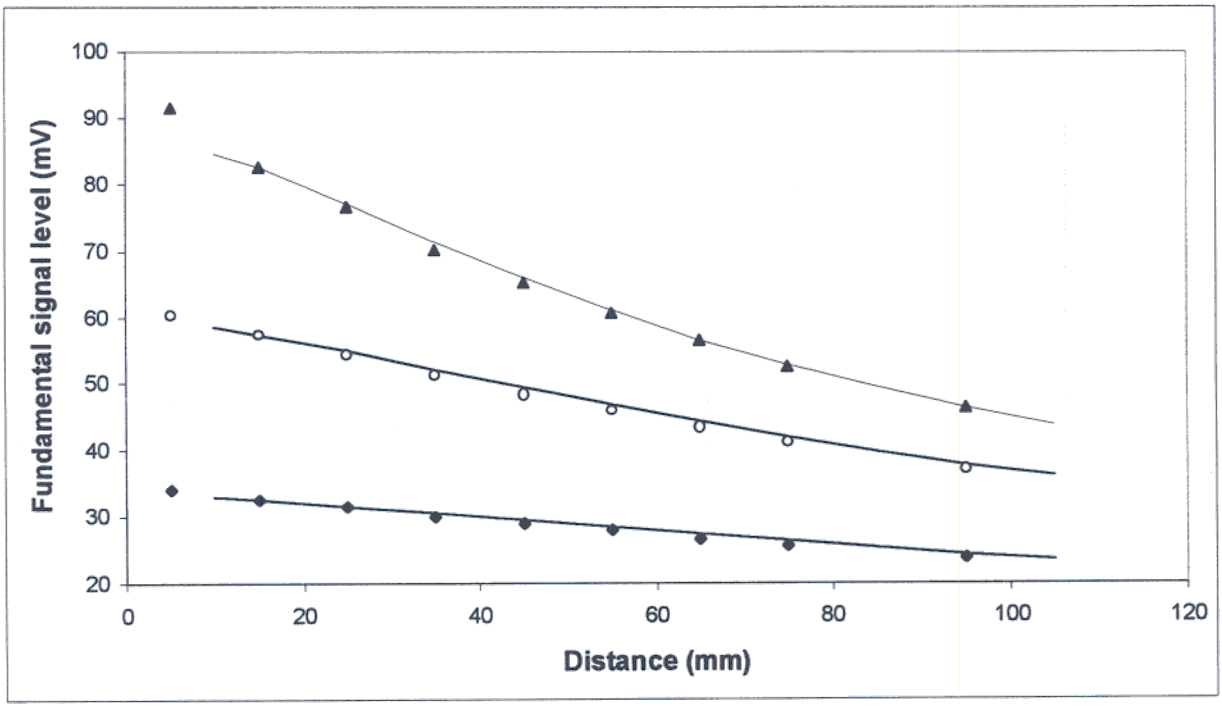


Figure 6.31 Axial variation of the fundamental voltage determined using the 75 mm active element diameter hydrophone, IP002. Measurements have been completed at drive settings of 250 mV (♦), 450 mV (o) and 700 mV (▲). Experiment, shown by individual data points, has been compared with theory (–) derived by propagating the waveform determined at 5 mm

It is clear from Figure 6.31 that the predicted nonlinear loss in the fundamental closely agrees with the observed variation. It should be noted that measurements and predictions shown in Figure 6.31 are those observed at the measurement site of interest and have not been corrected for attenuation in water.

6.3.4 Axial variation of generated second harmonic component

The axial variation of the second harmonic component, determined using the 75 mm hydrophone, is shown in Figure 6.32. Theoretical values, determined in the way specified above, have been normalised to the maximum fundamental signal levels displayed in Figure 6.31.

Again, the agreement between theory and measurement is encouraging: the general shape of the response and the axial position of the peaks being reliably reproduced. Differences in absolute level probably arise from uncertainties in the hydrophone model used in the convolution of the true acoustic waveform.

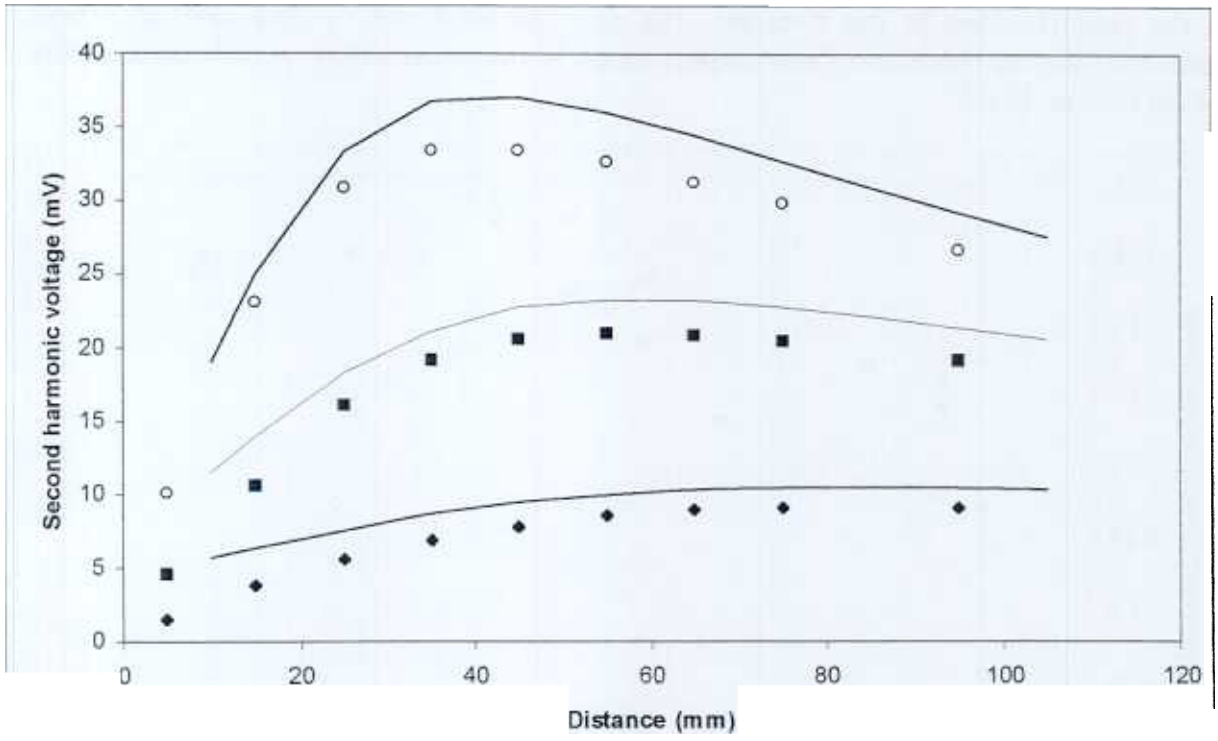


Figure 6.32: Axial variation of the second harmonic voltage determined using the 75 mm active element diameter hydrophone, IP002. Measurements have been completed at drive settings of 250 mV (♦), 450 mV (o) and 700 mV (▲). Experiment, shown by individual data points, has been compared with theory derived by propagating the waveform determined at 5 mm

6.4 EXPERIMENTAL INVESTIGATIONS OF THE 'TRANSDUCER CORRECTION'

6.4.1 Low drive level measurements

The 'magnomic' procedure, as highlighted in Section 3, involves acquiring four acoustic waveforms, two at the closest position possible to the transducer (in this case 5 mm) and two at the measurement site of interest (70 mm). At each position, waveforms are acquired at both 'high' and 'low' drive levels. In this context, the 'low' drive condition is sufficiently low to ensure that there is no nonlinear loss during propagation between the two sites. This measurement is carried in order to assess the effect of 'transducer imperfections' on the waveform at the further measurement site.

These imperfections were studied by performing a beam-scan along the acoustic axis of the 10 MHz transducer after the hydrophone had been carefully aligned on its acoustic axis. Results for the two hydrophones IP010 and IP901 are shown in Figure 6.33, where each individual measurement point was derived from acquiring the acoustic waveform and performing an FFT to extract the 'fundamental' signal level. The fundamental is again defined as the peak response in the spectrum. The two individual sets of data have each been normalised to their respective 5 mm measurements. Measurements were carried out at a drive setting level of 50 mV.

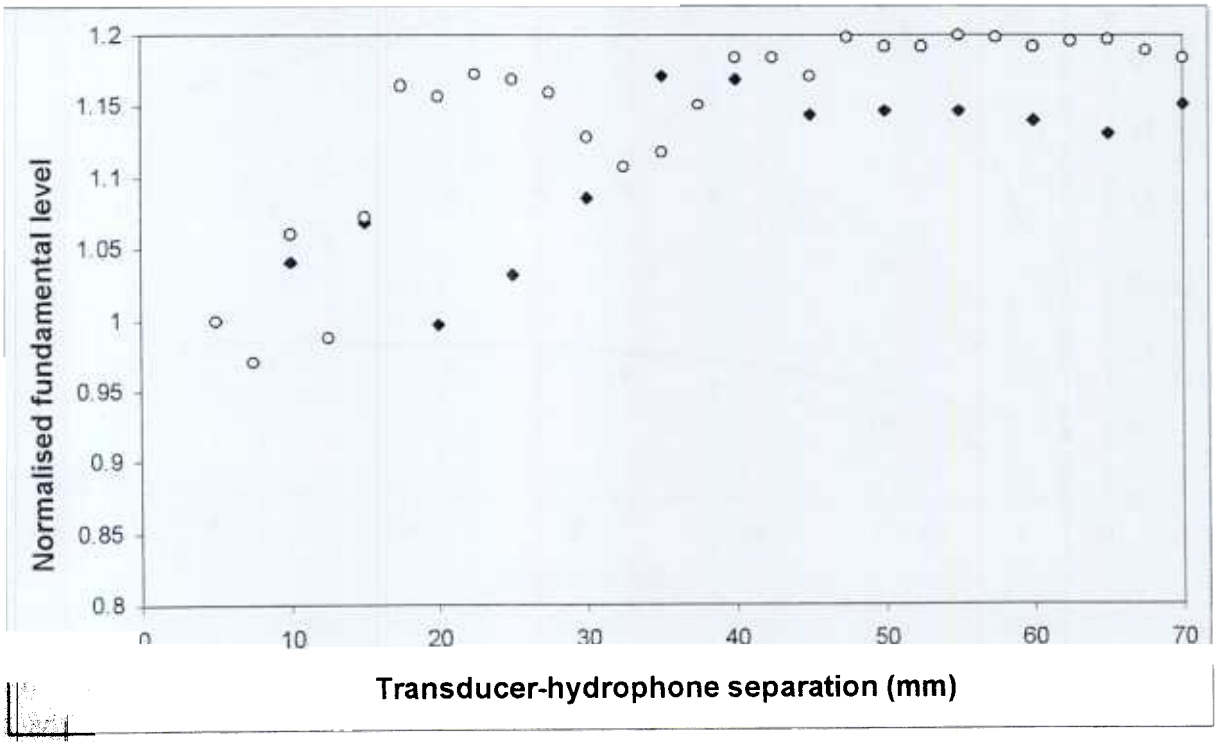


Figure 6.33: Comparison of the axial dependence of the fundamental signal level, determined using the two membrane hydrophones IP010 (♦) and IP901 (o). The transducer was operated in the 'linear' regime at a drive-level setting of 50 mV. Results have been corrected for small signal attenuation and have been normalised to the 5 mm voltage value.

The two hydrophones would appear to indicate a similar dependence for the water corrected fundamental voltage levels, the magnitudes increasing steadily until, at 30 mm, pressures 15% higher are noted. The fundamental signal levels determined at the face in the two cases were: 0.8 mV (IP010) and 4.2 mV (IP901). For the hydrophone IP901, a Precision Acoustics (PA) 28 dB gain amplifier was additionally used after the 55391001 preamplifier to boost the signal level.

As indicated previously, the transducer correction may be established from the acquisition of two low drive waveforms at 5 mm and 70 mm. Assuming simply attenuation (small signal) in water at 10 MHz over the intervening path, then the 10 MHz component of the waveform should decrease to a factor of 0.8528 (taking literature values of the attenuation of ultrasound in water at 21° C). Anything above or below this figure may be ascribed to departures in plane-wave behaviour of the acoustic field.

Table 6.4 represents a compilation of measurements made on the four hydrophones of interest. Values in the table are given for the fundamental signal level determined using the FFT facility of the LeCroy 9450A oscilloscope (frequency resolution of 0.1 MHz). These are given at the two relevant separations and two drive settings.

One of the problems encountered when making these measurements, certainly for the low drive settings, are the small voltage levels and the influence of extraneous electrical or vibrational noise on the measurements. In an attempt to improve measurement signal-to-noise, the output from amplifier 55391001 was coupled to the PA amplifier and a 200 kHz low pass filter was used. As the relative changes in 10 MHz signal level were important, the 20 MHz bandwidth limit on the oscilloscope was also used.

Measurement set, hydrophone	Distance information	Signal level 50 mV drive (mV)	Signal level 700 mV drive (mV)	Derived nonlinear loss	Comments
(1) IP904	At 5 mm At 70 mm Ratio	64.923 57.764 (0.88972)	887.3 574.2 (0.6471)	0.727	55391001/PA amplifier
(2) IP904	At 5 mm At 70 mm Ratio	58.75 56.48 (0.9614)	777 560.4 (0.7212)	0.75	55391001/PA amplifier
(3) IP904	At 5 mm At 70 mm Ratio	2.985 2.286 (0.766)	41.32 24.34 (0.589)	0.769	55391001
(4) IP904	At 5 mm At 70 mm Ratio	4.87 (*) 4.88 (*) (0.98)	31.8695 25.2475 0.7922	0.808	55391001
(5) IP016	At 5 mm At 70 mm Ratio	105.235 94.2 (0.8395)	1,434 918.7 (0.6407)	0.763	55391001/PA amplifier
(6) IP016	At 5 mm At 70 mm Ratio	4.3894 3.8977 (0.888)	61.177 39.566 (0.6468)	0.728	55391001
(7) IP016	At 5 mm At 70 mm Ratio	4.74 3.958 (0.835)	64.549 39.103 (0.606)	0.725	55391001
(8) IP016	At 5 mm At 70 mm Ratio	4.1443 4.0735 (0.9829)	49.744 41.138 (0.827)	0.841	55391001
(9) IP901	At 5 mm At 70 mm Ratio	48.66 45.55 (0.9361)	645.2 458.95 (0.7113)	0.76	55391001/PA amplifier
(10) IP901	At 5 mm At 70 mm Ratio	2.4625 1.9584 (0.7953)	34.164 19.888 (0.5821)	0.732	55391001
(11) IP901	At 5 mm At 70 mm Ratio	1.9635 1.9320 (0.984)	26.538 20.257 (0.7633)	0.776	55391001
(12) IP010	At 5 mm At 70 mm Ratio	41.184 35.840 (0.8703)	558.75 356.87 (0.6387)	0.734	55391001/PA amplifier
(13) IP010	At 5 mm At 70 mm Ratio	43.839 36.969 (0.8433)	573.12 363.71 (0.6346)	0.753	55391001/PA amplifier
(14) IP010	At 5 mm At 70 mm Ratio	too low 1.3846 N/D	6.1472 3.334 (0.5423)	N/D	55391001

(*) Measurements were made at a HP drive setting of 100 mV, due to poor signal-to-noise on 50 mV setting.

N/D Not derivable.

Table 6.4 Compilation of fundamental signal levels acquired at 5 and 70 mm for high and low drive levels. Also presented are figures for the derived nonlinear loss. Details of the amplification chain used for the measurements is given in the text

Some features of Table 6.4 will now be described:-

• The use of the PA amplifier and the resultant improvement in signal-to-noise generates more stable derived nonlinear loss values (0.748 ± 0.015 for the PA and 0.768 ± 0.04, for the amplifier 55391001);

• Taking individual hydrophones, there appears to be some variability regarding the low drive fundamental ratios (given in the third column of the Table). For IP904, the ratios are in the range 0.766 to 0.98. Note that in the former case (Set number 3), the corresponding high drive measurement seems similarly low (0.589) so that the derived nonlinear loss of 0.769 is similar to values derived by Sets 1 and 3. It is not clear what causes this variability, whether it is slight differences in alignment (particularly at the 5 mm separation), or whether the transducer is genuinely operating differently due to changes in temperature or soaking;

• Assuming that the PA amplifier derived results are the most reliable, Table 6.5 below, summarises the 'two-point' transducer imperfection correction, after normalising for the expected attenuation in water between 5 mm and 70 mm.

Hydrophone serial number	'Transducer correction'
IP010	1.02; 0.99
IP016	0.98
IP901	1.10
IP904	1.04; 1.13

Table 6.5: Comparison of the transducer 'corrections' derived for the four hydrophones used within this study, two bilaminars (IP010 and IP016) and two coplanars (IP901 and IP904)

The data set shown in Table 6.5 is fairly limited, so it is difficult to draw any definitive conclusions. It is of concern to the general applicability of the 'magnomic' method that, although tentatively stated, the correction does appear different for different hydrophone types. Bilaminar hydrophones, exhibit a correction which generally appears small (within 2%). By contrast, for coplanar hydrophones, the correction seems to be 10% or so. However, these measurements should be qualified by the fact that even for the same hydrophone, the evaluated 'correction' can display significant variability, as indicated above.

The deviations from plane-wave behaviour clearly provide an important limiting factor relating to the accuracy of the 'magnomic' calibration method. Due to this, a systematic comparison of the axial variation in peak-pressure has been undertaken for each of the hydrophones used in the study, for the pulse excitation used for the 'magnomic' calibrations described in Section 7.

Figure 6.34 reveals this axial variation determined for each of the hydrophones with the transducer operating at low drive (linear) conditions. They illustrate an increase in pressure along the axis out to the calibration position of 70 mm, and are consistent with the beam-plotting measurements presented previously in Section 6.1, although it should be noted that these earlier measurements were carried out using the excitation drive which included the extra cycle.

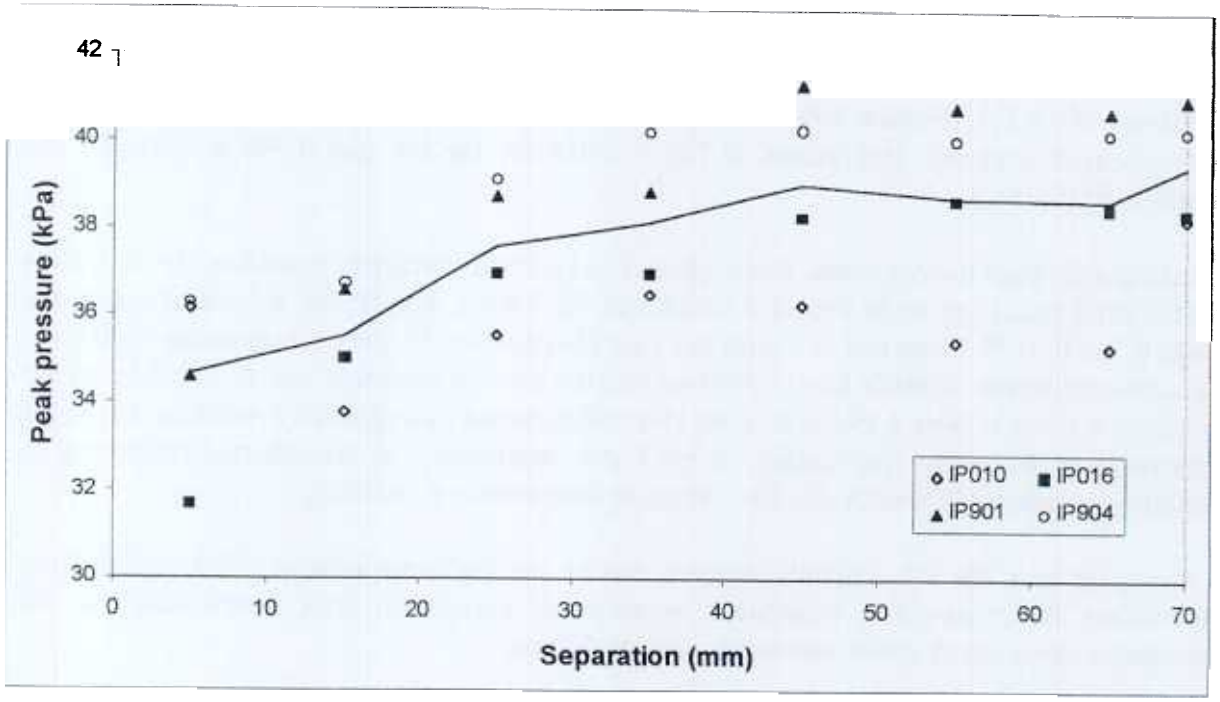


Figure 6.34: Axial-variation in peak-pressure determined using the four hydrophones. Measurements have been made with the 10 MHz transducer operating under low drive conditions (HP setting 50 mV). The full line gives the average pressure at each position, derived from the four hydrophones. Values have been corrected for attenuation in water at 10 MHz. For a true plane-wave, there should be no variation along the axis, the peak-acoustic pressure all along the axis being equal to the value measured close to the transducer face

These axial plots demonstrate a low acoustic pressure, relative to the averaged pressure in the plane, close to the transducer face. This increases in value up to roughly the same level of the averaged pressure with increasing distance from the transducer. Due to the low sensitivity of IP010, peak-pressure measurements made using this hydrophone tend to be more susceptible to noise, and results derived using this device do tend to show a greater spread. Nevertheless, agreement between the four hydrophones is acceptable and they indicate a increase of 13% in the acoustic pressure relative to the value at the transducer face. It is encouraging that all of the devices appear to show the same variation, indicating that it is a property of the acoustic field rather than a device-dependent parameter; a conclusion slightly at odds with that made previously. The other potentially key quantity relevant to calculating the effect of transducer imperfections on 'magnomic' calibrations is the average pressure increase along the axis from 5 mm to 70 mm. From the mean dependence portrayed in Figure 6.34, this corresponds to 1.09 times the pressure at the face.

Figure 6.35 shows the variation in the fundamental level derived from waveform acquisitions carried out at each position along the axis. Again, results are presented for all four hydrophones and these have been normalised to the fundamental signal level determined at a separation of 45 mm. Results are broadly in line with those shown for peak pressures in Figure 6.34, as expected, although they do seem to indicate a small decrease in the fundamental level of roughly 5% from 45 mm out to 70 mm.

It should be noted that although results were derived under different excitation conditions, the variation shown in Figure 6.35 is consistent with that presented in Figure 6.32, another encouraging factor which indicates that the variation is real and is a consequence of the manner in which the transducer surface vibrates.

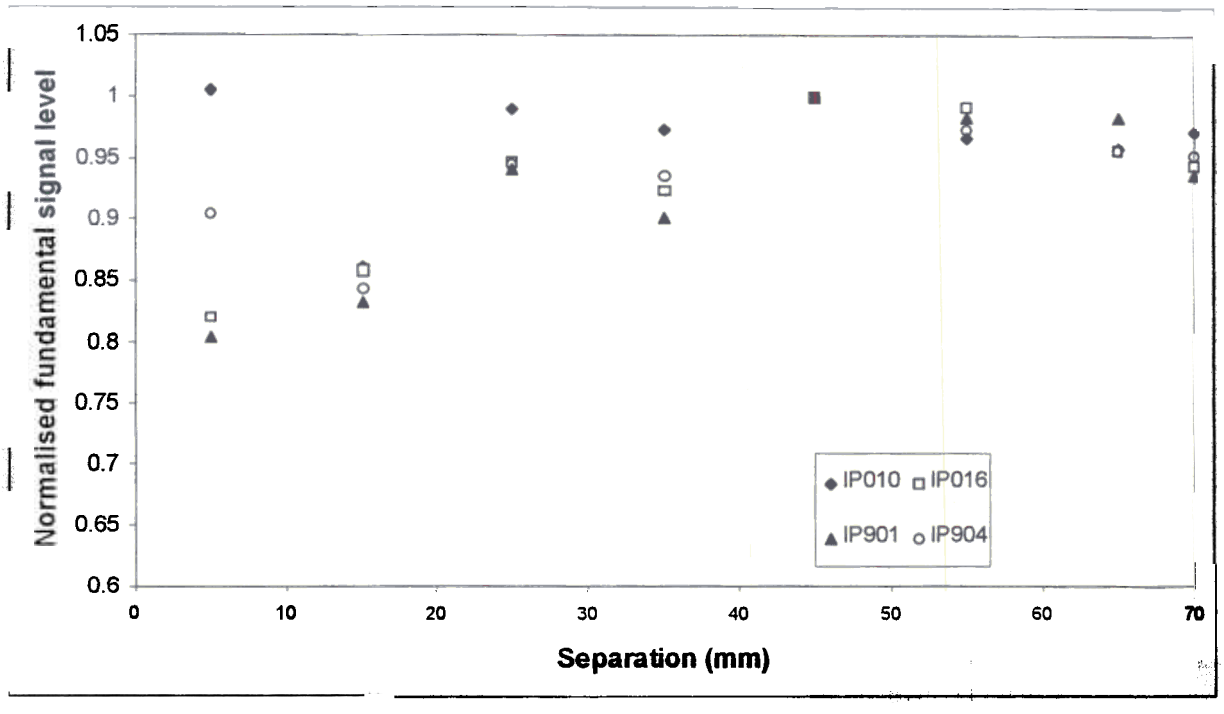


Figure 6.35 Variation in the fundamental signal level determined along the axis of the 10 MHz transducer derived using four hydrophones from FFT's obtained from waveform data. Signal level values have been normalised to their values obtained at a separation of 45 mm

6.4.2 Drive setting behaviour for the axial dependence of the fundamental signal level

It is clearly of interest to investigate the way in which the fundamental level varies with the axial position in the field, for higher drive voltages. It is tacitly assumed in the 'magnomic' method that the low amplitude correction is still valid at the higher applied drives. The axial variation of the fundamental level is shown in Figure 6.36, for two of the three drive voltage levels (200 mV and 700 mV), in addition to the low drive conditions which have already been displayed in Figure 6.33. All have been derived using the hydrophone IP010. Each individual set was obtained by repeating the alignment procedure described in Section 5.6.1. The fundamental values were derived through FFT's carried out on the waveforms acquired at each position. Again, the fundamental is defined as the peak in the response at each position.

Whilst the two higher drive levels clearly display nonlinear decay from 40 mm onwards, there are no obvious similarities between the four curves. However, one striking feature which is common to the higher drive setting curves is the rapid fall off in the level of the fundamental close to the transducer, which is of the order of 20% to 30%.

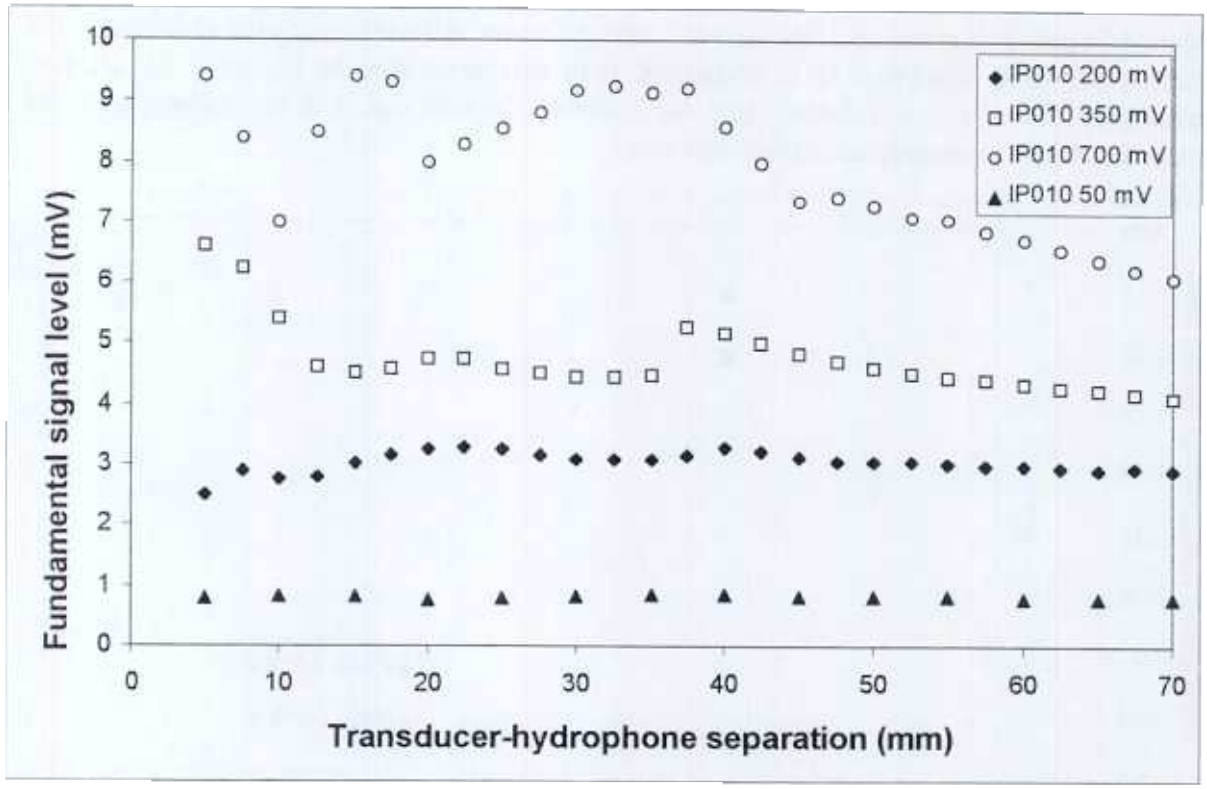


Figure 6.36: Variation in the fundamental signal level determined using the 0.2 mm active element hydrophone IP010 for four drive settings of the 10 MHz transducer. Waveform acquisitions have been completed at each of the positions and the fundamental content of the signal derived following through an FFT of the relevant truncated waveform

6.5 THE EFFECT OF DECONVOLUTION

In Section 6.3.2, the measured nonlinear loss derived using the 75 mm active element hydrophone, IP002, was used to compute the pressure being generated at the transducer face. This implicitly assumed that the waveform acquired at the face of the transducer is an accurate representation of the true acoustic waveform which is strictly only true if the sensitivity of the hydrophone is flat over the frequency range of interest, typically between 5 and 15 MHz. Whilst this may be appropriate for the wider bandwidth hydrophones used in this study such as IP901, IP904, IP010 and IP016, it is less likely to be the case for the 75 mm active element hydrophone, IP002, whose overall film thickness of 50 μm produces a resonance at 20 MHz. To investigate this, the measured waveform at 5 mm was deconvolved with the response of the hydrophone to generate the 'true' acoustic waveform, the two being compared in Figure 6.37.

The 'true' acoustic waveform has been propagated to a separation of 70 mm using the Mitome routine and scaled to generate the observed nonlinear loss of 0.755. This has required the use of a peak pressure of 0.636 MPa, 6% higher than the value derived through taking the hydrophone waveform indicated in Section 6.3 directly . The difference arises due to quite subtle changes in the shape of the spectrum. This slight modification does not alter the general conclusions of Section 6.3 concerning the modelling of the behaviour of the 75 mm hydrophone.

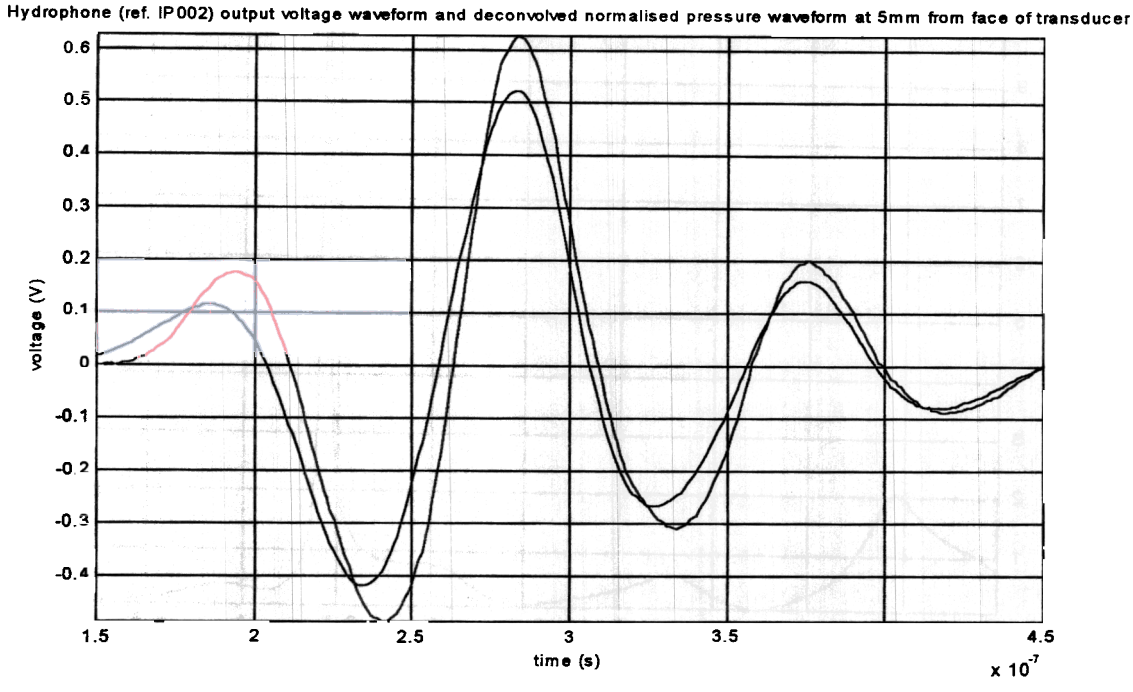


Figure 6.37: Normalised pressure obtained by deconvolution of voltage waveform at 5 mm from the face of transducer using the theoretical hydrophone response normalised for 10 MHz value (–) and the voltage measured 5 mm from transducer face (–), derived for hydrophone IP002. The absolute pressure at the separation of 5 mm has been matched to produce a nonlinear loss at 70 mm of 0.755. This yields a peak-pressure value of 0.636 MPa

It is also of interest to investigate the effect of deconvolution on waveforms propagated using the Mitome routine for some of the other hydrophones used within this study. First, Figure 6.38 illustrates the theoretical response calculated for the 9 μm bilaminar hydrophone IP016, in the way described in Appendix D.

This response, coupled with that of the amplifier, has been used to deconvolve the hydrophone waveform acquired at 5 mm, to derive the true acoustic waveform. This has then been propagated using the Mitome routine to the 70 mm position and compared with the propagated (non-deconvolved) hydrophone waveform to investigate the influence of variations in the response of the hydrophone over the bandwidth of the acoustic pulse. The two waveforms are compared directly in Figure 6.39. It can be seen that the agreement is very good, indicating that, certainly to a first order, variations in the sensitivity of the hydrophone have a small effect on the propagated waveform.

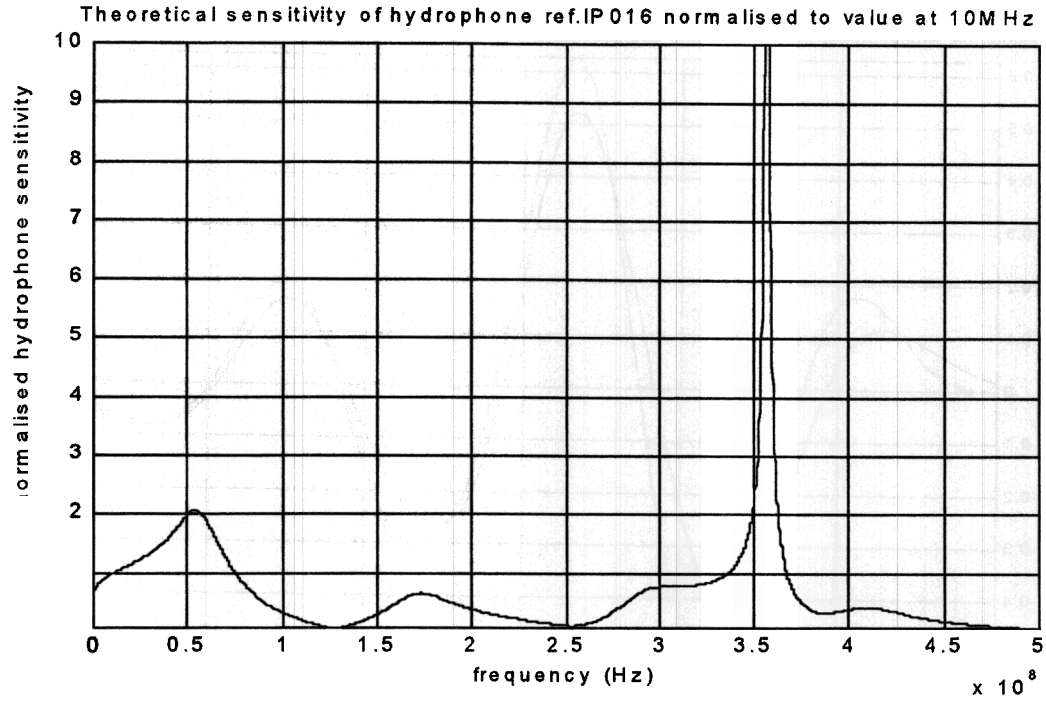


Figure 6.38: Theoretical response for the hydrophone IP016 normalised to the value at 10 MHz.

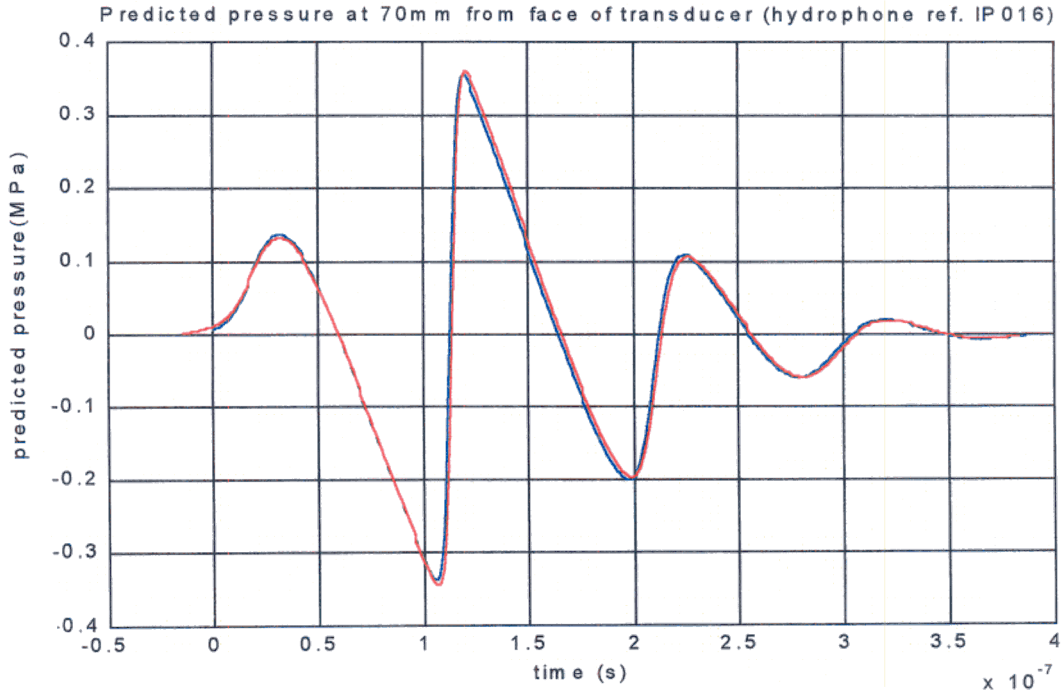


Figure 6.39: Predicted pressure at 70 mm from face of transducer obtained by scaling the initial voltage using the known hydrophone sensitivity at the fundamental frequency (–) and by deconvolving the initial voltage waveform with the theoretical hydrophone sensitivity (–), for the bilaminar hydrophone IP016

7 RESULTS - 'MAGNOMIC' CALIBRATIONS

Prior to the presentation of the calibration results, some aspects critical to the calibration process will be described and studies, which investigate their influence, presented. These study areas relate to the positioning of the hydrophone in the acoustic field and investigations of the repeatability of waveform acquisition.

7.1 INVESTIGATION OF WAVEFORM ACQUISITION REPEATABILITY

It is of interest to compare waveforms acquired at given drive levels for various hydrophones. By normalising the waveforms to their respective maxima and comparing their overall shapes, the repeatability of the waveform acquisition process can be assessed. In the first instance, it will be assumed that each hydrophone has a flat frequency response as well as linear phase over the frequency content of the voltage waveforms acquired at 5 mm from the face of the transducer. This is justifiable considering the limited frequency content of the pulses acquired close to the transducer face. However, it is acknowledged that strictly a deconvolution of the measured voltage waveform with the transfer function of the hydrophone-amplifier combination should be carried out to derive the true acoustic waveform.

Waveforms acquired 5 mm from the face of the transducer will be considered first, as they form an important part of the 'magnomic' calibration process. In total, the five hydrophones listed in Section 6 have been used to complete the acquisitions.

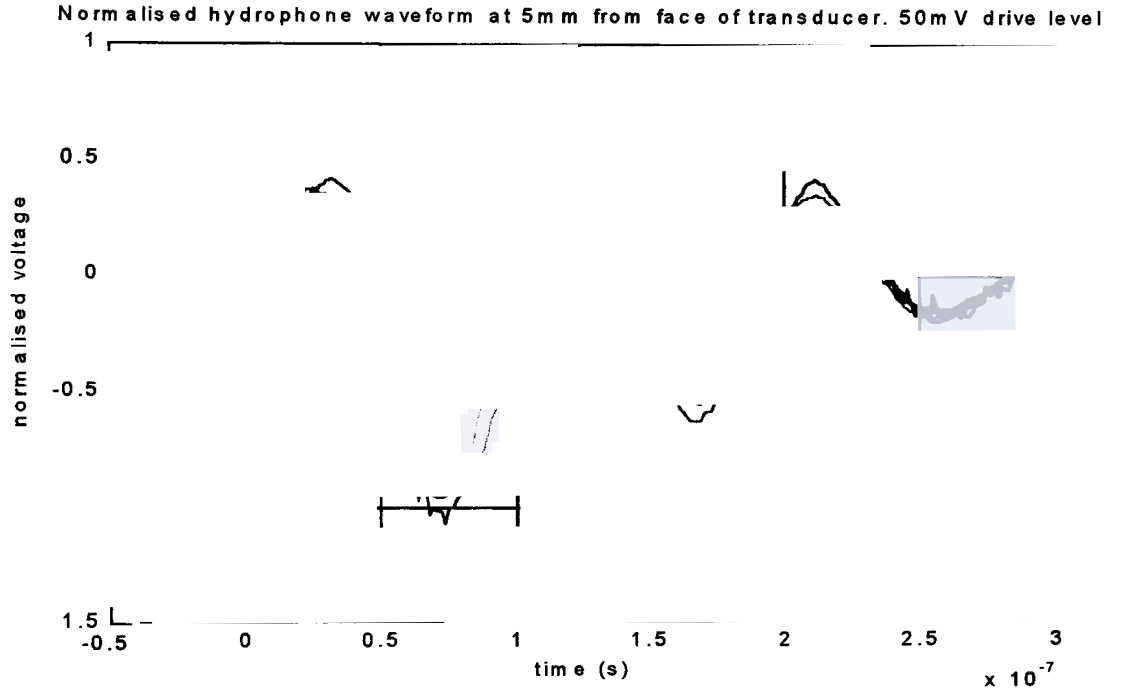


Figure 7.1: Voltage waveforms acquired 5 mm from face of the 10 MHz transducer derived using various hydrophones, for the 50 mV drive level. Hydrophones used: — IP010, — IP016, — IP901, — IP904, — IP002

Both Figures 7.1 and 7.2 show that the agreement between the waveforms measured at the face of the transducer is not always as anticipated. This may arise due to alignment problems. As noted in Section 6.1, significant structure in the pressure amplitude distribution exists close

to the transducer face, and the variability of the waveform acquisition embodied in Figures 7.1 and 7.2 may reflect differences in amplitude or phase produced by slight variations in the positioning of the hydrophone. It is also tentatively noticeable, particularly in Figure 7.2, that coplanar hydrophones appear to have a subtly different response to bilaminars, especially noticeable, due to the way the normalisation has been carried out, in the region of the peak-negative pressure.

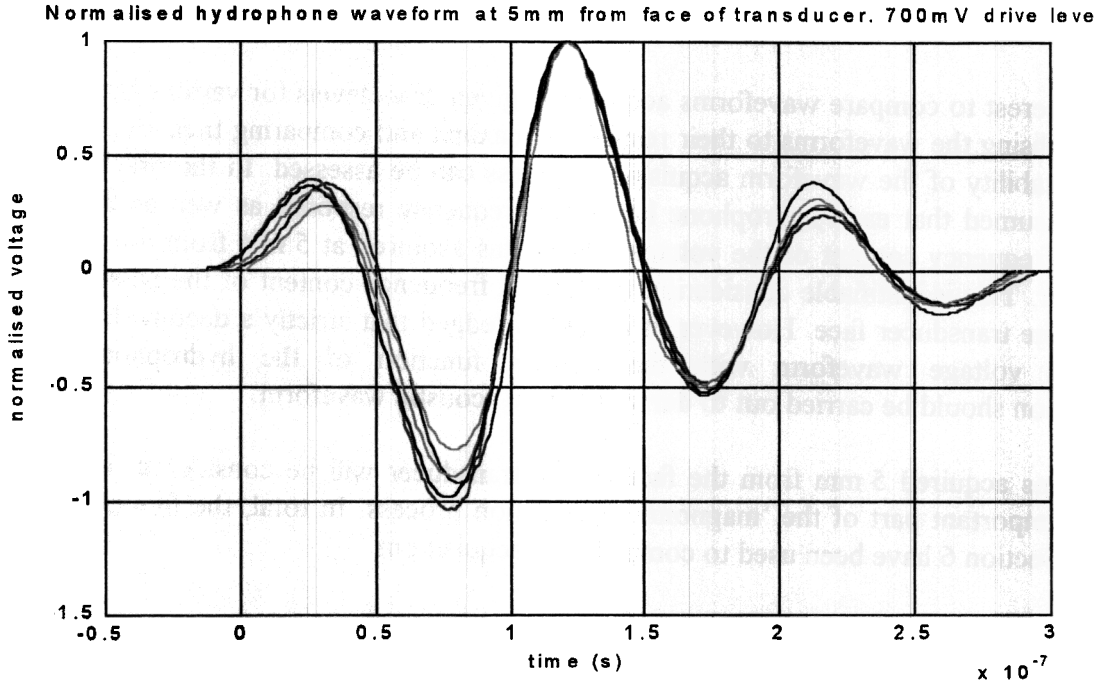


Figure 7.2: Voltage waveforms acquired 5 mm from face of the 10 MHz transducer derived using various hydrophones, for the 700 mV drive level. Hydrophones used: — IP010, — IP016, — IP901, — IP904, — IP002

A second aspect of the repeatability of the measurement process relates to waveform acquisition for a particular hydrophone at each of the two positions of the acoustic field used for the calibration. This is investigated in Figures, 7.3 to 7.10, where the repeatability of re-positioning and acquisition is assessed following the initial process, described in Section 5.6.1, whereby the beam-alignment axis of the transducer is first established. It should be noted that these acquisitions were completed using the earlier power amplifier and therefore exhibit an additional cycle.

Although these waveforms were never used for 'magnomic' calibrations the comparisons serve a useful purpose as they illustrate the repeatability of the waveform acquisition which can realistically be achieved. It can be seen that, in general, this is very good, although variations can sometimes occur (see Figure 7.5 for the hydrophone IP901). The origin of this is unclear, it appears not to be related to the stability of the hydrophone as later measurements, carried out using the alternative calibration drive amplifier, did not show this effect. As a general statement, alignment and positioning of the hydrophone tends to be easier at 70 mm where the field distribution is broader (more closely approaching a plane-wave).

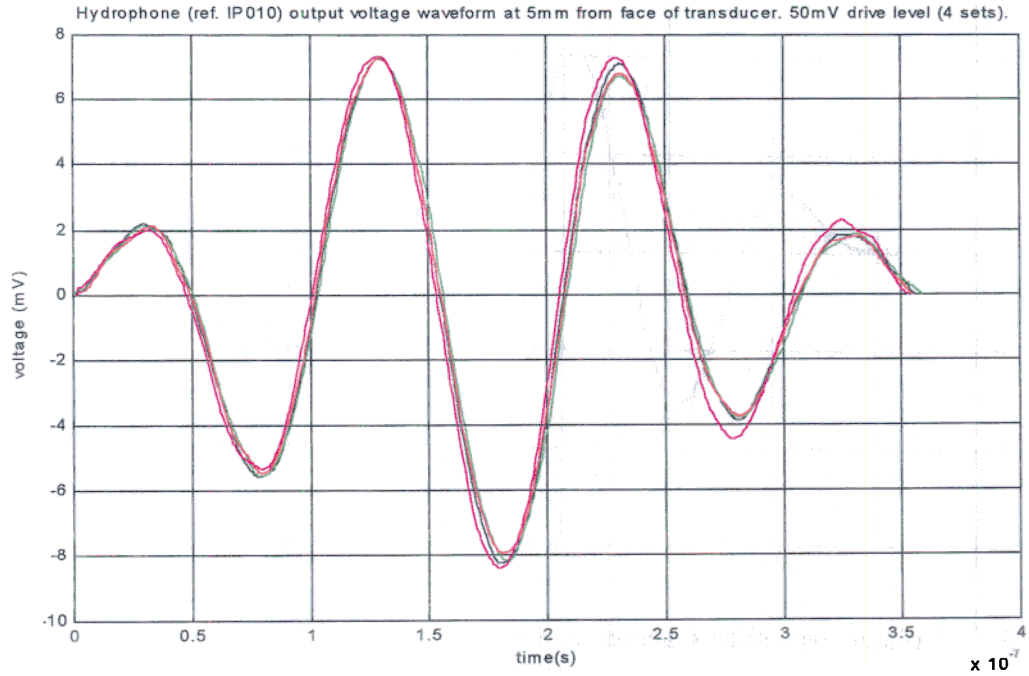


Figure 7.3: Voltage waveforms acquired at 5 mm from face of the 10 MHz transducer (4 repeated acquisitions, 50 mV drive level, for hydrophone IP010)

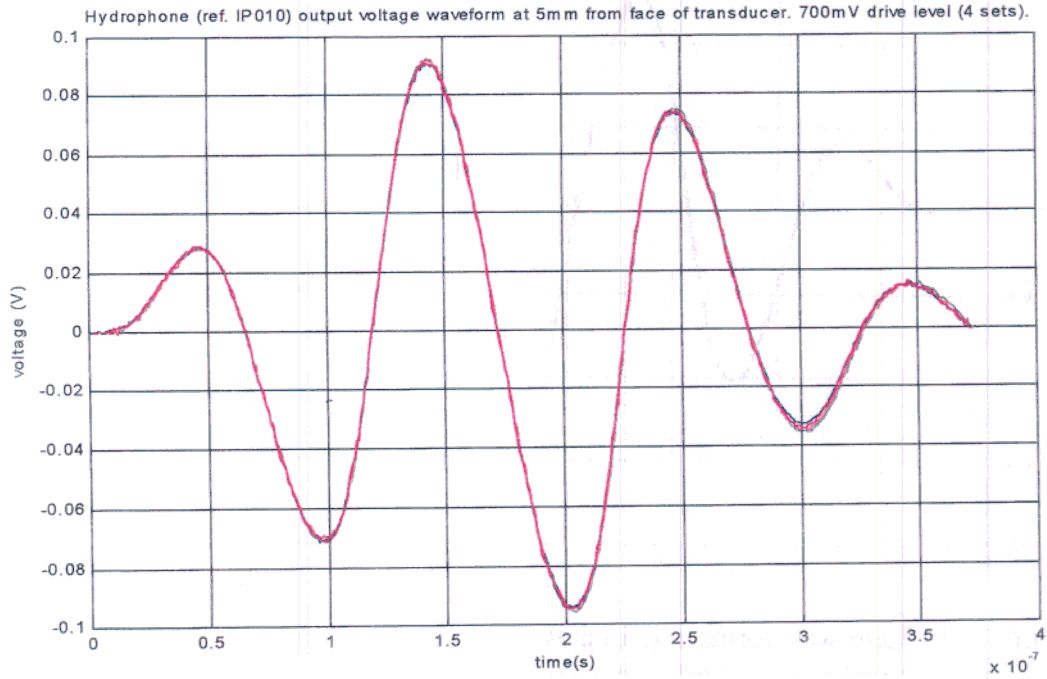


Figure 7.4: Voltage waveforms acquired 5 mm from face of the 10 MHz transducer (4 repeated sets, 700 mV drive level, for hydrophone IP010)

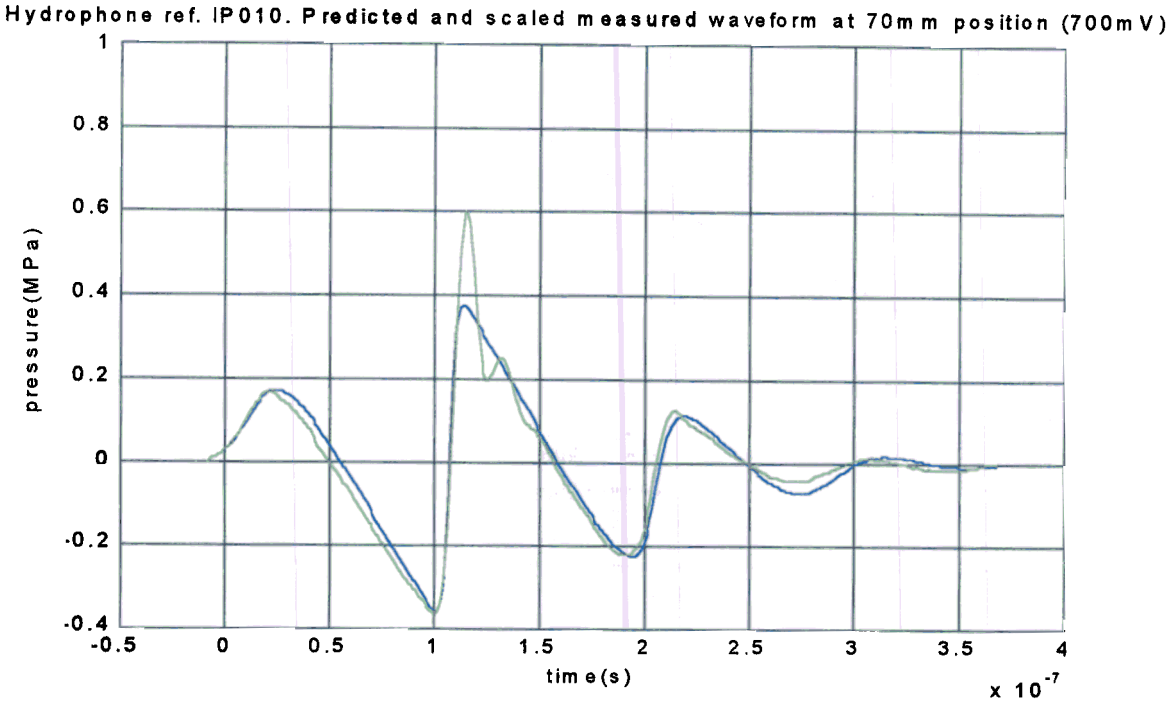


Figure 7.15: Predicted pressure (–) and scaled measured voltage waveform (–) determined at 70 mm from the transducer face for the 700 mV drive level using hydrophone IP010. The predicted waveform was derived using Method 1

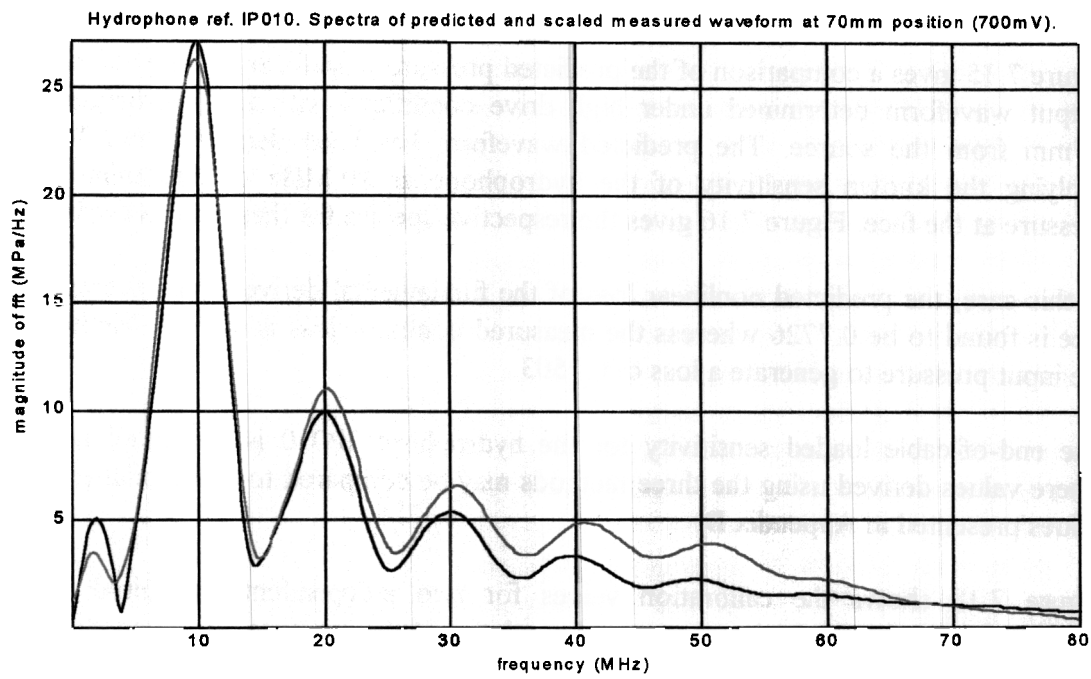


Figure 7.16 Predicted amplitude spectrum (–) and the scaled measured spectrum (–) derived from the hydrophone output voltage determined at 70 mm from face of transducer, at the 700 mV drive level for hydrophone IP010. The spectra were derived from the two waveforms shown in Figure 7.15

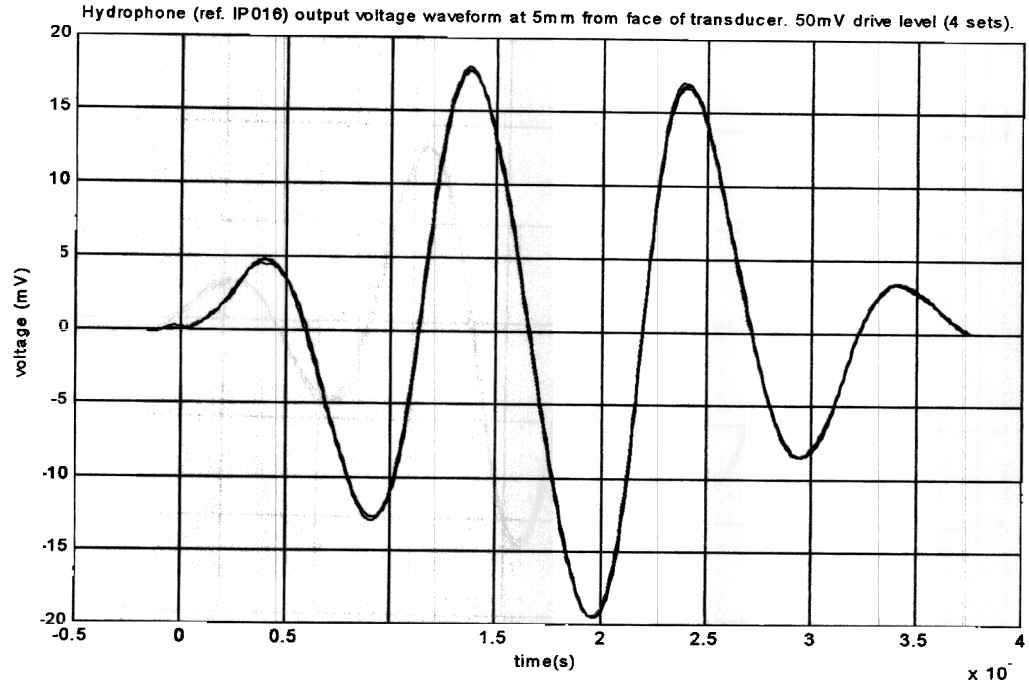


Figure 7.7: Voltage waveforms acquired 5 mm from face of the 10 MHz transducer (4 repeated sets, 50 mV drive level, for hydrophone IP016)

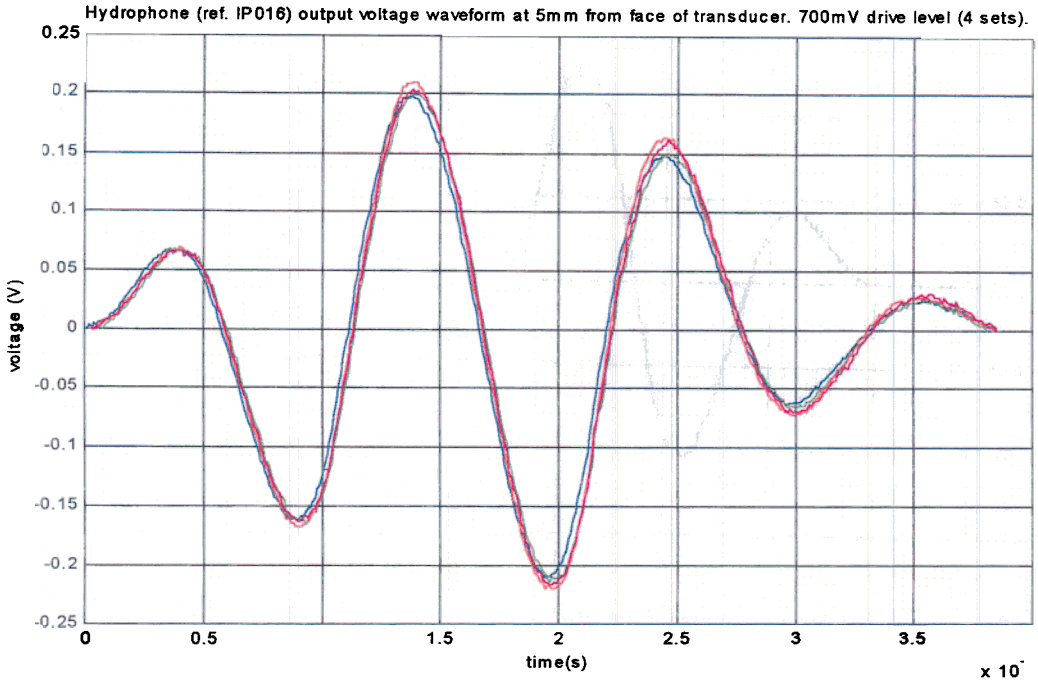


Figure 7.8: Voltage waveforms acquired 5 mm from face of the 10 MHz transducer (4 repeated sets, 700 mV drive level, for hydrophone IP016)

In this case, the predicted nonlinear loss of the fundamental derived from the pressure at the face is found to be 0.798 whereas the measured nonlinear loss is 0.778. Method 2 matches the input pressure to generate a loss of 0.778.

The end-of-cable loaded sensitivity of the hydrophone IP016 is presented in Figure 7.13 where values derived using the three methods may be compared to a compilation of reference values presented in Appendix B.

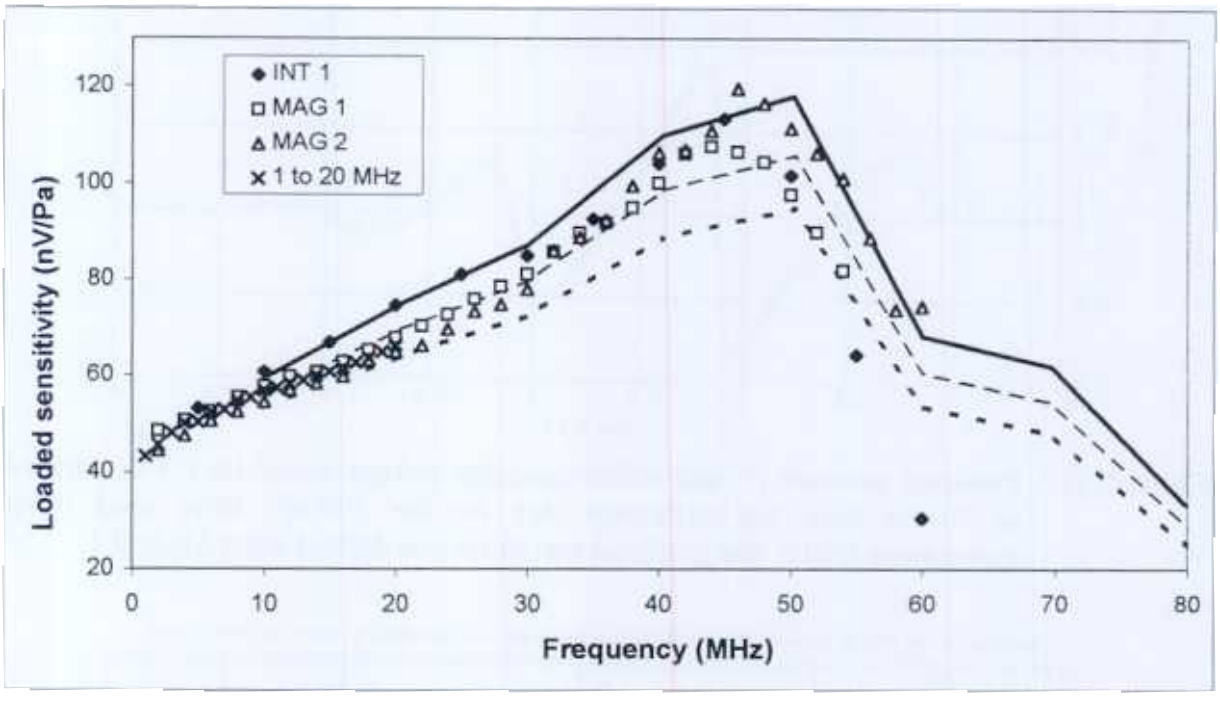


Figure 7.13: Estimated hydrophone sensitivity (continuous line) derived during the current study for hydrophone IP016 compared with reference values tabulated in Appendix B. These originate from previous "magnomic" work (labelled MAG1 and MAG 2), interferometer (INT) and conventional 1 to 20 MHz based calibration methods. Also shown in the figure are the results derived from Methods 2 (long dashes) and 3 (short dashes).

Figure 7.14 shows the calibration values for two independently acquired sets of data, calculated using Method 1, i.e. through a knowledge of the pressure being generated at the face of the transducer.

'magnomic' derived calibrations described in detail in Section 7.2. Note the significant variations between the two sets, in the range 5% to 18% for the low drive measurements and 1% to 17% for the high drive measurements. The two IP901 sets show the greatest difference. However, this variability will not affect the application of the 'magnomic' method as the four waveforms are acquired together, over a short-time without realigning the transducer-hydrophone. It is therefore short-term stability which is more important.

	Hydrophone IP010	Hydrophone IP016	Hydrophone IP901	Hydrophone IP904
Peak-pressure, Set 1 (kPa)	37.3	34.0	33.6	36.9
Peak-pressure, Set 2 (kPa)	30.6	32.0	33.7	33.6

Table 7.1: Peak pressures determined 5 mm from face of the 10 MHz transducer obtained by scaling the voltage waveforms using the known sensitivity of the hydrophone at the fundamental frequency (for 50 mV drive level)

	Hydrophone IP010	Hydrophone IP016	Hydrophone IP901	Hydrophone IP904
Peak-pressure Set 1 (MPa).	0.538	0.485	0.449	0.515
Peak-pressure Set 2 (MPa).	0.521	0.428	0.471	0.489

Table 7.2: Peak-pressures determined 5 mm from face of the 10 MHz transducer obtained by scaling the voltage waveforms using the known sensitivity of the hydrophone at the fundamental (for 700 mV drive level)

7.2 'Magnomic' hydrophone calibration

7.2.1 Overall description

Within the analysis of calibration methods presented here, a number of methods will be presented. The first three of these all assume that the transducer behaves as a perfect plane-piston, producing a plane-wave over the particular aperture plane of interest. The final Section deals briefly with deviations from plane-wave behaviour of the acoustic field, termed transducer imperfections, and how these might be included in the calibration process.

First, the three methods used to derive 'magnomic' calibrations will be described, and these are distinguished by the way in which the experimental data is analysed, as follows:

Method 1 Using the known sensitivity of the hydrophone at 10 MHz

It is assumed that the pressure waveform at the face of the transducer may be obtained by simply dividing the voltage by the known sensitivity of the hydrophone at 10 MHz (taken from the reference values presented in Appendix B). Two waveforms are acquired under high drive (700 mV) conditions, one at 5 mm and one at 70 mm from the face of the transducer. The 5 mm waveform is converted from voltage to pressure and is propagated using the algorithm described in Section 4, to the 70 mm position. The spectral components of the hydrophone output voltage waveform are then divided by the frequency components of the predicted acoustic waveform to yield the hydrophone response (after adjusting for the amplifier gain). Note that this division is only carried out at local frequency maxima, as significant problems with signal-to-noise ratio may occur for other points.

Method 2 Matching predicted and measured losses in the fundamental magnitude

This method does not assume a value for the sensitivity of the hydrophone at 10 MHz. Rather, it takes the measured nonlinear loss in the fundamental between the two positions 5 mm and 70 mm, after correction for absorption in water. It then scales the pressure of the waveform acquired close to the face in such a way that, following propagation of the waveform to 70 mm, this nonlinear loss is matched. Once this is achieved, propagated spectra and measured spectra are again compared to derive the frequency dependent sensitivity of the hydrophone.

Method 3. Applying the nonlinear loss derived from the 75 mm diameter hydrophone, IP002

In Method 2, it is assumed that the measured nonlinear loss is accurately determined. However, from the work carried out on the 75 mm bilaminar hydrophone in Section 6.3, we know that the nonlinear loss at a drive level of 700 mV is 0.755 (although this loss is measured over a much larger aperture). In Method 3, the voltage waveform obtained at 5 mm is scaled so that, following propagation and correction for water attenuation, the predicted nonlinear loss is 0.755, equal to the 75 mm hydrophone derived result. Once this is achieved, the propagated spectra and measured spectra are again compared to derive the frequency dependent sensitivity of the hydrophone.

Each of these methods will be applied to the four reference hydrophones in turn, with plots of predicted and measured waveforms and spectra being presented for Method 1. Values of sensitivity derived for these hydrophones using each method will then be compared with a summary of the reference values presented in Appendix B. Derived sensitivities will be presented for two independent calibration runs, labelled Set 1 and Set 2, but using only the Method 1 analysis.

7.2.2 Hydrophone IP016

Figure 7.11 gives a comparison of the predicted pressure waveform and the actual hydrophone output waveform determined under high drive conditions with the hydrophone positioned 70 mm from the source. The predicted waveform has been derived using Method 1, by applying the known sensitivity of the hydrophone at 10 MHz to determine the acoustic pressure at the face. Figure 7.12 gives the respective spectra for these two waveforms.

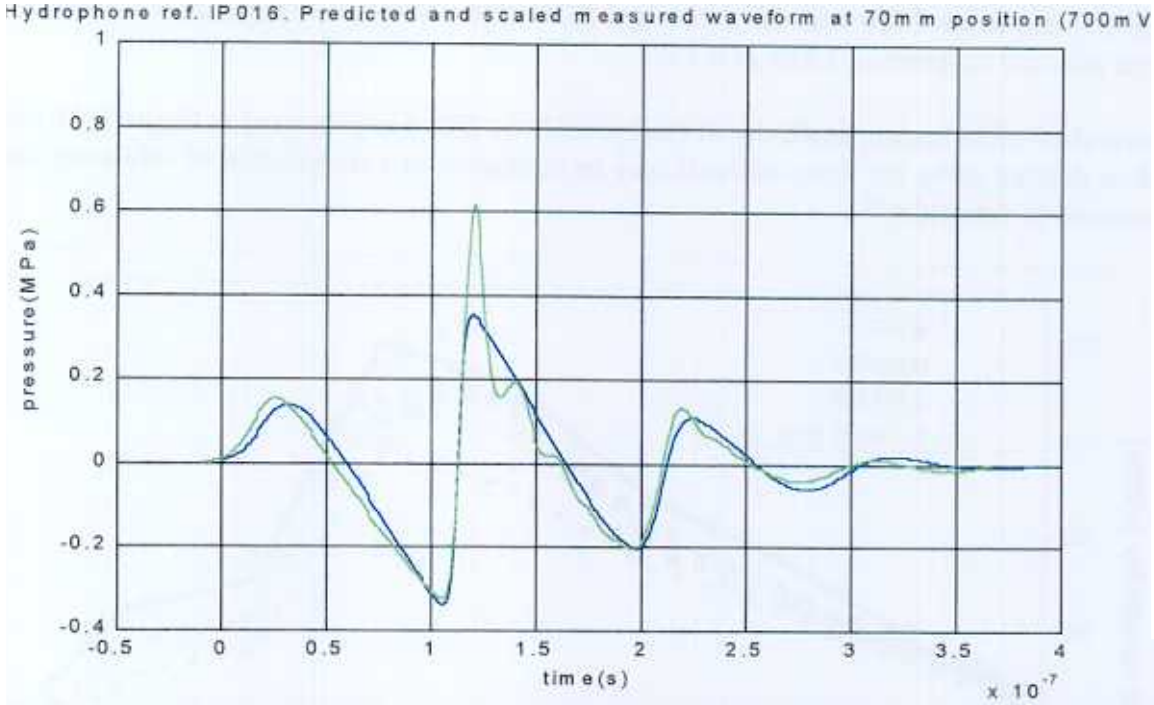


Figure 7.11: Predicted pressure (–) and scaled measured voltage waveform (–) determined at 70 mm from the transducer face for the 700 mV drive level using hydrophone IP016. The predicted waveform was derived using Method 1

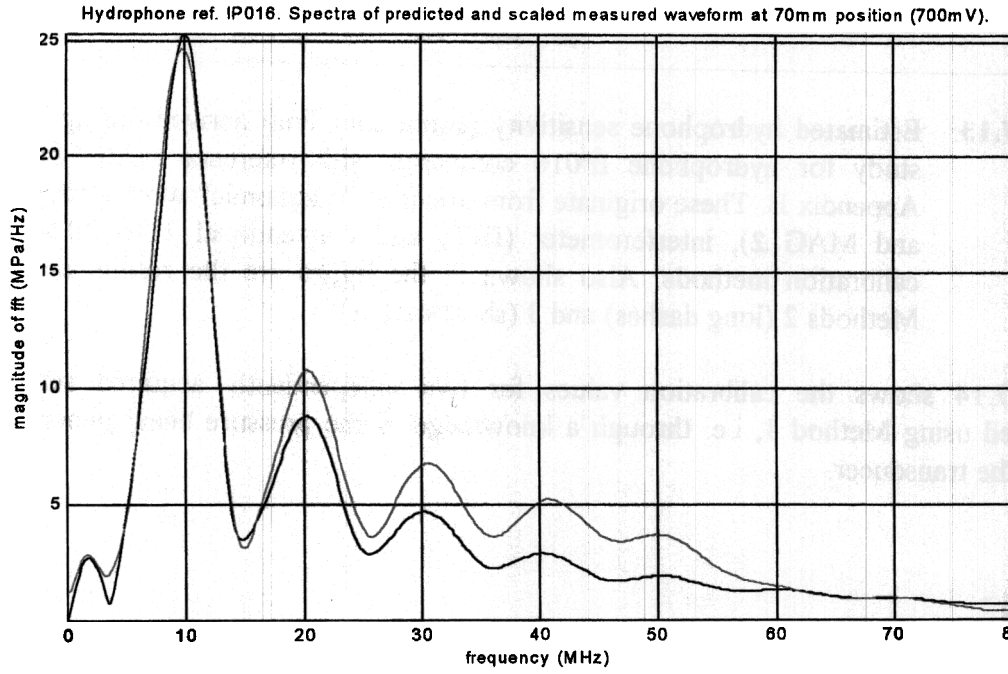


Figure 7.12: Predicted amplitude spectrum (–) and the scaled measured spectrum (–) derived from the hydrophone output voltage determined at 70 mm from face of transducer, at the 700 mV drive level for hydrophone IP016. The spectra were derived from the two waveforms shown in Figure 7.11

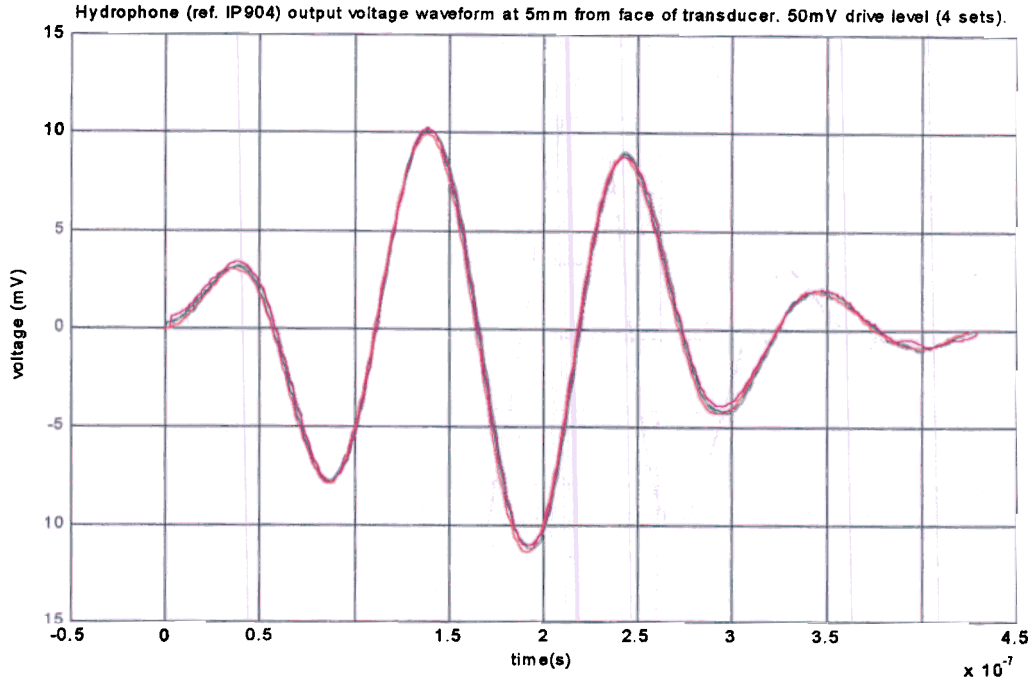


Figure 7.9: Voltage waveforms acquired 5 mm from face of the 10 MHz transducer (4 repeated sets, 50 mV drive level, for hydrophone IP904)

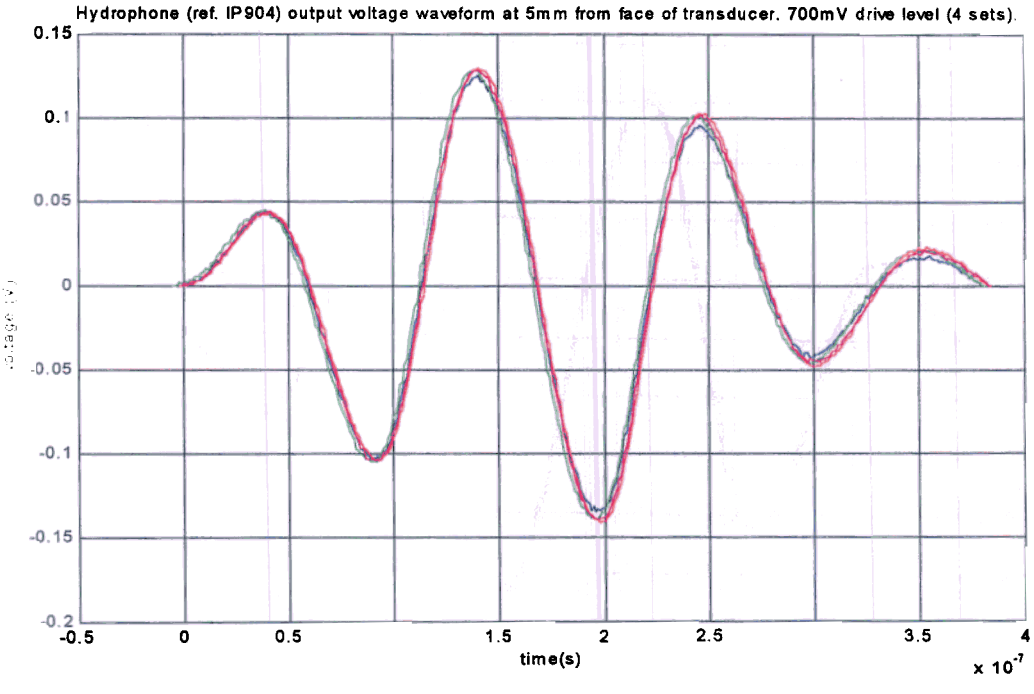


Figure 7.10: Voltage waveforms acquired 5 mm from face of 10 MHz transducer (4 repeated sets, 700 mV drive level, for hydrophone IP904)

The peak-pressures determined using the various hydrophones, all determined at a transducer-hydrophone separation of 5 mm, are summarised in Tables 7.1 and 7.2. Two independent sets of data are presented, the resultant variation being characteristic of the whole data acquisition process, including the ability to consistently establish the beam-alignment axis. Note that the pressures shown in Tables 7.1 and 7.2 were derived from the waveforms actually used for the

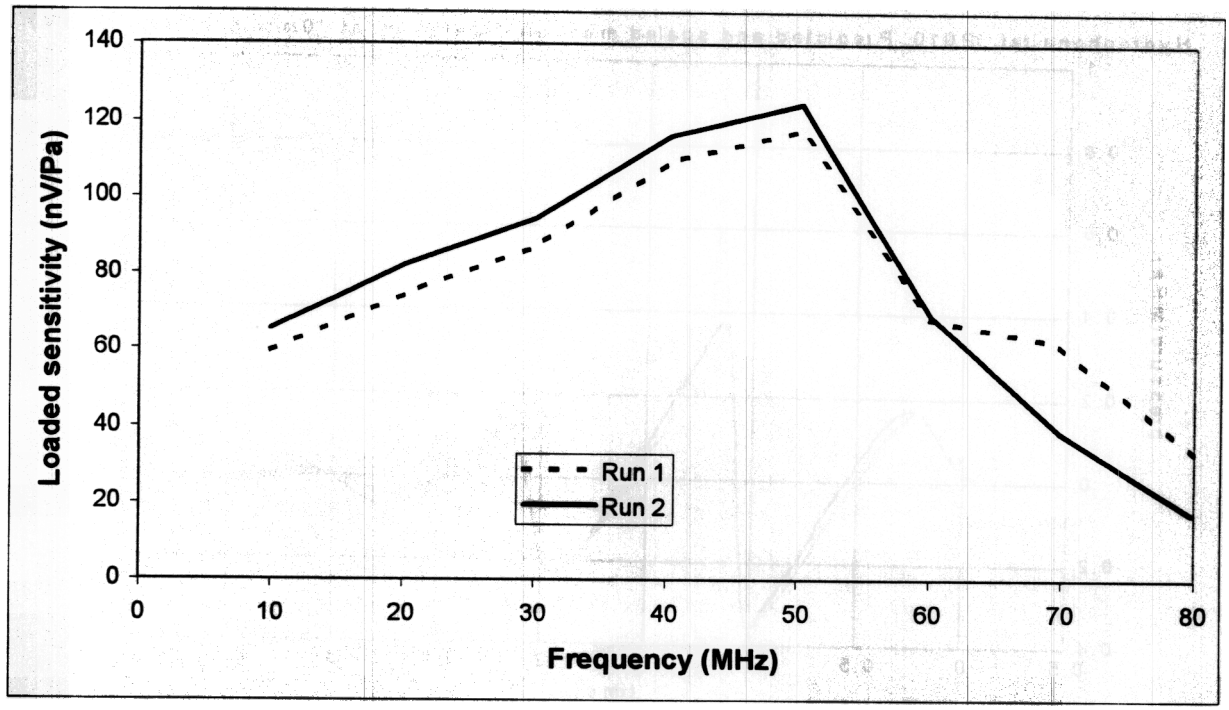


Figure 7.14: Comparison of two independent runs for the hydrophone IP016, using the Method 1 analysis

7.2.3 Hydrophone IP010

Figure 7.15 gives a comparison of the predicted pressure waveform and the actual hydrophone output waveform determined under high drive conditions with the hydrophone positioned 70 mm from the source. The predicted waveform has been derived using Method 1, by applying the known sensitivity of the hydrophone at 10 MHz to determine the acoustic pressure at the face. Figure 7.16 gives the respective spectra for these two waveforms.

In this case, the predicted nonlinear loss of the fundamental derived from the pressure at the face is found to be 0.7726 whereas the measured nonlinear loss is 0.7503. Method 2 matches the input pressure to generate a loss of 0.7503.

The end-of-cable loaded sensitivity for the hydrophone IP010 is presented in Figure 7.17 where values derived using the three methods may be compared to a compilation of reference values presented in Appendix B.

Figure 7.18 shows the calibration values for two independently acquired sets of data, calculated using Method 1 i.e. through a knowledge of the pressure being generated at the face of the transducer.

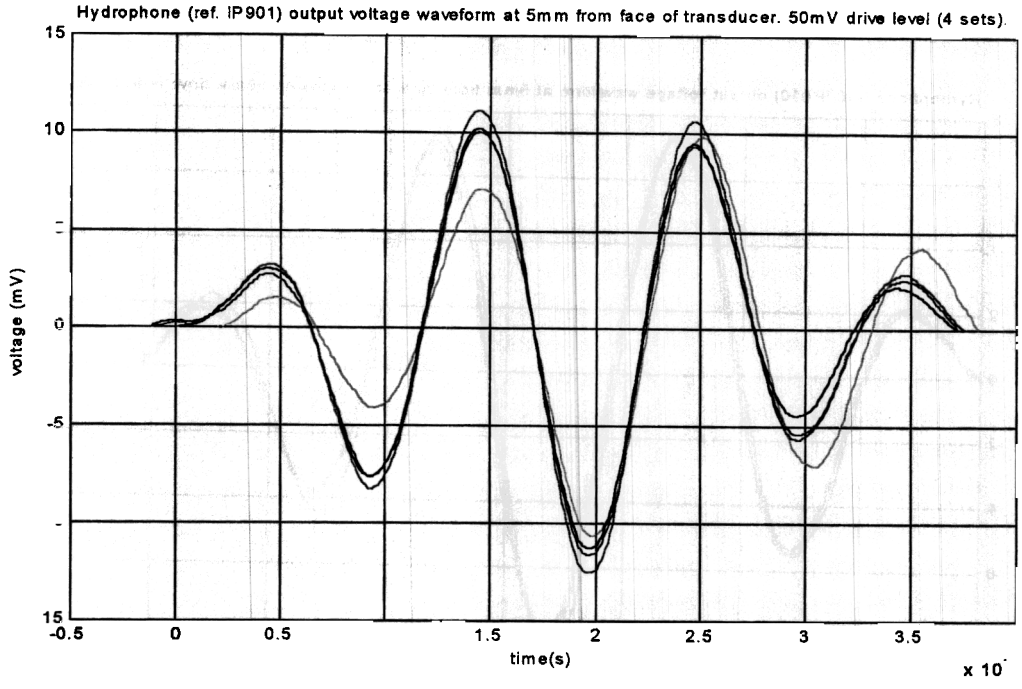


Figure 7.5 Voltage waveforms acquired 5 mm from face of the 10 MHz transducer (4 repeated sets, 50 mV drive level, for hydrophone IP901)

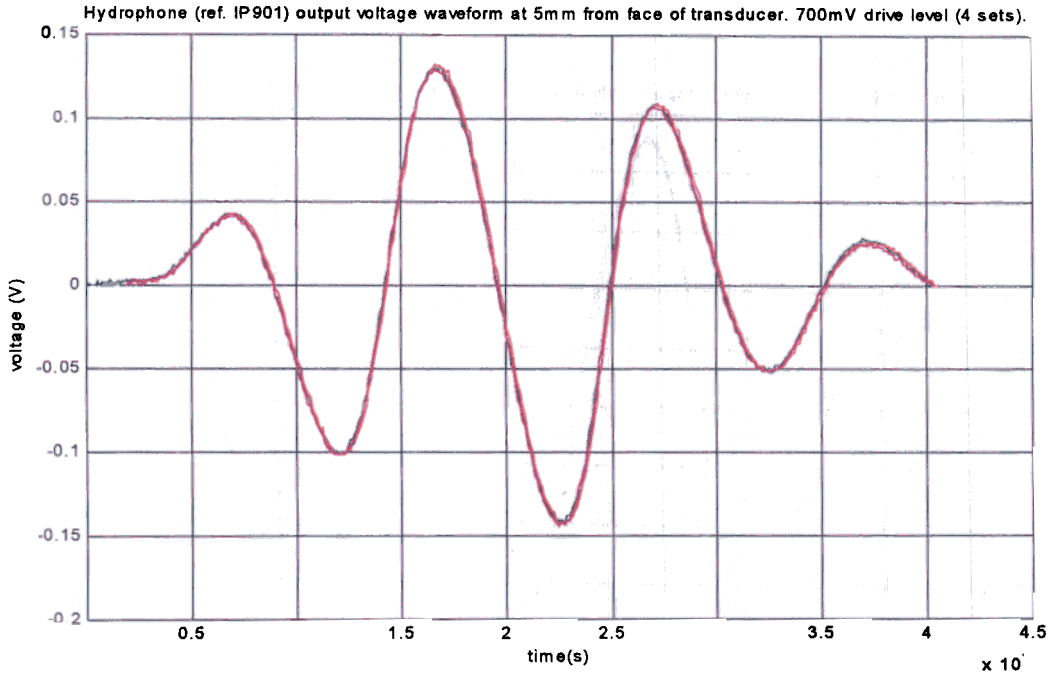
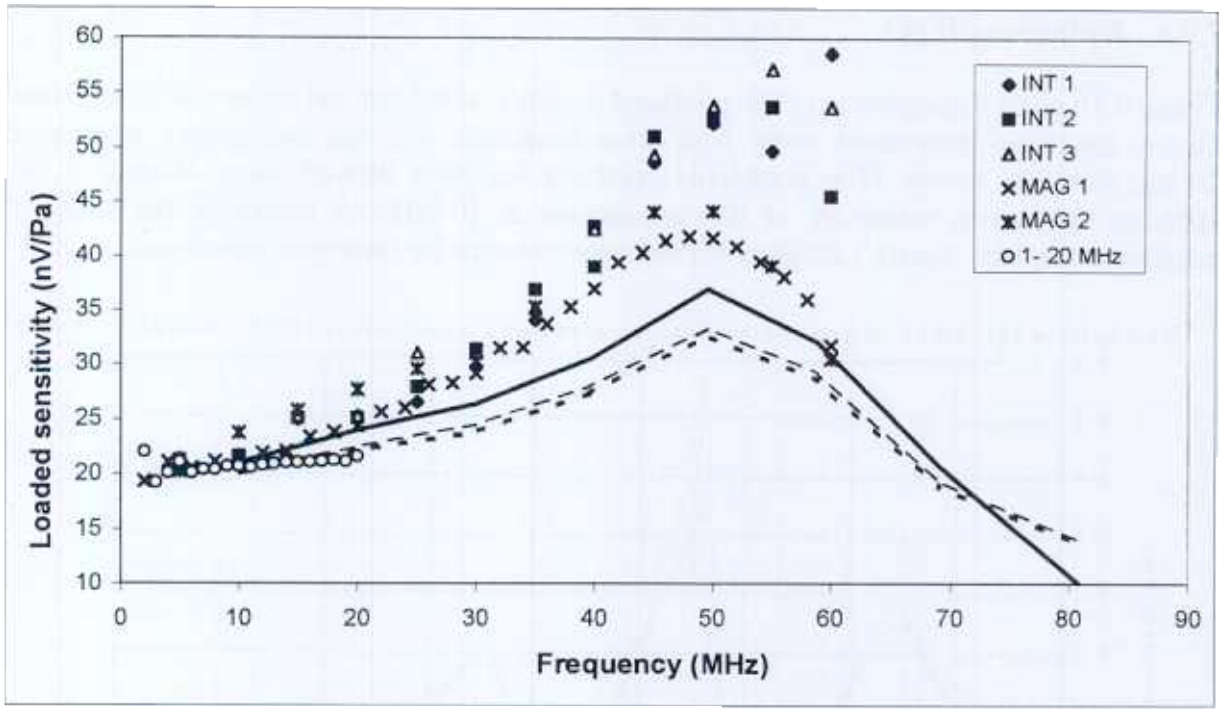


Figure 7.6: Voltage waveforms acquired at 5 mm from face of the 10 MHz transducer (4 repeated sets, 700 mV drive level, for hydrophone IP901)



Estimated hydrophone sensitivity (continuous line) derived during the current study for hydrophone IP010 compared with reference values tabulated in Appendix B. These originate from previous "magnomic" work (labelled MAG 1 and 2), interferometer (labelled INT 1,2 and 3) and conventional 1 to 20 MHz based calibration methods. Also shown in the figure are the results derived from Methods 2 (long dashes) and 3 (short dashes)

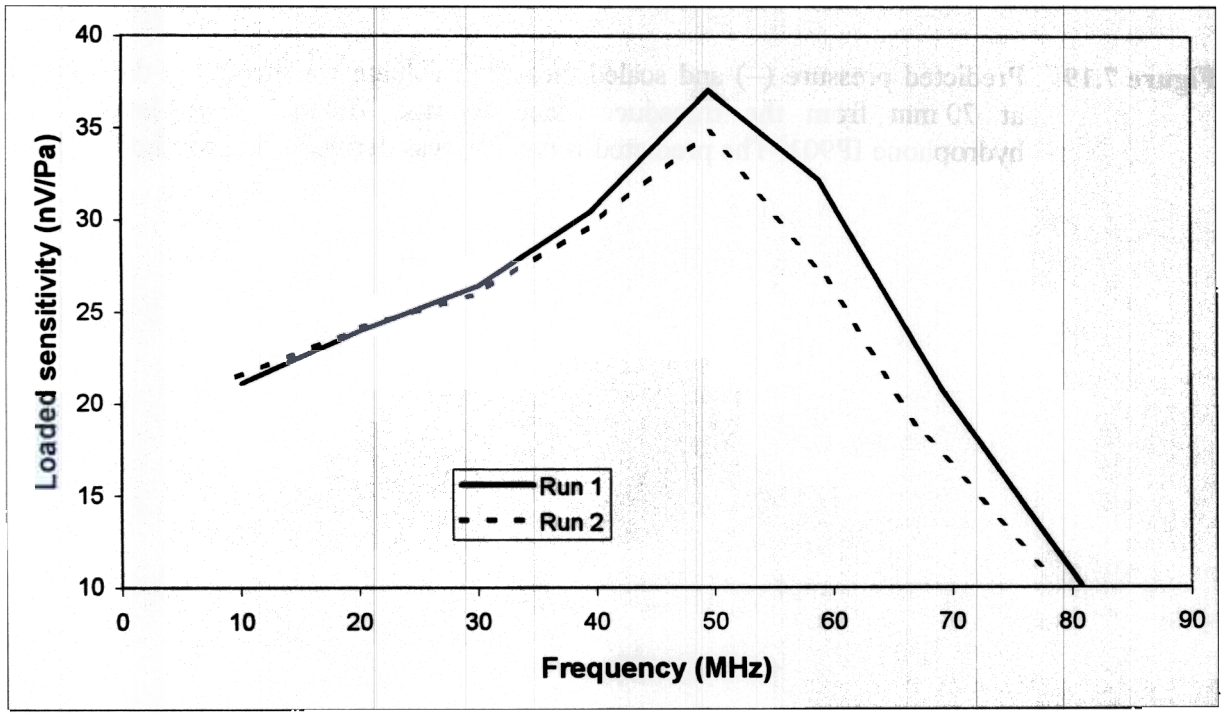


Figure 7.18: Comparison of two independent runs for the hydrophone IP010, using the Method 1 analysis

7.2.4 Hydrophone IP901

Figure 7.19 gives a comparison of the predicted pressure waveform and the actual hydrophone output waveform determined under high drive conditions with the hydrophone positioned 70 mm from the source. The predicted waveform has been derived using Method 1, by applying the known sensitivity of the hydrophone at 10 MHz to determine the acoustic pressure at the face. Figure 7.20 gives the respective spectra for these two waveforms.

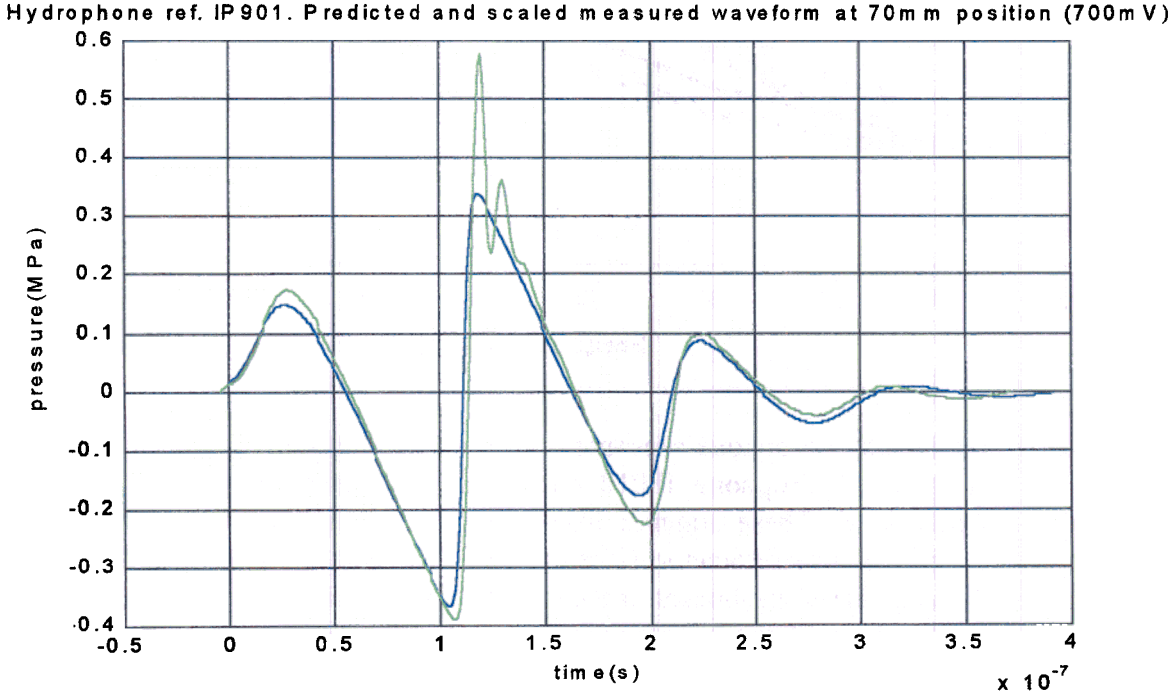


Figure 7.19: Predicted pressure (–) and scaled measured voltage waveform (–) determined at 70 mm from the transducer face for the 700 mV drive level using hydrophone IP901. The predicted waveform was derived using Method 1

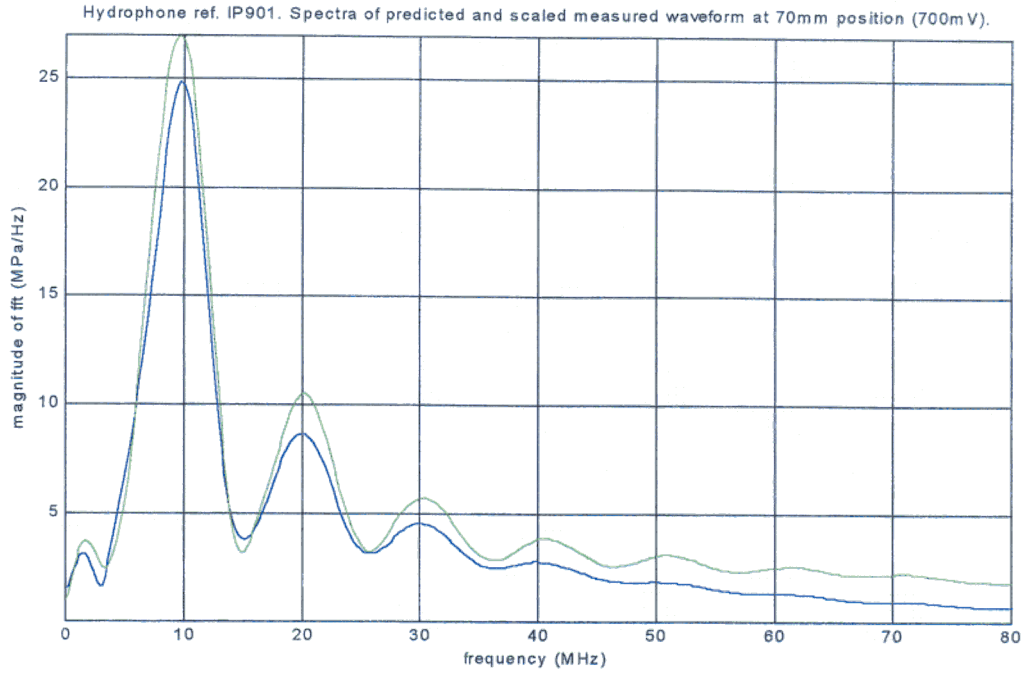


Figure 7.20: Predicted amplitude spectrum (–) and the scaled measured spectrum (–) derived from the hydrophone output voltage determined at 70 mm from face of transducer, at the 700 mV drive level for hydrophone IP901. The spectra were derived from the two waveforms shown in Figure 7.19

In this case, the predicted nonlinear loss of the fundamental derived from the pressure at the face is found to be 0.7983 whereas the measured nonlinear loss is 0.8663. Method 2 matches the input pressure to generate a loss of 0.8663.

The end-of-cable loaded sensitivity for the hydrophone IP901 is presented in Figure 7.21 where values derived using the three methods may be compared to a compilation of reference values presented in Appendix B.

Figure 7.22 shows the calibration values for two independently acquired sets of data, calculated using Method 1 i.e. through a knowledge of the pressure being generated at the face of the transducer.

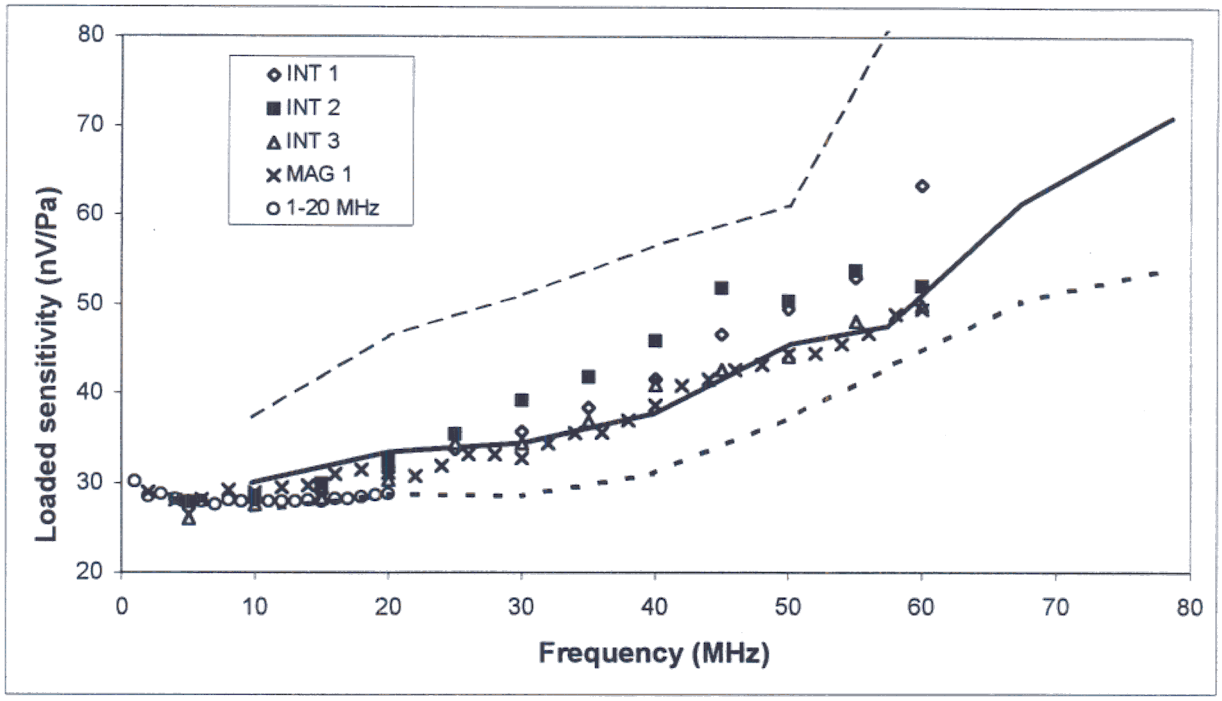


Figure 7.21: Estimated hydrophone sensitivity (continuous line) derived during the current study for hydrophone IP901 compared with reference values tabulated in Appendix B. These originate from previous "magnomic" work (MAG), interferometer (labelled INT 1, 2 and 3) and conventional 1 to 20 MHz based calibration methods. Also shown in the figure are the results derived from Methods 2 (long dashes) and 3 (short dashes).

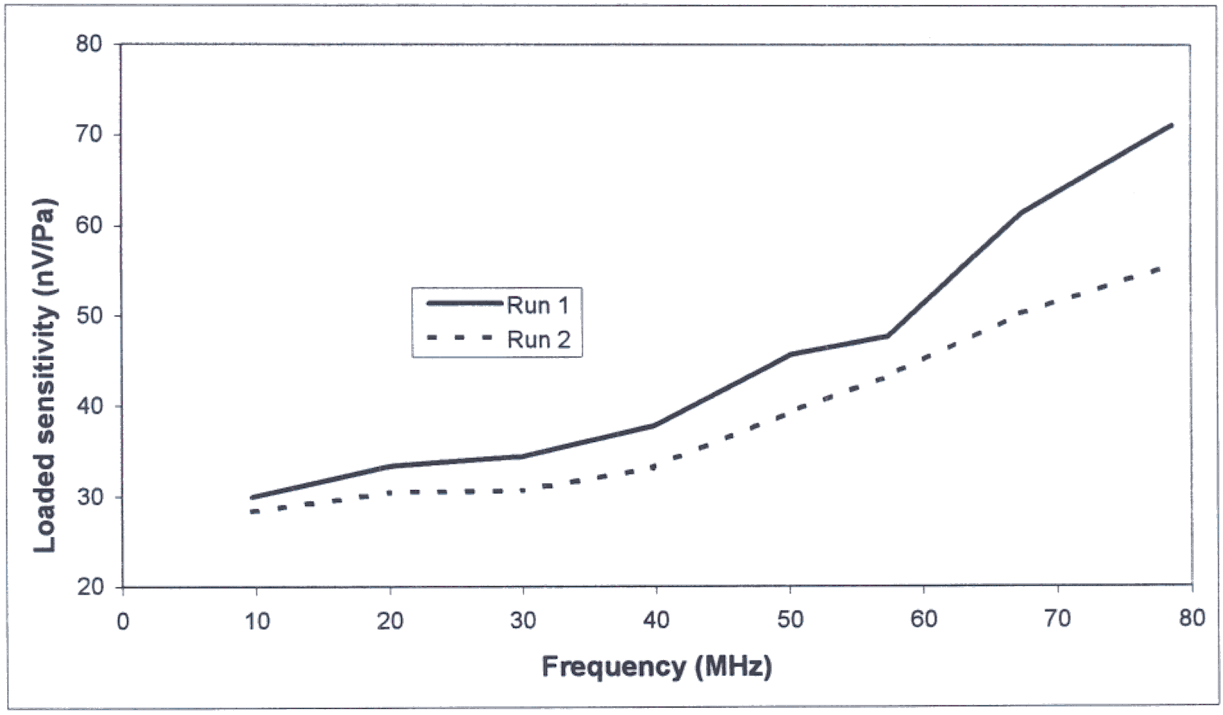


Figure 7.22: Comparison of two independent runs for the hydrophone IP901, using the Method 1 analysis

7.2.5 Hydrophone IP904

Figure 7.23 gives a comparison of the predicted pressure waveform and the actual hydrophone output waveform determined under high drive conditions with the hydrophone positioned 70 mm from the source. The predicted waveform has been derived using Method 1, by applying the known sensitivity of the hydrophone at 10 MHz to determine the acoustic pressure at the face. Figure 7.24 gives the respective spectra for these two waveforms.

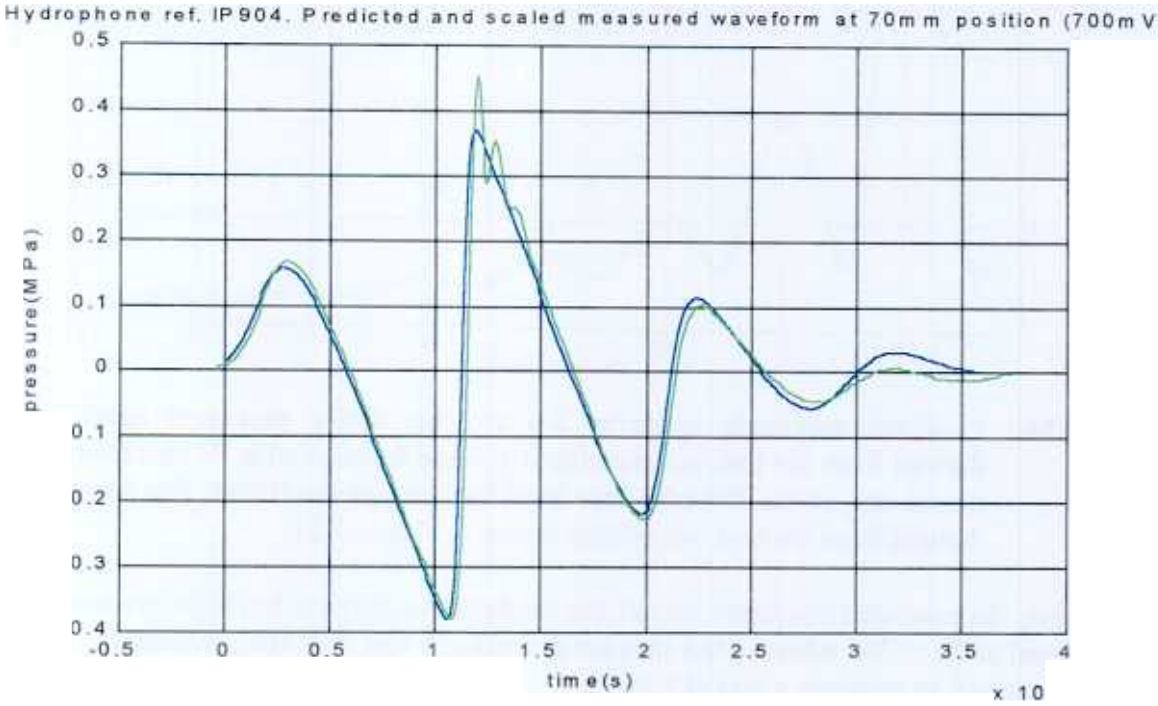


Figure 7.23: Predicted pressure (–) and scaled measured voltage waveform (–) determined at 70 mm from the transducer face for the 700 mV drive level using hydrophone IP904. The predicted waveform was derived using Method 1

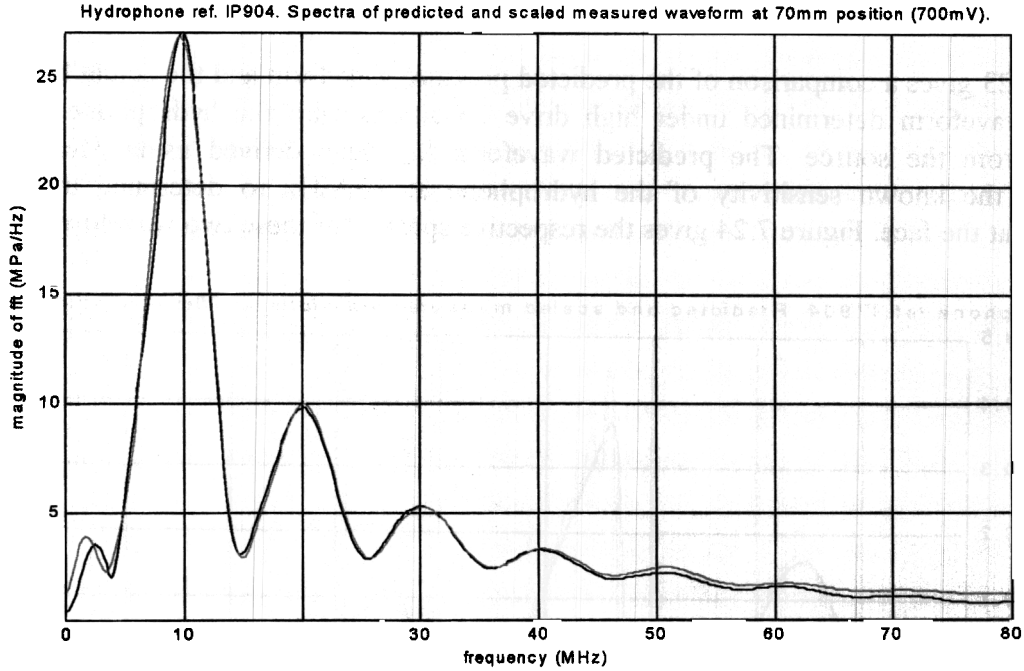


Figure 7.24: Predicted amplitude spectrum (–) and the scaled measured spectrum (–) derived from the hydrophone output voltage determined at 70 mm from face of transducer, at the 700 mV drive level for hydrophone IP904. The spectra were derived from the two waveforms shown in Figure 7.23

In this case, the predicted nonlinear loss of the fundamental derived from the pressure at the face is found to be 0.766 whereas the measured nonlinear loss is 0.7603. Method 2 matches the input pressure to generate a loss of 0.7603.

The end-of-cable loaded sensitivity for the hydrophone IP901 is presented in Figure 7.25 where values derived using the three methods may be compared to a compilation of reference values presented in Appendix B.

Figure 7.26 shows the calibration values for two independently acquired sets of data, calculated using Method 1 i.e. through a knowledge of the pressure being generated at the face of the transducer.

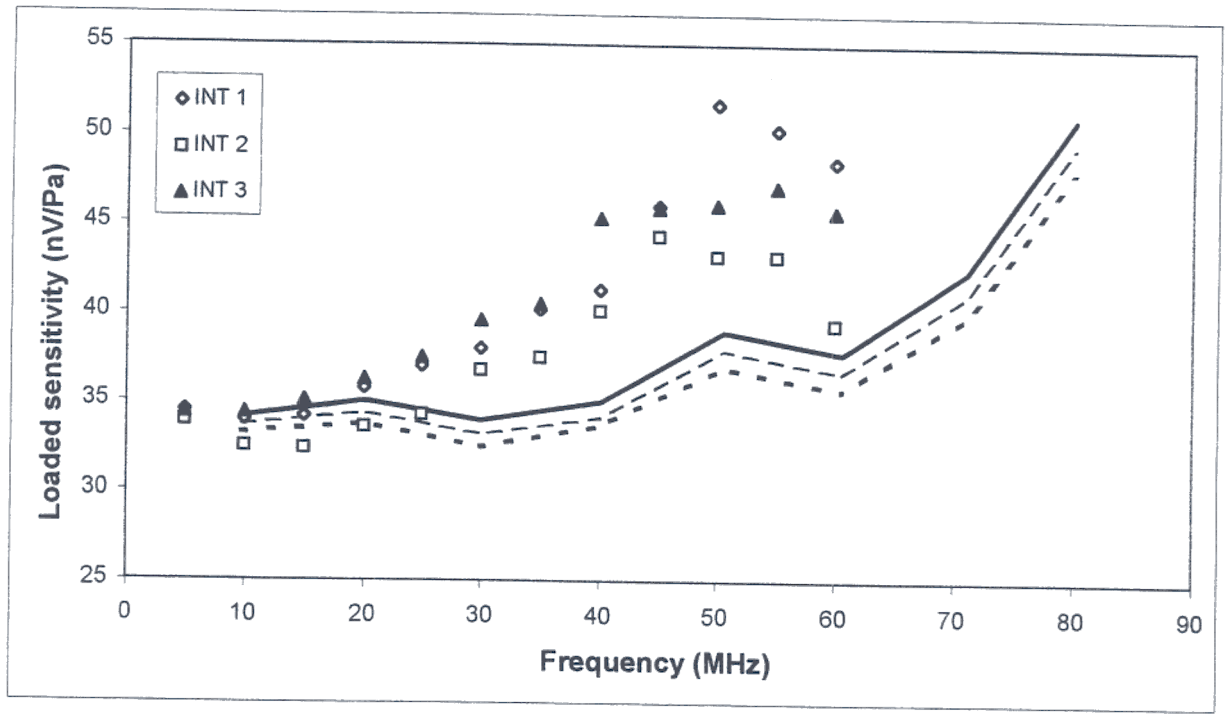


Figure 7.25: Estimated hydrophone sensitivity (continuous line) derived during the current study for hydrophone IP904 compared with reference values tabulated in Appendix B. The reference values have been taken from three independent interferometer runs. Also shown in the figure are the results derived from Methods 2 (long dashes) and 3 (short dashes)

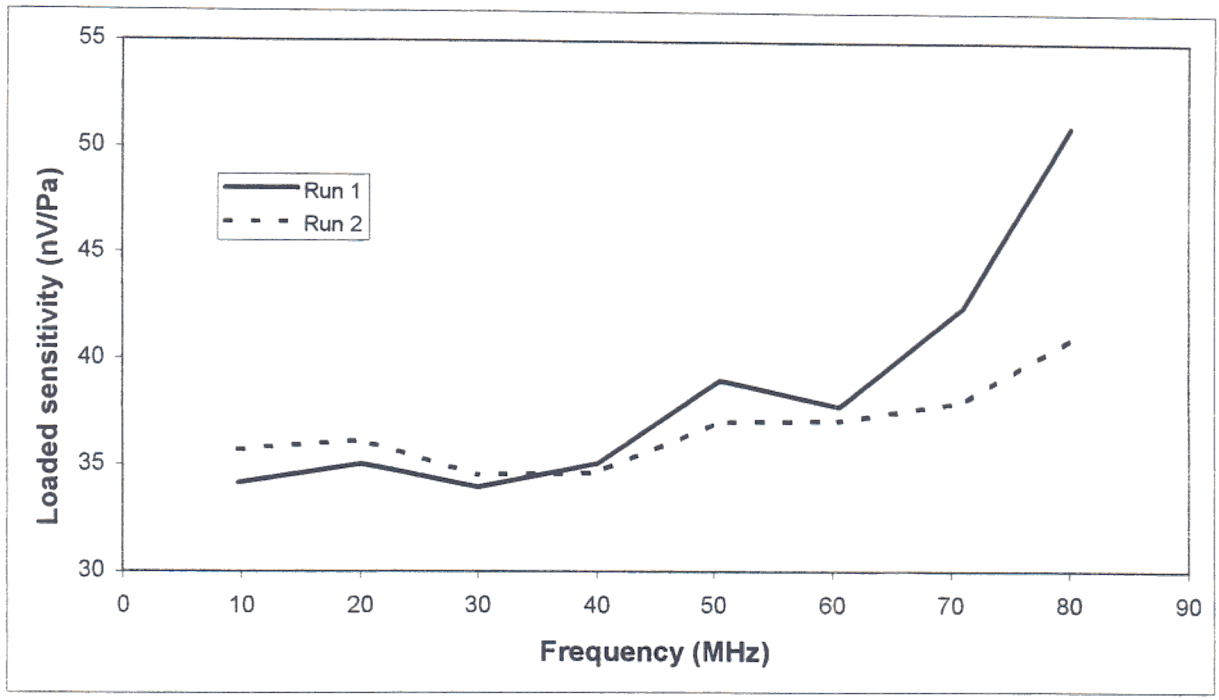


Figure 7.26: Comparison of two independent runs for the hydrophone IP904, derived using the analysis of Method 1

7.3 CORRECTING FOR TRANSDUCER IMPERFECTIONS

It is clear from the beam-plotting results shown in Section 6.1 that the central assumption of plane-wave propagation from the source to the measurement site does not hold. Rather, the results shown in Figures 6.34 and 6.35, indicate an increase in pressure along the transducer axis, exhibited using all four hydrophones used within this study. The issue which must now be addressed is whether corrections can be meaningfully applied in a justifiable manner to account for these departures from the idealised plane-wave behaviour. In this context it is instructive to develop a simple model which considers the 'transducer imperfection correction', as it may provide some insight into how the 'magnomic' calibration may be influenced.

From the low drive measurements of the axial pressure variation (Figure 6.34), the pressure may be seen to increase along the axis, to a final value at 70 mm of p_f. The net result of this is to increase the value of the nonlinear distortion parameter (σ) relative to that of a plane-wave travelling from the transducer surface. This increase will be dependent on the average pressure increase along the path and will be taken as $\delta\sigma$. It is possible to derive a value for $\sigma(z)$, which is given by:-

$$\sigma(z) = \sigma_o + \delta\sigma = \beta k z (p_o + \delta p)/(\rho c^2)$$

where p_o is the peak acoustic pressure at the source and $\sigma_o = \beta k z p_o$ is the nonlinear distortion parameter at 70 mm for a plane-wave of amplitude p_o propagating from the source. The value of $\sigma(z)$ defines the nonlinear loss at the position z, $L(\sigma(z))$, so that if we now consider the ratio of the fundamental level at z to that at the source (derived from the 5 mm measurement), we have:-

$$p_f \,.\, \exp(-\alpha \,.\, z) \,.\, L(\sigma(z)) / p_o$$

In fact the ratio p_f .exp $(-\alpha \,.\, z)/ p_o$ is determined from low amplitude measurements (linear regime) when $L(\sigma(z))$ is equal to unity. From the low amplitude axial variation in pressure shown in Figure 6.34, values for p_f and δp are 1.13 p_o and 1.09 p_o respectively, although there is seen to be some experimental scatter. It is instructive to calculate the effect this has on the value of σ at the measurement site.

From Table 7.2, the average peak-pressure determined at 5 mm using the various hydrophones was 0.50 MPa. Note that it will be assumed that absorption over the 5 mm path between the transducer and the hydrophone positioned at its closest position is small: in reality a correction could be applied. Using this pressure, the value of σ_o at 70 mm may be computed as 2.4, which corresponds to a nonlinear loss of 0.79. Assuming the values for p_f and δp given earlier, the modified value of $\sigma(z)$ becomes 2.63 which corresponds to an increased nonlinear loss of 0.765. This is a significant difference. It has a substantial effect on the computed harmonic content at 70 mm and therefore on the 'magnomic' calibration values.

This analysis predicts that the observed nonlinear ratio of the fundamental signal level at the two measurement positions under high drive conditions, should be of the order 0.864 (after correction for small signal absorption in water). In fact, as indicated in Section 7, the nonlinear loss values for the two hydrophones for the two sets of measurements show great variability, being in the range 0.7503 to 0.867. The average value is 0.80. It should be noted that implementation of such a correction will result in an increase in the predicted harmonic

magnitudes at 70 mm, which will tend to decrease the derived sensitivity values at the elevated frequencies. A detailed comparison of the results will be given in Section 8, but, in general, this will tend to degrade the agreement observed between the 'magnomic' values and those derived from the interferometer.

The second factor to be taken into consideration is the change in the frequency content of the low-drive waveforms between the two measurement positions, 5 mm and 70 mm. If we assume that $v_{11}(t)$ is the voltage waveform measured at 5 mm from the transducer face under low drive conditions (50 mV) and, accordingly, let $v_{12}(t)$ the low-drive voltage waveform determined at 70 mm. If we now take $V_{11}(f)$ and $V_{12}(f)$ as the two respective Fourier transforms, then at a given frequency we should have:-

$$|T(f)| = \left| \frac{V_{12}(f)e^{0.065\alpha(f)}}{V_{11}(f)} \right| \approx 1$$

where $\alpha(f)$ is the attenuation in water as a function of frequency. In practice, this does not turn out to be the case. Figure 7.27 shows this 'transducer correction factor', defined as $|T(f)|$, over the frequency range 5 to 15 MHz. It can be seen that the shape of the correction has a similar shape for each of the four hydrophones with the correction factor at the fundamental frequency (10 MHz) being in the range 1.04 to 1.12.

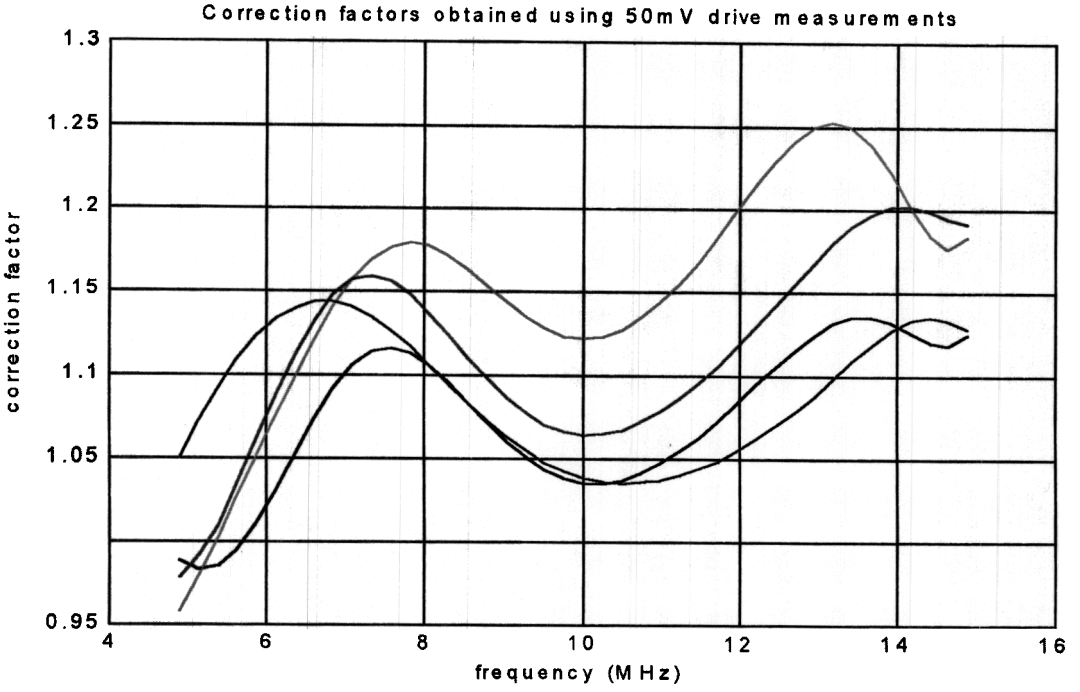


Figure 7.27 Correction factors for the four hydrophones used within this study: IP010 (—) IP016 (—) IP901 (—) IP904 (—). The values have been derived from low amplitude measurements (70 mV), by comparing the spectra of waveforms acquired at 5 mm and 70 mm, after correcting for the frequency dependent water absorption through the intervening path

In principle, the curves depicted in Figure 7.27 can be used to correct the high drive waveforms acquired at the face, which may then be propagated forward to the measurement position, 70 mm., in an attempt to correct for the changes in the spectral content. It is instructive to consider at a qualitative level the anticipated changes in the calibration values which this will produce, although no specific results will be presented.

Let $v_{21}(t)$ be the voltage waveform determined at 70 mm from the transducer under high drive conditions. Then, under the same drive conditions, let $v_{22}(t)$ be the voltage waveform measured at 70 mm. Taking again the corresponding Fourier transforms as $V_{21}(f)$ and $V_{22}(f)$, in order to obtain the corrected waveform at the 5 mm position, the quantity $V_{21}(f)$ must be multiplied by the 'correction' transfer function $T(f)$, over the frequency range 5 to 15 MHz. This process will lead to an increase in the fundamental pressure level at the face of the transducer, hence the level will be higher than that obtained in Method 1. The net result of this is a higher value of σ value at 70 mm, an increased nonlinear loss and higher pressures for the elevated harmonics. The results of this will be that the calibration curves shown in Figures 7.13, 7.17, 7.21 and 7.25 will all be pulled down, again degrading the level of agreement with the interferometer derived results for most of the hydrophones.

8 DISCUSSION

It is clear from the results of this study that an accurate determination of the nonlinear loss plays an important role in the 'magnomic' process. The compilation of calibration values for the four hydrophones presented in Section 7.2 support this statement. It can be seen that for the hydrophone IP016, a 2.6% change in the nonlinear loss shifts the sensitivity at 30 MHz by 10% (see Figure 7.13). Other hydrophones show a similar sensitivity, for IP010, a 3% change in the loss value from 0.7726 to 0.7503, results in a downward shift in the sensitivity of 13%. Leaving aside the issue of transducer departures from plane-wave behaviour it should be possible to determine the loss, which is a relative measurement, reasonably accurately, although care must be taken when considering truncation effects as noted in Section 6.2. Even so, uncertainties of ±1% in the loss values due to windowing are probably realistic, with a significant effect on the derived sensitivity. In view of this, the variability in the derived loss values, both between hydrophones and for the same hydrophone repeated, is of concern. It may arise from the problems of alignment close to the transducer face, or due to the low signals being measured for some hydrophones in the low drive case.

One significant new feature of this study has been the use of the large-aperture hydrophone, IP002, in order to try to establish an independent value for the nonlinear loss. The results obtained using this hydrophone are shown in Section 6.3, and indicate good agreement between theory and measurement concerning the predicted plane-wave propagation behaviour, both for the fundamental loss and the variation of the second harmonic. The large active element size of this hydrophone (75 mm diameter) means that it averages over the whole cross-section of the acoustic beam, and therefore determines some averaged nonlinear loss over the measurement plane. The results are not therefore expected to be of direct relevance to the nonlinear loss determined using the small hydrophones, which is determined along the beam-alignment axis but they should nonetheless provide some guide. It is interesting to note that the diametrical beam-plots shown in Figure 6.3 show an approximate uniformity of the field, beyond a distance of ±1 mm off-axis. Taking the 'average' peak pressure as 0.635 MPa (determined from the observed nonlinear loss of 0.755), and equating this with the average observed for the beam plots, then the indicated pressure minima seen in Figure 6.3 is 0.44 MPa. It is interesting to note that this is 11% lower than the 0.49 ± 0.03 MPa peak-pressure measured using the various hydrophones shown in Table 7.2.

The results of beam-plotting measurements at various positions in the transducer field given in Section 6.1 clearly indicate strong departures from the required plane-wave behaviour. Measurements performed across the axis at a variety of axial positions have demonstrated that in planes close to the transducer, i.e. those which provide 'source' waveforms for use in the 'magnomic' calibration routines, the peak-positive acoustic pressure can change by as much as 50% over a central region of just 2 mm, when examined with a miniature needle hydrophone. This result strongly suggests that this particular transducer may not be the ideal source to provide the input waveforms for the calibration method. In principle it is possible to correct for these imperfections although it is not clear from the original 'magnomic' work given in Appendix A how exactly this was brought about. Within this study, due to these uncertainties in the correction mechanism, it has not been attempted

Instead, the approach of Method 1 given in Section 7 has been one of taking the pressure waveform at the face of the transducer determined using the 10 MHz sensitivity of the hydrophone, propagating it forward to the measurement site and comparing predicted and

observed harmonic magnitudes. In view of the simplicity of this approach and the transducer imperfections in the plane-wave structure commented upon earlier, it is a little surprising that this approach gives reasonable results, although the agreement with alternative methods appears to depend on the hydrophone.

The comparison of results derived using the interferometer and the current 'magnomic' project will now be carried out in detail. However, first, it is worth emphasising that there are considerable uncertainties associated with the interferometer calibrations of hydrophone sensitivity, particularly above 50 MHz, so comparisons at the higher frequencies need to be considered with some care.

For IP016, the 9 μm bilaminar membrane hydrophone, for example, the random (Type A) uncertainties at 50 MHz are ±14% whilst at 60 MHz they are ±40% (see Appendix B.1). Agreement between the interferometer calibrations and the results of the current study is actually very good, being within the measurement uncertainties for the interferometer up to 50 MHz (for Set 1). Both interferometer and current 'magnomic' calibrations appear to be higher than the old 'magnomic' data and the conventional 1 to 20 MHz calibration method. The differences are as follows: 7.3% (10 MHz); 11.7% (20 MHz) and 9.6% (30 MHz). The results for Set 2 are shifted up by roughly 4%, and agreement with other methods is consequently slightly poorer. It is of interest to note that the sensitivity at the fundamental frequency is higher than other methods: this would imply that the fundamental pressure generated by propagating the waveform forward to 70 mm is too low. This may arise due to the fact that transducer imperfections have not been accounted for, leading to an increase in the fundamental pressure at the measurement site and a resultant pulling down of the 10 MHz sensitivity.

The hydrophone IP010 is the second 9 μm bilaminar studied. The interferometer results are shown in Appendix B.3 and these indicate random uncertainties above 50 MHz which again degrade, being typically ±15% to ±20%. Additionally, this hydrophone has been calibrated several times using the old 'magnomic' hydrophones in a relative comparison method. The interferometer sensitivity results are considerably higher than those determined during the current study using the 'magnomic' method. The differences are apparent over the whole frequency range, the slope of the two curves over the frequency range 10 to 40 MHz being appreciably different up to the resonance observed at approximately 50 MHz. Differences between the interferometer results and the current 'magnomic' calibrations are 37% (40 MHz), 2% (50 MHz) and 74% (60 MHz). Calibrations transferred from the old 'magnomic' hydrophones through the comparison method appear to be in much closer agreement with the current calibration, differences being 11.5% (30 MHz); 23% (40 MHz) and 13.5% (50 MHz). Agreement between the various techniques at the fundamental frequency 10 MHz is very good. The two independent calibrations carried out on IP010 show good agreement (Figure 7.18), being very close up to 50 MHz.

IP901 is a 9 μm coplanar membrane hydrophone whose prior calibrations have been summarised in Appendix B.2. Typical calibration uncertainties for the interferometer derived values again degrade above 50 MHz, the random uncertainties increasing from typically 10% at 50 MHz to 20% at 60 MHz. The results derived from the current 'magnomic' study and alternative techniques are portrayed in Figure 7.21. Agreement between the interferometer and current 'magnomic' methods is actually very acceptable, being 9% at 30 MHz, 10% at 40 MHz, and 11% at 50 MHz. Agreement between various methods at the fundamental

frequency is again acceptable, although the current 'magnomic' calibration values are 5% higher which is still within the uncertainties for the various methods. The calibrations derived from the old 'magnomic' hydrophones agree very well with the current results. Unfortunately, the agreement for the second set of calibrations (Run 2) is poorer, again the calibrations appear to be crudely shifted down by typically 10%.

The second 9 μm coplanar hydrophone used was IP904, whose limited reference calibrations are presented in Appendix B.4. These are restricted to three interferometer calibrations. These results are compiled along with the results of the current study in Figure 7.25. It is clear that agreement between the interferometer and the 'magnomic' results is poor, the two sets of data appear to show an entirely different frequency dependence. Again, agreement at 10 MHz is good, but above this frequency the two curves diverge. Differences are 10% (30 MHz); 20% (40 MHz) and 21% (50 MHz). The interferometer results again are higher. Note than there is some spread in values between the three interferometer sets, especially above 50 MHz. It should also be recorded that, although the two hydrophones IP901 and IP904 are nominally identical, they do produce different waveforms at the 70 mm position. In Figure 7.23 (IP904), it is clear that the observed thickness resonance is not as strong as that displayed by IP901, shown in Figure 7.19. The hydrophones would therefore appear to possess different resonances, approximately 85 MHz for IP901, in excess of 110 MHz for IP904.

9 SUMMARY

A systematic investigation has been undertaken of the 'magnomic' method of hydrophone calibration. The basis of the technique lies in modelling the propagation of finite-amplitude plane-waves in water, and comparing the measured harmonic content of a distorted acoustic waveform with that predicted through modelling. The technique has been used to calibrate four GEC-Marconi membrane hydrophones over the frequency range 10 to 60 MHz, the results being compared with other methods, primarily the results of the first high frequency hydrophone calibrations derived using the NPL primary standard laser interferometer.

A number of conclusions may be drawn from the study:-

• a single 10 MHz transducer has been used to define a region close to the transducer face where plane acoustic waves are produced. The transducer was identical to the one used in the original 'magnomic' work. Beam-plotting measurements carried out using miniature hydrophones both along and perpendicular to the transducer beam-alignment axis show that a plane-wave is not in fact produced. This manifests itself in a local on-axis minimum close to the transducer and a pressure distribution which, when corrected for absorption in water, gradually increases along the acoustic axis;

• ignoring the effect of these transducer imperfections on the nonlinear waveform, calibrations at frequencies up to 60 MHz can be achieved through a knowledge of the pressure at the measurement position close to the transducer face, derived using the 10 MHz sensitivity of the hydrophone being calibrated. Through carrying out calibrations in this way, agreement with interferometer results and calibrations derived from prior 'magnomic' studies is very variable, appearing to depend on the hydrophone;

• it is not clear how best to correct for transducer imperfections in a justifiable way. Using a quite simple model, corrections applied for some hydrophones would appear to degrade the observed agreement with the interferometer results.

In terms of the way the results of this study impact on the NPL ultrasonics standards programme, a number of recommendations may be made, as follows:-

- the studies presented have been carried out on a single transducer, and it is possible that alternative sources of such devices could be investigated to establish those which come nearest to the required plane-wave behaviour;

- there is a general need to improve our modelling capability for nonlinear diffractive acoustic fields. This would be important in this and other areas of ultrasonic metrology. For the 'magnomic' work, this might enable corrections to be applied for deviations from plane-wave behaviour;

- these two approaches might be necessary should there be a need to extend hydrophone calibration capability above its current limit of 60 MHz - this may well be most readily achieved using a variant of the 'magnomic' technique;

- currently, due to the uncertainties outlined in the 'magnomic' method, it is not possible to advocate the technique as a standard method of hydrophone calibration;

- the 60 MHz calibrations derived from the interferometer were established within the framework of the 1995 - 1998 NMS Acoustics Programme. This work has emphasised the inadequacies of calibrations above 50 MHz (typically ±20% to ±25%), arising principally from signal-to-noise issues. This is being addressed within the current (1998 - 2001) NMS programme, where a five-fold improvement in signal-to-noise is being sought;

- the interferometer remains the most promising method of calibrating hydrophones up to 60 MHz with reasonable calibration uncertainties.

10 ACKNOWLEDGEMENTS

The authors acknowledge the technical work of Dr David Bacon, and the financial support of the National Measurement System Policy Unit of the UK Department of Trade and Industry.

11 REFERENCES

BACON, DR (1982). *Characteristics of a pvdf membrane hydrophone for use in the range 1 - 100 MHz.* IEEE Trans. **SU 29**, p18-25

BACON DR (1986). *Finite amplitude propagation in acoustic beams.* PhD Thesis, University of Bath.

BLACKSTOCK DT (1964). *Thermoviscous attenuation of plane, periodic finite-amplitude sound waves,* J. Acoust. Soc. Am., **36,** p534-542.

CARSTENSEN EL, LAW WD, McKAY ND and MUIR, TG (1980). *Demonstration of nonlinear acoustic effects at biomedical frequencies and intensities.* Ultrasound Med. Biol. **6**, p359-368.

COSTA ET, LEEMAN S and HODDINOTT, JC (1986). *A new approach to measurements of three-dimensional pulses: linear and non-linear fields.* In Physics of Medical Ultrasound II (Institute of Physical Sciences in Medicine Report No. 57), p87-93.

COSTA ET, HODDINOTT JC and LEEMAN S (1986a). *Artefact free measurement of attenuation, impedance and dispersion.* 1986 Ultrason. Symp. Proc., p963-966.

COSTA ET, LEEMAN S and JONES JP (1990). *Reflectivity measurements using a large-aperture hydrophone.* 1990 IEEE Ultrasonics Symposium Proceedings, p1043-1046.

ESWARD TJ, ROBINSON SP and ZEQIRI, B. (1997*). Extending the frequency range of the NPL primary standard interferometer to 60 MHz.* NPL Report No. CMAM(INT)001.

HAMILTON MF and BLACKSTOCK DT (1997). *Nonlinear Acoustics.* Academic Press Ltd, London.

IEC 60866 (1987) *Characteristics and calibration of hydrophones for operation in the frequency range 0.5 MHz to 15 MHz.* International Electrotechnical Commission, 1987

IEC 61101 (1991) *The absolute calibration of hydrophones using the planar scanning technique in the frequency range 0.5 to 15 MHz.* International Electrotechnical Commission, 1991

IEC 61102 (1991) *Measurement and characterisation of ultrasonic fields in the frequency range 0.5 MHz to 15 MHz.* International Electrotechnical Commission, 1991

MITOME H. (1989). *An exact solution for finite-amplitude plane sound waves in a dissipative fluid.* J. Acoust. Soc. Am. **86**, p2334-2338.

MUIR TG and CARSTENSEN EL. (1980). *Prediction of nonlinear acoustic effects at biomedical frequencies and intensities.* Ultrasound Med. Biol. **6**, p345-357.

PRESS WH (1992). *Numerical recipes in FORTRAN. The art of scientific computing.* Cambridge University Press, Cambridge, Chapter 4, p134-135.

ZEQIRI B (1989). *Field parameter measurements using a large-aperture hydrophone.* Ultrasonics International 89 Conference Proceedings, p989-994.

APPENDIX A: HIGH FREQUENCY 'MAGNOMIC' HYDROPHONE CALIBRATION

This Appendix is made up of extracts from an NPL Internal document, produced in September 1993, which describes the 'magnomic method'. It was intended as a series of notes on the basic method and some guidance on the software used. It has been reproduced here purely for reference purposes.

A. DESCRIPTION OF CALIBRATION METHOD

A.1.1 General description of the method

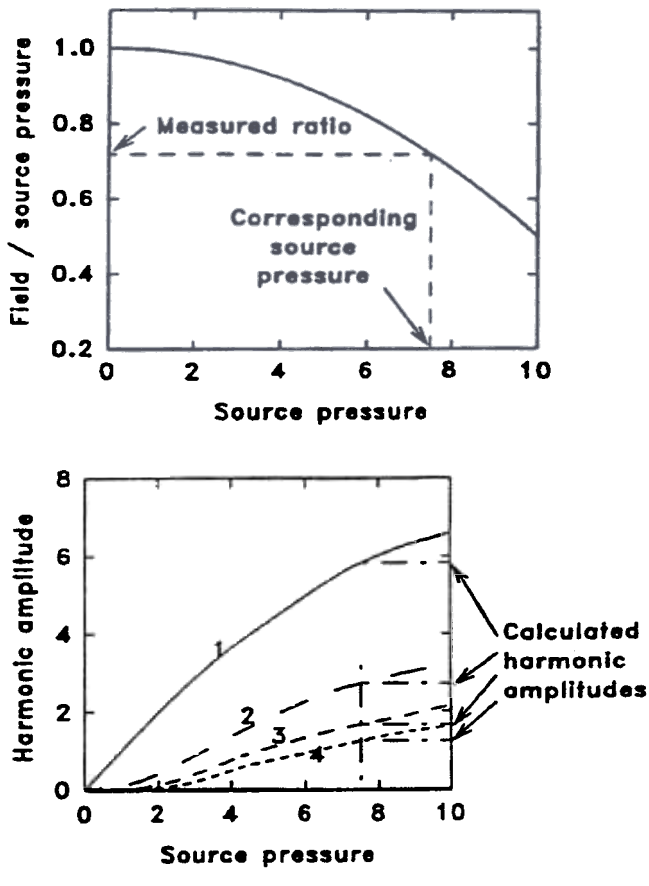


Figure A.1: Principle of the magnomic calibration method

Magnomic hydrophone calibration methods rely on predicting the nonlinear relationship between the source and field amplitudes. If the propagation loss, for instance, can be both modelled and measured, then the measurement can be compared with theory and the amplitude inferred. Nonlinear propagation produces harmonics of the starting frequency, so there is the potential for calibration at multiple frequencies. This general approach is illustrated in Figure A.1. There are generally two stages. In the first stage, measurements of the propagation loss (typically measured at a low frequency corresponding to the source waveform) are compared with theoretical predictions. This propagation loss is a monotonic function of the source amplitude and, by matching the observed and predicted losses, this amplitude can be inferred.

The second stage involves using the propagation algorithm to calculate the total waveform (including its harmonic content) at a field point. These results are then compared with the measured waveform from the hydrophone and comparison of the two permits the calibration to be made. Early methods (Bacon 1982, 1986) used tone-burst fields, which gave calibration results at multiples of the source frequency.

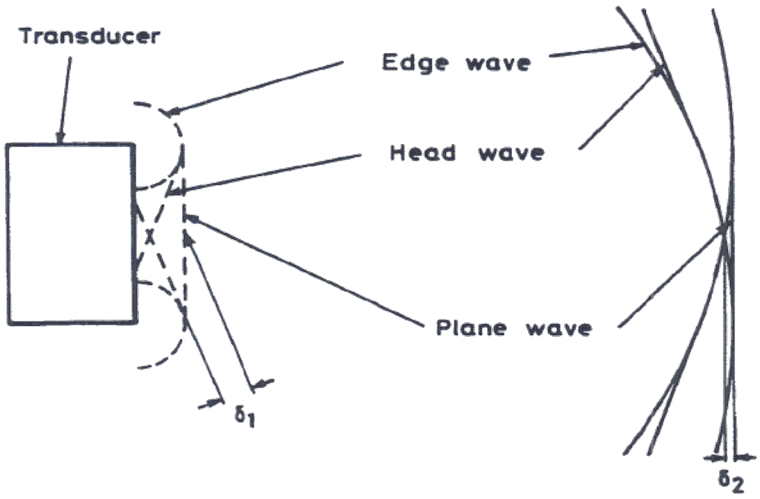


Figure A.2: Field geometry, showing plane, edge and head-waves.

The calibration method using tone-burst fields has been shown to agree with other methods, but it is somewhat unsatisfactory because it relies on an approximate model of the propagation. This could be overcome with a better theoretical model, but each calculation of sensitivity would require several computations of the field and this could prove to be expensive in computer time. An alternative is to use a plane-wave field, because the nonlinear propagation for this situation can be solved fairly readily, using the Cole-Hopf transformation. Such a plane-wave can be obtained if the source transducer is pulsed. The field of a plane-piston transducer can be considered to be the sum of two parts: the edge-wave and the plane-wave components (see Figure A.2). If the transducer emits a pulse of ultrasound then, for a short period of time, the field at a particular point corresponds to that of a plane-wave. After this time, the signal from the periphery of the transducer arrives (the edge-wave) and the field can no longer be considered plane. The time δt, for which the plane-wave exists in isolation varies with position and can be evaluated from simple geometric considerations to be, (on the acoustic axis):

$$\partial t = \frac{\sqrt{z^2 + b^2} - z}{c} \qquad \text{(A.1)}$$

where c is the sound velocity, z is the propagation distance and b the radius of the piston source. By equating δt with the pulse length, the maximum distance over which the plane and edge-waves are separable is obtained. Some of the measurements were obtained with a transducer of diameter 19 mm and a pulse length of about 270 ns (for which the acoustic pressure was less than about 1 % of the peak). Equation A.1 indicates that a propagation path of up to 110 mm could be used before there is interference from the edge-wave. To obtain calibration results at this distance the amplitude needs to be sufficiently high to cause significant nonlinear losses. The plane-wave shock parameter (σ) is given by:

$$\sigma = \frac{\beta p k z}{\rho c^2} \tag{A.2}$$

where p is the acoustic pressure amplitude at the source, β is the nonlinearity parameter, k the acoustic wavenumber and ρ the density. For a frequency of 10 MHz and a distance of 110 mm, the condition for σ to be greater than 2 is that the acoustic pressure must be at least 0.27 MPa. This can be achieved in practice, so the method is viable. Other measurements for propagation distances up to 100 mm used a 5 MHz transducer which was 25 mm in diameter. In principle, a similar approach to that described above can be used - the results at low frequencies can be used to determine the source waveform and then this can be used in determining the sensitivity for the harmonics. For a pulsed wave, however, there are several component frequencies present at the source. This means that the initial waveform cannot be determined uniquely from a knowledge of the propagation loss, unless the frequency response of the hydrophone at low frequencies is known. There are a number of ways to overcome this problem, such as calibrating the hydrophone at low frequencies using another technique, modelling the frequency response of the hydrophone and utilising an analysis algorithm to determine the low frequency response from the finite amplitude measurements. This last method is possible in principle (see A.3 below), because there are the same number of known parameters (viz. the nonlinear changes in amplitude at each frequency) as unknown variables (the hydrophone sensitivity at these frequencies). In practice, however, it can be difficult to obtain a reliable value for the sensitivity if the nonlinear change in amplitude at a particular frequency is small. Here, these difficulties are avoided by using a hydrophone with a sensitivity that is essentially constant over the frequency range of interest.

The experimental arrangement is shown in Figure A.3. A high-frequency preamplifier was used (having a gain of 0.5 when connected to a 50 Ω load) and was connected with 50 Ω cable to a broadband signal amplifier and then to the digitiser with a 50 Ω termination. To make it possible to calibrate the amplification chain, a discrete 50 Ω termination was used, rather than selecting the 50 Ω input option on the digitiser. (It would be possible, and preferable, to use the 50 Ω input on the digitiser if one wanted to calibrate the whole system, for use subsequently in making pressure measurements directly. The configuration used here was the optimum for hydrophone calibration.) The function generator was an HP8165A, operated in burst mode with a single-cycle burst of the correct sign so as to give the maximum shock amplitude (it may also be possible to use the HP8116A).

It is important to align the system very carefully, so as to be sure that the measurements are made on the axis. One of the reasons for this is to minimise the effect of edge-waves (which arrive sooner off-axis). The edge-waves themselves are used for this alignment - initially one can use the pulsed field, but a more precise location of the position can be made by exciting the transducer with a few cycles. Alignment is made at distances where there is expected to be a minimum of pressure on the axis.

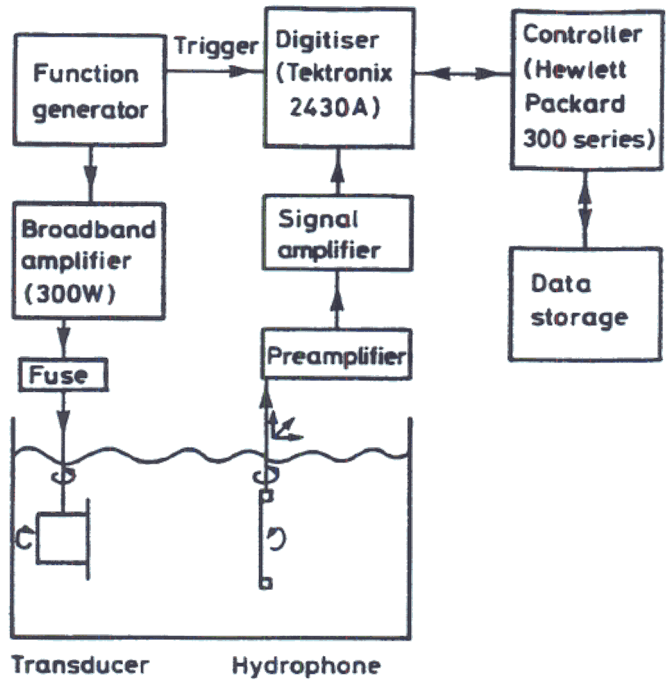


Figure A.3: Block diagram of the experimental arrangement

A major practical difficulty that has to be overcome is the fact that some commercial transducers are not perfect and do not produce a plane-wave, even for the initial interval defined by Equation A.1. This effect has been noted previously for commercial transducers and has been attributed to non-uniformities in the transducer backing. When the hydrophone is moved along the acoustic axis, the measured harmonic amplitudes are not constant, but increase with propagation distance. The analysis algorithm has therefore to be modified to take account of this phenomenon. Other features of the analysis include the need for windowing. This is because there is often little gap between the plane-wave and the other following waves. The end of the plane-wave does not, therefore, always match the ideal zero-amplitude and zero-slope conditions that would ensure the absence of end-effects. A diagram of the algorithm is given in Figure A.4.

Fortunately, these modifications appear to be sufficient to describe the effects, as can be seen from Figure A.5, where the calculated and measured waveforms at a field point are compared. In Figure A.6 the waveforms at the source and at 90 mm are compared. The edge-wave is clearly seen for the waveform at 90 mm, which is just beginning to overlap the plane-wave at this distance.

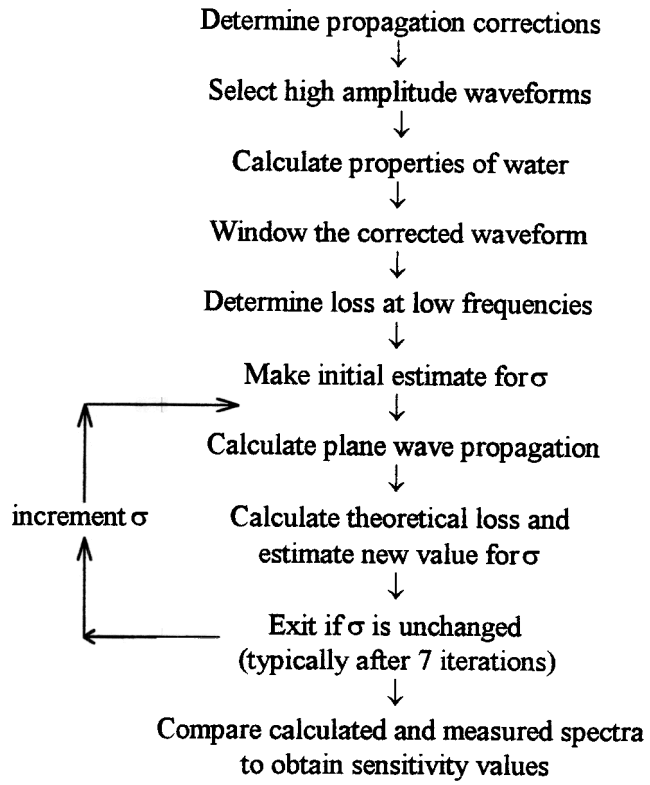


Figure A.4: Computer algorithm

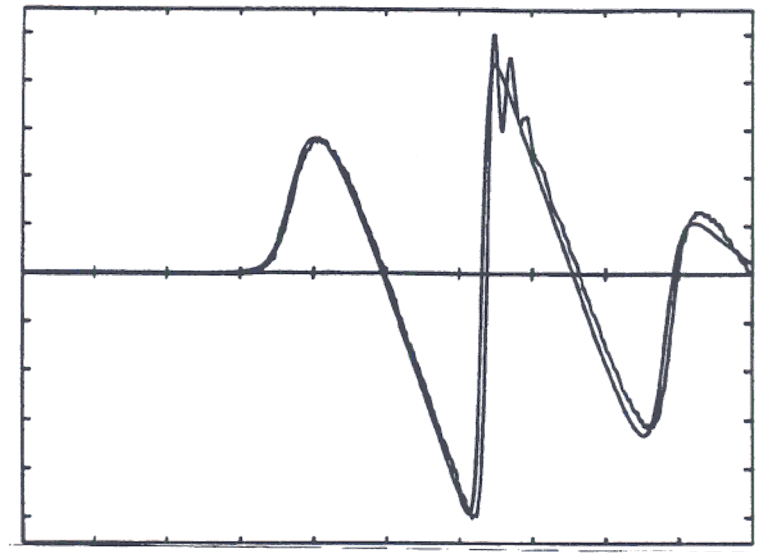


Figure A.5: Comparison of the calculated (smooth curve) and measured (irregular curve) waveforms at 111 mm. The two curves have been displaced slightly in time.

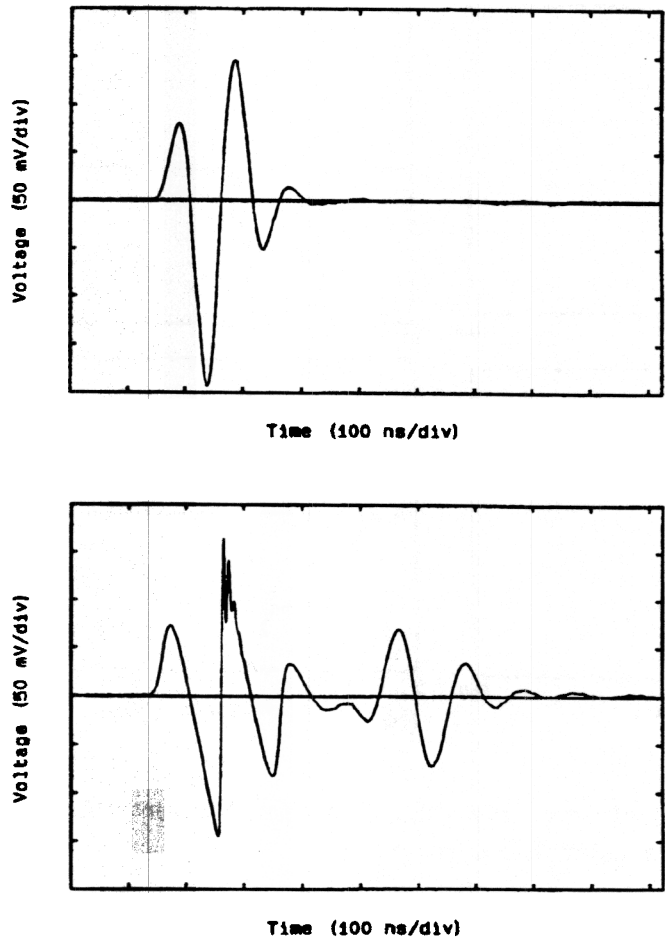


Figure A6: Measured waveforms at 3 mm (upper curve) and 90 mm (lower curve) from the 10 MHz transducer.

The uncertainties have yet to be assessed in detail, but include the effects of the linearity and slew-rate of the digitiser, the gain and input impedance of the hydrophone amplifier, the uncertainty in the nonlinearity coefficient and attenuation coefficient of water, the non-uniformity of the transducer field and any variation in frequency response of the hydrophone at low frequencies. One important test of the method is to model the calibration process. Here, an amplitude and phase response is assumed for a device and waveforms synthesised to model what might be observed experimentally. The calibration algorithm was then used on these waveforms and the results compared with the original assumed hydrophone response. These results are presented in Figures A.7 to A.9 for calculations that assumed a 10 MHz source transducer. For these theoretically-derived (noise-free) results, the shape of the response is reproduced well, even up to the calculation limit of 250 MHz.

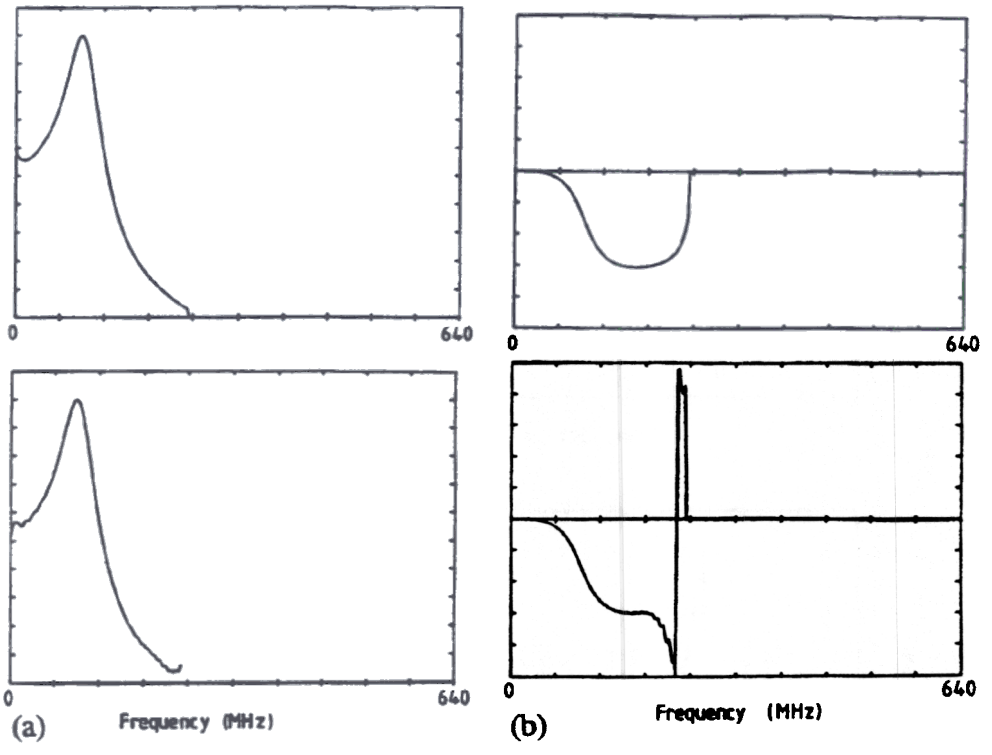


Figure A.7: Comparison of input and calculated response for a 9 μm thick membrane hydrophone: (a) amplitude; (b) phase.

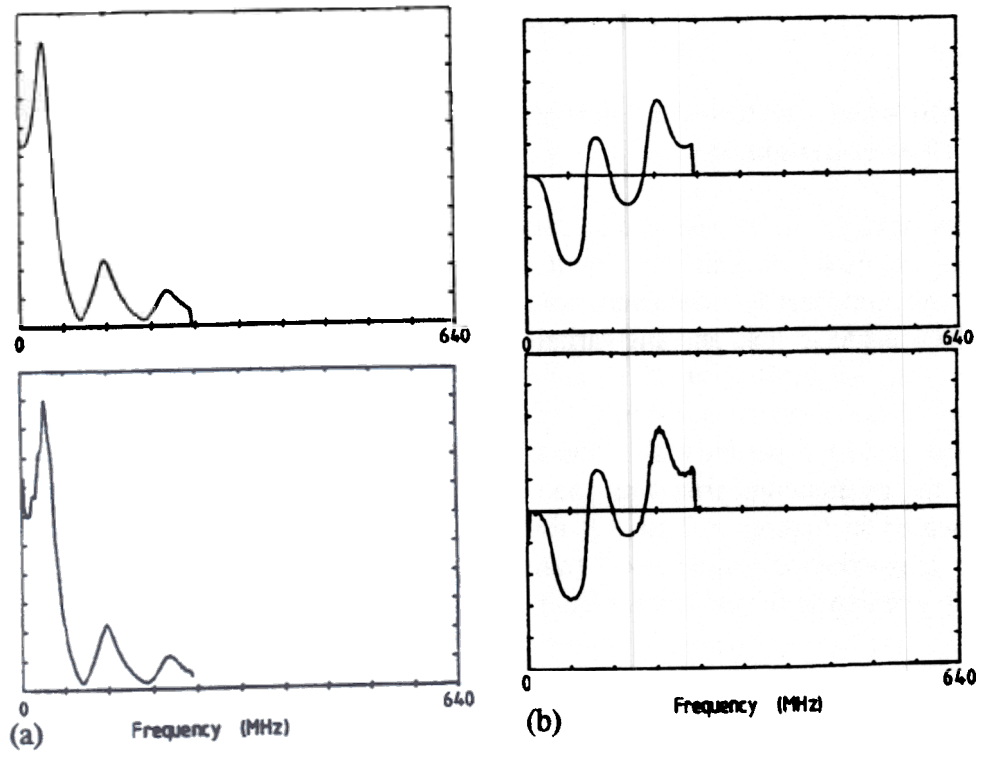


Figure A.8: Comparison of input and calculated response for a 25 μm thick membrane hydrophone: amplitude; (b) phase.

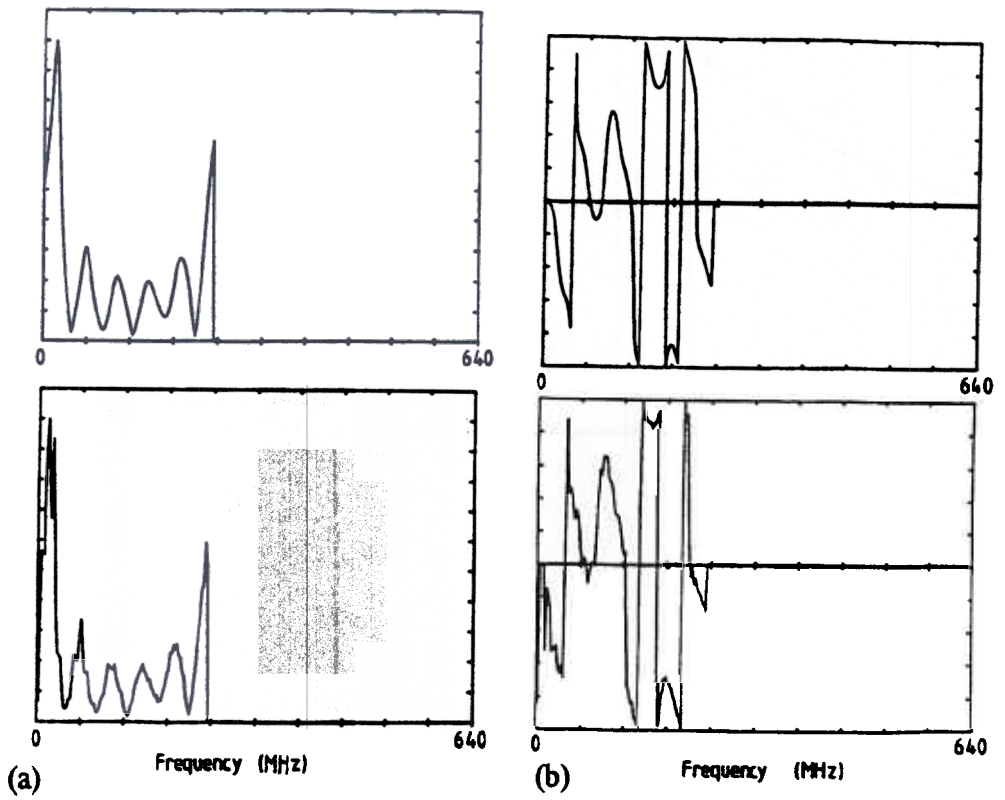


Figure A.9: Comparison of input and calculated response for a 50 μm thick (bilaminar) membrane hydrophone: (a) amplitude; (b) phase.

In Figure A.9, it can be seen that some of the values for frequencies that are not multiples of the fundamental frequency are beginning to deviate from the expected result. Figure A.10 gives the sensitivities at 10 MHz intervals from 10-100 MHz. It can be seen that the agreement is within about 3% for all devices. In general, the results for the bilaminar hydrophone which is 50 μm thick are less good than for the others.

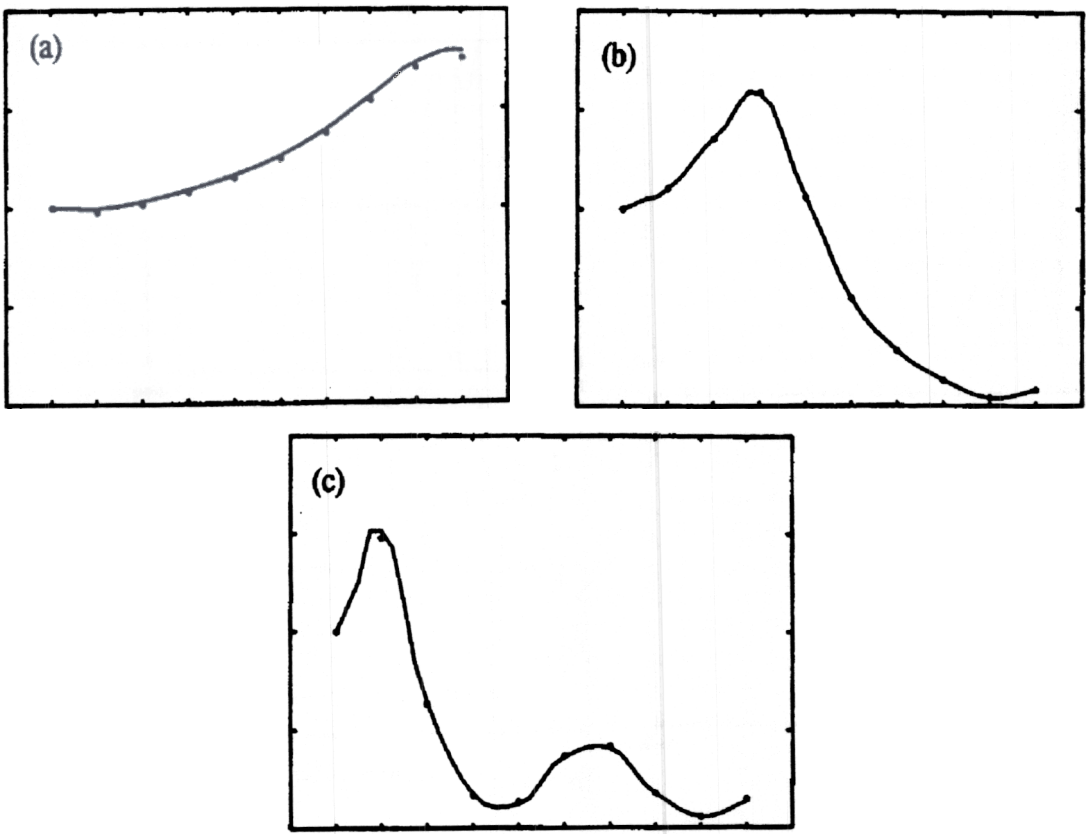


Figure A.10: Comparison of calculated (•) and input (-) sensitivities from 10-100 MHz when modelling the calibration process. Hydrophones had thicknesses of: (a) 9 μm, (b) 25 μm and (c) 50 μm.

These results give justification for the use of a lower frequency (5 MHz) transducer for calibrating a bilaminar hydrophone, although even this may not be ideal. This is because the frequency response of a bilaminar hydrophone is not usually constant, even at low frequencies.

The method has been applied to calibrate a membrane hydrophone made from 6 μm PVDF film in the frequency range 10 to 100 MHz. The hydrophone was used in conjunction with a preamplifier and digitiser, so the calibrations apply to the sensitivity of the whole measuring system and not just the hydrophone. Such a calibration has practical significance, since it can be applied directly to measurements that are subsequently made with the same system. At the fundamental frequency of 10 MHz, the measured sensitivity was 0.410 V/MPa, whereas the value obtained by reference to the NPL Primary Standard Laser Interferometer (Bacon 1988) was 0.408 V/MPa. At 20 MHz, the two methods gave the same sensitivity value of 0.411 V/MPa. At frequencies above 20 MHz, the results were verified by comparing them with the model of the hydrophone frequency response. The effects of the bandwidth of the preamplifier and digitiser had to be measured and incorporated into the predictions of the system response, as well as the effect of the electrical loading of the hydrophone by the preamplifier. This last effect gave rise to a resonance in the system response, which can be seen as a ringing in the experimentally measured waveforms (Figures A.5 and A.6). The difference between the two sets of data is less than 2% up to 60 MHz, rising to 8.8% at 100 MHz.

The calibration method can equally well be applied to determining the amplitude and phase response of a hydrophone. Results for two hydrophones are plotted in Figures A.11 and A.12 and are detailed in Tables A.1 and A.2 below. In Figures A.11 to A.12, the sensitivity values are compared at 10 MHz with interferometer calibrations and at higher frequencies with predictions of the frequency response. The agreement shown provides further validation of the calibration method.

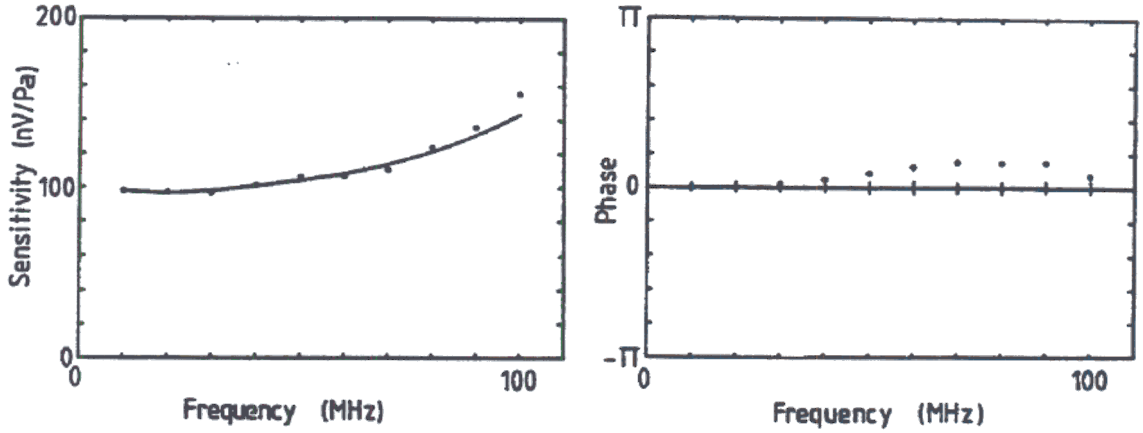


Figure A.11: Measured sensitivity (left) of a 6 μm thick membrane hydrophone (•), compared with results from interferometry combined with predictions of the frequency response (-); (right) measured phase response.

In addition to using this technique in calibrating hydrophones, it is possible to apply it to measure the nonlinearity coefficient (β) of water (or, in principle, any other medium), provided that the hydrophone sensitivity at the fundamental frequency is known. For the pulsed method as used here, this gives a value for β of 3.50, equivalent to a B/A value of 5.0. This result is equal to the currently accepted value obtained from thermodynamic calculations and gives another indication of the method's reliability.

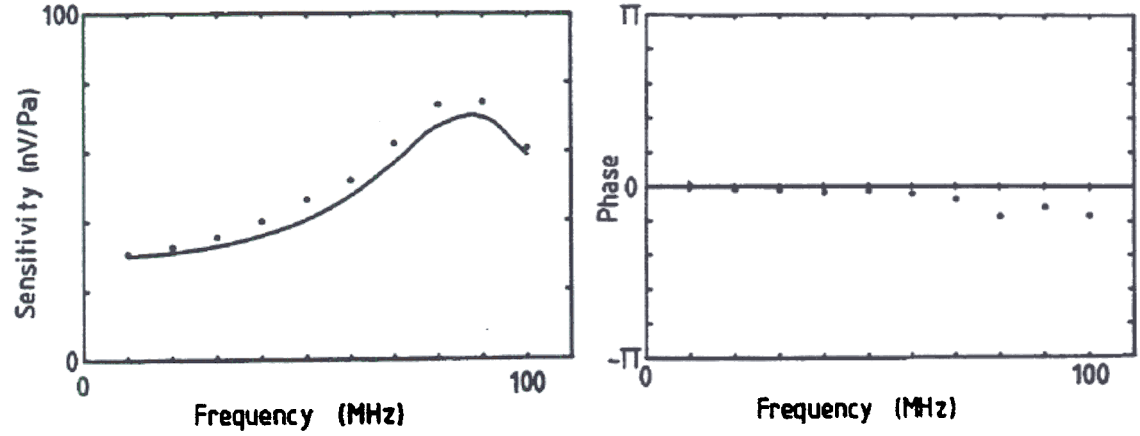


Figure A.12: Measured sensitivity (left) of a 9 μm thick membrane hydrophone (•), compared with results from interferometry combined with predictions of the frequency response (-); (right) measured phase response.

A.2 RESULTS FOR SPECIFIC HYDROPHONES

A.2.1 Sensitivity values

The measurements were obtained using the method described above, correcting them to end-of-cable open-circuit values. Only results obtained with the 10 MHz transducer have been processed. The results and random uncertainties (95% confidence) are given in Tables A.1 and A.2. It should be noted that calibration data for the whole measurement system is available up to 120 MHz for IP767, but we cannot measure impedances at this frequency and so cannot make the loading correction. At 10-30 MHz, results from the interferometer are given for comparison. At 30 MHz it should be noted that the results from the interferometer are not very reliable (the signal is small, spatial-averaging and possibly nonlinear propagation effects are significant), so no real credence can be given to the comparison. The measurements for the calibrations were performed on 15-19 January 1990, at water temperatures in the range 19.8-20.3 °C. The transducer used was number 886 (19 mm, 10 MHz Panametrics).

Frequency (MHz)	Interferometer results (nV/Pa)	Magnomic results (nV/Pa)	Random uncertainty (95% confidence) (%)	Number of measurements
10	97.51	97.84	1.0	14
20	96.87	97.02	0.6	13
30	109.8 (not accurate)	96.65	2.2	13
40		101.63	1.4	13
50		106.1	3.6	13
60		106.56	2.0	13
70		110.46	3.3	13
80		123.73	2.8	13
90		135.61	2.2	12
100		155.53	3.7	11
110		173.06	3.8	8

Table A.1: Results for IP767: 6 μm thick coplanar-shielded membrane hydrophone.

Frequency (MHz)	Interferometer results (nV/Pa)	Magnomic results (nV/Pa)	Random uncertainty (95% confidence) %	Number of measurements
10	29.95	30.76	0.8	12
20	31.62	32.58	1.1	12
30	37.41 (not accurate)	35.36	2.7	12
40		40.05	1.4	12
50		46.23	3.2	12
60		51.77	2.1	12
70		62.48	4.1	12
80		73.60	3.7	12
90		74.45	2.8	9
100		61.06	4.8	8
110		64.85	5.0	4

Table A.2: Results for IP027: 9 μm_thick, 0.5 mm diameter coplanar-shielded_hydrophone.

A.3 STEPS TO IMPROVE THE TECHNIQUE

A.3.1 Calibrations using the interferometer

There are several steps that could be taken to improve the calibration technique and its validation. If the interferometer were used to measure the source waveform precisely, then it could be used to check the magnomic method. If a distorted field waveform were to be measured, then it may be possible to get direct interferometer calibrations up to (say) 50 MHz. The main obstacle at present to interferometer calibrations above 20 MHz is that spatial averaging effects become very large with tone-burst fields. A plane-wave method would obviously overcome this difficulty. One further application would be to use the interferometer to calibrate the reference hydrophone at low frequencies. This would mean that the frequency response in the range 1-20 MHz would be known, so the reducing an assumption made by the magnomic method.

A.3.2 Repeat the measurements using the nonlinear system

Here, further measurements would be made at both 5 and 10 MHz, using similar transducers to those used before (there are some different transducers with the same dimensions). It may be possible that the size of the propagation artefact close to the transducer varies between devices.

A.3.3 Improve the calibration algorithm

At present, the algorithm assumes that it has a good idea of the initial waveform. This assumption can be eliminated using a different sort of optimisation algorithm. Initial work has

been performed using a matrix inversion method, but this does not seem to be a well posed problem from the mathematical point of view and is unstable. A more sophisticated method is therefore required. This would also mean that calibration values at intermediate frequencies could be obtained with better validity. (At present there is data at 2.5 MHz intervals for the results from the 10 MHz transducer, but we do not make use of it. The 5 MHz transducer would give results at about 1 MHz intervals.)

A.4 REFERENCES

BACON D R (1980). *Properties of a PVDF hydrophone with 100 MHz bandwidth for studying medical, nonlinear and other fields*. Proc. IEEE Ultrasonics Symp., p582-585.

BACON DR (1982). *Characteristics of a PVDF membrane hydrophone for use in the range 1-100 MHz*. IEEE Trans. Son. Ultrason., **SU-29**, p18-25.

BACON DR (1982). *A new method for ultrasonic hydrophone calibration.* Proc. IEEE Ultrasonics Symp., p700-704.

BACON DR (1986). *Finite amplitude propagation in acoustic beams*. PhD Thesis, University of Bath, UK.

BACON DR (1988*). Primary calibration of ultrasonic hydrophones using optical interferometry*. IEEE Trans. Ultrason. Ferroelectrics Eleq. Contr., **35**, p152-161.

BACON DR (1990). *Nonlinear Acoustics in Ultrasound Calibration and Standards*. In 'Frontiers of Nonlinear Acoustics: 12th ISNA' (Eds. M F Hamilton & D T Blackstock), p3-19.

APPENDIX B MEMBRANE HYDROPHONE REFERENCE SENSITIVITIES

This Appendix tabulates sensitivities for the four reference hydrophones used during this study. These values were derived earlier during this project and are summarised in the two early reports generated: Esward et al. (1997) and Zeqiri and Burford (1996), both of which constitute internal NPL reports. They are referenced explicitly for traceability purposes. Note that, in keeping with the arrangement used for this 'magnomic' calibration study, all sensitivities referred are end-of-cable loaded into Input B of the amplifier 55391001.

B.1 IP016

This is a 9 μm bilaminar membrane hydrophone of active element diameter 0.5 mm. Two sets of sensitivity data are presented.

B.1.1 Interferometer calibrations

The hydrophone was calibrated in November 1996, the results being summarised in CMAM(INT)001. The calibration was carried out using a 5 MHz focused transducer, Type V307, serial no. 110779, with the hydrophone positioned at the focus of the transducer (equivalent time delay of 98 μs or separation of 145 mm). The uncertainties appearing in the tabulation below relate to the standard deviation from four measurements.

Frequency (MHz)	End-of-cable loaded sensitivity (nV Pa $^{-1}$)
5	53.2 ± 0.9%
10	60.7 ± 2.6%
15	66.9 ± 2.9%
20	74.7 ± 3.1%
25	81.1 ± 3.5%
30	84.9 ± 4%
35	92.6 ± 5.7%
40	104 ± 9.4%
45	113.3 ± 14.8%
50	101.5 ± 14%
55	64.2 ± 22%
60	30.4 ± 40%

Experimentally derived spatial-averaging corrections have been applied to the measured sensitivities. These are presented in Appendix D of the report CMAM(INT)001 for the transducer in question. The correction is relatively small in relation to the random uncertainties given above, varying from 1 % at 5 MHz to just over 5% at 60 MHz.

The second 'magnomic' set of data for IP016 was obtained in December 1993. This calibration was carried out prior to the first customer calibration up to 40 MHz in order to validate the technique. The results shown are for a single run.

Frequency (MHz)	End-of-cable loaded sensitivity (nV Pa $^{-1}$)	Frequency (MHz)	End-of-cable loaded sensitivity (nV Pa $^{-1}$)
2	44.3	32	85.9
4	47.4	34	88.7
6	50.7	36	92.4
8	52.4	38	99.3
10	54.5	40	106.3
12	57.0	42	106.8
14	58.2	44	110.7
16	59.8	46	119.6
18	63.2	48	116.5
20	64.9	50	111.4
22	66.2	52	106.1
24	69.6	54	100.9
26	73.3	56	88.5
28	74.8	58	73.8
30	78	60	74.4

B.1.3 1 to 20 MHz nonlinear comparison technique

A substantial calibration history also exists for the device derived using the A7 customer hydrophone facility. This technique is based on a comparison using a 1 MHz fundamental distorted waveform to provide sensitivities at 1 MHz intervals up to 20 MHz. The results below represent an average of thirteen calibrations carried out over the last twelve years. Expanded uncertainties are given using a coverage factor, k, equal to 2.

B.1.2 'Magnomic' calibrations

During the early stages of the project, Milestone 1 (entitled "Establish service for hydrophone calibration in the frequency range 20 to 60 MHz") involved using a nonlinear comparison method to transfer 'magnomic' calibrations to two other high frequency hydrophones, one of which was IP016. The 'magnomic' hydrophone used was B767 and the work is described within the report "Study of a comparison method for the calibration of hydrophones in the frequency range 20 MHz to 60 MHz" (NPL Report CIRA(INT)005 August 1996). The uncertainty values tabulated correspond to the Type A uncertainties, calculated at a confidence level of approximately 95%.

Frequency (MHz)	**End-of-cable loaded sensitivity (nV Pa $^{-1}$)**	**Frequency (MHz)**	**End-of-cable loaded sensitivity (nV Pa $^{-1}$)**
2	48.5 ± 7%	32	85.7 ± 15.1%
4	50.7 ± 11%	34	89.6 ± 15.4%
6	52.4 ± 10.5%	36	91.8 ± 16.9%
8	55.4 ± 10.1%	38	95.0 ± 17.1%
10	57.6 ± 10.1%	40	99.9 ± 17.6%
12	59.8 ± 11.8%	42	106.0 ± 18%
14	60.7 ± 13.7%	44	107.6 ± 19.5%
16	62.8 ± 14.8%	46	106.5 ± 19.2%
18	65.2 ± 14.1%	48	104.3 ± 17.3%
20	67.7 ± 12.4%	50	97.6 ± 19.8%
22	70.4 ± 12.2%	52	89.7 ± 19.9%
24	72.7 ± 14.9%	54	81.9 ± 18.9%
26	75.9 ± 15.5%	56	72.6 ± 21.1%
28	78.6 ± 16.4%	58	65.4 ± 20.7%
30	81.1 ± 16.9%	60	58.3 ± 15.5%

Frequency (MHz)	End-of-cable loaded sensitivity (nV Pa $^{-1}$)
1	43.2 ± 6%
2	45.6 ± 6%
3	48.2 ± 6%
4	50.0 ± 6%
5	50.4 ± 6%
6	52.3 ± 6%
7	52.9 ± 6%
8	54.7 ± 6%
9	55.4 ± 7%
10	56.8 ± 7%
11	57.4 ± 7%
12	58.3 ± 7%
13	59.0 ± 7%
14	60.0 ± 8%
15	60.8 ± 8%
16	61.6 ± 8%
17	62.7 ± 9%
18	63.6 ± 10%
19	64.9 ± 11%
20	66.3 ± 12%

B.2 IP901

This is a 9 μm coplanar membrane hydrophone of active element diameter 0.5 mm. Three sets of sensitivity data, derived using various methods, are presented.

B.2.1 Interferometer calibrations

The hydrophone was calibrated twice using the interferometer. The first time was in November 1996, the results being summarised in CMAM(INT)001, when the calibration was carried out using two different 5 MHz focused transducers: Type V307; serial no. 110779, with the hydrophone positioned at the focus of the transducer (equivalent time-delay of 98 μs or separation of 145 mm) and Type V326 serial number 230041 (time-delay of 36 μs or 54 mm). The uncertainties appearing in the tabulation below relate to the standard deviation from at least three measurements.

Frequency (MHz)	End-of-cable loaded sensitivity (nV Pa^{-1}) Transducer 110779	End-of-cable loaded sensitivity (nV Pa^{-1}) Transducer 230041
5	27.1 ± 3.8%	27.8 ± 5.5%
10	27.9 ± 2.9%	28.5 ± 5.5%
15	28.9 ± 3%	29.9 ± 6.3%
20	31.3 ± 4.2%	32.6 ± 8.1%
25	33.8 ± 4.6%	35.4 ± 5%
30	35.7 ± 5.1%	39.2 ± 9.4%
35	38.4 ± 6.6%	41.8 ± 4.8%
40	41.6 ± 9.6%	45.9 ± 6.7%
45	46.7 ± 9.1%	51.9 ± 7.5%
50	49.5 ± 7.6%	50.48 ± 7.9%
55	53.1 ± 9.5%	53.9 ± 6.2%
60	63.5 ± 16.8%	52.2 ± 7.9%

Experimentally derived spatial-averaging corrections have been applied to the measured sensitivities. These are presented in Appendix D of the report CMAM(INT)001 for the two transducers in question.

IP901 was also calibrated using the interferometer in October 1997. The results given below have been corrected for spatial-averaging using beam-plots of the harmonic content of the nonlinear field. The uncertainties given in the tabulation below give the standard deviations for nine calibrations.

Frequency (MHz)	End-of-cable loaded sensitivity (nV Pa^{-1})
5	26.0 ± 4.2%
10	27.6 ± 4.9%
15	28.3 ± 5.6%
20	30.3 ± 6.2%
25	32.4 ± 7.1%
30	34.4 ± 8.2%
35	36.9 ± 9.1%
40	41.0 ± 9.9%
45	42.7 ± 14%
50	44.2 ± 17.3%
55	48.2 ± 19.3%
60	50.0 ± 22.5%

B.2.2 'Magnomic' calibrations

During the early stages of the project, Milestone 1 (entitled Establish service for hydrophone calibration in the frequency range 20 to 60 MHz") involved using a nonlinear comparison method to transfer 'magnomic' calibrations to two other high frequency hydrophones, one of which was IP901. The 'magnomic' hydrophone used was B767 and the work is described within the report "Study of a comparison method for the calibration of hydrophones in the frequency range 20 MHz to 60 MHz" (NPL Report CIRA(INT)005 August 1996). The uncertainty values tabulated correspond to the Type A uncertainties, calculated at a confidence level of approximately 95%.

Frequency (MHz)	End-of-cable loaded sensitivity (nV Pa $^{-1}$)	Frequency (MHz)	End-of-cable loaded sensitivity (nV Pa $^{-1}$)
2	29.0 ± 5.5%	32	34.4 ± 8.4%
4	28 ± 5.8%	34	35.5 ± 8.4%
6	28.1 ± 6%	36	35.6 ± 9%
8	29.2 ± 7.5%	38	37.0 ± 9%
10	28.9 ± 5.7%	40	38.7 ± 8.5%
12	29.5 ± 6%	42	40.9 ± 8.8%
14	29.7 ± 6.9%	44	41.6 ± 8.3%
16	31 ± 6.3%	46	42.7 ± 10%
18	31.5 ± 5.8%	48	43.2 ± 11%
20	31.1 ± 6%	50	44.5 ± 11.3%
22	30.8 ± 6.1%	52	44.6 ± 11.5%
24	31.9 ± 7.8%	54	45.6 ± 13.9%
26	33.2 ± 7.2%	56	46.8 ± 16%
28	33.2 ± 6.9%	58	49.0 ± 14.3%
30	32.8 ± 8.6%	60	49.6 ± 14.5%

B.2.3 1 to 20 MHz nonlinear comparison technique

A substantial calibration history also exists for IP901 device using the A7 customer hydrophone facility. This technique is based on a comparison using of a 1 MHz fundamental distorted waveform to provide sensitivities at 1 MHz intervals up to 20 MHz. The results below represent an average of ten calibrations carried out over the last twelve years. Expanded uncertainties are given using a coverage factor, k, equal to 2.

Frequency (MHz)	End-of-cable loaded sensitivity (nV Pa $^{-1}$)
1	30.2 ± 6%
2	28.5 ± 6%
3	28.7 ± 6%
4	28.2 ± 6%
5	27.9 ± 6%
6	27.9 ± 6%
7	27.6 ± 6%
8	28.0 ± 6%
9	27.9 ± 7%
10	28.0 ± 7%
11	27.9 ± 7%
12	27.9 ± 7%
13	27.9 ± 7%
14	28.0 ± 8%
15	27.9 ± 8%
16	28.2 ± 8%
17	28.2 ± 9%
18	28.4 ± 10%
19	28.6 ± 11%
20	28.7 ± 13%

B.3 IP010

This is a 9 μm bilaminar membrane hydrophone of active element diameter 0.2 mm. Two sets of sensitivity data are presented.

B.3.1 Interferometer calibrations

The hydrophone was calibrated in December 1996 and May 1997, the results being summarised in CMAM(INT)001, APPENDIX F. The calibration was carried out using a 5 MHz focused transducer, Type V307, serial no. 110779, with the hydrophone positioned at the focus of the transducer (equivalent time delay of 98 μs or separation of 145 mm). A second calibration was carried out using the focused transducer, Type V326, serial no. 230041 (equivalent time delay of 36 μs or separation of 54 mm). Both sets of data are tabulated below with the uncertainties representing the standard deviation from four measurements.

Frequency (MHz)	End-of-cable loaded sensitivity (nV Pa^{-1}) Transducer 110779	End-of-cable loaded sensitivity (nV Pa^{-1}) Transducer 230041
5	21.4 ± 0.5%	21.3 ± 1.8%
10	21.7 ± 0.8%	21.6 ± 2.4%
15	22.8 ± 1.2%	22.8 ± 3.5%
20	25.0 ± 4.3%	25.1 ± 4.1%
25	26.5 ± 4.5%	27.9 ± 4.8%
30	29.8 ± 6.3%	31.4 ± 5.6%
35	34.1 ± 5.2%	36.9 ± 6.3%
40	39.1 ± 4.9%	42.8 ± 7%
45	48.7 ± 11.1%	51.1 ± 8.5%
50	52.3 ± 16.2%	52.6 ± 8.2%
55	49.8 ± 17.2%	53.8 ± 11.2%
60	58.6 ± 27.8%	45.6 ± 10.8%

IP010 was also calibrated using the interferometer in October 1997. The results given below have been corrected for spatial-averaging using beam-plots of the harmonic content of the nonlinear field. The uncertainties given in the tabulation below give the standard deviations derived from eleven calibrations.

Frequency (MHz)	End-of-cable loaded sensitivity (nV Pa^{-1})
5	20.8 ± 4.2%
10	21.7 ± 4.9%
15	23.0 ± 5.6%
20	25.3 ± 6.2%
25	27.7 ± 7.1%
30	31.1 ± 8.2%
35	35.2 ± 9.1%
40	42.5 ± 9.9%
45	49.4 ± 14%
50	53.9 ± 17.3%
55	57.2 ± 19.3%
60	53.8 ± 22.5%

B.3.2 'Magnomic'-derived calibrations

IP010 has also been calibrated using a piston transducer operating at 2 MHz to generate a strongly distorted waveform. The calibration, carried out in August 1998 as part of the customer job A8/98/299, were derived relative to the hydrophone IP901 using the 'magnomic' values for this hydrophone. The uncertainties are Type A only, given at a confidence level of approximately 95%, and have been derived from four calibrations. They figures are unusually small and should not be considered as typical for the intercomparison method at these frequencies.

Frequency (MHz)	End-of-cable loaded sensitivity (nV Pa $^{-1}$)	Frequency (MHz)	End-of-cable loaded sensitivity (nV Pa $^{-1}$)
2	19.3 ± 0.8%	32	31.5 ± 1.2%
4	21.1 ± 1.0%	34	31.6 ± 1.1%
6	20.6 ± 1.5%	36	33.8 ± 1.4%
8	21.2 ± 1.2%	38	35.3 ± 2.2%
10	21.5 ± 1.2%	40	37.0 ± 4.6%
12	21.9 ± 1.3%	42	39.5 ± 2.2%
14	22.1 ± 1.6%	44	40.4 ± 1.4%
16	23.4 ± 1.2%	46	41.5 ± 2%
18	23.8 ± 2.2%	48	41.9 ± 1.6%
20	24.4 ± 1.8%	50	41.8 ± 1.2%
22	25.7 ± 0.8%	52	41.0 ± 4.1%
24	26.0 ± 1.6%	54	39.6 ± 4.7%
26	28.1 ± 1.7%	56	38.2 ± 1.2%
28	28.3 ± 3.2%	58	36.1 ± 3.4%
30	29.2 ± 3.2%	60	31.9 ± 4%

A calibration through comparison for IP010 was carried out over the frequency range 5 to 60 MHz in May 1997 in support of the project AM023020. This was completed by comparing the response of IP010 with IP901 and IP016 in the field radiated by the 5 MHz focused transducer number 230041. Calibration figures for the end-of-cable-loaded sensitivity were derived through comparison with the two 'magnomic' hydrophones IP901 and IP016.

Frequency (MHz)	IP010 end-of-cable loaded sensitivity RE: IP016 (nV Pa^{-1})	IP010 end-of-cable loaded sensitivity RE: IP901 (nV Pa^{-1})	Average end-of-cable loaded sensitivity (nV Pa^{-1})	Mean random uncertainty (95%)
5	21.5	18.8	20.2	± 4.4%
10	23.6	23.7	23.7	± 7.2%
15	25.3	26.2	25.8	± 4.4%
20	27.5	27.9	27.7	± 3.6%
25	29.4	29.9	29.6	± 5.4%
30	31.2	31.4	31.3	± 8.3%
35	34.7	35.9	35.3	± 8.6%
40	37.5	40.7	39.1	± 7.5%
45	42.2	45.9	44.1	± 8.9%
50	42.4	45.9	44.2	± 9.2%
55	38.2	40.3	39.2	± 9.9%
60	28.6	32.5	30.6	± 8.5%

B.3.3 1 to 20 MHz nonlinear comparison technique

A substantial calibration history also exists for IP010 device using the A7 customer hydrophone facility. This technique is based on a comparison method and uses a 1 MHz fundamental distorted waveform to provide sensitivities at 1 MHz intervals up to 20 MHz. The results below represent an average of fifteen calibrations carried out over the last twelve years. Expanded uncertainties are given using a coverage factor, k, equal to 2.

Frequency (MHz)	End-of-cable loaded sensitivity (nV Pa $^{-1}$)
5	34.5 ± 0.5%
10	34.0 ± 1.1%
15	34.2 ± 2.3%
20	35.8 ± 2.4%
25	37.0 ± 0.4%
30	38.0 ± 4%
35	40.2 ± 5.5%
40	41.3 ± 3%
45	46.0 ± 6.8%
50	51.7 ± 11%
55	50.3 ± 13.2%
60	48.5 ± 15.8%

The hydrophone was calibrated in April 1997, the results being summarised in CMAM(INT)001. The calibration was carried out using a 5 MHz focused transducer, Type V326, serial no. 230041, with the hydrophone positioned at the focus of the transducer (equivalent time delay of 41 μs or separation of 61 mm). The uncertainties appearing in the tabulation below relate to the standard deviation from four measurements.

Frequency (MHz)	End-of-cable loaded sensitivity (nV Pa $^{-1}$)
5	33.9 ± 0.4%
10	32.5 ± 1.4%
15	32.4 ± 1.7%
20	33.6 ± 3%
25	34.3 ± 3.6%
30	36.8 ± 5.6%
35	37.5 ± 5%
40	40.1 ± 7.7%
45	44.3 ± 8.2%
50	43.2 ± 11%
55	43.2 ± 10.4%
60	39.4 ± 16.4%

IP901 was also calibrated using the interferometer in October 1997. The results given below have been corrected for spatial-averaging using beam-plots of the harmonic content of the nonlinear field. The uncertainties given in the tabulation below give the standard deviations for nine calibrations.

Frequency (MHz)	End-of-cable loaded sensitivity (nV Pa $^{-1}$)
5	34.4 ± 4.2%
10	34.4 ± 4.9%
15	35.1 ± 5.6%
20	36.3 ± 6.2%
25	37.5 ± 7.1%
30	39.6 ± 8.2%
35	40.5 ± 9.1%
40	45.3 ± 9.9%
45	45.9 ± 14%
50	46.1 ± 17.3%
55	47.1 ± 19.3%
60	45.7 ± 22.5%

B.5. References

ESWARD TJ, ROBINSON, SP and ZEQIRI B (1997). *Extending the frequency range of the NPL primary standard interferometer to 60 MHz.* NPL Report No. CMAM(INT)001.

ZEQIRI B and BURFORD PA (1996). *Study of a comparison method for the calibration of hydrophones in the frequency range 20 MHz to 60 MHz.* NPL Report No. CIRA (INT)005.

APPENDIX C GAIN VALUES FOR AMPLIFIER 55391001

The frequency dependent gain of the amplifier 55391001, Input B is tabulated below.

Frequency (MHz)	Gain	Frequency (MHz)	Gain
1	6.7210	**31**	6.4796
2	6.6829	**32**	6.4550
3	6.6563	**33**	6.4275
4	6.6397	**34**	6.3982
5	6.6316	**35**	6.3681
6	6.6307	**36**	6.3381
7	6.6354	**37**	6.3082
8	6.6444	**38**	6.278
9	6.6562	**39**	6.2473
10	6.6695	**40**	6.2157
11	6.6826	**41**	6.1831
12	6.6943	**42**	6.1500
13	6.7031	**43**	6.1168
14	6.7075	**44**	6.0841
15	6.7061	**45**	6.0523
16	6.6980	**46**	6.0221
17	6.6846	**47**	5.9938
18	6.6674	**48**	5.9679
19	6.6484	**49**	5.9450
20	6.6292	**50**	5.9254
21	6.6114	**51**	5.9094
22	6.5953	**52**	5.8957
23	6.5809	**53**	5.8831
24	6.5682	**54**	5.8701
25	6.5572	**55**	5.8552
26	6.5477	**56**	5.8377
27	6.5387	**57**	5.8189
28	6.5286	**58**	5.8007
29	6.5163	**59**	5.7849
30	6.5002	**60**	5.7734

APPENDIX D TRANSFER FUNCTION OF A HYDROPHONE

This Appendix presents a model for the transfer function of a hydrophone and applies it to predict the response of three designs of hydrophone of the membrane type.

D1 THEORETICAL CONSIDERATIONS: DESCRIPTION OF THE MODEL

The aim of this Section is to outline the theory used to calculate the pressure reflection and transmission coefficients as well as the absorption coefficient of a hydrophone consisting of n layers of material when placed in a given medium.

Consider a transducer consisting of n-2 layers where the top-most and bottom-most layers are in contact with a specific medium. It is assumed that only plane waves are normally incident on the surface of the top-most layer. Let x be the direction for normal propagation. Let p_i and u_{xi}, where $1 \le i \le n-1$, be the pressure and normal component of the particle velocity respectively at the top of the i^{th} layer, where i=1 corresponds to the top of the backing medium (see Figure D.1).

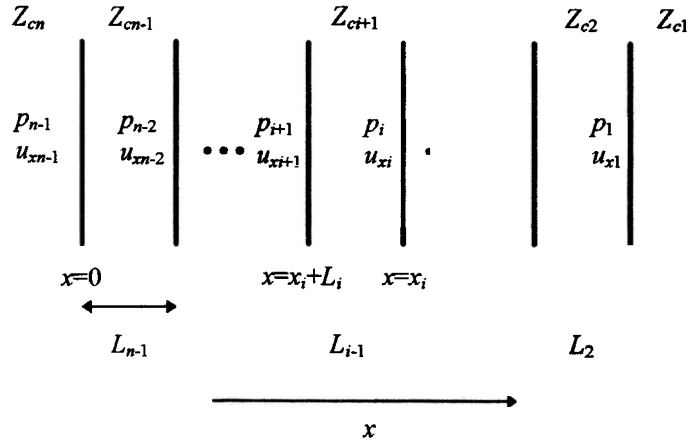


Figure D.1: Schematic diagram of the multi-layered hydrophone model

Z_{ci} and L_i are respectively the characteristic impedance of the medium and the thickness corresponding to the i^{th} layer. Note that L_1 and L_n are not defined since these are associated with semi-infinite media on either side of the transducer.

It is of interest to be able to determine the pressure reflection and transmission coefficients as well as the absorbent coefficient of the transducer for a normally incident plane wave on the top-most layer.

The pressure at the top-most layer will consist of an incident and reflected component:

$$p_{n-1} = \left(A_{n-1}e^{-jk_n x_{n-1}} + B_{n-1}e^{jk_n x_{n-1}}\right)e^{j\omega t} \qquad \text{(D1)}$$

where k_n is the complex wave number associated with the medium, x_i is the value of the x coordinate at the top of the i^{th} layer and ω is the angular frequency.

The normal particle velocity at the top-most layer is given by:

$$u_{xn-1} = -\frac{1}{j\omega\rho_n}\frac{\partial}{\partial x}p_{n-1} = \frac{1}{Z_{cn}}\left(A_{n-1}e^{-jk_n x_{n-1}} - B_{n-1}e^{jk_n x_{n-1}}\right)e^{j\omega t}$$

where ρ_n is the density of the medium and Z_{cn} is the characteristic impedance of the medium ($Z_{cn}=\rho_n c_n$, where c_n is the velocity of sound in the medium).

The pressure reflection coefficient is defined as:

$$R = \frac{B_n}{A_n}$$

From Equations D1, D2 and D3, it may be shown that

$$R = \frac{Z_{sn-1} - Z_{cn}}{Z_{sn-1} + Z_{cn}}$$

where $Z_{sn-1}=p_{n-1}/u_{xn-1}$ is the surface impedance of the top-most layer.

The absorption coefficient is defined as:

$$\alpha = 1 - |R|^2 \tag{D5}$$

Hence, it can be seen that if the surface impedance of the hydrophone can be determined, so can both the pressure reflection coefficient and the absorption coefficient.

Consider now the pressure and normal particle velocity at the top of layer i

$$p_i = \left(A_i e^{-jk_{i+1}x_i} + B_i e^{jk_{i+1}x_i}\right)e^{j\omega t} \tag{D6}$$

$$u_{xi} = \frac{1}{Z_{ci+1}}\left(A_i e^{-jk_{i+1}x_i} - B_i e^{jk_{i+1}x_i}\right)e^{j\omega t} \tag{D7}$$

By combining Equations D6 and D7, the following expressions may be obtained

$$A_i = \frac{1}{2}\left(p_i + Z_{ci+1}u_i\right)e^{jk_{i+1}x_i} \tag{D8}$$

$$B_i = \frac{1}{2}\left(p_i - Z_{ci+1}u_i\right)e^{-jk_{i+1}x_i} \tag{D9}$$

Consider now the pressure and normal particle velocity at the top of layer i+1. From pressure continuity, we have:

$$p_{i+1} = \left(A_{i+1}e^{-jk_{i+2}x_{i+1}} + B_{i+1}e^{jk_{i+2}x_{i+1}}\right)e^{j\omega t} = \left(A_i e^{-jk_{i+1}(x_i - L_i)} + B_i e^{jk_{i+1}(x_i - L_i)}\right)e^{j\omega t} \tag{D10}$$

and from continuity of particle velocity:

$$u_{xi+1} = \frac{1}{Z_{\cdot\cdot}}\left(A_{i+1}e^{-jk_{i+2}x_{i+1}} - B_{i+1}e^{jk_{i+2}x_{i+1}}\right)e^{j\omega t} = \frac{1}{Z_{c}}\left(A_i e^{-jk_{i+1}(x_i - L_i)} - B_i e^{jk_{i+1}(x_i - L_i)}\right)e^{j\omega t} \quad \text{(D11)}$$

By substituting Equations D8 and D9 into Equations D10 and D11, the following matrix equation may be obtained:

$$\begin{Bmatrix} p_{i+1} \\ u_{xi+1} \end{Bmatrix} = \begin{bmatrix} \cos(k_{i+1}L_i) & jZ_{ci+1}\sin(k_{i+1}L_i) \\ \frac{j}{Z_{ci+1}}\sin(k_{i+1}L_i) & \cos(k_{i+1}L_i) \end{bmatrix} \begin{Bmatrix} p_i \\ u_{xi} \end{Bmatrix} \quad \text{(D12)}$$

or

$$\begin{Bmatrix} p_{i+1} \\ u_{xi+1} \end{Bmatrix} = [T_{i+1}] \begin{Bmatrix} p_i \\ u_{xi} \end{Bmatrix} \quad \text{(D13)}$$

where $[T_{i+1}]$ is the transfer matrix of the i+1$^{\text{th}}$ layer.

Note that if the characteristic impedance of a given layer is large, there will be a large difference in magnitude between the two off-diagonal terms. Hence, to insure better numerical stability, it is worthwhile re-writing Equation D12 in terms of the pressure normalised to the characteristic impedance:

$$\begin{Bmatrix} \frac{p_{i+1}}{Z_{ci+1}} \\ u_{xi+1} \end{Bmatrix} = \begin{bmatrix} \frac{Z_{ci}}{Z_{ci+1}}\cos(k_{i+1}L_i) & j\sin(k_{i+1}L_i) \\ j\frac{Z_{ci}}{Z_{ci+1}}\sin(k_{i+1}L_i) & \cos(k_{i+1}L_i) \end{bmatrix} \begin{Bmatrix} \frac{p_i}{Z_{ci}} \\ u_{xi} \end{Bmatrix} \quad \text{(D13)}$$

or

$$\begin{Bmatrix} \frac{p_{i+1}}{Z_{ci+1}} \\ u_{xi+1} \end{Bmatrix} = [T_{i+1}] \begin{Bmatrix} \frac{p_i}{Z_{ci}} \\ u_{xi} \end{Bmatrix} \quad \text{(D14)}$$

From D14, it follows that:

$$\begin{Bmatrix} \frac{p_{n-1}}{Z_{cn-1}} \\ u_{n-1} \end{Bmatrix} = [T_{n-1}][T_{n-2}]\cdots[T_2] \begin{Bmatrix} \frac{p_1}{Z_{c1}} \\ u_{x1} \end{Bmatrix} \quad \text{(D15)}$$

or

$$\begin{Bmatrix} \frac{p_{n-1}}{Z_{cn-1}} \\ u_{n-1} \end{Bmatrix} = [T] \begin{Bmatrix} \frac{p_1}{Z_{c1}} \\ u_{x1} \end{Bmatrix} \quad \text{(D16)}$$

where $[T]$ is the transfer matrix associated with the hydrophone.

Note that p_1 is the pressure transmitted into the medium backing the transducer.

Consider Equation D12. If the expression for p_{i+1} is divided by that for u_{xi+1}, a recurring relationship between the surface impedances of 2 consecutive layers may be obtained:

$$Z_{si+1} = \frac{p_{i+1}}{u_{xi+1}} = \frac{Z_{si}Z_{ci+1}\coth(\gamma_{i+1}L_{i+1}) + Z_{ci+1}^2}{Z_{ci+1}\coth(\gamma_{i+1}L_{i+1}) + Z_{si}} \tag{D17}$$

where $Z_{si} = \frac{p_i}{u_{xi}}$ and $\gamma_i = jk_i$.

The initial value Z_{s1} of the surface impedance is the value of the characteristic impedance of the backing medium. Hence, $Z_{s1}=Z_{c1}$. By knowledge of the characteristics of each layer of the hydrophone, it is therefore possible to obtain the surface impedance Z_{sn-1} at the top-most layer. The pressure reflection coefficient R as well as the absorption coefficient α may then be evaluated using Equations D4 and D5.

In order to evaluate the pressure transmission coefficient T, consider the total pressure and particle velocity at the top-most layer of the hydrophone (see Equations D1 and D2). At the op-most layer, x=0. By making use of this and by dividing D1 by D2, the following equation may be obtained:

$$u_{n-1} = \frac{p_{n-1}}{Z_{cn}}\frac{1-R}{1+R} \tag{D18}$$

From Equation D16, the transmitted pressure from the hydrophone into the medium may be obtained through inversion of the transfer matrix and by making use of Equation D18:

$$p_1 = T_{11}^{-1}p_{n-1}\frac{Z_{c1}}{Z_{cn-1}} + T_{12}^{-1}p_{n-1}\frac{Z_{c1}}{Z_{cn}}\left(\frac{1-R}{1+R}\right) \tag{D19}$$

where $[T]^{-1} = \begin{bmatrix} T_{11}^{-1} & T_{12}^{-1} \\ T_{21}^{-1} & T_{22}^{-1} \end{bmatrix}$

From Equation D1, it is easily shown that the incident component of the pressure wave at the top-most layer is:

$$A_{n-1} = \frac{p_{n-1}}{1+R} \tag{D20}$$

By definition, the pressure transmission coefficient T is the ratio of the transmitted pressure to the incident pressure or:

$$T = \frac{p_1}{\cdot} = T_{11}^{-1}\frac{Z_{c1}}{Z_{cn-1}}(1+R) + T_{12}^{-1}\frac{Z_{c1}}{Z_{cn}}(1-R) \tag{D21}$$

It is of interest to evaluate the average pressure $\bar{p}$ across the layer(s) of *pvdf*, as this is in fact what the hydrophone will measure. This is given by:

$$\bar{p} = \frac{1}{L_i}\int_{x_i}^{x_i+L_i} p_i(x)dx \tag{D22}$$

for the coplanar case, if the *pvdf* layer corresponds to the i^{th} layer and

$$\bar{p} = \sum_{k=i,j}\frac{1}{L_k}\int_{x_k}^{x_k+L_k} p_k(x)dx \tag{D23}$$

for the bilaminar case where the *pvdf* layers are the i^{th} and j^{th} layers. x_i corresponds to the value of x at the top of layer i.

If we assume that unit pressure is incident on the top-most layer (i.e. the face of the transducer where x=0), there is an input pressure of $e^{j\omega t}$. By definition the value of the average pressure obtained in this case is the frequency response function $H_1(\omega)$ between the face of the hydrophone and the layer(s) of *pvdf*.

$$H_1(\omega) = \bar{p}(\omega) \tag{D24}$$

Assume that a pressure wave is incident on the face of the transducer. The output average pressure can be obtained by convolving the time history $p(t)$ of this pressure wave with $h_1(t)$, where

$$h_1(t) = F^{-1}\left[H_1(\omega)\right] \tag{D25}$$

and F^{-1} denotes the inverse Fourier transform.

D.2 RESULTS

The general theory has been implemented in MATLAB so that, given the material density, the sound speed, the attenuation and the thickness associated with each layer, the following quantities may be obtained:

- pressure reflection coefficient R
- pressure transmission coefficient T
- absorption coefficient α
- frequency response function H_1
- response to a pulse.

The following material properties have been assumed:

Material	Velocity of sound ($m.s^{-1}$)	Material density ($kg.m^{-3}$)	Attenuation ($Np\ m^{-1}\ MHz^{-1}$)
Water	1485.39	998	N/A
Gold	3240	19281	N/A
Chromium	6608	7194	N/A
PVDF	2300	1780	111

N/A Not available, negligible attenuation assumed in the model

Table D1: Compilation of material properties used for the transfer function calculations.

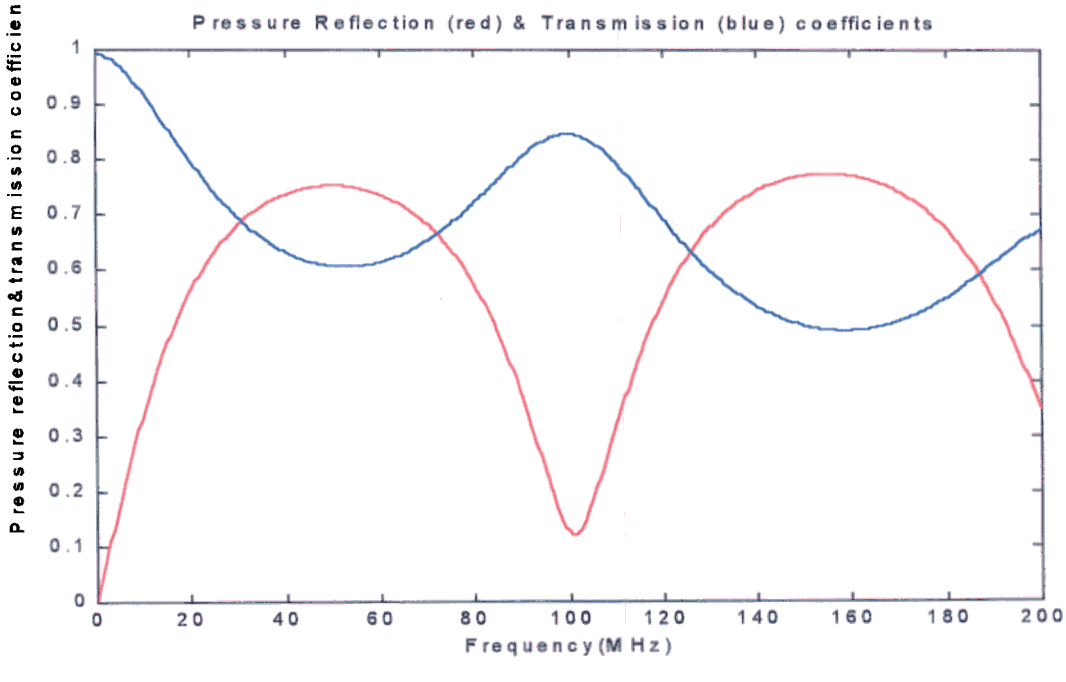
In total, three hydrophones have been examined; two coplanar and 1 bilaminar design. The hydrophones are assumed to be placed in water.

D.2 Coplanar hydrophone, Type 1

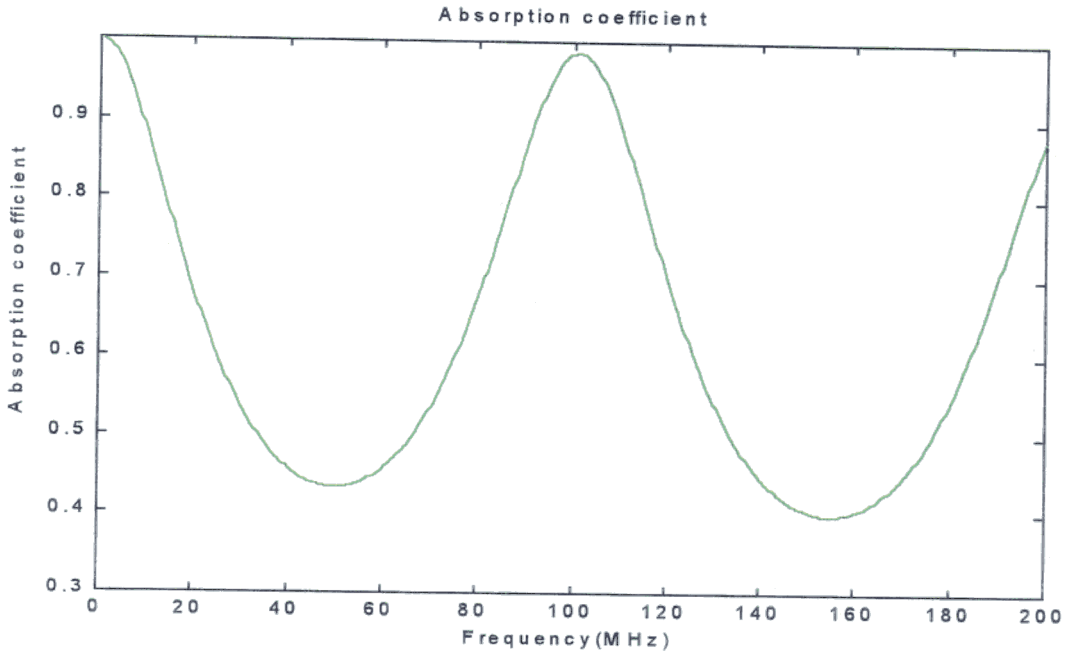
This type of hydrophone comprises 3 layers. A layer of *pvdf* sandwiched between 2 layers of gold. In this example, the following thicknesses have been used:

- gold thickness: 0.1μm
- PVDF thickness: 9μm

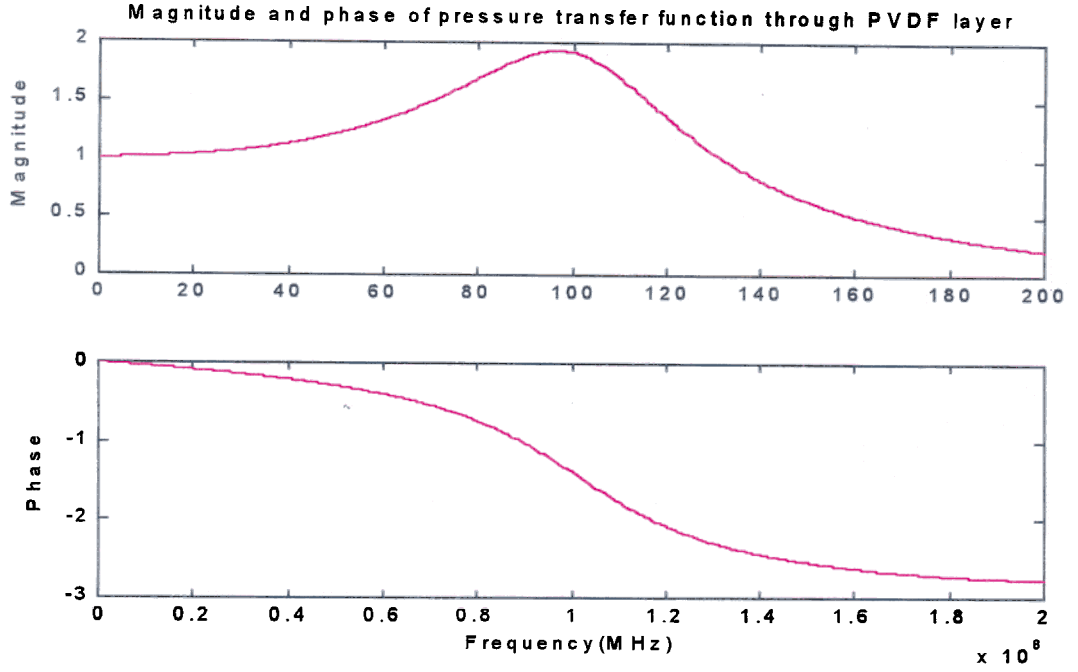
D.2.1 Pressure transmission and reflection coefficients



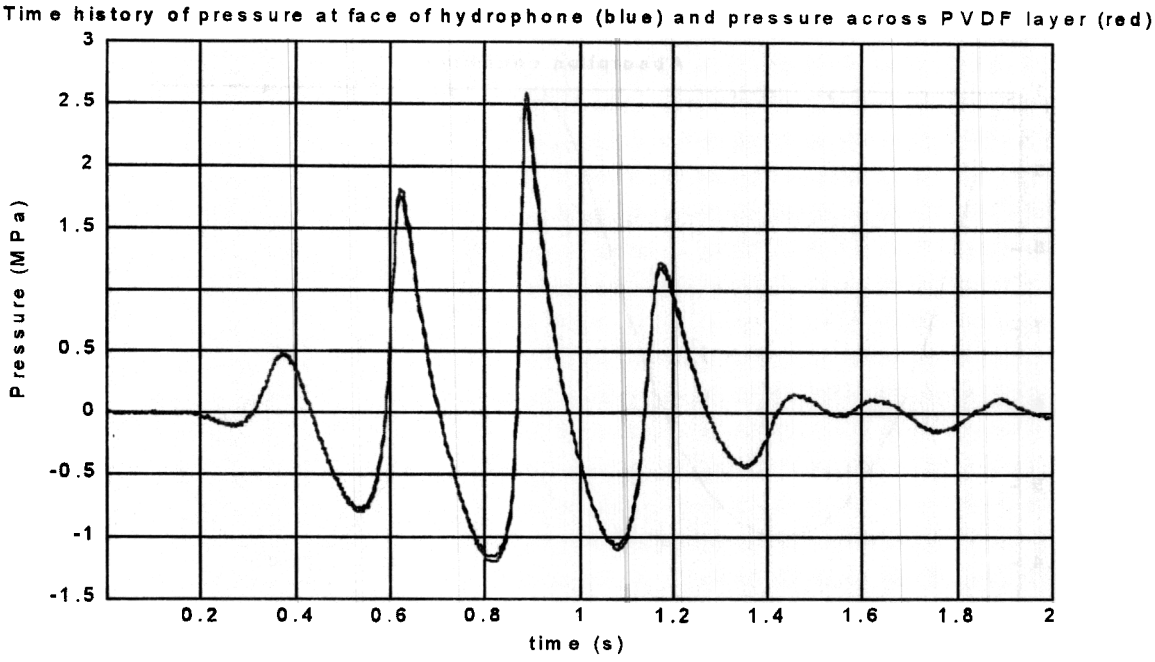
D.2.1.2 Absorption coefficient



D.2.1.3 Frequency response



D.2.1.4 Response to a pulse



D.2.2 Coplanar hydrophone, Type 2

This type of hydrophone comprises 5 layers arranged in the following way:

gold - chromium - PVDF - chromium - gold.

In this example, the following thicknesses have been used:

- gold thickness: 0.2μm
- PVDF thickness: 9μm
- chromium thickness: 0.05μm.

Frequency (MHz)	End-of-cable loaded sensitivity (nV Pa $^{-1}$)
1	22.0 ± 6%
2	19.2 ± 6%
3	20.1 ± 6%
4	21.1 ± 6%
5	20.1 ± 6%
6	20.4 ± 6%
7	20.4 ± 6%
8	20.7 ± 6%
9	20.7 ± 7%
10	20.7 ± 7%
11	20.6 ± 7%
12	20.8 ± 7%
13	20.9 ± 7%
14	21.0 ± 8%
15	21.0 ± 8%
16	21.1 ± 8%
17	21.2 ± 10%
18	21.3 ± 10%
19	21.2 ± 11%
20	21.6 ± 13%

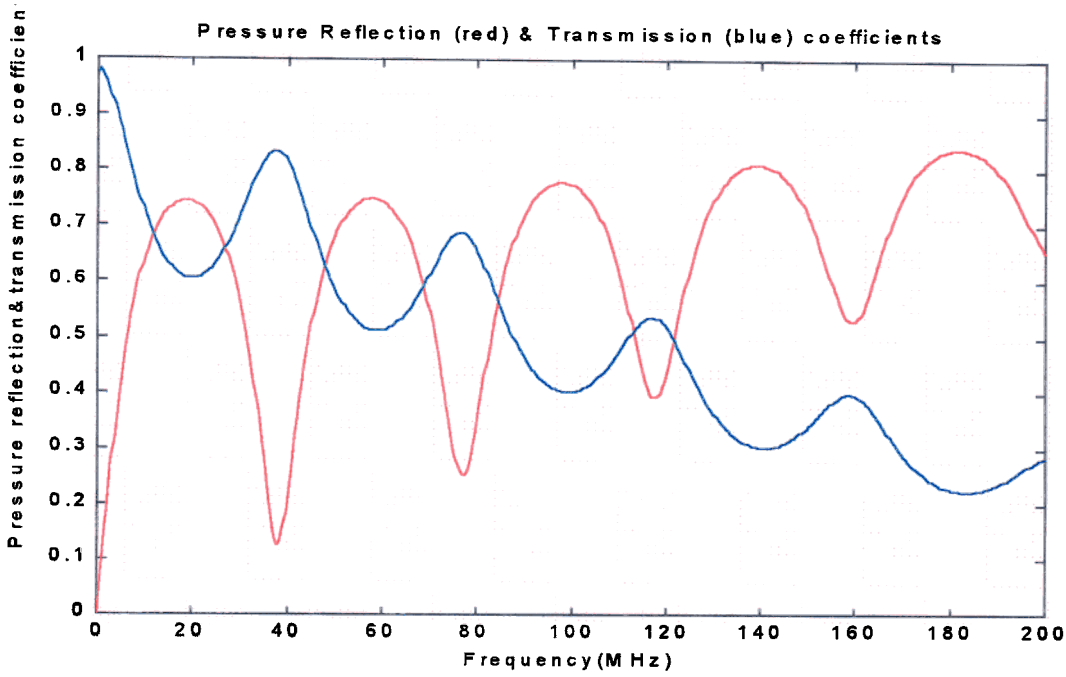
B.4. IP904

This is a 9 μm coplanar hydrophone of active element diameter 0.5 mm. Two sets of sensitivity data are presented.

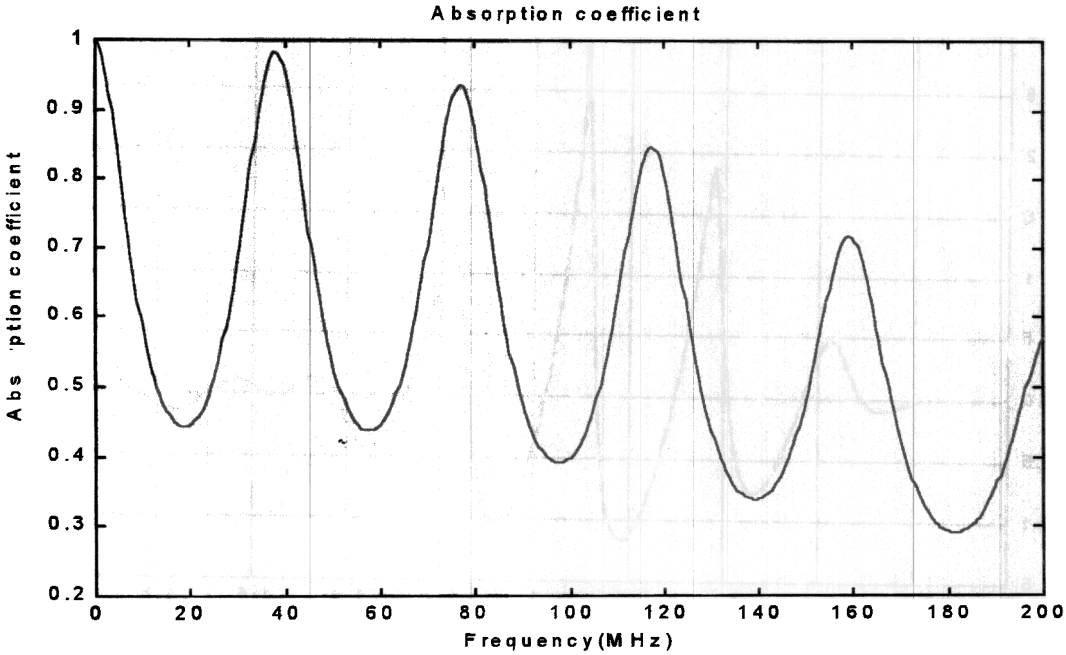
B.4.1 Interferometer calibrations

The hydrophone was calibrated in November 1996, the results being summarised in CMAM(INT)001. The calibration was carried out using a 5 MHz focused transducer, Type V307, serial no. 110779, with the hydrophone positioned at the focus of the transducer (equivalent time delay of 98 μs or separation of 145 mm). The uncertainties appearing in the tabulation below relate to the standard deviation from four measurements.

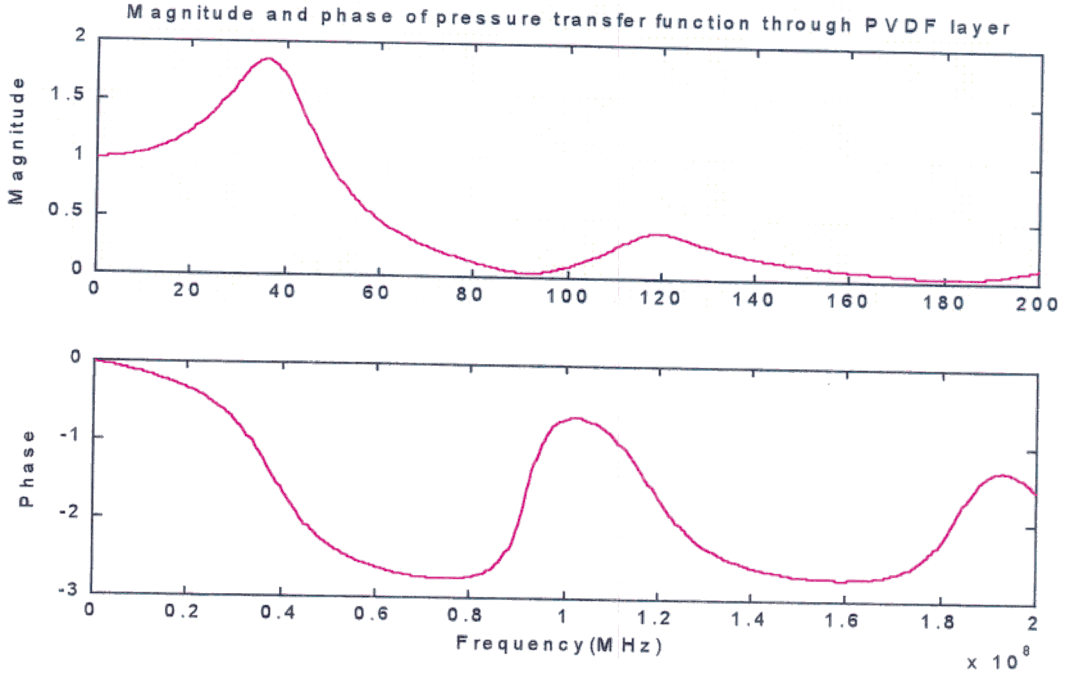
D.2.2.1 Pressure transmission and reflection coefficients



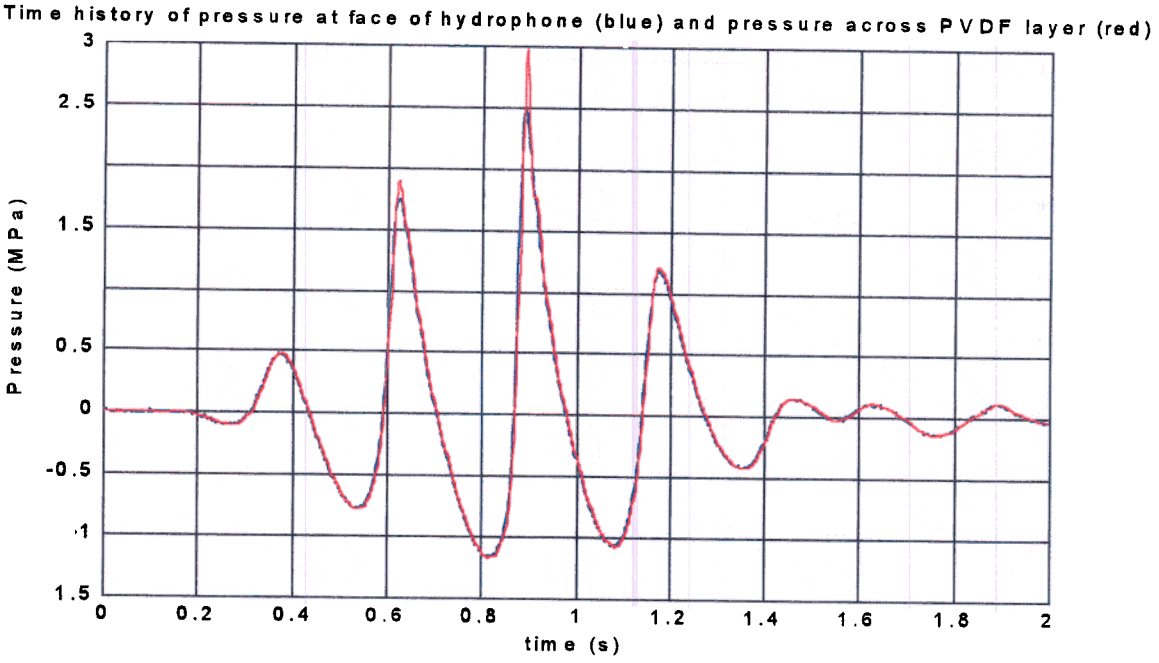
D.2.2.2.2 Reflection coefficient



D.2.2.3 Frequency response



D.2.2.4 Response to a pulse



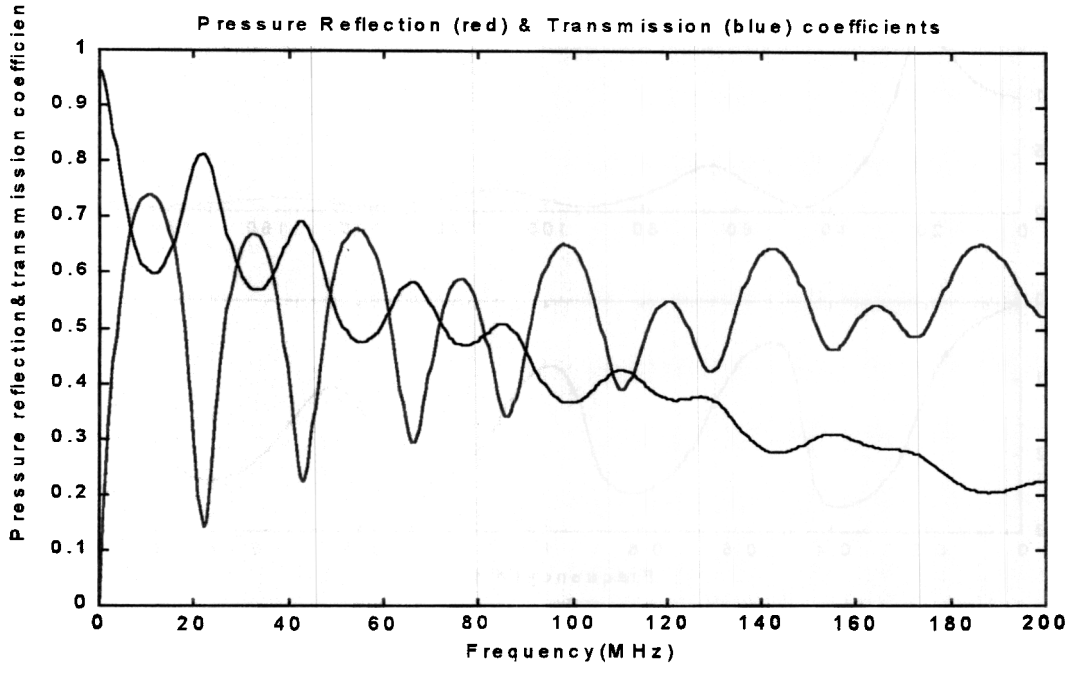
D.2.3 Bilaminar hydrophone

This type of hydrophone comprises 5 layers. 2 layers of *pvdf* inter-spaced by a layer of gold and sandwiched between 2 layers of gold. In this example, the following figures have been used:

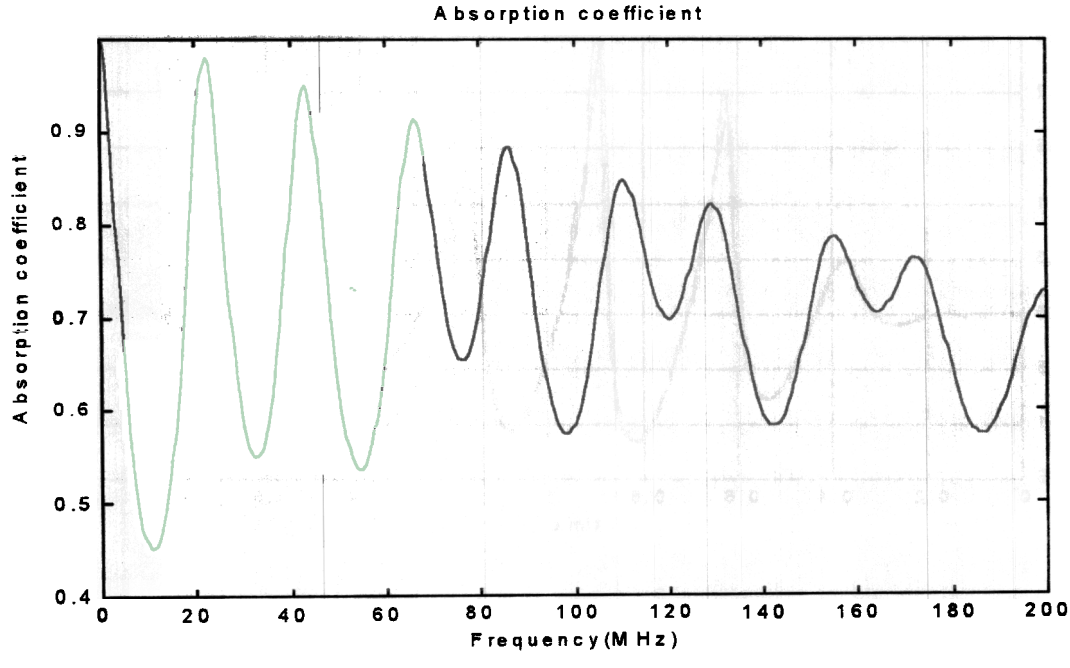
- gold thickness: 0.1μm

- *pvdf* thickness 25μm

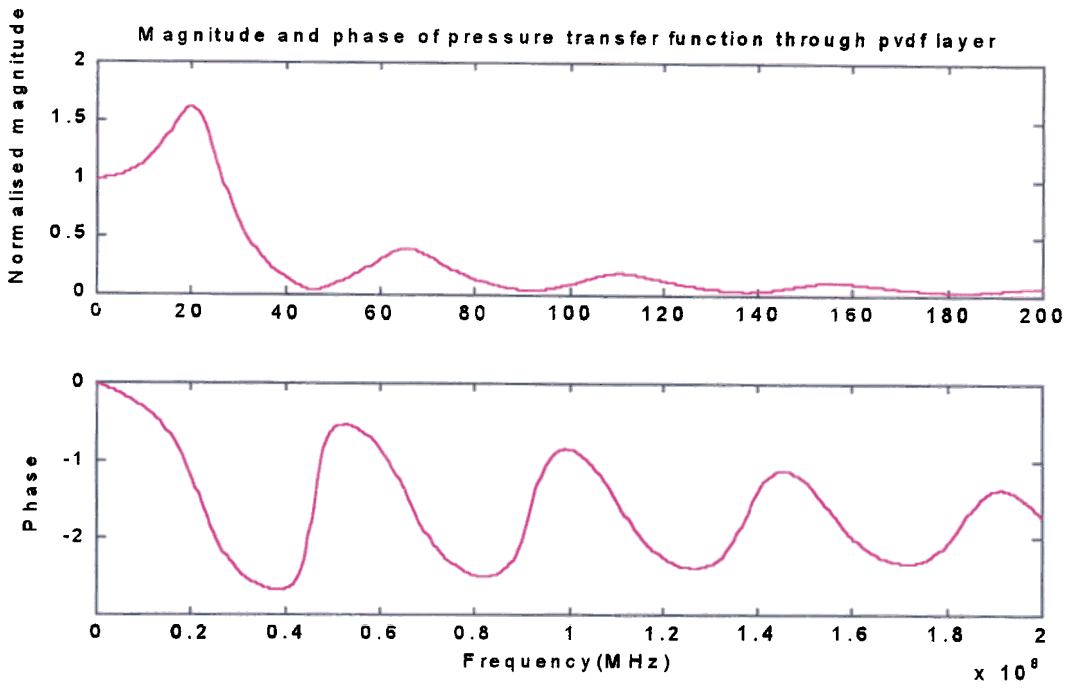
D.2.3.1 Pressure transmission and reflection coefficients



D.2.3.2 Absorption coefficient



D.2.3.3 Frequency response



D.2.3.4 Response to a pulse

